

Interaction of small molecules with thin NiO layers and related metal surfaces studied with high resolution X-ray photoelectron spectroscopy

Der Naturwissenschaftlichen Fakultät
der Friedrich-Alexander-Universität Erlangen-Nürnberg
zur
Erlangung des Doktorgrades Dr. rer. nat.

Vorgelegt von

Michael Lorenz

aus Schwabach



Als Dissertation genehmigt von der Naturwissenschaftlichen Fakultät der
Friedrich-Alexander-Universität Erlangen-Nürnberg

Tag der mündlichen Prüfung: 05. 03. 2012

Vorsitzender der

Promotionskommission: Prof. Dr. Rainer Fink

Erstberichterstatte: Prof. Dr. Hans-Peter Steinrück

Zweitberichterstatte: Prof. Dr. Jörg Libuda

Table of contents

1 Introduction.....	1
2 Theory.....	4
2.1 Basics of X-ray photoelectron spectroscopy (XPS).....	4
2.2 Vibrational splitting in XPS.....	5
2.3 Surface sensitivity of XPS and damping of XP spectra.....	7
2.4 Synchrotron radiation.....	13
2.5 Low energy electron diffraction (LEED).....	14
2.6 Super sonic molecular beam.....	15
3 Technical Details.....	17
3.1 Experimental setup.....	17
3.2 Crystal surfaces.....	20
3.3 Overview of used chemicals.....	20
3.4 Data analysis.....	21
4 Growth of nickel oxide.....	25
4.1 Oxygen interaction with Ni(111).....	25
4.1.1 The p(2x2) oxygen layer on Ni(111).....	27
4.1.2 Oxidation of Ni(111) at room temperature.....	28
4.1.3 Oxidation of Ni(111) at temperatures of 500 K and above.....	37
4.1.4 Discussion of oxygen coverages and estimation of NiO layer thickness.....	42
4.2 Growth of thin NiO layers on Cu(111).....	45
4.2.1 Oxygen interaction with Cu(111).....	45
4.2.2 Preparation of nickel layers and characterization with CO Titration.....	46
4.2.3 Oxidation of thin Ni layers on Cu(111).....	48
4.2.4 Preparation of NiO clusters on Cu(111).....	56
4.3 Comparison of the different preparations and summary.....	62
5 Adsorption on and reaction of C ₂ H _x species on clean and oxygen precovered Ni(111).....	68
5.1 Ethylene.....	71
5.1.1 Ethylene on clean Ni(111).....	71
5.1.2 Ethylene coadsorbed with O on Ni(111).....	77
5.2 Ethane.....	81
5.2.1 Ethane on clean Ni(111).....	81
5.2.2 Ethane coadsorbed with O on Ni(111).....	87
5.3 Acetylene.....	94
5.3.1 Acetylene on clean Ni(111).....	94
5.3.2 Acetylene coadsorbed with O on Ni(111).....	100

5.4 Concluding discussion.....	104
6 Adsorption of hydrocarbons on Cu(111) and thin NiO layers.....	109
6.1 Acetylene adsorption and reaction on Cu(111) and thin NiO surfaces.....	109
6.1.1 Acetylene adsorption on clean Cu(111).....	109
6.1.2 Acetylene adsorption on thin NiO lay.....	113
6.1.3 Thermal evolution of acetylene adsorbed on thin NiO layers.....	118
6.1.4 Acetylene adsorption on NiO clusters on Cu(111).....	128
6.2 Physisorption of hydrocarbons on Cu(111) and thin NiO Layers.....	135
6.2.1 Physisorption of hydrocarbons on Cu(111).....	135
6.2.1.1 Propylene physisorption on Cu(111).....	136
6.2.1.2 Interaction of ethane, ethylene and propane with Cu(111).....	140
6.2.2 Physisorption of hydrocarbons on NiO layers.....	143
6.3 Concluding discussion.....	152
7 Formation and thermal evolution of NiOH and NiCO ₃	158
7.1 Introduction.....	158
7.2 Water adsorption.....	161
7.2.1 Determination of damping factor.....	161
7.2.2. Water interaction with copper and nickel surfaces.....	163
7.2.3 Water adsorption on NiO.....	167
7.2.4 Thermal evolution of hydroxide layers.....	174
7.3 CO ₂ interaction with NiO layers.....	181
7.3.1 CO ₂ interaction with pure metal surfaces.....	181
7.3.2 CO ₂ adsorption on NiO.....	183
7.3.3 Thermal evolution of carbonate layers.....	191
7.4 CO interaction with NiO layers.....	196
7.4.1 CO interaction with nickel and copper surfaces.....	196
7.4.2 CO Adsorption and thermal evolution on NiO/Ni(111) and 2 ML NiO/Cu(111).....	200
7.4.3 CO interaction with NiO clusters on Cu(111).....	209
7.5 Coadsorption experiments on NiO layers.....	211
7.6 Concluding Discussion.....	213
8 Summary.....	221
9 Zusammenfassung.....	225
Literature.....	229

1 Introduction

Even though chemical reactions on surfaces have been studied for quite some time now, this field still remains interesting today. One of the main reasons for the interest in this field is heterogeneous catalysis, where the educts adsorb on the surfaces, react to the products there and these products then desorb again. Catalysts can significantly reduce the energy required for a particular reaction to occur, by lowering actual energies. This leads to large reductions in production costs for certain products, which can in turn open up new markets and enable cheaper production of other goods. The aim of lowering energy consumption is also extremely important today, as it lowers the CO₂ emissions, as still most of the energy is generated by burning of fossil fuels. The reduction of these CO₂ emissions, which are a main contributor to the global warming, is one of the big challenges of our time.

The prime example for an application of a heterogeneous catalyst is the modern three-way catalyst used for cleaning the exhausts of cars. Other important applications are, e.g., the Haber-Bosch process for ammonia synthesis, hydrogen production through steam reforming and sulfuric acid synthesis. For the optimization of existing catalysts and the development of new ones it is very important to understand the chemical reactions on these catalysts in great detail. This includes studies on the molecular level of the adsorption and reaction behavior of all relevant substances. Real catalysts often consist of metal particles on a support material, typically an oxide. As both components can play a role in a catalytic process, it is important to study the interaction of these relevant substances with the individual components to fully understand the system. Studying model systems reduces the complexity which helps in understanding the reaction pathways. The most common approach for studying the reactions on the individual components is to use single crystal surfaces as model systems. This approach is valid, as metal particles on real catalysts show several different facets, which consist of defined crystallographic faces, with e.g.(111) or (100) orientation [1]. Within this thesis, adsorption and reactions of small molecules on Ni(111) and Cu(111) crystal surfaces are discussed. The molecules studied are mainly small hydrocarbons. These are of special interest as they are among the most important raw materials in chemical industry [2].

For the study of the chemical reactions on surfaces we choose X-ray photoelectron spectroscopy (XPS). XPS is a versatile tool to study chemical reactions on surfaces. Different oxidation states of an atom normally lead to peaks at different binding energies, and consequently the distinction of, e.g., several oxygen-containing species on a surface is possible. The use of synchrotron radiation as the excitation source in XPS enhances the surface

sensitivity due to the tunable excitation energy. It also provides sufficient intensity to follow reactions in situ and to detect very small quantities of 0.01 ML or even less of reaction products. Synchrotron radiation also provides a very high resolution of the spectra, high enough to resolve vibrations in the spectra. This vibrational resolution opens an additional route to identify reaction products, see e.g. C₂H₂ on Ni(111) in Chapter 5. As the adsorption site of a molecule also has an influence on the binding energy, high resolution XPS can be used to help in identification of adsorption sites. This is used in Chapter 5 to solve the puzzle of the adsorption site of ethylene (C₂H₄) on Ni(111), which has been discussed controversially in literature.

A real catalyst is often in contact with various substances besides the desired educts and products. This can have a variety of different effects. On metal single crystal surfaces one approach to study some of these effects is to adsorb a species on to a crystal surface where already another species has been adsorbed. This can lead both to changes in the adsorption behavior of the studied species, and reactions between the two adsorbates. Oxygen is a much used substance for such coadsorption experiments, both due to its reactivity and its behavior to adsorb on surfaces in well defined structures. On Ni(111) oxygen adsorbs in a p(2x2) structure [3] with a coverage of 0.25 ML. In Chapter 5 we discuss the coadsorption of C₂H₂, C₂H₄ and C₂H₆ with 0.25 ML oxygen on Ni(111). The oxygen leads both to a change in adsorption site and a different thermal evolution of the adsorbed hydrocarbons.

In order to learn about the behavior of catalysts, it is also interesting to study oxide surfaces. These are interesting both because oxides are a common substrate for metal particles in catalysts, and because they can be catalytically active themselves.

NiO is used as a main or co-catalyst in a wide range of important reactions, e.g. photocatalytic water splitting [4, 5], ethene dimerization [6-9], butane isomerization [7, 9], oxidation of azodyes [10], steam reforming of hydrocarbons for the generation of H₂ from biomass [11], and hydrogenation of benzene [12] among others. In Chapter 6 we investigate the adsorption and thermal evolution of various small hydrocarbons with differently prepared NiO layers.

However, Nickel oxide (NiO) also has interesting properties for a wide range of other applications. Its antiferromagnetic nature and high Neel Temperature make it an interesting material for applications in devices using giant magnetoresistance [13, 14]. In spintronics devices NiO is used as a precursor for Ni layers that retain the morphological and crystalline properties of the NiO

layer. The properties of the NiO layers on the other hand can be influenced by the growth conditions of the NiO [15, 16].

In molten carbonate fuel cells, NiO is used directly as the cathode [17, 18]. On Ni electrodes in alkaline solutions [19] and in solid oxide fuel cells [20] it is known that NiO is growing on the nickel electrodes during operation, or during interruptions in the operation. As this hinders the functionality of the electrodes it is interesting to study the growth and decay conditions of the NiO. Other applications worth mentioning are the use of NiO in an all solid state electrochromic device [21], the use of p-doped NiO as a hole collector in dye-sensitized solar cells [22] and its use as a gas sensor [23]. It has also recently been shown that NiO can be grown in the form of small nanosized walls [24], which is useful for the fabrication of future nanodevices. Chapter 4 of this thesis deals with studying the growth and thermal stability of NiO layers on Ni(111) and Cu(111) crystals. The growth of NiO from Ni layers evaporated on Cu(111) allows a control of the thickness of the NiO layers. This is interesting as the thickness of a layer can have a large influence on its reactivity.

Several of the mentioned applications fall into the area of science which is today summed up by the term nanotechnology, i.e. they contain functional parts which are in the range of 1-100 nm in size in at least one dimension. Nanotechnology is receiving considerable interest at the moment. One of the reasons for this is the miniaturization of the processing structures in computer chips, but there are also hopes for numerous other applications, ranging from memory storage over steel improvement to medical applications like filtration or drug delivery. This trend towards very small structures has an interesting implication: if a structure of any kind is getting smaller, the surface to volume ratio is going up. This means that the properties of the structure are getting more and more dependent on the properties of the surface instead of the bulk properties. The properties of surfaces, however, can change a lot when they interact with adsorbates. In this context, it is especially interesting to study the interaction of the surfaces with gases that are parts of the ambient atmosphere, as many of the existing and planned nanostructures can come into contact with air. In the context of this thesis, in Chapter 7 we thus study the interaction of the NiO surfaces with H₂O, CO₂ and CO. All of these gases led to adsorbate layers with a thermal decay over a wide temperature range, which can be explained by major restructuring of the surface.

2 Theory

2.1 Basics of X-ray photoelectron spectroscopy (XPS)

Photoelectron spectroscopy makes use of the photoelectric effect explained by Einstein [25]. If a photon with sufficient energy hits an electron in an atom the energy of the photon can be used to overcome the binding energy (E_B) of the electron and emit it from the atom. The kinetic energy of the electron (E_{kin}) is then given by

$$E_{kin} = h\nu - E_B \quad (1)$$

where h is the Planck constant and ν is the frequency of the incident photon.

The electrons are detected with an electron energy analyzer, where they are filtered with an electric field. The work function Φ of the electron analyzer has to be considered as well for the kinetic energy of the electrons giving us the following formula

$$E_{kin} = h\nu - E_B - \Phi \quad (2)$$

Depending on the incident energy of the photons, electrons from different energy levels within an atom can be probed. Before the use of synchrotron radiation for photoelectron spectroscopy, electrons from the valence levels of the atoms were probed by ultraviolet light generated with gas discharge lamps, mostly Helium lamps. Due to this use of ultraviolet light the term ultraviolet photoelectron spectroscopy (UPS) is typically used for such experiments. For core level electrons on the other hand much higher photon energies are required to remove them from the atoms. As these energies typically lie in the X-ray regime of the electromagnetic spectrum, the photoelectron spectroscopy of core levels is commonly known as X-ray photoelectron spectroscopy (XPS).

As different elements have different core level binding energies, XPS can be used to identify different chemical species. Although the core levels of the atoms do not participate in chemical bonds, they are nonetheless influenced by their chemical surroundings, and this is visible in the spectra. Due to these so called chemical shifts, the interpretation of XP spectra allows to obtain information about e.g. oxidation states or adsorption sites. The amount of emitted electrons from a specific core level, and thus the XPS signal intensity is proportional to the number of adsorbate atoms, which makes XPS a quantitative technique. Due to this it is also denoted as “electron spectroscopy for chemical analysis” (ESCA).

A very detailed discussion of XPS can be found in the book by Hüfner [26].

2.2 Vibrational splitting in XPS

In a XP spectrum besides the main peaks, satellites may appear due to a variety of initial or final state effects. The most important of these effects within this thesis is the vibrational excitation in the core hole state. The excitation of the electrons from the ground state to the core hole state with its different vibrational levels is assumed to be a vertical, also denoted as Franck-Condon transition, as shown in Figure 2.1.

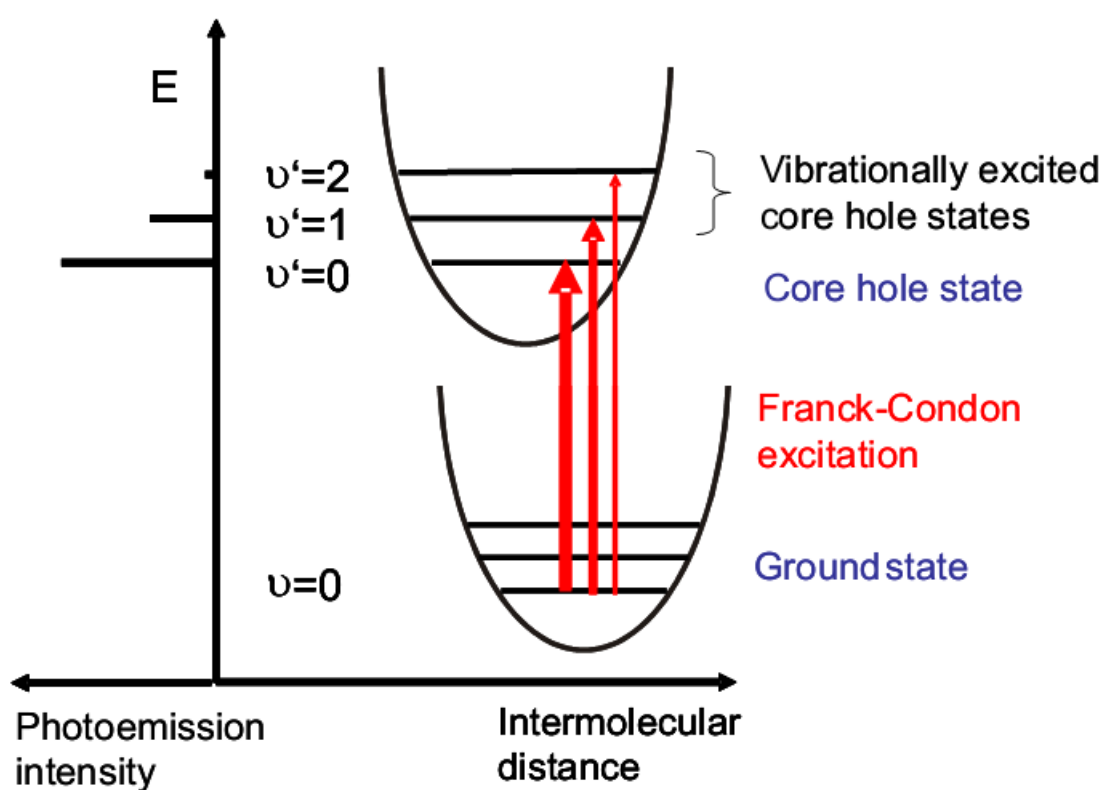


Figure 2.1: Schematic drawing to illustrate the Franck-Condon transition between a neutral molecule AB and an ionized core hole state AB^+ within Born-Oppenheimer approximation. Picture taken from [27].

If the transition of the electron leads to a vibrationally excited state, this leads to a lower kinetic energy of the electrons in regard to a transition from ground state to ground state, which is known as an adiabatic transition. For a C-H stretching vibration this typically leads to peak with a distance of ~ 400 meV to the main peak (see [28] and references therein). This energy difference is well above the resolution of 200 meV which is typically achieved for the C 1s

spectra discussed in this thesis, and thus these satellites have to be included in the analysis.

This analysis is usually performed within the linear coupling model by Cederbaum and Domcke [29]. There it is assumed that both the ground state and the electronically excited state (the core hole state) can be described by the same harmonic potential, and differ only in the equilibrium position and the energy. Then the distribution of the transitions to the different vibrationally excited states, and subsequently the intensity distributions in the photoemission spectrum, is given by a superposition of all totally symmetric vibrations $I(0 \rightarrow \nu)$ according to a Poisson function [30]:

$$I(0 \rightarrow \nu) = e^{-S} \frac{S^\nu}{\nu!} \quad (3)$$

ν is the vibrational level in the ionic final state, and S is the so called S-factor. The S-factor can be thought of as an average vibrational quantum number, and it can be determined directly from the photoelectron spectra as the ratio between the intensities of the ground state and the first vibrationally excited state [30, 31]:

$$S = \frac{I(0 \rightarrow 1)}{I(0 \rightarrow 0)} \quad (4)$$

Within the harmonic oscillator approximation the S-factor is calculated as follows according to [30, 31]:

$$S = \frac{m\mu\omega(\Delta r)^2}{2\hbar} \quad (5)$$

with ω as the vibrational frequencies, Δr the change of the minimum in the potential energy curve upon excitation, μ as the reduced mass and m as the number of equivalent C-H bonds. Thus the S-factor is directly proportional to the number of C-H bonds, which is used within this thesis to identify adsorbed species and reaction products.

An overview on vibrational structures in XP spectra with a detailed discussion of the theory can be found in reference [32].

2.3 Surface sensitivity of XPS and damping of XP spectra

If a particle, like in our case an electron, travels through a medium it can undergo collisions with other particles, which can be either elastic or inelastic. In the case of an inelastic collision the electron loses some of its kinetic energy (typically several eV). As in XPS the kinetic energy of the electrons is probed this has the direct consequence that inelastically scattered electrons do not contribute to the intensity of a peak for a defined electronic state, which is comprised of electrons which travel from the source to the detector without any collisions. The inelastically scattered electrons are still detected at lower kinetic energies (i.e. apparently higher binding energies) and contribute to the background of the spectra. The average distance between two inelastic collisions defines the inelastic mean free path (IMFP) λ . This inelastic mean free path can also be interpreted as the average distance between the source and the first inelastic collision, which removes an electron from contributing to a peak. Thus the IMFP is of great relevance in respect to the surface sensitivity of XPS. The attenuation of a photoelectron signal due to inelastic collisions of the photoelectrons is given by the Beer-Lambert law:

$$I(d) = I_0 * e^{-d/\lambda} \quad (6)$$

where $I(d)$ is the attenuated signal, d is the distance the electrons have to travel in the attenuating layer, I_0 is the not attenuated signal and λ is the IMFP.

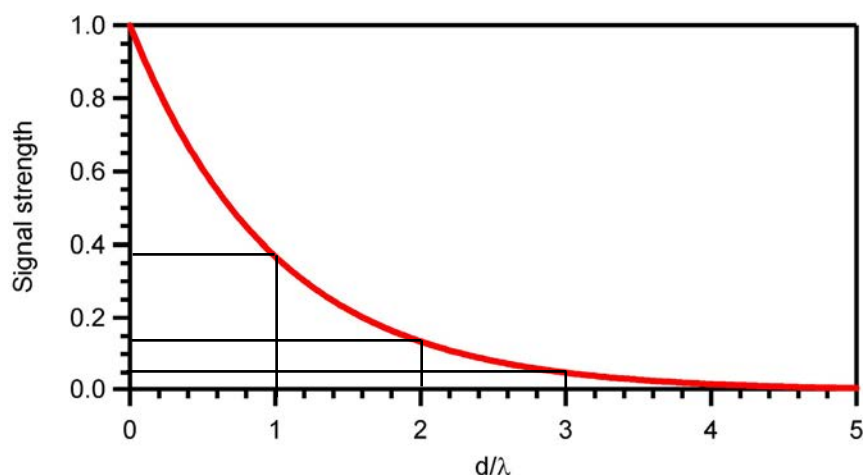


Figure 2.2: Attenuation of the photoelectron signal according to Beer-Lambert law

As can be seen from the equation and the plot in Figure 2.2 the remaining intensity depends on the ratio of the distance d the electrons travel through an attenuating layer and the inelastic mean free path λ within this layer. When the attenuating layer has the same thickness as the IMFP, the signal is damped by 63%, giving a remaining intensity $I(d)$ of 37%; if the layer is three

times the IMFP the signal is already reduced by 95%. The quantity 3λ is called information depth. Surface sensitivity is a very important concept in surface science. By achieving a high surface sensitivity almost all of the experimental observations concern processes happening on the surface, suppressing observations from the bulk of the material. This is favorable to observe, e.g., adsorption processes on the surface. In XPS one method to increase this surface sensitivity is minimizing the inelastic mean free path of the electrons, because a low IMFP leads to a low escape depth of the electrons suppressing the electrons coming from the bulk of the sample.

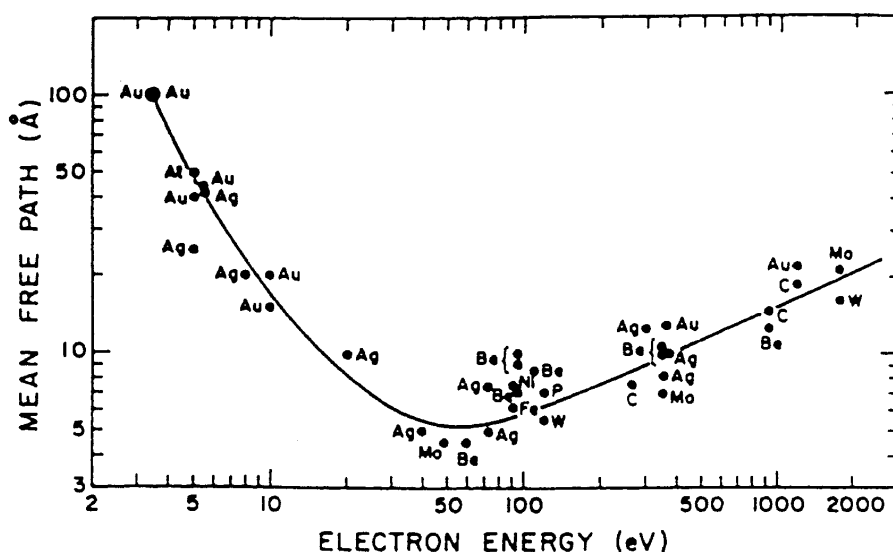


Figure 2.3: “Universal curve” for inelastic mean free paths in several materials, depending on electron kinetic energy, taken from [33], after [34]

The IMFP mainly depends on the kinetic energy of the electrons, but also on the material. Figure 2.3 shows the so called “universal curve” for the dependence of the IMFP on the kinetic energy of the electrons. Seah and Dench [34] found this curve by compiling approximately 350 IMFP and applying a least squares fit. The curve has a minimum around 50-100 eV, so the best surface sensitivity is reached by bringing the kinetic energy of the electrons close to 100 eV. Laboratory X-ray sources are limited to the natural energy levels of the cathode material. If e.g. a C 1s species with a typical binding energy of 283.0 eV is studied, the two most common laboratory sources for XPS, X-ray tubes with an aluminum or magnesium cathode produce X-rays with an energy of 1486.6 or 1253.6 eV, leading to kinetic energies of 1103.6 and 970.6 eV, respectively, which is far from the optimal value of 100 eV. As discussed in Chapter 2.4, synchrotron sources are tunable X-ray sources that allow to choose a matching photon energy for the optimized study of a given core level. In Table 2.1 the different atomic core levels that were investigated in this thesis are given together with the photon

energies used to study them. Also for all core levels the kinetic energies of the photoelectrons are shown. They are close to 100 eV and thus give us high surface sensitivity.

Core level	Typical adsorbate binding energy [eV]	Photon energy ($h\nu$) [eV]	Kinetic energy [eV]	Routinely achieved resolution [meV]
C 1s	283.3 (<i>C₂H₂ on Ni(111)</i>)	380	96.7	230
O 1s	529.6 (<i>O on Ni(111)</i>)	650	120.4	290
Ni 2p _{3/2}	853.1 (<i>core level of Ni crystal</i>)	950	96.9	350
Cu 2p _{3/2}	933.0 (<i>core level of Cu crystal</i>)	1030	97.0	430

Table 2.1: Core levels and the photon energies for their study relevant to this thesis

It should be noted, however, that there is also a downside to this choice of kinetic energy for the photoelectrons. Photoelectron diffraction (PhD) [35], which is caused by the interference of the original electron wave field with elastically scattered components (due to e.g. surrounding adsorbates) of the same wave field, is of greater concern for electrons with low kinetic energies than for those with higher energies. This effect makes the quantitative analysis of the XP spectra more challenging, especially if an adsorbate is studied under a different angle than the reference adsorbate. Thus in most experiments presented in this thesis the observation angle was kept constant, unless otherwise noted.

To calculate damping effects, the knowledge of the inelastic mean free path of a material is important. For materials or kinetic energies where no experimental values are available from literature, the IMFP in Å can be estimated with an equation developed by Tanuma, Powell and Penn [36]:

$$\lambda = \frac{E}{E_p^2(\beta \ln(\gamma E) - C/E + D/E^2)} \quad (7)$$

with the following parameters

$$\beta = -0.0216 + \frac{0.944}{\sqrt{E_p^2 + E_G^2}} + 7.39 * 10^{-4} \rho \quad (8)$$

$$\gamma = 0.191 \rho^{-0.5} \quad (9)$$

$$C = 0.065/U^2 - 0.130/U + 1.11 \quad (10)$$

$$D = 1.91/U^2 - 5.12/U + 35.3 \quad (11)$$

$$U = N_v \rho / A \quad (12)$$

$$E_p = 28.8 \sqrt{\frac{N_v \rho}{A}} \quad (13)$$

λ is the inelastic mean free path, E is the kinetic energy of the electrons, E_p is the free electron Plasmon energy in eV, E_G is the band gap energy for nonconductors (in eV), ρ is the bulk density (in g/cm³), A is the atomic or molecular weight and N_v is the number of valence electrons per atom or molecule.

In some experiments, most importantly for the reaction of nickel oxide layers with carbon dioxide and water discussed in Chapter 7, it is important to correct the quantitative coverages of some of the adsorbates, which are reduced by damping effects of the layers above. This correction has to be applied to help understanding the reaction mechanisms. More details about the applied correction for each case will be given in the corresponding chapters, but the general ideas and formulas behind the correction will be outlined below.

If a surface has a smooth adsorbate layer adsorbed on it with a coverage of 1 ML (e.g. 1 ML Ni evaporated on to Cu(111), which forms a flat layer [37]) the signal intensity of the core levels of the initial (clean) surface is damped to a certain extent. This remaining intensity we define as the damping factor a , which is identical with $I(d)$ for d =thickness of one adsorbate layer. The damping factor is thus calculated with equation (6), which means that it depends on the thickness of the adsorbate layer and the IMFP. In a simple model, which will be called Model 1, we can then calculate the remaining intensity of a layer in a multilayered system with equation (14), if we assume

that all layers above the examined layer share the same damping properties, i.e. have the same IMFP.

$$I(a, \Theta) = I_0 * a^{\Theta} \quad (14)$$

$I(a, \Theta)$ is the observed remaining intensity, I_0 is the undamped initial intensity, a is the damping factor and Θ is the total amount of the damping layers in ML coverage.

This Model 1, however, disregards the fact that for partially covered adsorbate layers only a part of the electrons coming from the lower layers will have to travel through the adsorbate layer and thus are damped.

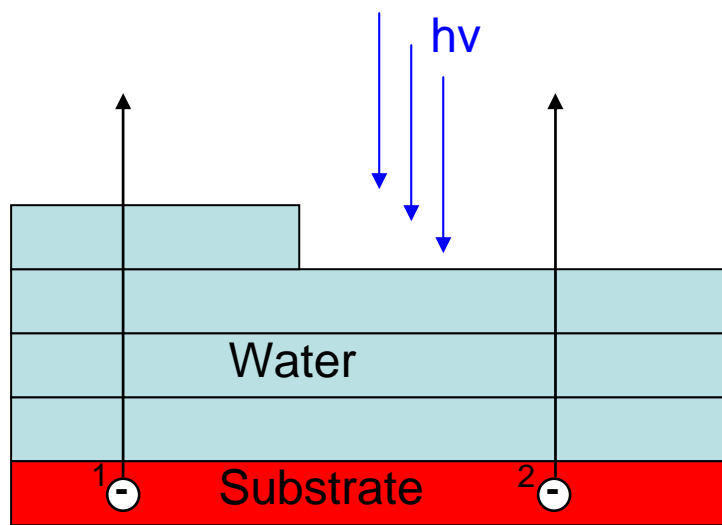


Figure 2.4: Model for the damping of the photoelectrons. For details see text.

Figure 2.4 shows a simplified model for such a situation, with the assumption of 3.4 ML water adsorbed on a substrate. This model will be called Model 2. A layer-by-layer growth, also known as a Frank-van der Merwe [38] growth mode, is assumed for this model. In the example above, an electron that is excited at position #1, which is representative for 40% of the total electrons since the fourth layer is complete up to 40%, needs to travel through 4 layers of water before it escapes the surface region. On the other hand an electron from position #2 only needs to travel through 3 layers of water. These 60% of the electrons are thus less damped than the 40% that need to travel through four layers of water. In this example the total remaining intensity $I_{\text{substrate}}$ can be written as:

$$I_{\text{substrate}} = I_0 * (0.4 * a^4 + 0.6 * a^3) \quad (15)$$

From this a more general formula can be devised:

$$I(a, n, f) = I_0 * (f * a^{n+1} + (1 - f) * a^n) \quad (16)$$

$I(a, n, f)$ is the observed remaining intensity, I_0 is the undamped initial intensity, a is the damping factor, n is the number of complete adsorbate layers and f is the fraction of coverage of the incomplete outermost adsorbate layer.

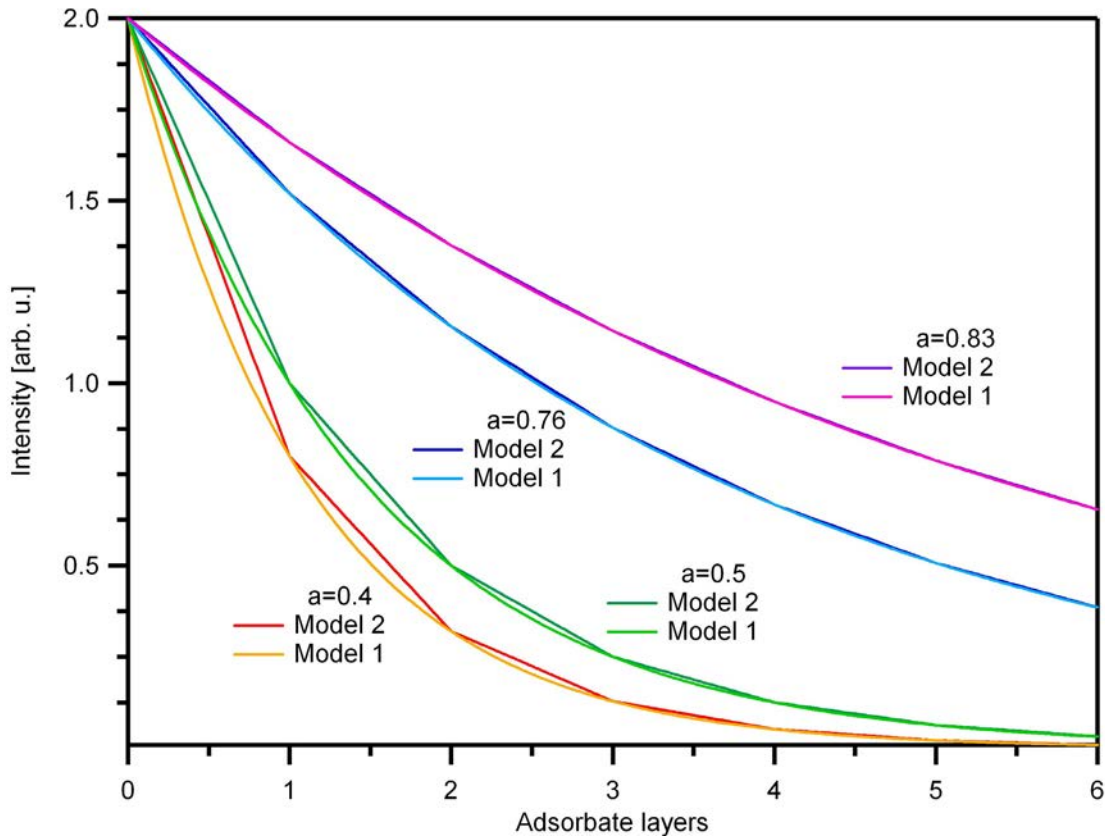


Figure 2.5: Comparison of the two models for damping

Figure 2.5 shows a comparison of the expected damping for the two models for four different damping factors. Model 1 exaggerates the signal damping when compared with Model 2. However several things have to be noted. For completely covered layers both models give the same intensity, which can be understood by the fact that equation (16) gets reduced to equation (14) for $f=0$ or 1. On the other hand the highest difference is found for $f=0.5$. The magnitude of this difference is also influenced by the value of the damping factor. For a damping factor of 0.4, which corresponds to an IMFP which is ~ 1.1 times the thickness of a monolayer, a clear difference between the two curves is visible, with a maximum difference of $\sim 10\%$. For a damping factor of 0.83 on the other hand the two curves lie almost on top of each other and

have a maximum difference of $< 0.5\%$. If Model 2 is used to calculate either $I(\mathbf{a}, \mathbf{f}, \mathbf{n})$ or I_0 one has to keep in mind that if the number of layers increases during an experiment, the formula has to be adjusted for the new number of n , i.e. over the course of an experiment several different version of equation (16) might be needed to calculate the desired quantities.

2.4 Synchrotron Radiation

A charged particle that is accelerated emits radiation according to electrodynamics. If a charged particle is accelerated away from his linear orbit, usually with a magnet, e.g. to move it around a corner in an accelerator, such radiation is emitted. The radiation has been termed synchrotron radiation as it was first witnessed at a synchrotron-type accelerator in 1947 [39]. Due to the energy loss associated with this radiation emission it was first an undesired side effect in accelerators dedicated to particle physics. However, due to the interesting properties of this radiation, including a wide spectral range and a high intensity, today dedicated facilities are constructed for the generation of synchrotron radiation. In such facilities electrons are accelerated close to the speed of light and then inserted into a so called storage ring, where they stay for a period of several hours. It should be noted that the relativistic kinetic energy of the electrons is in the low GeV range and thus much lower than the TeV energy range currently used in accelerators dedicated to particle physics research. In third generation synchrotron radiation sources the electrons are first accelerated and then stored at a constant energy. The storage rings are equipped with several so called insertion devices for the actual generation of the synchrotron radiation. In these insertion devices, the electrons are forced on an oscillating path by a series of very strong permanent magnets with alternating poles, which leads to a greater radiation intensity. Insertion devices known as undulators are constructed in a way that they lead to a constructive interference of the radiation sent out by the different electrons travelling through the undulator providing an even higher intensity. This also leads to a narrow energy distribution of the photons, whereas “normal” synchrotron radiation has a wide spectral range. The energy of the photons can be varied by changing the gap between the two opposite rows of alternating magnets, making it tunable over a wide range dependent on the design parameters of the undulator and storage ring. The photons are then guided to the experiment stations via so called beam lines attached to the storage ring. These beam lines include optical elements like monochromators, apertures and mirrors to monochromatize and further improve the light quality. During the timeline of this thesis the electron beam current in the storage ring at BESSY II typically

was refreshed to a value of 300 mA three times a day, after which it decayed exponentially. This is important as the photon flux, and subsequently the spectral intensity is directly dependent on the electron beam current.

Detailed further information on synchrotron radiation can be found in these books: [40-42]

2.5 Low energy electron diffraction (LEED)

Equation (17) describes the wavelength of an electron depending on its kinetic energy, according to the work of De Broglie [43]:

$$\lambda_e [nm] = \frac{h}{m_e v} = \sqrt{\frac{1.5eV}{E_{kin}}} \quad (17)$$

Using this equation we see that electrons with low kinetic energies around 20-500 eV have a wavelength in the order of interatomic distances. Thus they are diffracted by the surface atoms. This is used to study e.g. the surface ordering of a crystal. As discussed in Chapter 2.3, the mentioned electron energies lead to low values of the IMFP, making LEED a surface sensitive technique.

Adsorbates often form superstructures on surfaces, with larger periodicity than the substrate. As the LEED pattern is an image of the reciprocal space, these superstructures lead to additional spots in between the substrate spots. As these superstructures often have very defined coverages, LEED is an ideal tool in the preparation of layers with defined coverages for calibration purposes, for which the technique is also used within this thesis. To describe the arrangement of the molecules within the superstructures on the surfaces two notation methods are commonly used. The most common notation was developed by Wood [44]. It is based on the ratios between the lattice vectors of the superstructures and those of the substrate lattice as well as on the rotation angle in between these two lattices, with the additional letters p and c set before these informations to distinguish between primitive and centered surface structures. As this notation is not applicable to all superstructures, also a matrix notation [45] is sometimes used, giving the transformation matrix between the substrate and the superstructure lattice.

For a longer introduction see [46] and for detailed information on LEED please refer to these books: [47-50].

2.6 Supersonic molecular beam

When a gas with a high pressure, p , is expanded through a nozzle into a region with lower pressure, p_b , like the background pressure of a vacuum system, its behavior is determined by the ratio between the two pressures according to equation (18) [51]:

$$\frac{p}{p_b} = \left(1 + \frac{\gamma - 1}{2} M^2\right)^{1/(\gamma - 1)} \quad (18)$$

with M as the Mach number and γ as the adiabatic index. For an ideal gas, with a ratio of $p/p_b > 2.1$, the velocity of the gas molecules reaches values higher than the local speed of sound. The expansion cone in this case is shown in Figure 2.6.

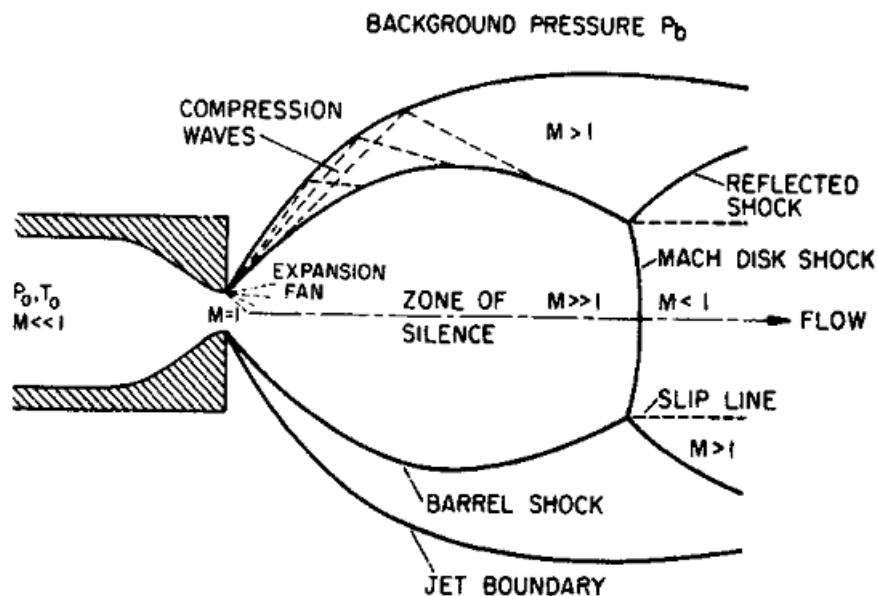


Figure 2.6: Super sonic expansion of a gas from a nozzle. Picture taken from [51].

This expansion is an adiabatic process, in contrast to the expansion from an effusive Knudsen source. During the expansion a lot of collisions between the gas molecules lead to a conversion of the thermal energy of the molecules to kinetic energy, with a velocity vector in the direction of the expansion. However, it could be shown that only the translational and rotational degrees of freedom are easily converted to kinetic energy, vibrational degrees of freedom remain almost unchanged [51]. Ideally, in the expanded gas all molecular velocities would be the same; however, in praxis a small distribution of velocities is found. This distribution is always narrower than the Maxwell-

Boltzman distribution and can be made even narrower with higher Mach numbers.

The kinetic energy of the molecules after expansion depends on the temperature of the molecules before expansion, and thus it can be increased by heating the nozzle. Further increases can be achieved by mixing the gas with a lighter gas like Helium, which is called seeding [51]. As the velocity of all molecules is similar after expansion, the intermixing leads to a higher kinetic energy of the molecules of the heavier gas [51].

When building a supersonic molecular beam source, the supersonic “zone of silence”, shown in Figure 2.6, is cut out of the gas beam by a small orifice with sharp edges, which is called skimmer. Such a setup was first realized by Becker and Bier [52]. The beam then usually passes through two additional pumping stages, before entering the vacuum chamber. The supersonic beam used within this thesis is described in detail in [53] and in [54] information can be found on kinetic energies achieved for seeded and heated CH_4 and C_2H_6 beams.

For a detailed coverage of atomic and molecular beams see [51].

3 Experimental Details and Data analysis

3.1 Experimental Setup

All experiments discussed within this thesis, with the exception of the STM pictures shown in Chapter 4, were done using a transportable UHV apparatus described in detail in [53] and [55]. The experiments were conducted at the third generation synchrotron source BESSY II in Berlin, at the beamline U49/2-PGM 1 [56].

The UHV apparatus, which is shown in Figure 3.1, consists of three separate chambers. The preparation chamber is used for sample preparation and is equipped with a sputtering gun, a LEED optics and an electron beam evaporator and a quartz crystal microbalance for preparing the nickel layers. The analysis chamber is equipped with a quadrupole mass spectrometer for gas analysis and leak testing, and the electron analyzer (Omicron EA 125 U7 HR). The monochromator shown in Figure 3.1 was not used within this thesis, but instead at this location the apparatus was connected to the beamline. In the connection between chamber and beamline a beamflag was included that was moved by compressed air. This beamflag was used to block the photon flux on the sample in between spectra, in order to minimize beam damage. An overview of the resolutions typically achieved within this thesis in the different core levels is given in Table 2.1. The base pressure in the analysis chamber was below $2 \cdot 10^{-10}$ mbar. In the preparation chamber the base pressure typically was between $5 \cdot 10^{-10}$ and $1 \cdot 10^{-9}$ mbar. As almost all preparations discussed in this thesis, except the evaporation of nickel on Cu(111), but including the oxidation of said nickel layers, were performed in the analysis chamber, this relatively high pressure in the preparation chamber was of no concern.

The molecular beam chamber is attached to the analysis chamber. It consists of three differential pumping chambers, with the pressure in the third chamber being equal or lower than the pressure in the analysis chamber. The molecular beam was blocked by a fast moving flag to allow for defined gas exposures. The nozzle used for gas expansion had a nominal diameter of 100 μm and was made of molybdenum. For providing a constant gas flux to the nozzle the machine is equipped with two flow controllers, one with a maximum flux of 500 sccm and the other of 50 sccm. As the analysis chamber is spherical, the sample may be positioned in the middle so that both the molecular beam and the photons can hit the sample at the same time, and the electrons can travel directly to the electron analyzer. Additional to the molecular beam, a gas dosing system was available (not shown in Figure 3.1). This gas dosing system could be used both with gases in

minicans or confined volumes and liquids in glas-metal tubes. The gases were introduced to both chambers by multicappillary array dosers.

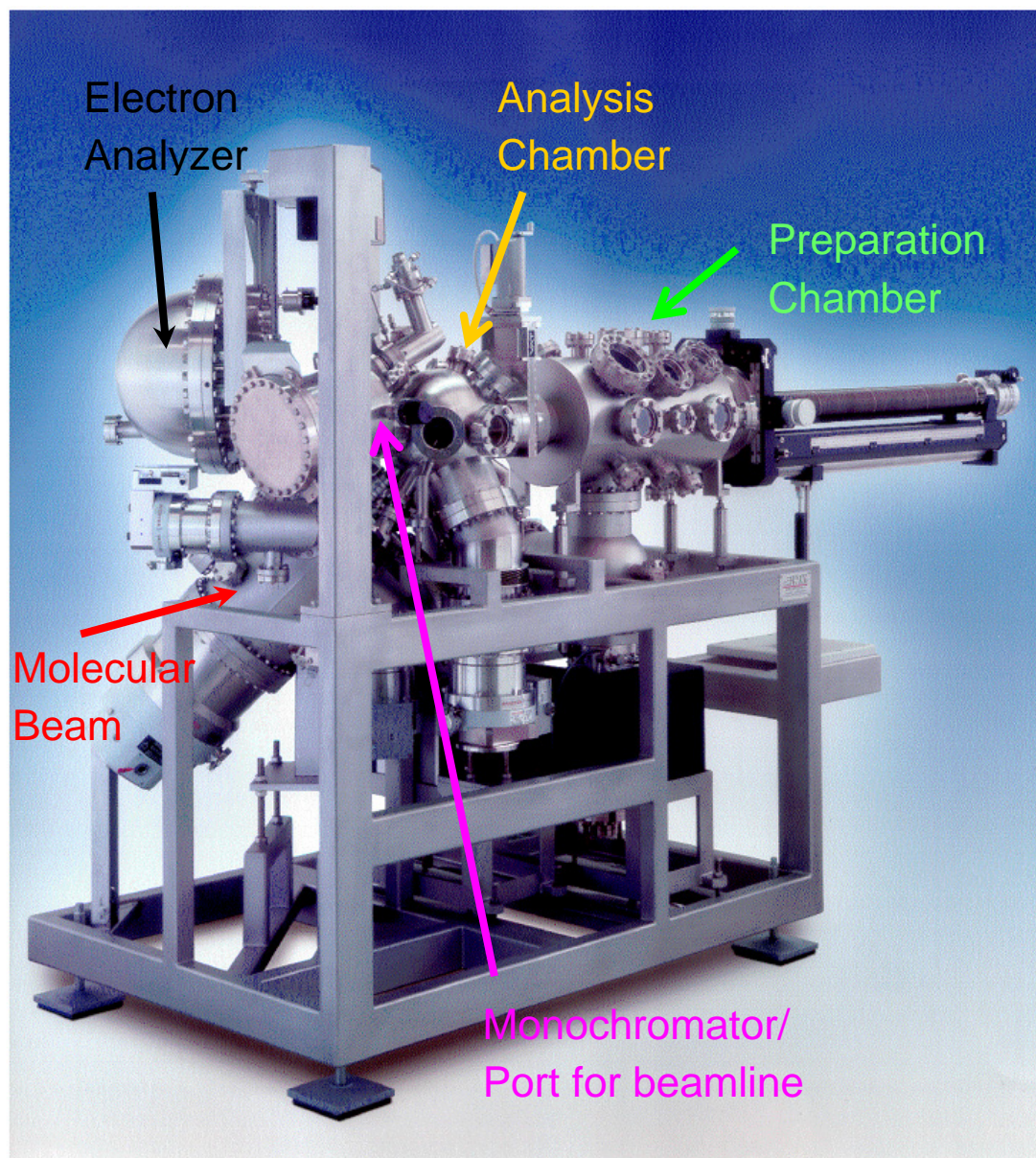


Figure 3.1: Picture of the UHV apparatus without cables and prevacuum pumps. Picture taken from [53].

The manipulator and sample holder allow for a rotation of the sample in two angles. Thereon the sample can be positioned in any orientation within the analysis chamber; however, only two distinct positions were used within this thesis, one normal to the molecular beam and one normal to the electron emission. The angle between these two positions is 45° . The sample can be cooled with liquid nitrogen down to ~ 100 K, and heated resistively up to 1400 K. As resistive heating has an effect on the spectra, a filament in bispiral form is mounted behind the sample for heating during measurement. With this filament temperatures up to ~ 500 K can be reached, however, the final

temperature is sometimes limited due to a massive increase in background pressure as the filament also heats the sample holder.

The two crystals, Ni(111) and Cu(111), were mounted slightly differently. The Ni(111) crystal was spotwelded to two tantalum wires with diameters of 0.5 mm on opposite sides of the sample. These wires then were spotwelded to tungsten rods with diameters of 2 mm, which were inserted into the sample holder. In between the tantalum wires and the tungsten rods a platinum foil with 0.1 mm thickness was inserted, in order to make the spotwelding easier. On both the free sides of the crystal a type K thermocouple pair was spotwelded. These wires had a thickness of 0.125 mm each.

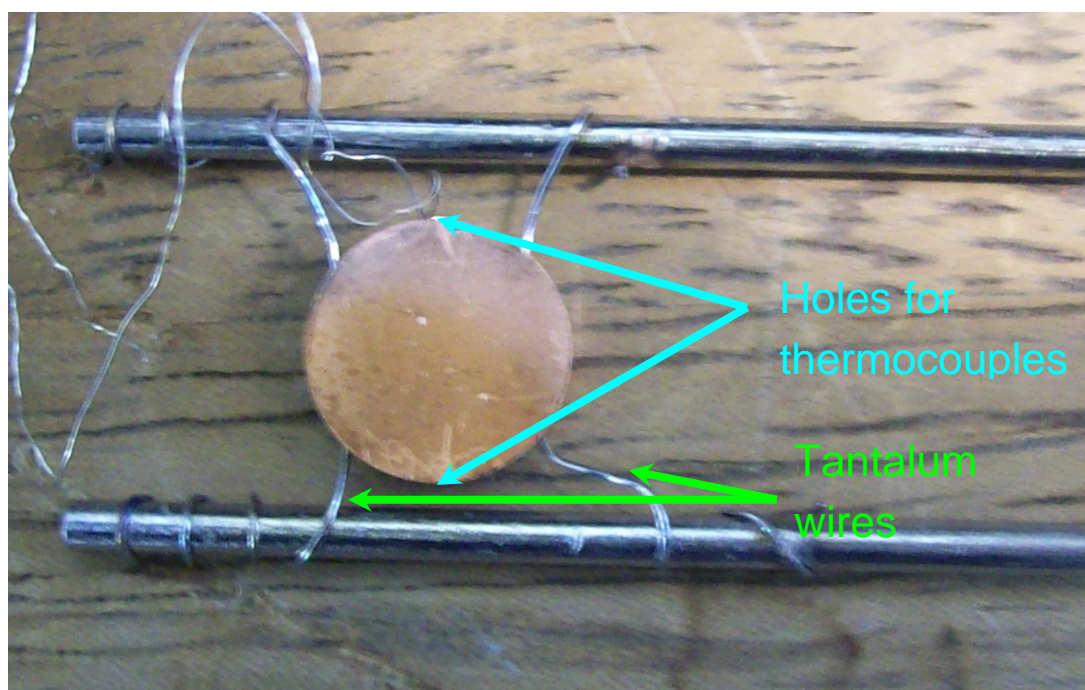


Figure 3.2: Photograph of the mounted Cu(111) crystal outside of the sample holder

As the Cu(111) crystal could not be spotwelded, a different approach was used there, shown in Figure 3.2. The crystal had circular shape with a diameter of 10 mm and a thickness of 1 mm. On opposite sides of the crystal, the left and right side in Figure 3.2, small holes are drilled through the crystal, with a diameter of ~0.3 mm. Through both these holes tantalum wires with a diameter of 0.3 mm are lead, and then coiled several times around tungsten rods with a diameter of 2 mm and spotwelded to them. These wires keep the crystal in place and allow for both electrical and thermal contact. The tungsten rods were then inserted into the sample holder. The other two sides, the upper and lower side in Figure 3.2, contained small holes. The two thermocouple wires of a type K pair, with wire diameters of 0.125 mm, were spotwelded together and the excess wire segments beyond the spotwelding spot carefully removed. The pair was then inserted into one of the holes, and

jammed into place with small segments of copper wire of suitable diameter. The same procedure was repeated for another thermocouple pair.

3.2 Crystal surfaces

Nickel has the atomic number 28 and is located in the periodic table in the fourth period as the head of the 10th group and thus is a transition metal. It crystallizes in a fcc crystal structure with a lattice parameter of 3.524 Å [57]. Thus the (111) face of the crystal is hexagonal with a next neighbor distance of 2.49 Å.

Copper has the atomic number of 29, and is located next to nickel in the periodic table and also a transition metal. It crystallizes in a fcc structure with a lattice parameter of 3.615 Å [58]. The close match of this value with the value found for nickel helps in the growth of flat nickel layers on Cu(111) [37]. The (111) face of the crystal is hexagonal with a next neighbor distance of 2.56 Å.

Prior to experiments, the crystals were cleaned using standard procedures [59]. Argon sputtering cycles typically lasted for 15 minutes on Ni(111) and 20 minutes on Cu(111), and were performed with an accelerating voltage of 1000 V at an argon pressure of $5 \cdot 10^{-6}$ mbar. After sputtering, the Ni(111) crystal was annealed to 1000 K and the Cu(111) crystal to 850 K. Subsequently the C 1s and O 1s regions were checked for remaining adsorbates. We also checked each time for common crystal impurities, i.e. sulfur on both crystals. Other impurities were not detected during overview scans over a wide spectral range at the beginning of each beamtime and in infrequent intervals in between the experiments.

The NiO layers on Ni(111) were removed from the surface by annealing to 1250 K for some minutes. On Cu(111), however, the NiO layers always had to be removed by sputtering as annealing led to a segregation of the oxide oxygen into the bulk, a process that was reversed upon cooling the crystal down again. This process is discussed in Chapter 4.

3.3 Overview of used chemicals

Table 3.1 lists all chemicals used in this thesis together with their respective purities. Helium was used as a seeding gas in methane and ethane beams in order to achieve higher kinetic energies. The helium gas line was led through a cooling trap filled with liquid nitrogen in order to remove water from the gas stream. The gas line of methane, ethane and ethene was led through

a cooling trap filled with ethanol and cooled down with liquid nitrogen in order to remove water from the gas. The same measure was sometimes taken for oxygen when preparing the oxide layers, as detailed in the respective chapters. Water was filled into a glas-metal tube and mounted on the dosing system. In order to remove gases, several cycles of freezing the water and pumping off the gas phase were performed, until no bubbles showed upon melting of the ice.

Substance	Chemical Formula	Purity
Methane	CH ₄	3.5
Ethane	C ₂ H ₆	3.5
Ethene	C ₂ H ₄	3.5
Acetylene	C ₂ H ₂	2.6
Propane	C ₃ H ₈	3.5
Propylene	C ₃ H ₆	3.5
Carbon monoxide	CO	3.7
Carbon dioxide	CO ₂	4.5
Oxygen	O ₂	4.8
Helium	He	6.0

Table 3.1: List of used gasses and their respective purities

3.4 Data analysis

All data analysis was performed with the program Igor Pro 5.05A on the basis of a script programmed by Martin Kinne [53].

As both the sample and the electron analyzer are grounded they have a common Fermi level, which is commonly used as a reference for the binding energies. The position of the Fermi level (E_F) is determined by measuring a spectrum in the respective binding energy region and fitting this spectrum with a Gaussian error function, i.e. the integral of the Gaussian normal distribution [60]. Such a fit is shown in Figure 3.3 The position of the Fermi level is then determined by the position of the inflection point of the Gaussian error function.

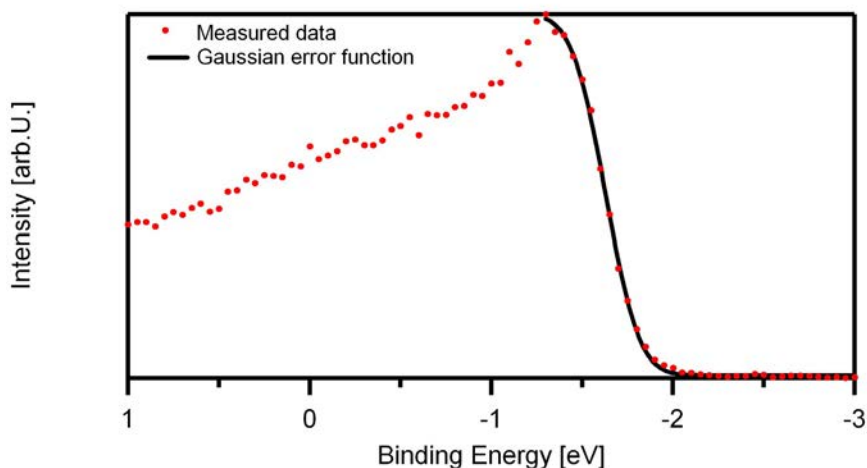


Figure 3.3: Sample fit of a Fermi edge with a Gaussian error function. The excitation energy used was 950 eV.

Please note that unlike for laboratory experiments, where the Fermi edge is usually determined once and then used for all spectra, for synchrotron XPS experiments like the ones discussed in this thesis, the Fermi edge has to be determined every time a different core level is studied. This is because for different core levels different excitation energies are used in order to achieve the highest surface sensitivity in all cases, and the Fermi level was found to change slightly upon a change in excitation energy.

In a first step in data analysis the binding energy scale was shifted by $-E_F$, so that the Fermi edge itself shifted to a value of 0.00 eV. Next the binding energy range of the spectra was cut down to a certain binding energy range, e.g. 526 to 538 eV for most O 1s spectra discussed within this thesis. In the next step all spectra were normalized to a common background value. This was done, as the intensity of all spectra is dependent on the photon flux, which in turn is directly dependent on, among other factors, the electron beam current within the storage ring. During the timeline of this thesis, this electron beam current at BESSY II typically was refreshed to a value of 300 mA three times a day, after which it decayed exponentially. Thus the spectral intensity is constantly decreasing over time.

As most XP spectra sit on top of a linearly increasing background, this linear background was subtracted in the next step in order to make the spectrum parallel to the binding energy axis. Where possible this linear background was determined from an adsorbate free spectrum or, in the case of the oxide surfaces, the spectrum of the oxide surface before it was exposed to other adsorbates. A special case occurred for the C 1s spectra of the NiO surfaces.

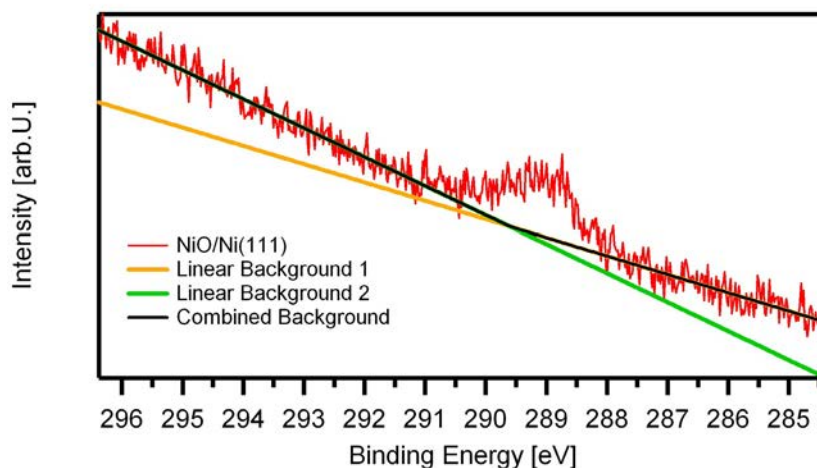


Figure 3.4: Illustration of the background subtraction for C 1s spectra on NiO surfaces.

As shown in Figure 3.4 the background of the C 1s region of NiO surfaces has a kink around 289.6 eV. The peak above this kink is due to 0.01 ML carbonate (see Chapter 7.3). The cause of this kink is unclear. To determine a background the regions left and right of the kink were treated separately, with a linear background determined for each region. Then a combined background was constructed out of these two linear backgrounds, as shown in Figure 3.4, which was subsequently subtracted from the spectra. Please note that the approach was only used for the C 1s spectra discussed in Chapter 7, as the adsorbates discussed in Chapter 6 had their main spectral features at lower binding energies so that this kink was of no concern and thus a single linear background could be used. Due to secondary processes the background is higher on the high binding energy side of a peak than on the low binding energy side. This effect was taken into account by subtracting a Shirley background [61] of all O 1s, Ni 2p and Cu 2p spectra as well as the C 1s spectra discussed in Chapter 7. For the C 1s spectra discussed in chapters 5 and 6 better fits could be obtained when no Shirley background was subtracted.

After the subtraction of the background, the spectra were fitted with asymmetric Doniach-Sunjich [62] functions convoluted with a Gaussian to obtain quantitative information. Parameters within these fits were the peak position and height, the asymmetry and the Gaussian and Lorentzian widths. For adsorbates on metal surfaces the Gaussian width was usually determined from the width of the Fermi edge, while it remained free for the studies on NiO. For peaks belonging to the same adsorbate, i.e. the adiabatic and vibrational peaks in the spectra of the hydrocarbons on the metal surfaces the same values were used for the asymmetry and the Gaussian and Lorentzian widths.

The absolute coverages were determined by integrating the total area of the spectra. As argued above, the spectral intensity, and thus this area, is dependent on the photon flux. This was taken into account by dividing the integrated areas by the background intensity, which is also dependent on the photon flux. This value was then compared with the corresponding value of a reference structure with known coverage. The used reference substances were ethylene on Ni(111) discussed in Chapter 5.1.1. and CO layers on Ni(111) and Ni and Cu(111) discussed in Chapter 7.4.1.

4 Growth of nickel oxide

Nickel(II)oxide (NiO) is a green crystalline solid. It crystallizes in the rocksalt (NaCl) structure with a lattice parameter of 4.177 Å [63]. As Ni has a lattice parameter of 3.524 Å [57] with a facecentered cubic (fcc) lattice, the oxidation of a nickel crystal leads to a volume increase of ~70%. In nature, NiO appears in the form of the rare mineral bunsenit that was first described by Bergemann in 1858 [64] and named after Robert Bunsen. Since in the rocksalt structure the unit cell contains two layers in the (100) direction, which are both composed of each 0.5 ML Ni and 0.5 ML O, the distance between two layers is 2.089 Å, which is half of the lattice parameter. In the (111) direction, where the layers are alternatively composed of pure Ni and pure O layers the distance is 2.41 Å.

4.1 Oxygen interaction with Ni(111)

The interaction of oxygen with and the oxidation of Ni(111) has been attracting interest by a large number of authors. At low exposures, before the onset of oxidation, oxygen dissociatively adsorbs in a hollow-fcc site as shown by NEXAFS [65], LEED-IV [66] and DFT calculations [67]. Two ordered structures have been found for chemisorbed oxygen on Ni(111): At first a $p(2 \times 2)$ structure with a nominal coverage of 0.25 ML is formed after adsorption of 1 L oxygen at room temperature [3, 65, 68, 69], and secondly a $(\sqrt{3} \times \sqrt{3})R30^\circ$ structure, which has been reported to mainly exist in the range between 3-20 L [3, 65, 70, 71]. These two structures are interpreted as the first step of a three stage oxidation model, that was suggested for metals in general by Fehlner and Mott [72], and was first shown to be valid for Ni by Holloway and Hudson [68, 73], with later confirmations by various other groups [70, 74-78]. In this model the oxidation of metal surfaces happens in three stages: First fast chemisorption due to a sticking coefficient close to unity (leading to the aforementioned superstructures), then fast oxidation of the first layer and in the last stage slower oxidation which leads to a thickening of the oxide. Most groups agree that the NiO layer has a thickness of 3-4 ML at saturation [71, 77, 79, 80] although some groups also report the growth of thicker films in the third phase [75, 81].

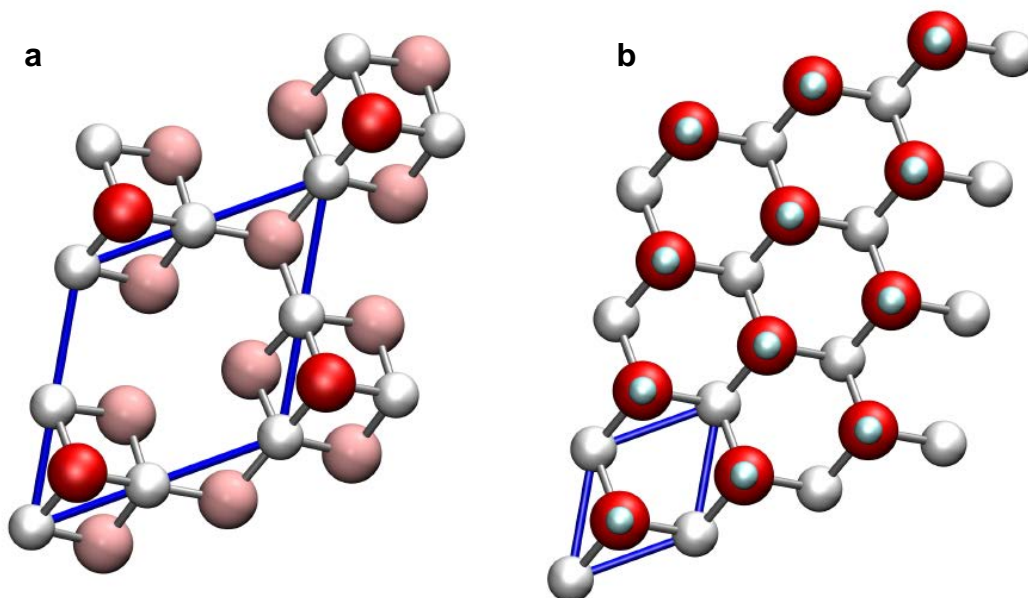


Figure 4.1: NiO (111) **(a)** (2x2) octopolar reconstruction **(b)** hydroxide terminated (1x1) surface. Nickel atoms in the second layer are shown in white, oxygen atoms in the first and third layer are shown in bright and shaded red, respectively. The hydrogen atoms of the OH groups are shown in light blue. Pictures taken from [82].

At room temperature NiO grows on Ni(111) with (111) orientation [68, 69, 76, 79, 83]. A recent STM study by Knudsen et al [76] shows that the NiO forms irregular islands on the surface. A fragmentation of the NiO(111) films into small grains of 2-4 nm size has also been reported by Kitakatsu et al [79]. The (unreconstructed) NiO(111) surface is a polar surface and thus it is thermodynamically unstable [82]. For such polar surfaces with rocksalt crystal structure Wolf [84] proposed a stabilizing p(2x2) octopolar reconstruction of the surface, in which $\frac{3}{4}$ of the atoms in the first layer and $\frac{1}{4}$ of the atoms in the second layer are missing. This structure is displayed in Figure 4.1 (a). Experimentally a (2x2) reconstruction for NiO(111)/Ni(111) was observed by Rohr et al. [85] with LEED after removing a hydroxyl layer on the NiO with thermal treatment, however this could not be directly identified as the suggested octopolar reconstruction. Ventrice et al. [86] observed the octopolar reconstruction with STM for NiO(111) films between 3 and 6 ML thickness grown on Au(111), and Barbier et al. [87] found it with GIXDS on a NiO(111) surface of a NiO crystal. On NiO(111)/Ni(111) the octopolar reconstruction was also suggested by Okazawa et al. [69]. In a recent DFT study Ebensperger and Meyer [82] showed that at elevated temperatures in a hydrogen free surrounding the oxygen terminated octopolar reconstruction is the most stable phase for NiO(111), although the nickel terminated octopolar reconstruction is very close in energy and can thus also be present. Another way for the polar surface to stabilize is the adsorption of water or hydrogen to form hydroxide, as displayed in Figure 4.1 (b). Several groups studying NiO

on Ni(111) in fact found that OH stabilizes the NiO(111) surface [79, 88, 89]. NiO(111) is generally very reactive to water, as reported by several groups using different techniques including HREELS [85, 88-90], LEED [79, 85, 88, 89], AES [79, 88], STM [76, 79] and XPS [76, 79, 80, 88, 89, 91]. Due to this it is challenging to prepare OH free NiO layers.

Concerning the thermal stability of NiO(111)/Ni(111) one study reports destabilization of the layers starting at 420 K [92], however, several other groups place the threshold for destabilization in the range between 550-600 K [75, 83, 93], where oxygen starts to diffuse into the nickel bulk [94].

If oxygen is dosed on the clean surface at higher temperatures around 500 K the preferred direction of the initial NiO layer changes to (100) [79, 81, 83]. However, detailed STM Studies by Kitakatsu et al. [79, 93] revealed the presence of triangular islands with (111) orientation within the NiO(100) films, covering ~ 7% of the surface after an oxygen dosage of 25 L. Hildebrandt et al. [81] showed that these islands nucleate at around 15 L and grow in size with increasing oxygen exposures, covering ~ 9-10% (this value was extracted by analyzing Figure 6. in [81] and not explicitly given in the paper) of the surface after an exposure of 150 L, so for even higher oxygen dosages an even larger percentage up to 100 % of NiO(111) can be expected. Please note that all spectra within chapter 4.1 were recorded at an emission angle of 45°.

4.1.1 The p(2x2) oxygen layer on Ni(111)

In this thesis the p(2x2) oxygen layer on Ni(111) was studied both as a precursor to oxidation and also in the context of the coadsorption studies of oxygen and C₂H_x species presented in Chapter 5. The oxygen layer exhibiting a p(2x2) LEED structure was prepared by adsorbing 1.5 L oxygen at 600 K. The LEED pattern is shown in Figure 4.2 (b) and the respective O 1s spectrum is shown in Figure 4.2 (a).

The O 1s spectrum shows a single peak located at 529.6 eV. A detailed discussion of the binding energy position in respect to values reported in literature will be provided in the following chapters. It is noteworthy that the oxygen peak is highly asymmetric.

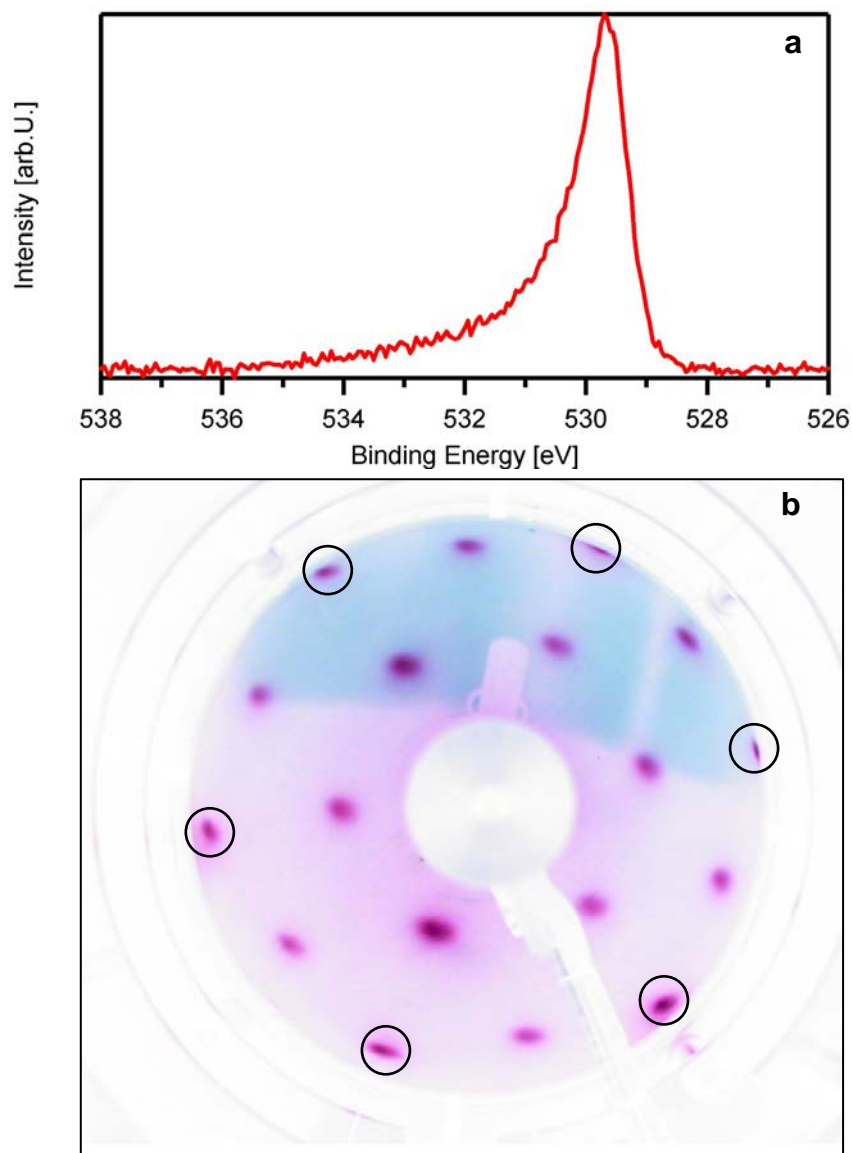


Figure 4.2: (a) O 1s spectrum of 1.5 L oxygen on Ni(111) (b) LEED picture of oxygen layer from (a) acquired at 79 eV, showing the p(2x2) pattern. Spots also visible for the (1x1) structure of the substrate are marked with circles.

4.1.2 Oxidation of Ni(111) at room temperature

To oxidize the Ni(111) surface, oxygen was dosed with the supersonic molecular beam on the surface at a temperature of 300 K. A gas flow of 5 sccm was used which gives a surface pressure of $\sim 1.1 \cdot 10^{-6}$ mbar. The oxidation of the surface near region was considered to be finished when the oxygen peak did not grow any more and no further change occurred in the Ni 2p region. The O 1s spectra of this experiment are displayed in Figure 4.3 (a). The orange spectrum resembles the O 1s spectrum of the O(2x2) layer, although the quantitative analysis depicted in Figure 4.3 (c)

reveals that it belongs to a higher coverage of 0.75 ML, which is consistent with the corresponding exposure of ~ 5 L. Just as for the O(2x2) layer the peak is located at 529.6 eV.

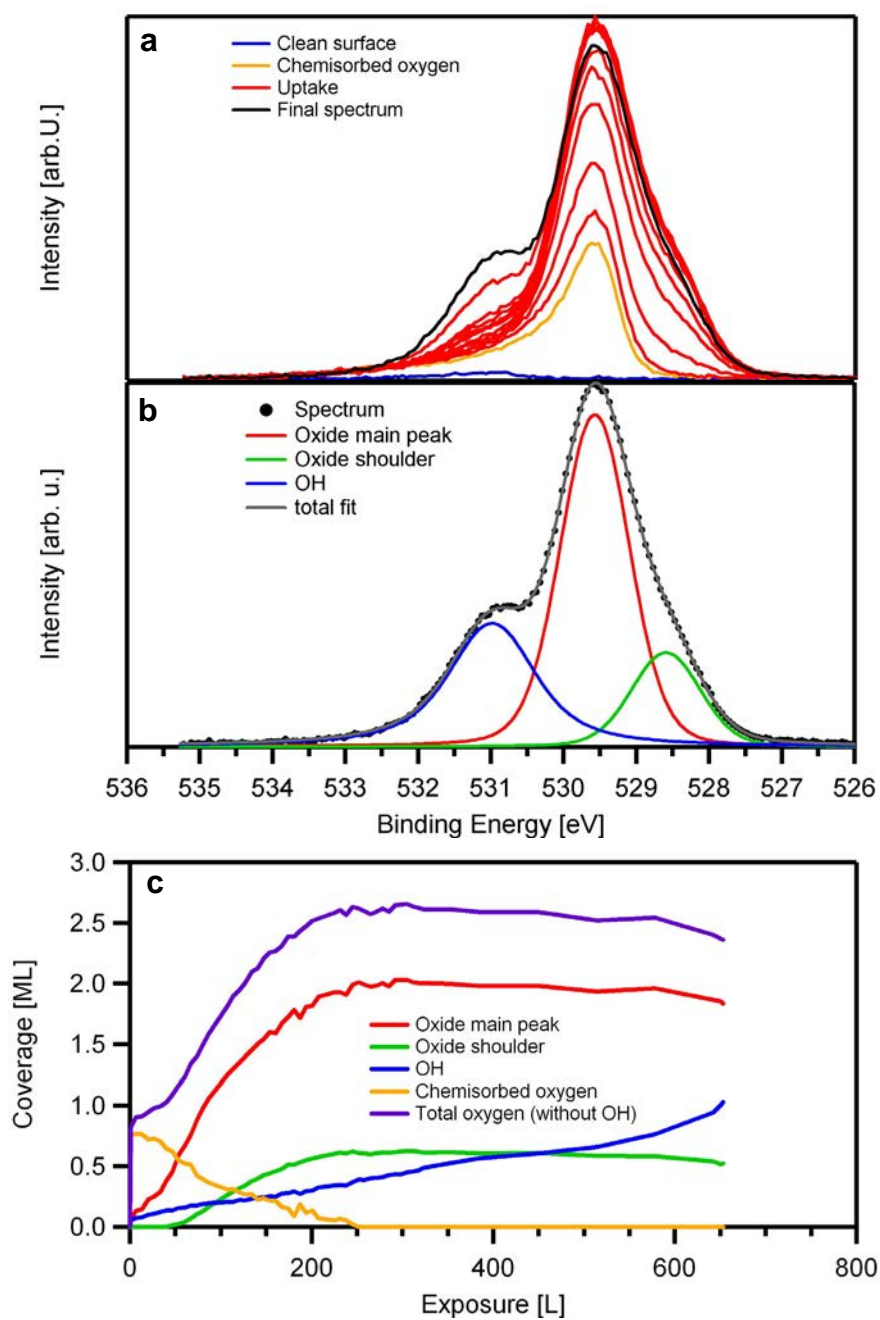


Figure 4.3: (a) Selected O 1s spectra acquired during dosing of 5 sccm oxygen on Ni(111) at 300 K (b) detailed fit of the final spectrum (c) Quantitative analysis of uptake experiment

For higher exposures the peak shape changes drastically. A detailed fit of the final spectrum of this oxygen adsorption experiment is shown in Figure 4.3 (b). The asymmetric peak of the chemisorbed oxygen has been replaced by a highly symmetric peak at the same binding energy of 529.6 eV. Domnick et al. [95] attributed the asymmetry of the chemisorbed oxygen peak to the strong

interaction between the chemisorbed oxygen atoms and the metallic nickel. Metals have a highly asymmetric peak due to excitations to the density of states at the Fermi level [96]. For nonmetallic adsorbates, in our case NiO, on the other hand the peak asymmetry is usually much smaller [97]. Due to this Domnick et al. [95] showed that the peak asymmetry of the oxygen peak disappears during the oxidation of thin nickel layers on Cu(111), and the final oxide peak is completely symmetric, just as the peak found here. Two additional peaks are found at 528.6 eV and 531.0 eV. At room temperature the oxide grows in (111) direction [68, 69, 76, 79, 83]. NiO (111) is unstable [84] and is stabilizing itself through the adsorption of water [79, 88, 89], leading to hydroxide. Thus we assign the peak at 531.0 eV to hydroxide. If we take the quantitative analysis shown in Figure 4.3 (c) into consideration, we see that the coverage of the peak at 528.6 eV (green line) increases roughly together with the main oxide peak, while the peak at 531.0 eV increases linearly over the whole timescale of the experiment and continues to increase even when the main oxide peak and the peak at 528.6 eV are saturated. As the two oxide peaks, which are generated from the directly dosed oxygen saturate, the different behavior of the species at 531.0 eV is consistent with a species that is generated from either the residual gas in the chamber or a minor contamination in the oxygen beam, pointing to OH.

XPS binding energies in the O1s region for the oxide and the hydroxide peaks found in literature are given in Table 4.1. Even though the peak positions differ by more than 1 eV between the publications, the relative binding energy position is consistent with $1.7 \text{ eV} \pm 0.1 \text{ eV}$, with only two exceptions in the works of Kitakatsu [79] and Lorenz [91]. Both found only small hydroxide shoulders making the determination of the peak position difficult.

The binding energy of 529.6 eV we find for the oxide peak is in good agreement with most values reported in literature. Both the absolute binding energy of the peak at 531.0 eV and the relative distance of 1.4 eV to the oxide peak, however, differ from the reported values. This difference to literature will be discussed in more detail in the study of water interaction with the NiO layers in Chapter 7.2, where it is shown that both the absolute and the relative binding energy of hydroxide depend both on the hydroxide coverage and the surface temperature. It should be noted that the coverage of the hydroxide peak was not the same for different oxidation experiments, but seems to depend on the partial pressure of the residual water in the chamber. It continued to grow in intensity over time even after the oxidation was finished and the oxygen beam was turned off. A similar behavior is found for a second important contamination, namely the formation of NiCO_3 . This species is discussed in detail in Chapter 7.3 and can be identified by a peak at 289.0 eV in the C 1s region, while in the O 1s region the binding energy of this

species is similar to the binding energy of OH. Due to this, a disambiguation of the two species is not possible from the O 1s region alone.

System	Oxide Peak	Hydroxide Peak	Difference between Oxide and Hydroxide	Source
NiO(111)/Ni(111)	529.6±0.1 eV	531.4±0.1 eV	1.8 eV	[79]
NiO(100)/Ni(111)	530.1±0.1 eV	532.1±0.1 eV	2.0 eV	[79]
NiO(111)/Ni(111) grown at 100 K	529.0 eV	530.7 eV	1.7 eV	[76]
NiO(111)/Ni(111)	529.7 eV	531.3 eV	1.6 eV	[80]
NiO(111)/Ni(111)	530.2 eV	532.4 eV	2.2 eV	[91]
NiO(111)/Ni(111)	Not given, ~ 529.8 eV	531.4 eV	1.6 eV	[89]
NiO(111)/Ni(100)	529.4 eV	531.2 eV	1.8 eV	[88]
NiO(100) crystal	529.7 eV	531.4 eV	1.7 eV	[98]
Heated β-Ni(OH) ₂	529.7 eV	531.4 eV	1.7 eV	[99]

Table 4.1: List of oxide and hydroxide binding energies reported in literature

The growth of the peak at 528.6 eV in Figure 4.3 (c) (green curve) starts 50 L after the growth curve for the main oxide peak; thereafter the shape of the coverage curves is very similar and both saturate above 200 L. Therefore we assign the peak at 528.6 eV to a second oxide species. Such a second oxide species, however, has not been reported in previous XPS studies of NiO. When considering this we have to bring two things to attention. First, due to the relatively low intensity of the 528.6 eV peak in respect to the very large intensity of the main peak it is not easy to spot the presence of this peak, which is even complicated by the fact that the presence of the peak is more clearly visible during the uptake (red lines in Figure 4.3 (a)) than in the final spectrum, which corresponds to a saturation of the oxide (black line in Figure 4.3 (b)). The clearer visibility during the uptake is due the subsequent growth of the two species: when the species at 528.6 eV starts to develop after 50 L, there is a visible change in the spectral shape. Due to its slightly earlier saturation in respect to the main oxide peak it later disappears again in the

low binding energy side of the main oxide peak. This lower visibility at saturation coverage, together with the fact that all previous XPS studies of the room temperature oxidation of Ni(111) [75, 79, 80] have been conducted with laboratory X-ray sources, which typically have a much lower resolution than the resolution of ~ 300 meV we achieve with synchrotron radiation, lead to the fitting procedure in the mentioned references ignoring this contribution, just using a broader peak at the main position at 529.6 eV. It should be noted that due to the symmetry of the peak this practice automatically will also underestimate the hydroxide content of the spectrum.

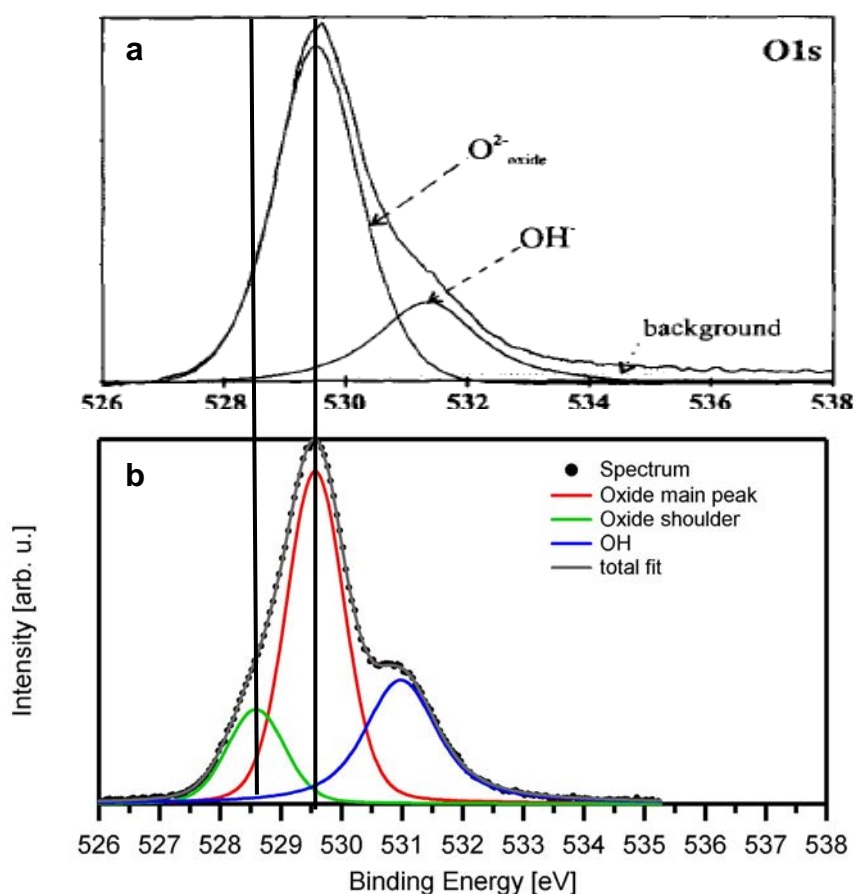


Figure 4.4 Comparison of literature data with our data (a) Data taken from Kitakatsu et al. [79], displaying oxide layer grown at 300 K (b) Spectrum of oxide layer grown at 300 K. Please note that for this comparison the binding energy axis is reversed

Figure 4.4 shows a comparison of data acquired by Kitakatsu et al. [79] to the data presented in Figure 4.3 (b). Please note that for this comparison the binding energy axis is reversed. On the low binding energy side, where the 528.6 eV peak is located the two spectra are very similar, while the small differences on the high binding energy side can be explained with the lower resolution of the laboratory source used by Kitakatsu et al. [79], and the different hydroxide coverage. Similar comparisons can be made for the data in the other two XPS studies [75, 80] of Ni(111) oxidation at room

temperature, leading to similar conclusions. We can therefore conclude that the peak at 528.6 eV is not a new feature unique to our experimental conditions but in fact simply was not resolved in the previous studies. What still remains to be discussed is the nature of the species. In Figure 4.3 (c), it can be seen that the coverage of the peak at 528.6 eV evolves in a similar fashion as the main oxide peak, and also saturates after approximately the same exposure. This points to the assignment of the 528.6 eV peak as a second oxide species

This assignment is further strengthened by DFT calculations from Ebensperger and Meyer [100], who indeed found a second oxide state on NiO(111) shifted to lower energies in respect to the main oxide state. A closer look at the evolution of the different species in the quantitative analysis depicted in Figure 4.3 (c) shows that the 528.6 eV oxide species only appears at an exposure of 50 L, when already a significant amount of the main oxide species is present on the surface. Therefore, the 528.6 eV species could belong to a surface oxide species. After an exposure of 230 L a stable coverage of 0.6 ML is reached for this species, which remains constant until above 500 L both oxides start getting damped significantly by the hydroxide. The evolution of the main oxide species starts already at exposures around 10 L, with a steady increase until a stable coverage is reached above 250 L exposure. While the oxidic contribution in the spectrum increases, the chemisorbed part continually decreases until it is completely gone around 250 L. The highest coverage for the chemisorbed component is 0.75 ML. This is close to a coverage of 0.8 ML oxygen which was suggested by Evans et al. [101] as the onset of subsurface diffusion of oxygen, which marks the start of oxidation of the surface. The shape of the total oxygen coverage (purple curve in Figure 4.3 (c)) is very similar to the coverage curves obtained by other groups [68, 70, 75, 77, 80].

An oxide layer with lower hydroxide content was heated to selected temperatures after growth at 300 K. The resulting O 1s spectra are shown in Figure 4.5 (a), with the quantitative results of the fitting procedure depicted in Figure 4.5 (b). The main oxide peak shifts from 529.6 eV to 529.9 eV and gains in intensity, while the oxide shoulder peak remains at a distance of -1 eV in respect to the main peak, leading to a shift from 528.6 eV to 528.9 eV at 600 K. In the quantitative analysis it is seen that the oxide shoulder loses intensity, suggesting its conversion to the main oxide species, which is also backed by the almost constant total coverage. A similar trend is found for the growth of NiO at higher temperatures, where the oxide shoulder species is found only to a smaller extent (see Chapter 4.1.3). The hydroxide peak is shifted from 531.0 eV to 531.6 eV and loses intensity. These two observations will be discussed in detail in Chapter 7.2.

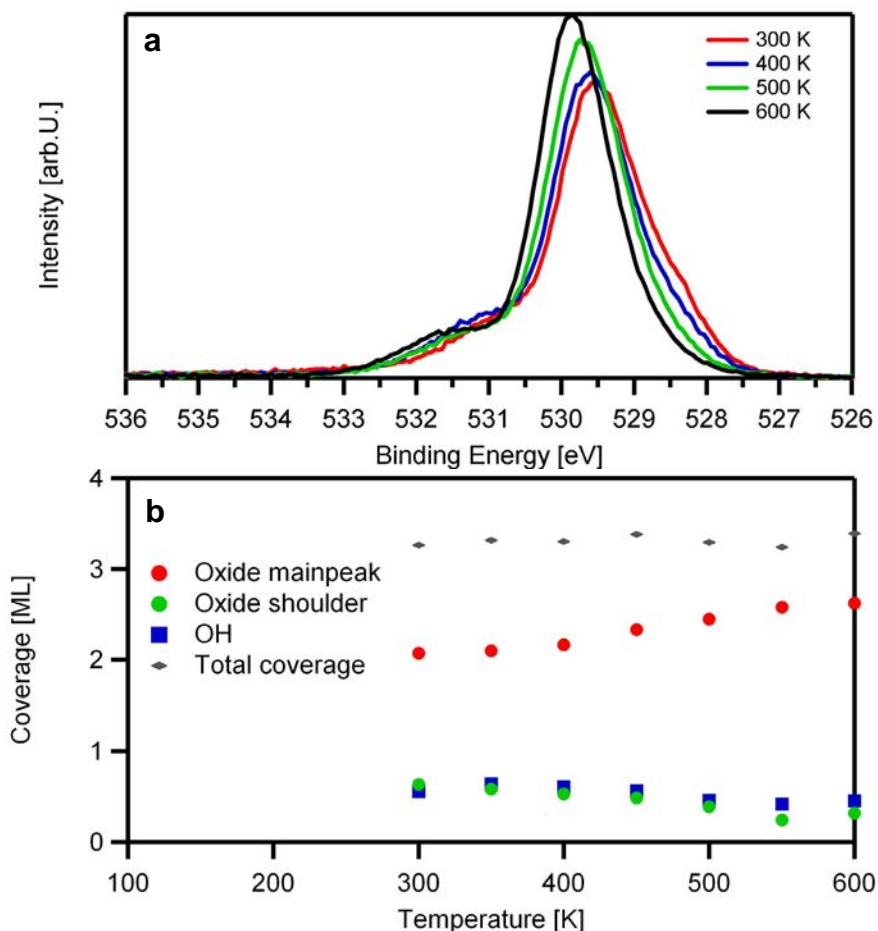


Figure 4.5: (a) Thermal evolution of NiO layer after growth at 300 K. (b) Quantitative analysis

Figure 4.6 (a) shows the Ni 2p spectra acquired during the oxidation of Ni(111) at room temperature. The spectrum of the clean surface (blue line in Figure 4.6 (a)) is dominated by a main peak at 852.9 eV, that is attributed to metallic nickel [79, 80]. At 858.7 eV, a satellite peak is found, the origin of which is the nature of an ongoing discussion in literature. Although it was initially attributed to a plasmon loss [102], an interpretation that is frequently revisited [103], other data points to it originating from a screened $2p^53d^9$ final state configuration [104] (the main line corresponds to a $2p^53d^{10}$ state). The spectrum of the oxidized surface (black line in Figure 4.6 (a)) shows three peaks located at 854.1, 855.7 and 861.0 eV. The peaks at 854.1 and 861.0 eV correspond to the main line, which has predominantly $3d^{10}\underline{L}^2$ character [105], and a satellite, respectively. The satellite is due to the finite overlap of the frozen ground state with the core electron removed with the unscreened final state which has mainly $3d^9$ character [105].

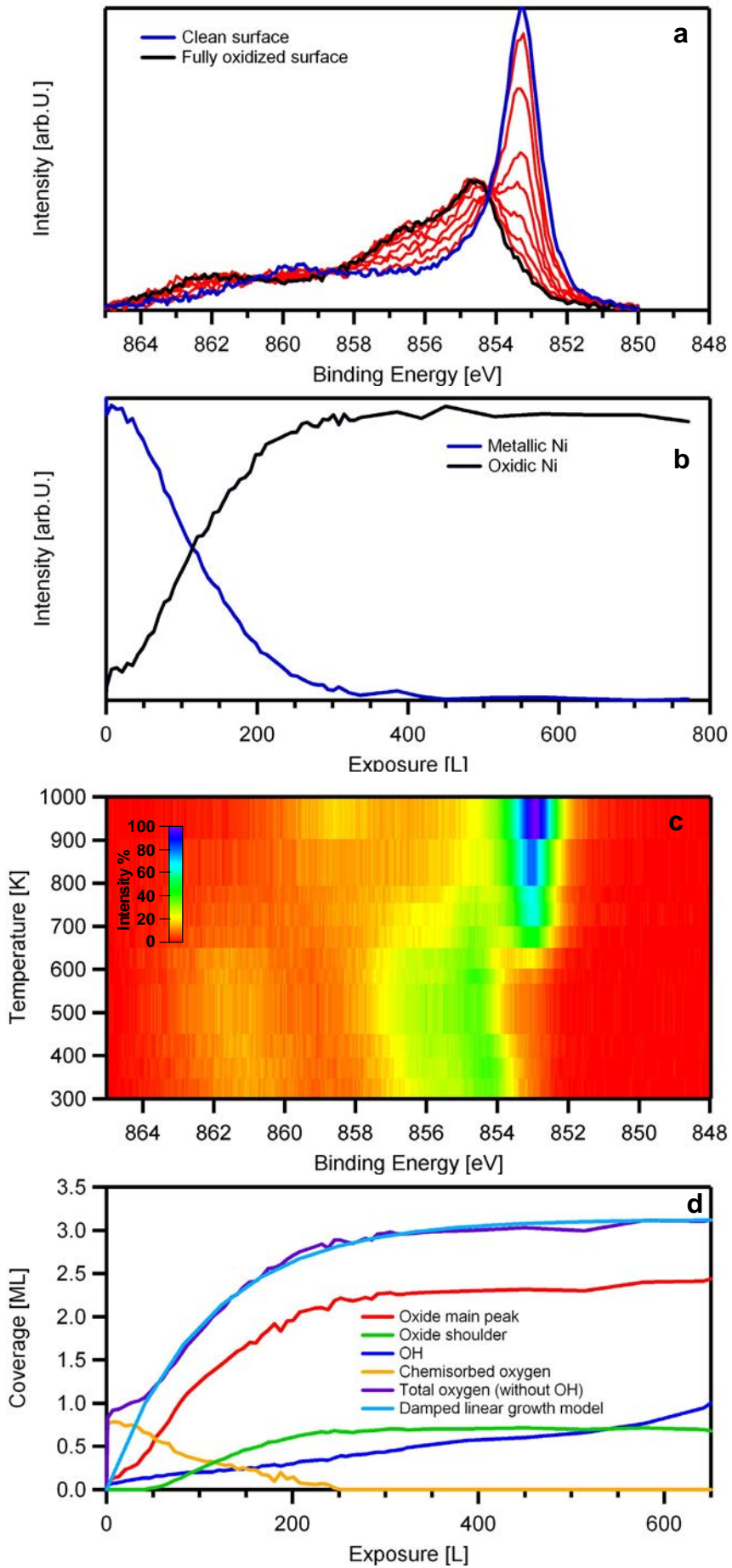


Figure 4.6 (on previous page): (a) Selected Ni 2p spectra acquired during dosing of 5 sccm oxygen on Ni(111) at 300 K (b) Relative intensities of metallic and oxidic nickel (c) Density plot for TPXPS of NiO layer grown at 300 K (d) Quantitative analysis of data from Figure 4.3 (a), corrected for damping by OH, together with fit assuming a damped linear growth of the oxide

The peak at 855.7 eV is attributed to undercoordinated nickel atoms from the surface [106] and contributions due to nonlocal screening effects, as shown by Sawatzki and coworkers [105, 107]. Possibly even more effects contribute to this peak, like a different Madelung constant at the surface [108] that would affect the charge transfer energy and also reduce the binding energy of the surface contribution. The spectral shape is identical with XP spectra both of poly- [98] and monocrystalline NiO [109], indicating complete oxidation within the escape depth of the photoelectrons.

To study the oxidation process the metallic spectrum was fitted with two peaks and the oxidized spectrum with three peaks. The resulting quantitative transition from the metallic to the oxidized state is shown in Figure 4.6 (b). Please note that the intensities for both metallic and the three oxidic contributions were added up to give the total metallic and oxidic contributions, respectively. As all of the Ni-atoms within our sampling depth get oxidized during the experiment a description in ML is not suitable as only an apparent coverage could be given, which is discussed together with the thickness of the films in Chapter 4.1.4. It should be noted, however, that the total intensity remains almost unchanged during the course of the experiment. The progression of the curve for oxidic Ni (black line in Figure 4.6 (b)) follows nicely the progression of the two oxide curves in Figure 4.3 (c). This clearly shows that the oxidation can be followed both in the O 1s and Ni 2p regions, yielding the same results. The oxidation is mostly finished after dosing 300 L of oxygen on the surface, with the last traces of metallic Ni gone after 425 L of oxygen. The slower oxidation after 200 L of oxygen would be consistent with the 3 stage oxidation model found by Holloway and Hudson [68] and mark the onset of the third stage, the slower thickening of the oxide. However, the curve shape is also consistent with the increased damping as the oxide thickens. Figure 4.6 (d) shows again the quantitative analysis of the data from Figure 4.3 (a), but in contrast to Figure 4.3 (c) it is now corrected for the damping by the hydroxide with the method detailed in Chapter 7.2. Included is also a curve (light blue) for a model, in which a linear growth for the oxide is assumed, independent of thickness, but that includes corrections for the selfdamping of the oxide layers. This selfdamping leads to smaller and smaller contributions to the coverage for the deeper layers of the oxide. The light blue line for this model fits the purple line for the total oxide coverage very well. If the oxide growth would indeed slow down like proposed in the

three stage model, the purple line would deviate from the blue line for higher exposures and feature an even lower slope. As this is not the case we can conclude that the curve shape is due to damping and the growth rate of the oxide is more or less constant. This also questions the thickness of 3 ML NiO reported in literature [71, 77, 79, 80] as saturation, because if the curve shape is due to damping effects the oxidation can be assumed to progress without saturating. The complete disappearance of the metallic nickel is not a sign of the complete oxidation of the whole crystal but rather the surface region of the crystal probed by the photoelectrons.

Figure 4.6 (c) shows Ni 2p spectra of a NiO layer grown at 300 K during stepwise heating to elevated temperatures in the form of a color coded density plot. The spectra were acquired after each heating step. Between 300 and 600 K the binding energy of all oxide peaks is shifted by 0.3 eV towards higher binding energies, which is the same shift we observed in the O 1s spectra during heating. Above 600 K at 852.9 eV the peak of metallic nickel starts to appear again, which indicates initial stages of decomposition of the NiO film. This is in good accordance with values of 550-600 K reported in literature [75, 83, 93] for the beginning of the decomposition.

4.1.3 Oxidation of Ni(111) at temperatures of 500 K and above

In order to minimize the initial OH impurities in the NiO layers another set of NiO layers were grown at higher temperatures. A surface temperature of 500 K during oxidation has two advantages. Firstly, the preferred NiO direction has been reported to be (100) [79, 81, 83], while at 300 K (111) is the preferred orientation [68, 69, 76, 79, 83]. Since the NiO(100) surface is not a polar surface its reactivity to water is much lower in respect to the NiO(111) surface. McKay [110] found for freshly cleaved NiO(100) surfaces only very weak interaction with water, which could be shown only to interact with defect sites. These findings were confirmed by several groups, both for freshly cleaved surfaces [111] and thin NiO films with (100) orientation [79, 88, 89]. It has to be mentioned, however, that the NiO(100) on Ni(111) was found to include small islands with (111) orientation [79, 81, 93] even for low oxygen doses of 15-25 L. By comparing these studies it is evident that the area covered by these islands increases for higher oxygen exposures. As the exposures we use for oxidation are higher by two orders of magnitude, in our case the majority or the whole surface should be covered by NiO(111). This is also backed up by an observed high reactivity towards water, as discussed below and in Chapter 7.2. This leaves us with the second advantage of the higher growth temperature. As shown in the calculations of Ebersperger and Meyer [82] at higher temperatures the hydroxylation of the surface is partially

lifted and the surface converted to the octopolar reconstruction. This is also supported by water adsorption experiments discussed in Chapter 7.2, where we found that the hydroxide coverage can be continuously lowered by annealing the surface. Thus a higher surface temperature should lead to lower hydroxide content.

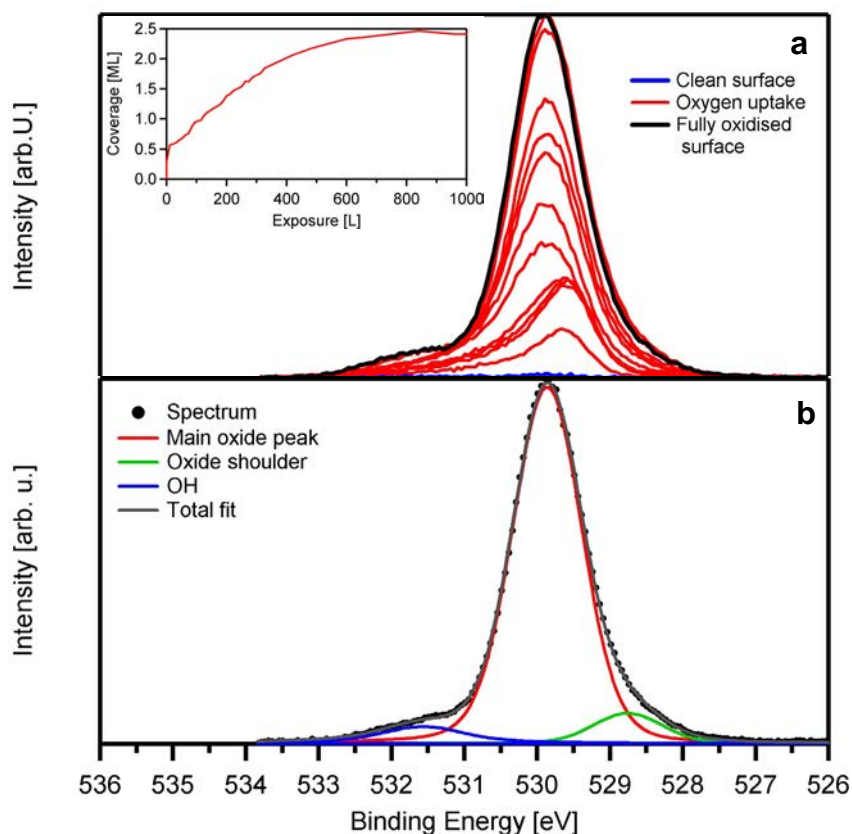


Figure 4.7: (a) Selected O 1s spectra acquired during dosing of 10 sccm oxygen on Ni(111) at 500 K **Inset:** Total oxygen (without OH) coverage versus exposure (b) detailed fit of the final spectrum.

To oxidize the surface at 500 K, 10 sccm oxygen were dosed on the surface with the molecular beam, giving an effective surface pressure of $2 \cdot 10^{-6}$ mbar. The surface temperature was kept at 500 K with resistive heating. The Fermi edge for the calibration of the binding energy was acquired at the same surface temperature, and spectra taken after the experiment without the resistive heating showed the same spectral height and peak intensity/background ratio. The corresponding O 1s spectra are displayed in Figure 4.7 (a), with the inset of that figure showing the evolution of the total oxygen coverage (without OH). The detailed fit of the fully oxidized surface is shown in Figure 4.7 (b).

The initial situation is very similar to the surface oxidation at 300 K. The first species to appear is a chemisorbed oxygen species at 529.6 eV with an

asymmetric peak shape. Afterwards, the peak shape changes to the symmetric shape of the oxide peak, just as observed for the oxide growth at 300 K. The oxide peak is located at 529.9 eV, the shoulder peak at 528.8 eV, and the hydroxide peak appears at 531.1 eV and shifts to 531.6 eV. All these binding energies are the same as for the oxide layer prepared at 300 K, after it was annealed to 600 K, as shown in Figure 4.5.

A clear difference to the oxide grown at 300 K is that both the oxide shoulder and the OH peak are smaller in relation to the oxide main peak. While for the 300 K oxide preparation the oxide shoulder contributed ~ 22% to the total oxide signal, here we only find a contribution of ~7%. This is also in good agreement with the thermal evolution of the 300 K oxide layer discussed in the previous Chapter, where the oxide shoulder lost intensity upon annealing, although there only a drop from 23 % down to 14 % was observed between 300 and 500 K.

A possible explanation for this is that the shoulder peak is due to some sort of defect sites, and growing the oxide at 500 K leads to a better ordered layer. Another possibility would be that the oxide shoulder is a feature of the flat, hydroxide stabilized NiO(111) surface. As discussed above, the (100) orientation of the NiO found by Kitakatsu et al. [79] for an oxidation temperature of 500 K should not dominate here, as our oxygen exposure was so large that the NiO(111) islands, who increase in size with higher oxygen exposures [79, 81], should be the majority species. As shown by Ebersperger and Meyer [82], at room temperature the most stable phase is a hydroxylated flat NiO(111) structure (see Figure 4.1 (b)), while at higher temperatures some of this hydroxylation is lifted and the surface converts itself to its octopolar reconstruction to stabilize itself (Figure 4.1 (a)). The relatively low hydroxide coverage of only 0.2 ML for the layer oxidized at 500 K points into the direction that we now have predominantly the octopolar reconstruction of the surface. The different oxide binding energies of 529.6 and 529.9 eV for the layers prepared at 300 K and 500 K, respectively, could also be indicative of a difference in surface structure, especially since such a shift in binding energy is also found during TPXPS experiments of hydroxylated surfaces as shown in Figure 4.5 and in Chapter 7.2. It should be mentioned, however, that both the NiO layers grown at 500 and 550 K, which is discussed below, have a very high reactivity to water at lower temperatures, despite having a low hydroxide content after growth. This is further indication of the conversion between the octopolar reconstructed and the hydroxide stabilized surface.

To further reduce the hydroxide content of the oxide layers, the oxidation temperature was raised to 550 K and the oxygen gas line was lead through a cooling trap to remove residual water in the oxygen. The resulting O 1s

spectra with a detailed fit and the evolution of the oxygen coverage are displayed in Figure 4.8.

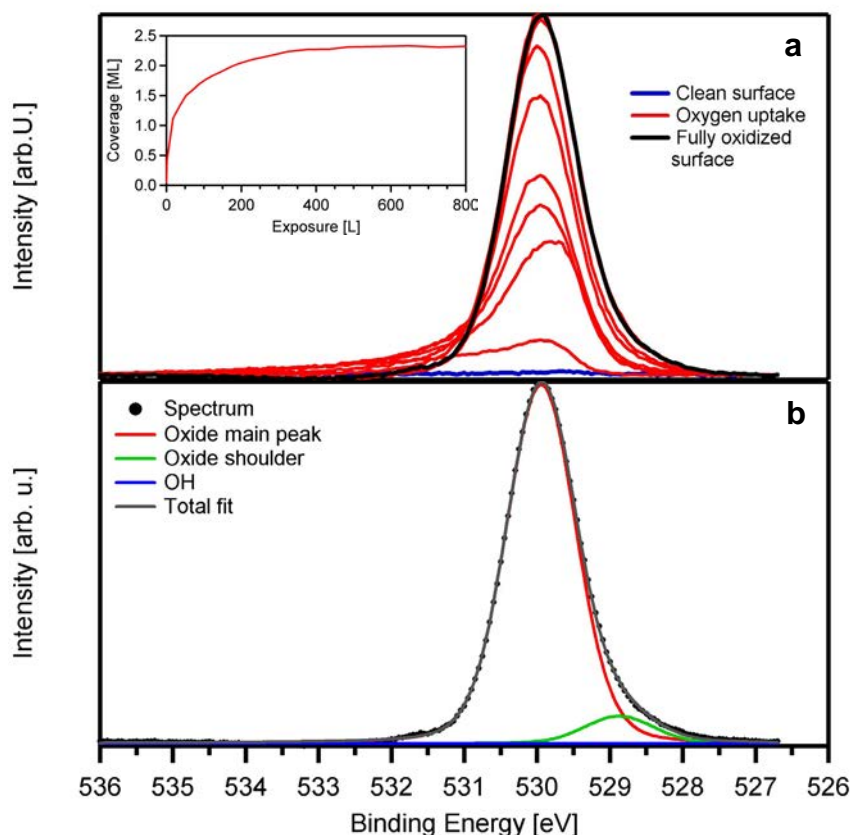


Figure 4.8 (a) Selected O 1s spectra acquired during dosing of 20 sccm oxygen on Ni(111) at 550 K **Inset:** Total oxygen coverage versus exposure **(b)** detailed fit of the final spectrum.

The spectra are similar to the ones for the preparation at 500 K, and also the binding energies for the chemisorbed oxygen, the oxide main peak and the oxide shoulder are the same, with values of 529.6 eV, 529.9 eV and 528.9 eV, respectively. The oxide shoulder contributes 6% to the total coverage, which is the same as for the 500 K oxide, within the margin of error. A hydroxide peak, however, was not present for the fully oxidized surface, as is very clear from the fit in Figure 4.8 (b). Another remarkable difference between the preparations at 550 K and 500 K is found in the insets of Figure 4.8 and Figure 4.7, respectively. While the oxidation process at 550 K is finished after an exposure of around 400 L of oxygen, at 500 K nearly double that exposure is needed to reach full oxidation within our sampling depth. Mitchel and Graham also found faster oxidation of the Ni(111) surface for higher temperatures [70].

The most likely explanation for this dependence on the temperature is a higher diffusion speed of either oxygen or nickel ions at higher temperatures. If we now compare these two oxidation curves with the oxidation curve at 300

K as shown in Figure 4.3 (c) it is clear, however, that the temperature is not the only important variable, as the oxidation at 300 K is even faster than at 550 K, although one might expect that it should be slower than at 500 K. This can be explained by the complicated structure of the surface at the higher temperatures, where the octopolar reconstruction displayed in Figure 4.1 (a) should dominate. At 300 K on the other hand the surface can grow flat as it is stabilized by the hydroxide, as displayed in Figure 4.1 (b). Since the formation of the octopolar reconstruction involves activated transport processes of NiO on the surface [82], this can explain the relatively slower oxidation at the temperatures where this surface structure dominates.

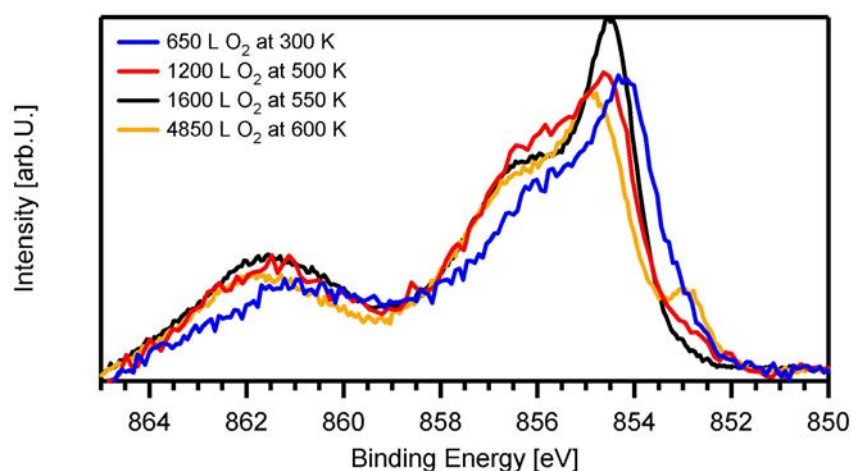


Figure 4.9: Ni 2p spectra of Ni(111) oxidized under different conditions

Slight differences between the layers prepared at the different temperatures are also visible in the Ni 2p region. The corresponding spectra are displayed in Figure 4.9. The overall shape of the spectra is similar for the three different preparation methods. However, the spectrum of the layer prepared at 300 K is shifted by 0.4 eV towards lower binding energies, in respect to the two spectra for the NiO layers prepared at higher temperatures. The O 1s spectra of the oxide are shifted by approximately the same amount and in the same direction. All three layers are fully oxidized. The oxidation at 500 K leads to a higher contribution from the peak at 856.1 eV as compared to the oxidation at 550 K, where the peak at 854.6 is more intense. As the nature of the peak at 856.1 eV is not fully understood yet, as discussed in the previous Chapter, it is not clear if this indicates a higher ordering for the layer grown at 550 K or not.

In order to determine whether the quality of the layers can be improved further by choosing an even higher oxidation temperature, 4850 L oxygen were dosed on the Ni(111) surface at 600 K. The resulting Ni 2p spectrum is displayed as the yellow line in Figure 4.9. A metallic contribution to the

spectrum at 852.9 eV indicates that, even after dosing a significantly larger amount of oxygen than in the other oxidation experiments, the surface is not fully oxidized. Since a beginning destabilization of the NiO layers in the temperature range 550-600 K has been reported in several publications [75, 83, 93], and oxygen was shown to start diffusing into the bulk in this temperature range [94], this result is not surprising, and thus this preparation has not been used for adsorption experiments.

4.1.4 Discussion of oxygen coverages and estimation of NiO layer thickness

To understand the observed saturation coverages the damping within the nickel oxide layers has to be discussed. The coverages are referenced to a well defined CO c(4x2) layer on Ni(111) (see Chapter 7.4). From the Ni 2p spectra of the NiO it could be seen that within the sampling depth of our photoelectrons all Ni atoms were fully oxidized, which means that no electrons from the metallic Ni-layers can escape without being inelastically scattered. XPS is a fully quantitative technique for submonolayer coverages, which means that the signal intensity scales linearly with the amount of adsorbate. If the adsorbate amount grows larger than 1 ML, however, any adsorbate molecule or atom that adsorbs on top of the already present adsorbate layer dampens the XP signal from that layer. This damping is calculated with equation (6) from Chapter 2.3. If more and more adsorbate layers are added, then the signal from the lowest layer can be damped so much, that it will have no contribution to the observed signal intensity. This effect limits the total signal intensity, which stops increasing even though the adsorbate layer can still grow in thickness. The coverage determined from such a layer is thus only an apparent coverage Θ_{apparent} . As this apparent coverage depends on the damping factor a (see Chapter 2.3) it can be used to make estimations on the inelastic mean free path of the adsorbate layer. To calculate Θ_{apparent} we just have to add up the signal intensity of each layer, which can be done using equation (14) from Chapter 2.3, since only fully closed layers are considered. This gives equation (19).

$$\Theta_{\text{Apparent}}(a) = \sum_{n=0}^{\infty} a^n \quad (19)$$

The uppermost (undamped) layer is represented by the factor for $n=0$. For a values <0.84 it is sufficient to include 25 layers, since all additional layers contribute with <0.01 ML to the total apparent coverage, minimizing the error of disregarding them, especially since this error is less than 1 % of the total apparent coverage.

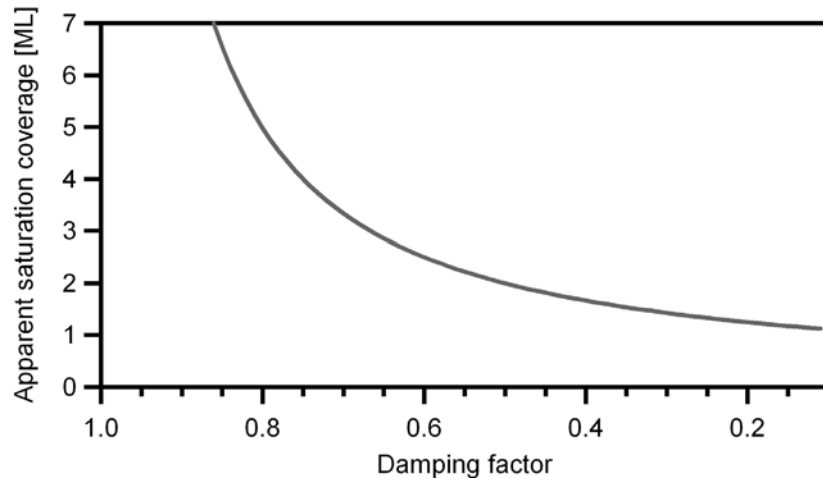


Figure 4.10: Apparent saturation coverages for several damping factors

Figure 4.10 shows that damping leads to quite low apparent saturation coverages; they are asymptotically approaching an apparent saturation coverage of 1 ML (i.e. the coverage of a single adsorbate layer on the surface, disregarding all layers beneath) for very low damping factors. If we now take the saturation coverage for our oxidic oxygen of $\sim 2.5 \pm 0.2$ ML we find a corresponding damping factor of 0.60 ± 0.03 . With equation (6) from Chapter 2.3, this can be translated to the IMFP for the electrons. The thickness of one layer of NiO(111) is 2.41 \AA . As all spectra in Chapter 4.1 have been recorded with an emission angle of 45° an effective layer thickness of $2.41 \text{ \AA} \cdot \sqrt{2} = 3.41 \text{ \AA}$ has to be used for the calculation. With this we find an IMFP in the range of $6.6 \pm 0.5 \text{ \AA}$.

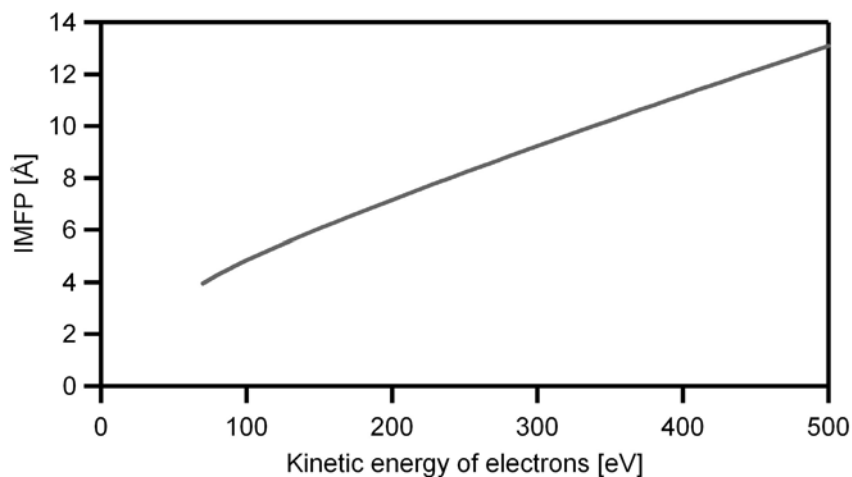


Figure 4.11: IMFP for NiO calculated after [36]

Since in literature no values of the IMFP in NiO for electrons with $\sim 100 \text{ eV}$ have been reported, we calculate the IMFP with equation (7) given in Chapter 2.3. The molecular weight of NiO is 74.7 g/mol and from this and the lattice constant of 4.177 \AA [63] the density is calculated to be 6.72 g/cm^3 . As

the value for the band gap we used the value of 4.3 eV found for bulk NiO [112], although it should be noted that for NiO thin films slightly smaller values have been found [113]. The valence electron number is 22. The resulting IMFP values are plotted in Figure 4.11. From Table 2.1 we find that the O 1s photoelectrons have a kinetic energy of 120 eV. The corresponding IMFP value of 5.3 Å is a bit lower than the values calculated from the effective coverage, but still close enough to support the coverage calibration.

With the lower limit for the IMFP of 6.1 Å (using the value of 6.6 Å and the error bar of 0.5 Å) calculated from the data and the effective NiO layer thickness of 3.41 Å it is now possible to calculate a lower limit for the thickness of the NiO(111) layer on Ni(111). In Chapter 2.3 we have seen that after $3*d/\lambda$ the intensity has dropped to 5 %. If we take this as the threshold we find a minimum number of 5.4 layers of NiO(111) on Ni(111). Since each layer contains 0.5 ML oxygen and 0.5 ML nickel atoms these 5.4 layers are equivalent to 2.7 ML NiO and thus very close to the 3 ML of NiO reported in literature [71, 77, 79, 80]. A rough upper limit for the film thickness can be estimated from the fact that the Fermi edge of metallic nickel is still visible even for fully oxidized layers even for the lowest kinetic energy of 380 eV (for the C 1s region) which we used. This apparent discrepancy – the Ni 2p region shows no sign of metallicity while it can be seen in the valence region – stems from the dependence of the IMFP of the electrons on their kinetic energy. The lowest kinetic energy (which corresponds to the lowest IMFP) we used was 380 eV for probing the Fermi edge with $h\nu=380$ eV as used for the C 1s region. As we have no means of determining the IMFP for 380 eV from our experimental data for the estimation of the layer thickness we use the IMFP calculated with equation (7) given in Chapter 2.3. For 380 eV this gives us an IMFP of 10.8 Å. If we now take the same 5 % threshold as before this gives as a rough upper estimate for the NiO layer thickness of 4.75 ML, corresponding to one oxygen and nickel per unit cell.

4.2 Growth of thin NiO layers on Cu(111)

For the study of thinner layers of NiO we chose Cu(111) as a substrate, as Ni was found to form flat layers on Cu(111) when evaporated at 120 K and annealed to 300 K [37]. This should allow growing layers of defined thickness. In previous studies on the oxidation of thin nickel layers on Cu(111) [95, 114], an oxidation temperature of 300 K was found to be necessary to fully oxidize a Ni layer of 2 ML thickness. For Ni evaporation in oxygen atmosphere [115] and direct evaporation of NiO [116, 117] the NiO grows in islands, with (111) orientation [116]. For the oxidation of thin nickel layers on Cu(111) at 300 K a cluster growth was also reported [114]. Please note that all spectra within chapter 4.2 were recorded at an emission angle of 0°.

4.2.1 Oxygen interaction with Cu(111)

In order to study the oxidation of submonolayer coverages of nickel on Cu(111), a situation where bare patches of the Cu(111) surface also come into contact with the oxygen, the interaction of the clean Cu(111) surface with oxygen was studied first. Habraken et al. [118] studied the adsorption of oxygen on Cu(111) at room temperature with AES, LEED and ellipsometry. A very low sticking coefficient for the adsorption of 10^{-3} was found, remaining constant over the range of the adsorption leading to a linear increase in oxygen intensity. After 1700 L a saturation coverage of 0.45 ML was found, with no ordered structure. Also for other coverages no ordered structure was found with LEED. Wiame et al. [119] studied the oxygen adsorption at room temperature with STM, STS, AES and LEED. No long range order was detected in this study as well, but with STM a local reconstruction of the surface was seen for exposures above 200 L, with triangular precursor structures to Cu₂O forming mainly at step edges. At saturation, however, the structures are less defined and consist mostly of a distorted, Cu₂O like structure. The long range order was not improved by annealing, even though ordered structures were found for higher temperatures during oxygen exposure. Annealing to 573 K removed a substantial amount of the oxygen, reducing the oxygen/copper AES peak ratio from 0.19 to 0.08.

Figure 4.12 shows O 1s and Cu 2p spectra before and after the adsorption of 5700 L oxygen on Cu(111) at 300 K. The O 1s region is dominated by an asymmetric peak at 529.7 eV with a very broad high energy tail around 533 eV. The Cu 2p region features a single peak at 932.9 eV that is damped slightly upon oxygen adsorption, but neither a noticeable shift nor a new component was found. Fleisch and Mains [120] report metallic copper at 932.4 eV, Cu₂O at 932.5 eV and CuO at 933.8 eV.

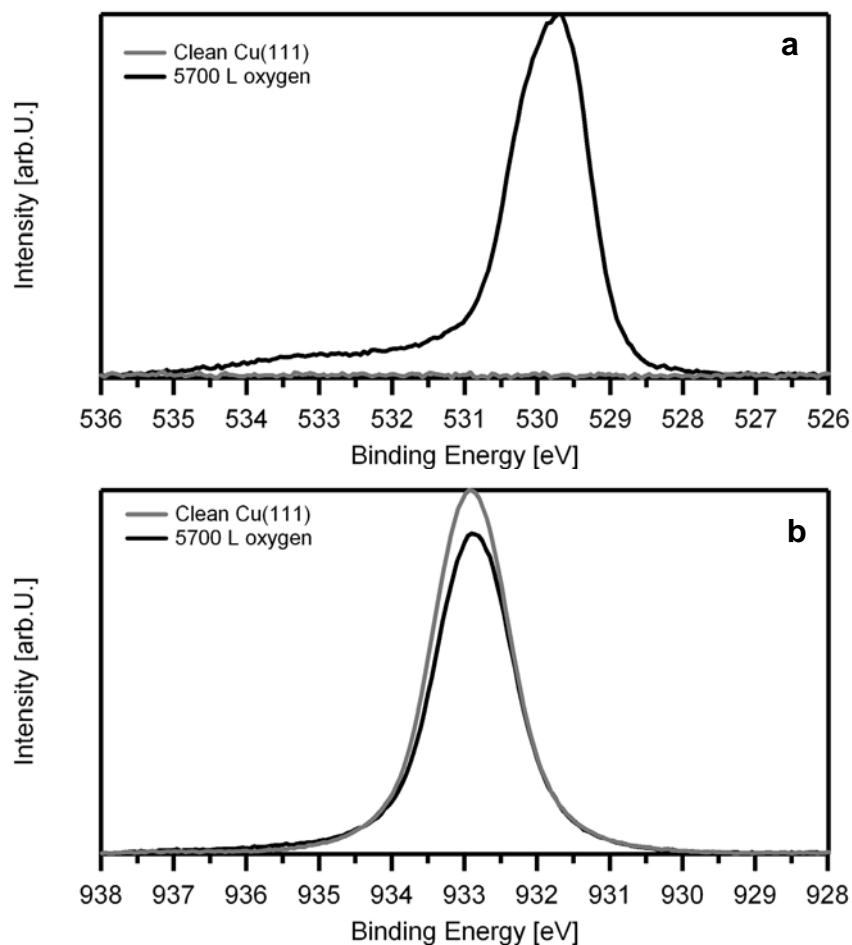


Figure 4.12: O 1s (a) and Cu 2p (b) spectra of a clean Cu(111) surface and after the exposure to 5700 L oxygen at 300 K. All spectra recorded at an emission angle of 0°

Since the clean surface shows no sign of oxygen or any other contamination it is clear that the peak at 932.9 eV can be attributed to metallic copper, and it is equally clear that upon oxygen adsorption no CuO is formed. Since the binding energies of metallic copper and Cu₂O are close a formation of Cu₂O can not be ruled out, even though the Cu 2p peak appears to undergo a very slight shift towards lower binding energies instead of the expected higher binding energies after oxygen adsorption.

4.2.2 Preparation of nickel layers and characterization with CO titration

Nickel was evaporated from a nickel rod onto a clean Cu(111) surface using an electron beam evaporator. The evaporation rate was monitored with a quartz crystal microbalance until it was constant for several minutes. From this evaporation rate the time necessary to grow nickel layers of either 2 or 0.5 ML thickness was determined. The thickness of 2 ML was chosen to get

a thin NiO layer of defined thickness, while the intention of the 0.5 ML Ni-layers is to grow NiO clusters on the Cu(111) surface. After oxidation the 2 ML Ni layers will from now on be called “thin NiO layers” while the 0.5 ML Ni layers will be referred to as “NiO clusters”. Before the start of the oxidation the surface was annealed to 200 K to get rid of any water or CO adsorbed on the surface. After that, in order to generate similar results to the ones obtained by Domnick et al. [37], the surface was cooled down to at least 150 K before the evaporation started. After the evaporation the surface was annealed to 300 K, again following the preparation method of Domnick et al. [37].

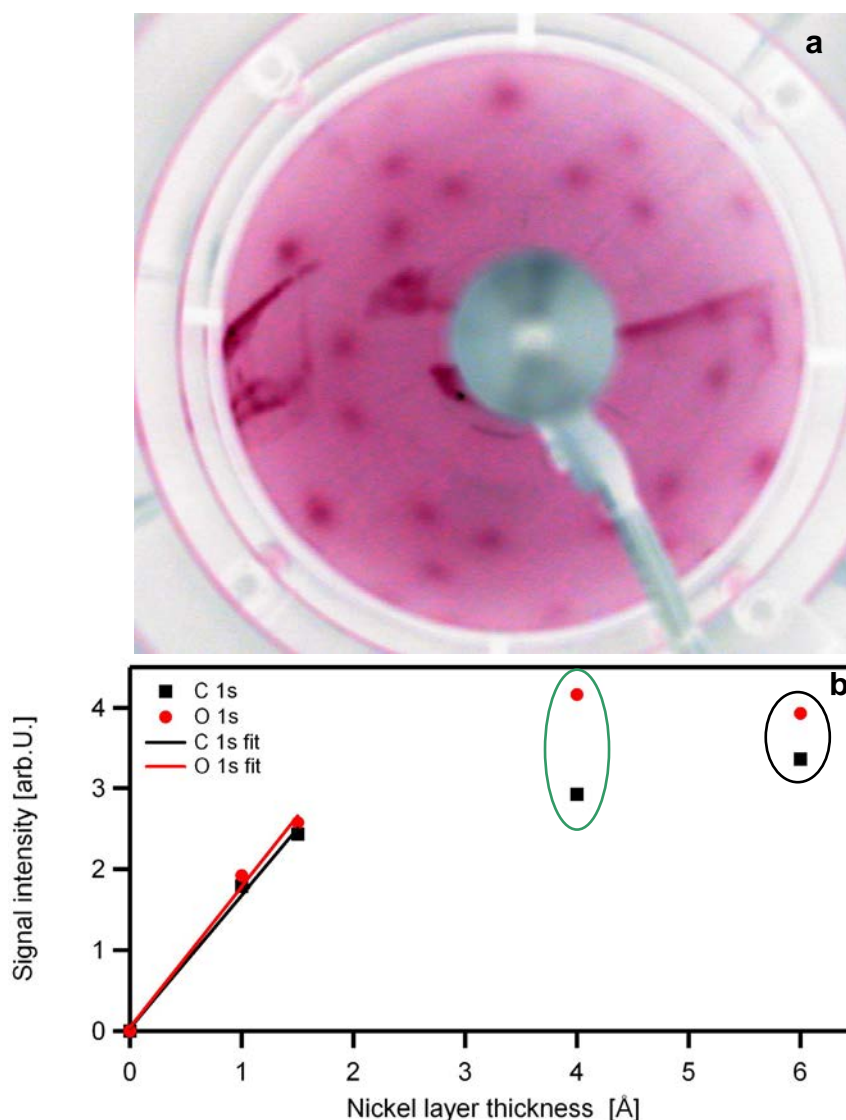


Figure 4.13: (a) LEED picture of $c(4 \times 2)$ structure of CO on 6 Å nickel evaporated on Cu(111) acquired at 79 eV (b) O 1s and C 1s signal intensities for saturated CO layers on various nickel layers on Cu(111). All layers for (b) were prepared by adsorbing CO at <220 K and subsequent annealing to 220 K.

To determine the actual coverage of nickel on the surface CO titration experiments were performed. CO desorbs from Cu(111) below 200 K [121, 122], while on Ni(111) the desorption starts above 250 K [123]. This difference in the desorption behavior allows for a clear distinction of CO adsorbed on the Cu(111) substrate or on the Ni(111) islands grown on the Cu(111). Koschel et al. [124] used this method successfully to characterize the inverse system, i.e. the growth of copper on Ni(111). CO was dosed on four different layers with 1, 1.5 and 6 Å of nickel on Cu(111) at less than 200 K, and then the temperature was raised to 220 K to desorb CO from bare Cu(111) patches but preserve all CO adsorbed on the Ni(111) patches. The layer with 6 Å thickness was chosen as a reliable reference for a fully closed layer. CO forms a c(4x2) structure on Ni(111) with a coverage of 0.5 ML, when adsorbed below 200 K and annealed to 320 K [125]. The LEED picture for CO dosed to saturation on the 6 Å thick nickel layer on Cu(111) at 120 K and subsequently annealed to 320 K is displayed in Figure 4.13 (a). Although the spots are rather diffuse a c(4x2) structure is visible [125]. This layer can thus be used as a reference layer, both for the CO titration and for coverage calibrations, analogous to the CO c(4x2) layer prepared on Ni(111) that is used for the coverage calibration of oxygen, CO, CO₂ and H₂O on the Ni(111) surface (see Chapter 7.4). The C 1s and the O 1s coverage obtained for this CO layer after the dosing at 120 K and subsequent annealing to 220 K is plotted in Figure 4.13 (b) in respect with values for CO layers on 1, 1.5 and 4 Å of nickel, as well as the zero remaining CO coverage after annealing a clean Cu(111) surface to 220 K. Although both the 6 Å (marked with a black circle in Figure 4.13 (b)) and the 4 Å layer (marked with a green circle in Figure 6.13 (b)) should be closed nickel layers, there is a rather large deviation for the coverages between the two layers. This is attributed to the strong photoelectron diffraction CO shows on Ni(111). Due to this photoelectron diffraction even a small change in angle can lead to an increase for the O 1s signal and a decrease for the C 1s signal, leading in both cases to a much larger separation of the two coverages than witnessed for the two lower nickel coverages. A line can be fitted to both the C 1s and the O 1s data for the lower nickel coverages, giving evidence that the coverages calculated from the evaporation rate were actually reached. Further evidence for this is found by examining the attenuation of the Cu 2p signal by the NiO layers, as discussed in the next chapter.

4.2.3 Oxidation of thin nickel layers on Cu(111)

Domnick et al. found that for temperatures above 300 K copper atoms segregate on top of thin nickel layers on Cu(111) [37]. Although in Chapter

4.1.3 it was shown that the oxidation at 500 K leads to cleaner layers compared with oxidation at 300 K, this segregation effect hindered higher oxidation temperatures than 300 K. In a different study Domnick et al. found that at temperatures below 300 K it is not possible to fully oxidize nickel layers that are thicker than 1 ML [114], so an oxidation temperature of 300 K was chosen. 20 sccm oxygen were dosed on the surface at 300 K, this is equivalent to a surface pressure of $2.7 \cdot 10^{-6}$ mbar.

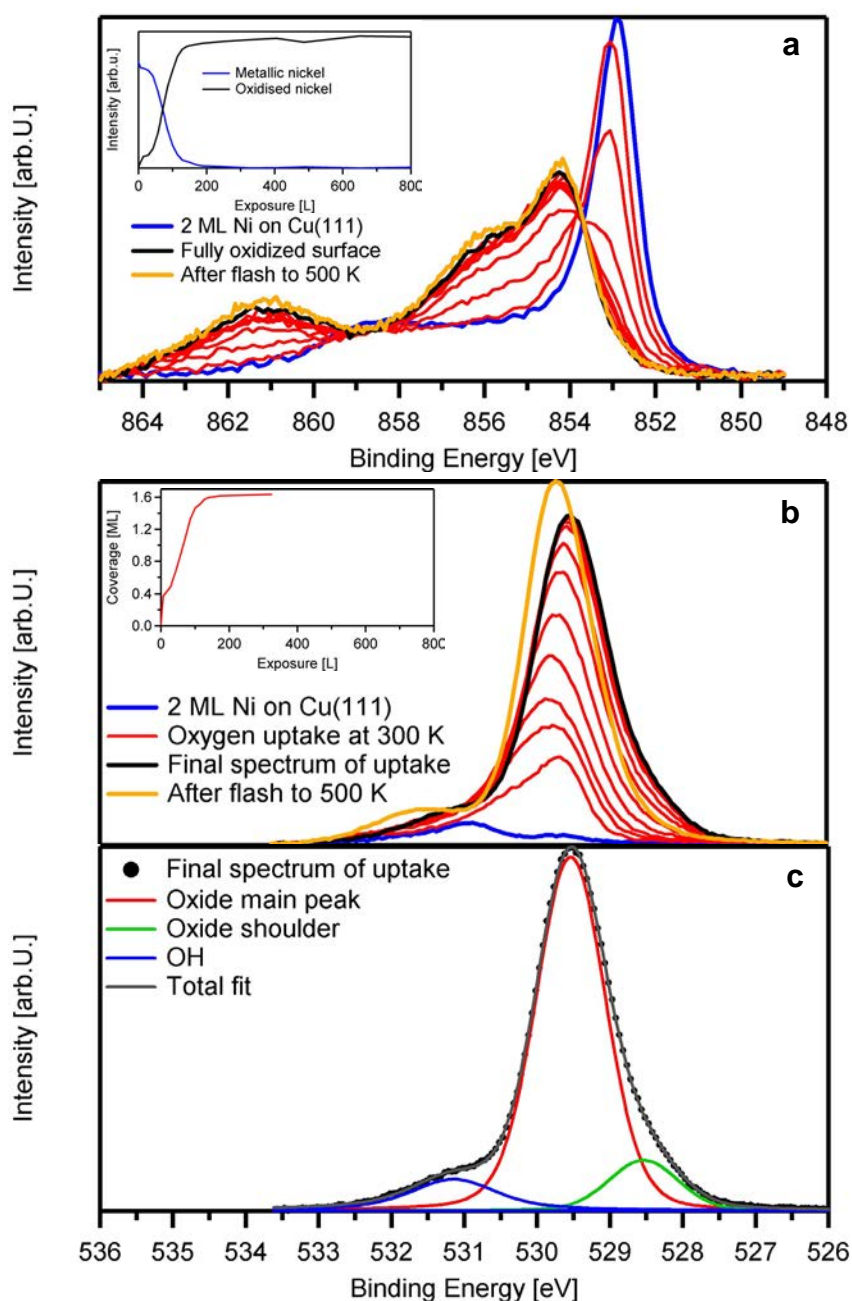


Figure 4.14: (a) Selected Ni 2p spectra of 2 ML nickel on Cu(111) during exposure to 20 sccm oxygen at 300 K; **Inset:** Evolution of metallic and oxidised nickel atoms (b) Selected O 1s spectra of 2 ML nickel on Cu(111) during exposure to 20 sccm oxygen at 300 K; **Inset:** Evolution of oxygen coverage (c) Detailed fit of the final spectrum acquired at 300 K

Figure 4.14 (a) shows Ni 2p spectra acquired during the oxidation of 2 ML nickel on Cu(111). From the spectral shapes it becomes clear that the oxidation is similar to the oxidation on Ni(111). The spectrum of the clean nickel layers show the same contributions as the Ni 2p spectrum of the bulk nickel crystal, with a metallic main peak at 852.8 eV and a satellite peak at 858.0 eV. While the main peak has basically the same binding energy as on the bulk nickel crystal, where it was located at 852.9 eV, the satellite peak is shifted by 0.7 eV towards lower binding energies relative to its position on Ni(111). As both the explanation of the satellite peak as a plasmon loss feature [102, 103], or as a screened $2p^53d^9$ final state configuration [104] depend on the electronic structure of the surface, the shift is attributed to the different electronic structure of the nickel due to the interaction with the underlying copper surface. Similar observations were made for thin nickel layers on Pd(100) [126], where for 3 ML thick layers the satellite peak is shifted by 1 eV towards lower binding energies, relative to the bulk value, and slowly shifts back to the bulk value as the layers grow bigger. The oxidized spectrum shows peaks at 854.1, 855.7 and 861.0 eV. These values are identical to the ones found for the 300 K oxidation on Ni(111), as discussed in Chapter 4.1.2. Since the oxidation temperature is the same in both cases, this result is not too surprising. Interestingly, the Cu(111) surface seems to have no influence on the electronic structure of the NiO layer, especially when considering that the satellite peak at 861.0 eV remains unshifted while the satellite at 858.0 eV of the unoxidized surface is shifted by 0.7 eV in respect to the Ni(111) surface. After the oxidation process the surface was annealed to 500 K in order to reduce the hydroxide content discussed below. The corresponding Ni 2p spectrum is shown as the orange line in Figure 4.14 (a). This spectrum is almost identical to the spectrum recorded at the end of the oxidation process. It is especially noteworthy that no intensity loss was found, since for the segregation of copper atoms on top of the nickel layer such an intensity loss would be expected. The copper signal during such an annealing process, which will be discussed in more detail later, is shown as the light blue line in Figure 4.17(a), and its relative intensity also remains constant between 300 and 500 K. So we can conclude that a segregation of copper atoms to the top is not taking place for the nickel oxide layers on Cu(111), while for unoxidized nickel layers on Cu(111) such an effect was reported above 300 K [37].

The inset of Figure 4.14 (a) shows the evolution of the oxidation process. The oxidation starts almost immediately and is finished after an exposure of 200 L, with the overall evolution very similar to the evolution of the 300 K oxidation on Ni(111) as displayed in Figure 4.6 (b). A difference is the earlier completion of the oxidation for the thin nickel layers on Cu(111). On Ni(111) between 200

and 425 L due to the self damping of the NiO layers the curve gets continuously flatter, until the metallic nickel is not visible any more. For the thin nickel layers on Cu(111) this region does not exist, because at a certain point all of the initial nickel atoms are oxidized and the nickel layer can not get thicker. Apparently the diffusion path lengths both for oxygen and nickel ions are short enough for 2 ML thick nickel films, that they do not play a significant role here, although that could also be due to the significant roughening of the surface upon oxidation discussed below. The increase in nickel coverage from the fully metallic to the fully oxidized surface seen in the inset of Figure 4.14 is not fully understood. During the oxidation of other nickel layers on Cu(111) the nickel coverage was found to remain constant or decrease, however, the changes were always in the order of $\pm 10\%$ of the coverage of the metallic surface. One possible explanation could be, that even at 300 K some copper atoms have diffused on top of the nickel layers, or nickel atoms into the copper bulk. The oxidation than leads to a reestablishment of the initial layer ordering, with all nickel atoms on top of the copper; and thus a change in nickel intensity.

Figure 4.14 (b) shows the O 1s spectra acquired during the oxidation of a 2 ML thick nickel layer on Cu(111). The spectrum for the freshly prepared nickel layer (blue line) shows a peak at 530.9 eV with a coverage in the order of 0.1 ML. Together with a peak found in the C 1s region (data not shown) at 285.2 eV this is identified as CO adsorbed in hollow positions on the (111) structured nickel layer [125]. This CO is not found after the oxidation, neither in the O 1s nor in the C 1s region. This is attributed to an oxidation of the CO to CO₂ by the dosed oxygen. A formation of NiCO₃ on NiO from the CO, as discussed in Chapter 7.4, is excluded as NiCO₃ coverages found after the oxidation process were found to have no correlation with the amount of CO present prior to the uptake.

The oxidation of the thin Ni layers on Cu(111) shows similar spectra in the O 1s region compared to the oxidation of the Ni(111) surface. A chemisorbed oxygen species is found at 529.6 eV. The oxide main peak appears at 529.8 eV and shifts towards 529.5 eV during the oxidation. The corresponding oxide shoulder is appearing at 528.8 eV and shifts to 528.5 eV. Also a small hydroxide peak is formed that is located at 531.2 eV. After the layer was annealed to 500 K (corresponding spectrum displayed as yellow line in Figure 4.14 (b)) the peaks shifted to 529.7, 528.6 and 531.7 eV, respectively. A detailed fit of the oxide spectrum at the end of the oxidation is displayed in Figure 4.14 (c). It should be noted that the spectra are fitted with the same fitting parameters used for the oxide layers on the Ni(111) surface. After the oxidation is finished the two oxide peaks have almost the same binding energies as the oxide peaks observed for NiO grown on Ni(111) at 300 K as

discussed in Chapter 4.1.2, and after annealing to 500 K the binding energy values are the same. This again highlights the great similarities between the oxide layers already found in the discussion of the Ni 2p spectra. The only remarkable difference found is the lower content of the 528.5 eV oxide species, which makes up 12.5 % of the oxide intensity compared to 22 % for the oxide on Ni(111). After annealing to 500 K the contribution of the oxide shoulder species falls to 3 %. The hydroxide coverage is in the range of 0.2 ML, and thus much lower than for the oxide preparation on Ni(111). As the reactivity towards water is similar for the two layers, see Chapter 7.2, the difference should mostly originate from a lower partial pressure of water in the chamber during the oxidation process of the thin nickel layers on Cu(111), leading to a lower hydroxide formation. Due to the relative low coverage of water, and as this coverage remains more or less unchanged upon heating, the intensity loss of the shoulder oxide species cannot be explained by a reduction in the hydroxide content. It is thus attributed to a restructuring of the surface towards the octopolar reconstruction. As the formation of this reconstruction involves some activated processes [82], this activation energy is provided by the higher temperature leading to a larger percentage of this reconstruction on the surface. This also explains the shift of the peaks towards higher binding energies upon annealing.

The coverage evolution of the oxide, which is shown in the inset of Figure 4.14 (b), is in agreement with the evolution of the oxidic nickel species depicted in the inset of Figure 4.14 (a). The oxidation is finished at 200 L and ends rather sharply due to the completed oxidation of all available nickel. Because both the O 1s and the Ni 2p region show that the reaction is finished at 200 L, all other NiO layers were prepared with a dose of 325 L oxygen in order to ensure full oxidation of the nickel on the one hand, while minimizing oxygen interaction with Cu(111) on the other hand. In the inset of Figure 4.14 (b) the total oxygen coverage of this experiment is shown, and saturation coverage of 1.6 ML oxygen is found. This value seems low for a full oxidation of 2 ML of nickel, but is explained by damping. Domnick et al. [114] found a coverage of 2 ML oxygen for two fully oxidized nickel layers on Cu(111), using a laboratory Al-K α X-ray source. Since our photoelectrons have lower kinetic energies, as discussed in Chapter 2.3, a lower IMFP and thus stronger damping is expected, explaining the lower apparent coverage for the oxygen. Due to the rough morphology of the surface, as discussed below, however, it is not possible to determine the true oxygen coverage.

After discussing the O 1s and Ni 2p regions the final interesting region is the Cu 2p region, as displayed in Figure 4.15 (a). The Cu 2p peak is located at 932.9 eV; only changes in intensity after the evaporation of 2 ML nickel on the Cu(111) surface are found, due to damping. Another reduction in intensity is

found upon oxidation. No oxidation of the copper was observed. As discussed in Chapter 4.2.1, Cu_2O is shifted by 0.1 eV towards higher binding energies in respect to metallic copper, and CuO is shifted by 1.4 eV [120]. Thus CuO can be directly ruled out. Due to its small binding energy difference in respect to the metallic copper the formation of some Cu_2O can not be completely ruled out. However, the Cu 2p peak of the NiO covered surface (black line in Figure 4.15 (a)) appears completely unshifted in respect to the peak of the clean surface (red line in Figure 4.15 (a)). There is also no shoulder visible on the high binding energy side. Furthermore, the oxygen coverage does not increase any more after the nickel is completely oxidized, making an ongoing oxidation of the copper surface after this moment unlikely. Lastly, as discussed in Chapter 4.2.1, the interaction of oxygen with copper is very unreactive. A saturation coverage of 0.45 ML was reached after dosing 1700 L molecular oxygen, and the coverage grows linearly [118], so the dose of 200 L used here would give a maximum of 0.05 ML oxygen binding to the copper. Due to these arguments the interaction of oxygen with the copper substrate can be disregarded.

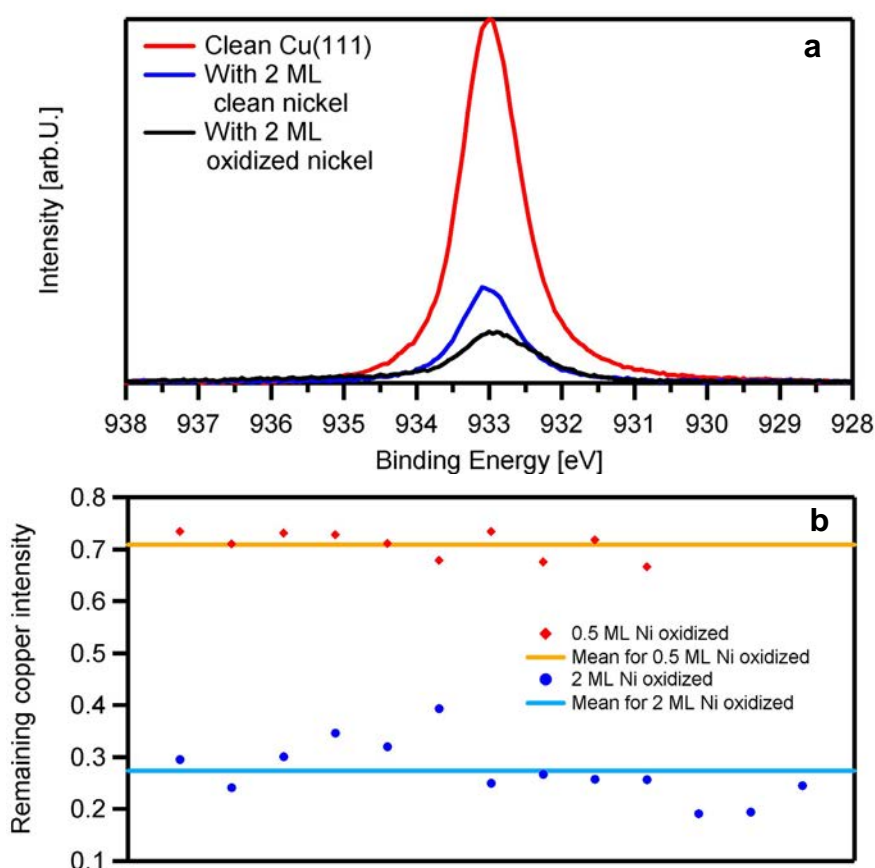


Figure 4.15: (a) Cu 2p spectra acquired during the different preparation steps for the thin NiO layers on Cu(111) (b) Damping of the Cu 2p signal by various NiO layer and NiO cluster preparations

The damping of the Cu 2p signal is used to further assure that the desired amounts of nickel have been evaporated. In Figure 4.15 (b) the remaining Cu 2p intensity after the preparation of various NiO layers and cluster on Cu(111) is shown. The spread for the NiO clusters, grown from 0.5 ML nickel on Cu(111) (the oxidation of these will be discussed in Chapter 4.2.4) is very low, with a mean remaining intensity of 0.71. If we now take the mean value of 6.75 Å from the range for the IMFP in NiO calculated from the experimental data in Chapter 4.1.4, this gives as a damping factor of 0.70. As 0.5 ML nickel should give approximately 1 ML NiO, the expected remaining intensity should be 0.70, which fits rather nicely to the value of 0.71, implying that the desired nickel amounts have been achieved. 2 ML of nickel should give 4 ML of NiO, leading to an expected remaining intensity of 0.24. Although the spread found in Figure 4.15 (b) for the thin nickel oxide layers, grown from 2 ML nickel, is much larger than for the nickel oxide clusters, the average value for the remaining intensity of 0.27 again fits rather nicely to the expected values. The larger spread is attributed to the longer evaporation times needed for the evaporation of 2 ML nickel compared to 0.5 ML nickel, which makes the evaporation process more sensible to fluctuations in the evaporation rate. It should be noted, however, that in this discussion the difference in damping behavior due to a surface roughening found for the NiO, as discussed below, has been disregarded as it is expected to be small.

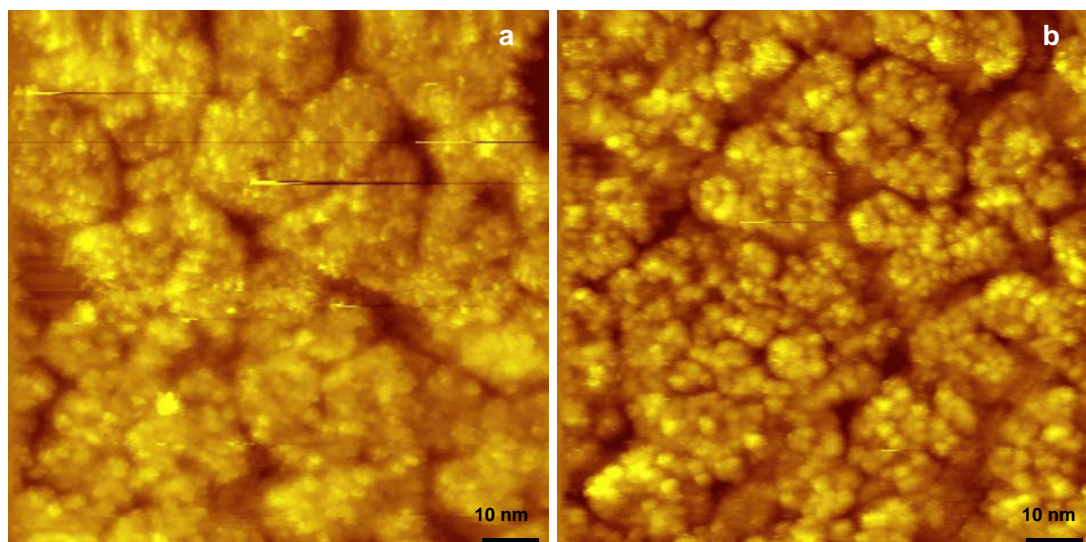


Figure 4.16: (a) 2 ML nickel on Cu(111) oxidized with 160 L of oxygen at room temperature (b) Same area after annealing to 500 K

As no long range order was found for the thin NiO layers when they were studied with LEED, STM measurements were performed by Florian Buchner, Elisabeth Zillner and Hubertus Marbach in order to elucidate the surface structure. The results are shown in Figure 4.16. The surface shows no defined structure, with the NiO growing in a bulky, cauliflower-like structure.

Figure 4.16 (b) shows the layer after the annealing to 500 K. This apparently increases the surface roughening even more, but also leads to better defined structures generating a sharper STM picture. The surface structure, however, is not improved, the whole surface appears very rough. Neither before nor after the annealing to 500 K gaps in the NiO layer reaching down to the Cu(111) are observed, indicating that the layers are closed. A very similar STM picture was found by Knudsen et al. [76] while studying the oxidation of Ni(111) at 300 K. This shows again the great similarity of these thin NiO layers on Cu(111) with the NiO layers grown on Ni(111) at 300 K.

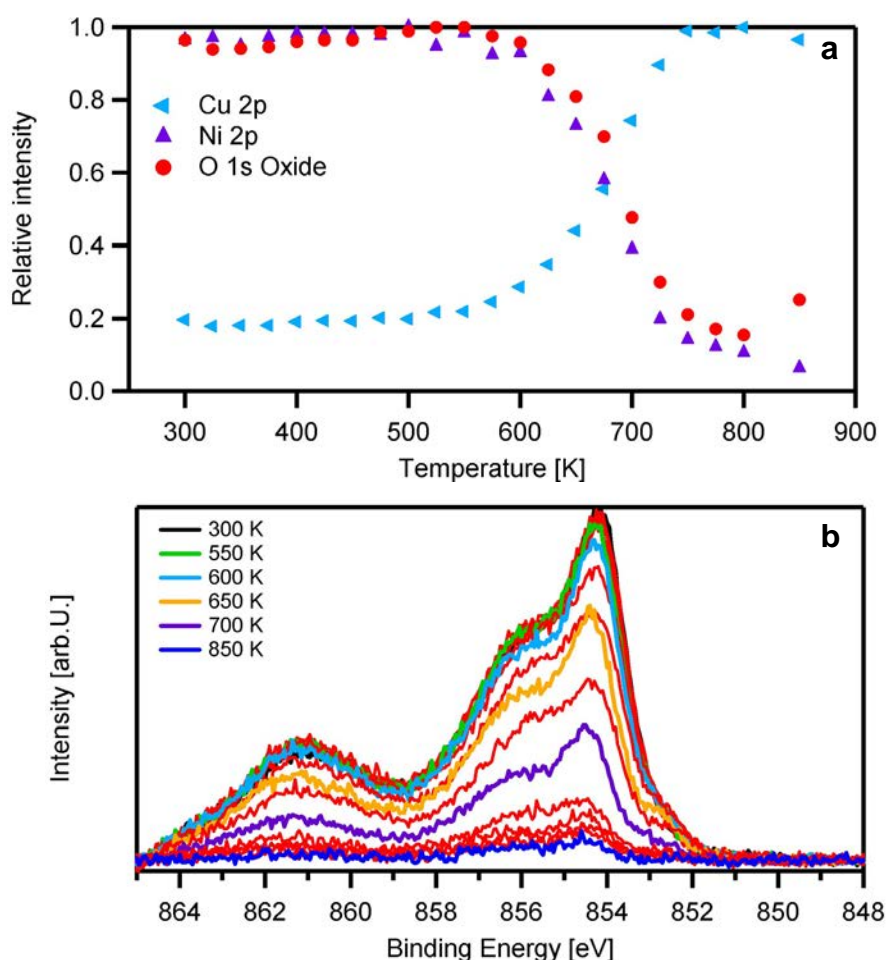


Figure 4.17: (a) Thermal evolution of the signal intensities from all relevant core levels for a thin NiO layer grown from 2 ML nickel on Cu(111). All signal intensities referenced to highest intensity in the corresponding core level. (b) Ni 2p region during TPXPS

In order to determine if any oxygen is lost during the annealing to 500 K after the oxidation at 300 K, and to determine whether or not copper atoms segregate on top of the NiO layers above 300 K, as they do for metallic nickel layers on Cu(111) [37], a freshly oxidized layer was heated resistively in 25 K steps up to 850 K, with a spectrum taken after each heating step for the Cu 2p, Ni 2p and O 1s core levels. The signal intensities for the Cu 2p and

Ni 2p regions and for the oxide peaks from the O 1s region is shown in Figure 4.17 (a).

Each intensity is referenced to the highest intensity observed for that particular core level. Between 300 and 550 K all intensities go up slightly. This is attributed to a lower damping due to the continuous reduction of the hydroxide coverage (data not shown). This reduction will be discussed in detail in Chapter 7.2. Above 550 K, both the oxygen and the Ni 2p intensity start to decrease, while the Cu 2p intensity starts to increase. The intensity increase of the Cu 2p spectra is attributed to reduced damping due to a loss of adsorbates. The intensity loss of the Ni 2p spectra shown in Figure 4.17 (b) is not accompanied by a spectral change. A decomposition of the NiO with loss of oxygen would lead to a spectral change, due to a reduction of NiO to metallic nickel. A possible desorption of the oxygen with a subsequent fast diffusion of the metallic nickel to the bulk is ruled out by looking at the final intensity for the oxygen in Figure 4.17 (a). At 850 K the oxygen coverage increases again, due to the oxygen diffusing from the bulk to the surface. From this we can conclude that both the nickel and the oxygen diffuse into the bulk above 600 K. Oxygen diffusion out of the bulk of the crystal to the surface was also witnessed after the experiment during the cleaning of the crystal. Due to this behavior the thin NiO layers and the NiO clusters were removed by sputtering instead of annealing. A similar segregation of nickel atoms to the surface at elevated temperatures was not found.

4.2.4 Preparation of NiO clusters on Cu(111)

NiO clusters were grown from 0.5 ML thick nickel layers on Cu(111). Due to the possible segregation effects for copper onto the nickel layers above 300 K [37], the oxidation temperature was again chosen as 300 K with subsequent annealing to 500 K, to obtain similar results as for the thicker nickel layers. As 320 L of oxygen were found to be sufficient to completely oxidize 2 ML of nickel on Cu(111), as discussed in the previous Chapter, the same amount was used for the 0.5 ML thick nickel layers. The corresponding Ni 2p and O 1s spectra during the different preparation steps are shown in Figure 4.18 (a) and (b), respectively. The metallic nickel prior to oxidation is characterized by the main peak at 852.5 eV and the satellite peak at 857.7 eV, as determined by fitting the data (fit not shown). Although the distance between the two peaks is the same as for 2 ML on Cu(111), both are shifted to lower binding energies by 300 meV. The main reason for this should be the stronger interaction between the adsorbed nickel and the copper substrate. Even for the 2 ML thick nickel layers the substrate certainly plays a role, as evident in the shift of the satellite peak by 0.7 eV compared to bulk nickel.

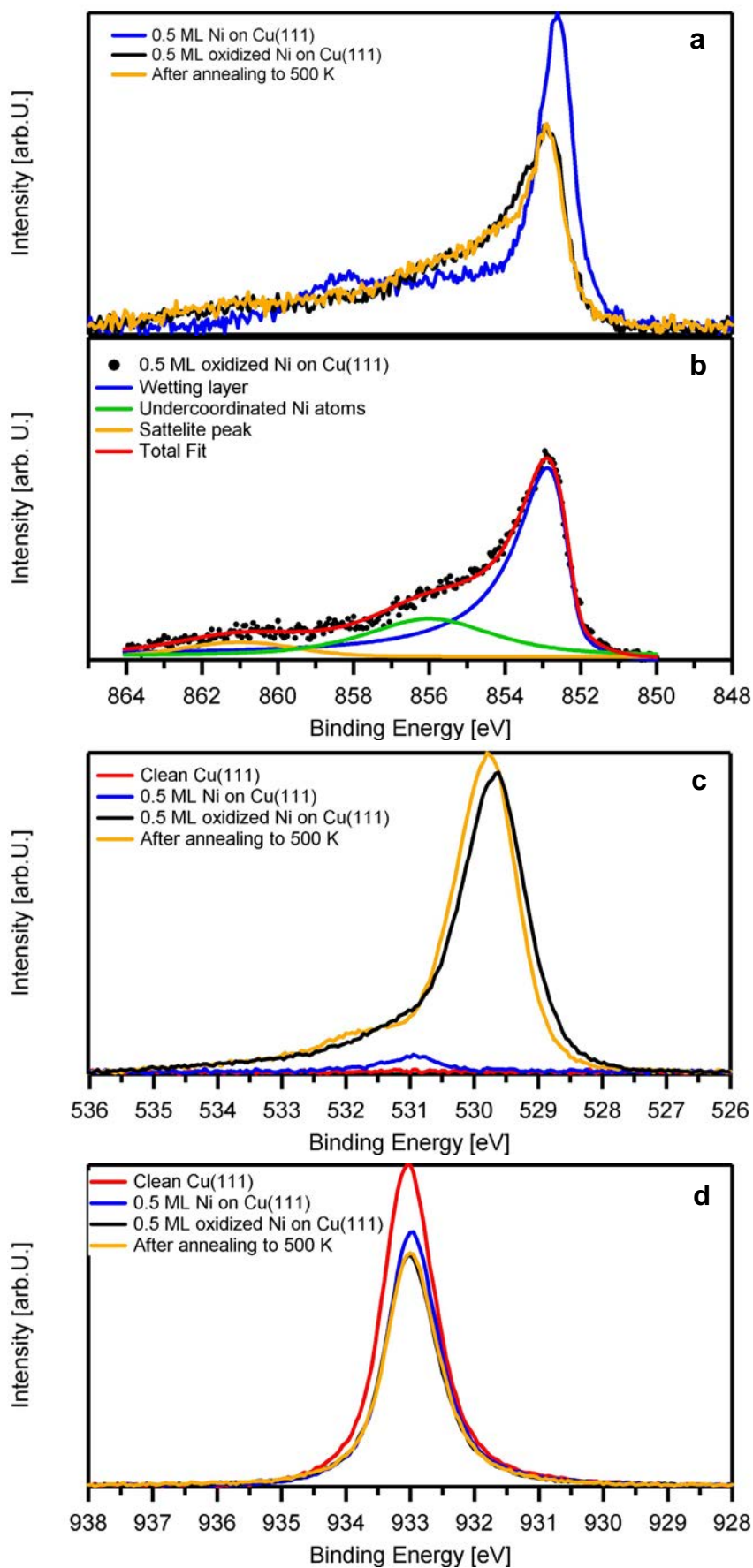


Figure 4.18 (on previous page): Preparation steps for NiO clusters grown from 0.5 ML nickel on Cu(111) (a) Ni 2p spectra (b) spectrum of the oxidized surface fitted with Pseudo-Voigt functions under the assumption of a model proposed by Höfert et al. [127] for NiO /Pd(100) (c) O 1s spectra (d) Cu 2p spectra

However, since in that case there are two nickel layers the substrate will certainly have less influence than for the 0.5 ML thick nickel layers, where all nickel atoms are directly on top of copper atoms instead of at least half of them on top of nickel atoms as is the case for the 2 ML thick layers. In the O 1s region again a small CO peak at 530.9 eV is seen for the metallic nickel layer, which is gone after the oxidation.

After oxidation the Ni 2p signal changes its shape to a shape that is somewhat reminiscent of the shape found for the two previously discussed NiO preparations, but which is significantly shifted towards lower binding energies. Two different interpretations are possible for this spectrum. If the spectrum is fitted with the same parameters used for the other NiO layers, the three NiO peaks are found at 853.0, 854.6 and 860.0 eV, meaning they are shifted by 1.1 eV towards lower energies in respect to the binding energies found for the thin NiO layers on Cu(111), which were prepared from 2 ML nickel. There is also a remnant of ~ 19 % metallic nickel, as determined from this low quality fit (fit not shown). In CO adsorption experiments on this surface, which are discussed in detail in Chapter 7.4, no peak for CO on nickel was found, so this metallic nickel component has to be due to undercoordinated atoms within the NiO and not due to larger unoxidized patches of nickel. If we further take into account the results we obtained for acetylene adsorption experiments on this surface, as discussed in Chapter 6.1.4, where acetylene adsorbs both on the NiO clusters and the bare Cu(111) patches in between them, but with much lower coverages than expected, it seems most likely that such undercoordinated atoms are mainly found at the edges of the clusters, influencing the electronic structures around them both for the NiO and the substrate in such a way that acetylene adsorption there is not possible any more.

An alternative explanation for the Ni 2p spectra is gained by comparing them with results obtained by Höfert et al. [127] for thin NiO layers on Pd(100). For this system Granozzi and coworkers [128-131] could show with a variety of methods that the first layer of NiO forms a wetting layer, which consists of Ni₃O₄. Höfert et al. [127] could show that this wetting layer also appears in high resolution Ni 2p XP spectra of this system, and developed a fitting procedure for it. Applying this model to the data presented here yields the fit displayed in Figure 4.18 (b). Please note that this fit was done with Pseudo-Voigt functions instead of the Donjac-Sunic function used for all other fits. This fit reveals three components, one at 853.1 eV which is attributed to the

wetting layer, one at 856.0 eV which is attributed to the undercoordinated nickel atoms on the surface [132] and the satellite located at 861.0 eV. This fit, which is in fact not much different from the fits used for the other NiO layers, as it has the same number of peaks with similar assignments, clearly shows that indeed the nickel is oxidized here as well. The observation that the binding energy of the main oxide peak is much closer to the metallic peak here as compared to the other NiO preparations can be attributed to the wetting layer nature of the NiO here. This can also be taken as a sign that we do not have stoichiometric NiO in this case, but rather some form of undercoordinated NiO like the Ni₃O₄, which was proposed for the wetting layer on Pd(100) [127]. If we add the OH coverage to the oxide coverage obtained from the O 1s spectra, we get a total amount of 0.67 ML, which would indeed give a Ni₃O₄ species considering the nickel coverage of 0.5 ML. This, however, does not take into account that the oxygen coverage has a relatively large error here, due to some oxygen adsorbed on the copper surface and also due to the complicated three-dimensional structures of the clusters, which lead to damping effects which cannot be easily corrected. This three-dimensional structure also explains the presence of the undercoordinated nickel atoms in the Ni 2p spectra, where the wetting layer peak is interpreted to arise from the base layer of the clusters, while the other peak is attributed to the rough surface of the clusters. As no other nickel oxide thicknesses besides the NiO clusters and the thin NiO layers have been prepared on Cu(111) within this thesis, no further information can be gained whether or not here really a wetting layer is formed or up to which coverages it exists. However, this model and its similarity to the interpretation used for the thicker NiO layers still show that the clusters indeed consist of NiO, although there is indication that the stoichiometry deviates from the thicker NiO layers.

After the oxidation, the surface was annealed to 500 K, to guarantee a similar preparation as the one used for 2 ML thick nickel layers. The spectra in Figure 4.18 (a) show that this had almost no effect on the Ni 2p spectrum, indicating that neither a migration of copper atoms on top of the NiO clusters, which would lead to dampening takes place, nor any nickel or oxygen is lost otherwise. Figure 4.18 (c) shows the O 1s spectra after the oxidation and after annealing to 500 K. The main oxide peak is found at 529.7 eV. The oxide shoulder peak found at the other oxide layers is also found at 528.7 eV, but only contributes around 3 % to the total oxide intensity. The total oxide coverage found in this case is 0.52 ML, which is in the expected oxygen range considering the nickel coverage of 0.5 ML. The high binding energy tail of the spectrum shows a hydroxide peak at 531.0 eV with a coverage of ~ 0.15 ML. Surprisingly only very minor carbonate contaminations of less than 0.01 ML

are found on the NiO clusters on Cu(111), this will be discussed in detail in Chapter 7.3. The long tail at high binding energies could be an indication of some oxygen on Cu(111), as it is also found in the corresponding spectrum (see Figure 4.12 (a)). On the other hand, if we consider that oxygen on Cu(111) saturates after 1700 L at a coverage of 0.45 ML, and the coverage grows linearly [118], a dose of 320 L as we used in this experiment should give no more than 0.085 ML oxygen on the Cu(111) surface. So the majority of the 0.52 ML oxygen found here is oxygen from the NiO. Considering this, the high energy tail of the spectrum could be a loss feature unique to the copper surface and not necessarily connected to oxygen directly adsorbed on Cu(111). Annealing to 500 K leads to a shift of the main oxide peak to 529.8 eV. The oxide shoulder peak is not found after the annealing experiment, and the hydroxide peak is shifted towards 531.5 eV. This shift to higher binding energies after the annealing is in good agreement with the NiO layers discussed previously, as well as the intensity loss for the oxide shoulder, and indicates a complete restructuring of the surface to the octopolar reconstruction. The slight difference in the O 1s binding energies compared to the binding energies found for the thin NiO layers in the previous Chapter is attributed to a stronger influence of the copper substrate, due to the thinner layers. The Cu 2p spectra are shown in Figure 4.18 (d). The evaporation of the nickel layer on top of the Cu(111) surface and the subsequent oxidation lead to a damping of the copper signal, as already seen for the thicker (2 ML) nickel layers discussed previously. No change in spectral shape is seen, which means that even though the copper surface is directly exposed to the oxygen beam during the oxidation of the nickel clusters the copper surface is not oxidized, which is in accordance with the oxygen adsorption experiments discussed in Chapter 4.2.1. Annealing the surface to 500 K has no effect at all on the copper signal. As seen already on the Ni 2p signal before, this is again evidence that no copper atoms segregate on top of the NiO clusters, indicating that the clusters are stable up to 500 K.

Figure 4.19 shows the STM results obtained for the oxidation of 0.5 ML nickel on Cu(111). The nickel grows in roughly hexagonal islands on the Cu(111) surface, see Figure 4.19 (a). Upon oxidation at 300 K, again the rough cauliflower like structure already observed for the thicker (2 ML) NiO layers on Cu(111) evolve again. The dark triangular features have been reported in literature [119, 133] to be a feature of the interaction of oxygen with Cu(111). They are attributed to a Cu_2O like terrace oxide, which starts to grow at step edges. In Figure 4.19 (c) these structures are gone after annealing to 500 K. As discussed in Chapter 4.2.1 the Cu 2p binding energy of Cu_2O is only different by 0.1 eV from the binding energy of metallic copper [120], and thus it is not possible to determine from the XPS data whether or not Cu_2O is

present on the surface. On the other hand the spectral shape of the Cu 2p (see Figure 4.18 (d)) remains unchanged both upon oxygen exposure and subsequent annealing to 500 K.

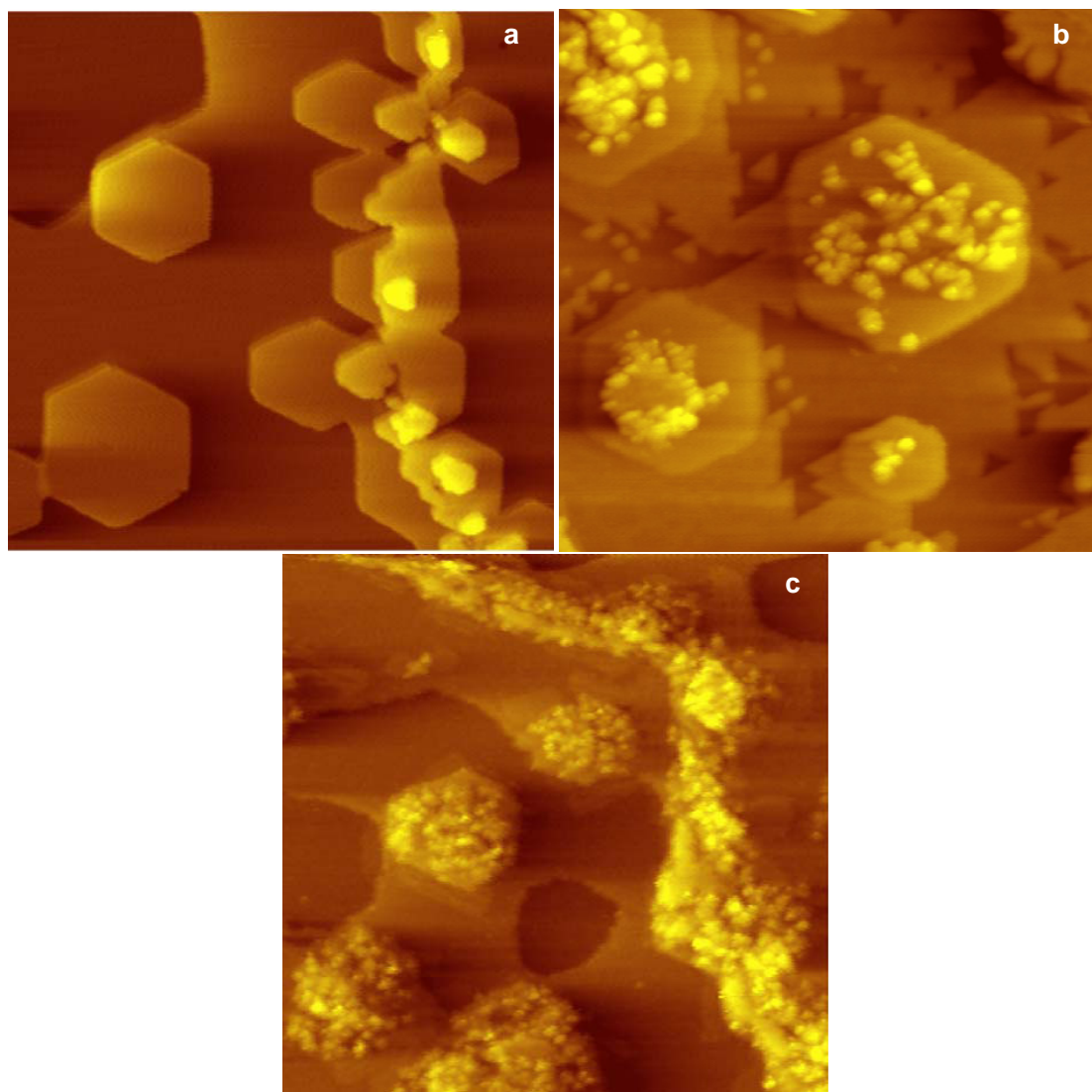


Figure 4.19: All pictures are 100 nm*100 nm **(a)** STM pictures of 0.5 ML nickel on Cu(111) **(b)** 0.5 ML nickel on Cu(111) oxidized with 160 L oxygen at 300 K **(c)** 0.5 ML nickel on Cu(111) oxidized with 160 L of oxygen at 300 K and subsequently annealed to 500 K

If the triangular structures seen in Figure 4.19 (b) really belong to a Cu_2O species instead of a chemisorbed oxygen species a slight spectral change in the Cu 2p spectrum would be expected both when they appear (i.e. after the oxidation of the 0.5 ML nickel on Cu(111)) and when they disappear again after annealing to 500 K. As such a change is not observed no Cu_2O should be present on the surface. The NiO structures appear to have grown after the annealing step, and look very similar to the structures found for the oxidation of the 2 ML thick nickel layers. From the STM picture it looks like the NiO is

distributed on the surface both in isolated islands and in longer stripes of connected smaller islands.

4.3 Comparison of the different preparations and summary

In this Chapter we studied the oxidation of a Ni(111) surface at various temperatures, and of two nickel layers of different thicknesses on Cu(111) at room temperature.

For low exposures of ~ 1.5 L of oxygen on Ni(111) the well known p(2x2) structure of chemisorbed oxygen [3, 65, 68, 69] with a coverage of 0.25 ML was prepared, with the LEED structure obtained for a surface temperature of 600 K. For higher exposures at 300 K, the highest coverage found for the chemisorbed oxygen species was 0.75 ML. The corresponding peak is found at a binding energy of 529.6 eV and shows an asymmetric peak shape. At even higher coverages the oxidation of the Ni(111) surface starts. The oxide peak has a symmetric peak shape, and the binding energies at which the main oxide peak is located for the various different preparations is listed in Table 4.2.

Surface and preparation	Binding energy of oxide main peak [eV]	Binding energy of oxide shoulder peak [eV]	Intensity ratio of total oxide intensity for oxide shoulder peak
Ni(111) oxidized at 300 K	529.6	528.6	22 %
After annealing to 500 K	529.7	528.7	14 %
After annealing to 600 K	529.8	528.8	11 %
Ni(111) oxidized at 500 K	529.9	528.8	7 %
Ni(111) oxidized at 550 K	529.9	528.9	6 %
2 ML nickel on Cu(111) oxidized at 300 K	529.8 (Start)- 529.5 (End)	528.8 (Start)- 528.5 (End)	12.5 %
After annealing to 500 K	529.7	528.6	3 %
0.5 ML nickel on Cu(111) oxidized at 300 K	529.7	528.7	3 %
After annealing to 500 K	529.8	-----	0 %

Table 4.2: Binding energies and intensity ratios for the two oxide species for the different NiO preparations

The binding energy of 529.6 eV is close to the values reported for NiO(111) on Ni(111) by several authors [79, 80, 89], and it is reported in literature that NiO(111) is the preferred orientation for these oxidation conditions [68, 69, 76, 79, 83]. A large hydroxide contamination of up to 1 ML also points to NiO(111) as the present surface orientation, as NiO(100) is very unreactive towards water, while the otherwise unstable NiO(111) surface was found to be stabilized by OH [79, 88, 89]. The position of the hydroxide peak shifts between 531.0 and 531.6 eV, dependent on coverage and annealing temperature, and is discussed in detail in Chapter 7.2. Another important contamination found was NiCO₃, which is mainly characterized by a peak in the C1s region at 289.0 eV. The O 1s binding energy of the carbonate is close to that of OH and thus cannot be distinguished. Like the OH contamination this contamination grows due to residual gases in the chamber over time. A detailed discussion of this species is given in Chapter 7.3. The Ni 2p spectra show a complete oxidation within the escape depth of the photoelectrons. From this escape depth an approximate IMFP for the photoelectrons of 6.6 Å and a rough estimation of the oxide layer thickness was made, giving a value between 5.4 and 9.5 ML (18-32 Å). The evolution of the oxide coverage shows both in the O 1s and the Ni 2p region an oxidation rate that seems to continuously decrease, but further investigation shows that the oxidation rate in fact is constant and the continuously slower increase of the oxygen coverage is due to the self damping of the NiO layers. Full oxidation within the escape depth of the photoelectrons is reached at 425 L. Annealing to higher temperatures leads to shifts of the oxide main peak both in the O 1s and Ni 2p region towards higher binding energies, and a reduction of the hydroxide content. These effects are discussed in Chapter 7.

An interesting aspect of the oxide layers is the appearance of a large “shoulder oxide” contribution in the O 1s spectra at ~ 1 eV lower binding energies in respect to the main oxide peak. This shoulder oxide peak was not detected up to now. The evolution of this peak during the surface oxidation, points to it as a second oxide species, which might be due to the surface structure of the oxide. This species is responsible for 22 % of the total oxide intensity for the fresh oxide layers grown at 300 K. If this second oxide structure is indeed found at the surface, i.e. the corresponding photoelectrons are not damped; this is equivalent to ~0.5 ML coverage for this species. In Table 4.2 the ratio decreases continuously upon annealing of the sample, while the total oxide intensity remains constant, which also points to an oxide species as the origin for this peak. A corresponding peak in the Ni 2p spectra was not found. If the surface is oxidized at higher temperatures the coverage of this species is even lower. As for higher oxidation temperatures the surface should mainly consist of the octopolar reconstructed surface structure

[82, 84], while the oxide layers oxidized at room temperature are flat and hydroxyl-stabilized, this points towards the shoulder species being mainly a feature of the hydroxylated flat surface. However, this species is also present in low concentrations of ~ 6% in the layers that are oxidized at 550 K, which were not hydroxylated. As the formation of the octopolar reconstruction involves activated transport processes of NiO, it is possible that also some intermediate structures are present on the surface due to kinetic limitations [82]. So this shoulder oxide species could also be due to these intermediate structures. The lower content of the oxide shoulder is attributed to the higher temperature, as an increase in temperature was shown to lower the content of this species also for the oxide layers grown at 300 K. No further insight in the nature of this species is gained from our XPS data, and for a clear assignment other methods, preferably theoretical simulations are needed.

The binding energies of the NiO grown at 500 K and above are shifted by 0.3 eV towards higher binding energies both in the O 1s and the Ni 2p region. Aside from the binding energy shift the Ni 2p spectra are very similar to the ones for the 300 K oxidation, again indicating complete oxidation of the layers within the escape depth of the photoelectrons. Due to this, the layer thickness is in the same range estimated for the oxide growth at 300 K. Apart from the binding energy shift and the lower contribution of the oxide shoulder peak the O 1s spectra also reveal a much lower hydroxide content. If the oxidation is performed at 550 K the hydroxide contamination was suppressed completely. For both oxidation temperatures the carbonate contamination was also found to be smaller. Another remarkable difference to the oxidation at 300 K is the evolution of the oxidation. At 500 K the oxidation within our sampling depth is only finished after an exposure of 800 L, which is almost double the exposure needed for the oxidation at 300 K. The general shape for the oxidation curve at 500 K is similar as that for the oxidation at 300 K. At 550 K the oxidation only needs 400 L of oxygen, confirming a reported faster oxidation for higher temperatures [70]. At 600 K, NiO was found to be unstable, allowing no complete oxidation within the escape depth of the photoelectrons, even for a total exposure of 4850 L oxygen.

If we compare the two oxidation temperature ranges we find many small differences that could indicate that the NiO grown at 300 K is different from the NiO grown at 500 K and above. These differences are the binding energy for the NiO both in the O 1s and the Ni 2p region, the oxidation speed, the intensity of the oxide shoulder peak and the hydroxide and carbonate content of the oxide layers. However, many of these differences can also be explained by the different surface temperatures, as all of these features were shown to be dependent on temperature in the respective Chapters of this thesis. There is also to consider that, even though the hydroxide content goes down to zero

for an oxidation temperature of 550 K, these layers are still shown to be very reactive towards water in Chapter 7.2. Towards other adsorbates, namely acetylene (see Chapter 6.1), CO₂ (see Chapter 7.3) and CO (see Chapter 7.4) these layers also exhibit a very similar behavior as the thin NiO layers on Cu(111), which are oxidized at 300 K and overall very similar to the NiO layers grown on Ni(111) at room temperature. All of these arguments point towards the interpretation that the layers prepared at 500 or 550 K have (111) orientation as well, even though literature reports a (100) orientation of the NiO [79, 81, 83] for oxidation temperatures of 500 K and above. The best explanation comes from the fact that STM studies reported that these NiO(100) films contain islands of (111) orientation [79, 81, 93]. These islands were reported to grow upon interaction with water [79, 93], and from a comparison between the studies it is also evident that the fraction of the surface covered with these islands increases with higher exposures. As this fraction is already around 10 % for an exposure of 150 L [81], the much higher exposures used within this thesis can easily lead to these islands covering the whole surface. Still the layers grown at 500 or 550 K are much cleaner, i.e. have a much lower hydroxide and carbonate content than the layers grown at 300 K. This, as well as the differences in binding energy, can be attributed to a restructuring of the surface at higher temperatures. At room temperature the surface is mainly flat and stabilized by hydroxide [82], as already reported in previous studies on this system [79, 88, 89]. For higher temperatures this hydroxylation can be partially lifted, and the surface is converted to the octopolar reconstruction [82].

In order to study thinner NiO layers and NiO clusters these were prepared by evaporating 2 ML and 0.5 ML nickel on a Cu(111) surface and subsequently oxidizing them at 300 K. A higher oxidation temperature, which would be preferable due to the lower contamination content by hydroxide and carbonate found for the oxidation of Ni(111) was not possible, as in a study by Domnick et al. [37] copper atoms were found to segregate on top of the nickel layers above 300 K. The overall oxidation behavior of the 2 ML thick nickel layers on Cu(111) was found to be very similar to the oxidation of Ni(111) at 300 K. The final binding energies for the NiO both in the O 1s and Ni 2p region are almost identical to the ones found for the NiO(111) on Ni(111). An interesting difference is that the two oxide peaks in the O 1s region shift by 300 meV during the course of the oxidation, which has to be due to either the influence of the copper substrate or the thin layer nature of the nickel. The oxide shoulder peak is found again and contributes 12.5 % to the total intensity, which is less than for the NiO(111) on Ni(111). The oxygen uptake curve also resembles the one for the 300 K oxidation on Ni(111) up to an exposure of 200 L, where it abruptly ends, due to the complete oxidation of all available

nickel atoms. Due to the great similarities in the spectra and the oxygen uptake curve between the two 300 K oxidations on Ni(111) and the thin nickel layers on Cu(111) it seems reasonable to assume that NiO(111) is growing on Cu(111) under these conditions, which is also in agreement with a study where NiO was directly evaporated on Cu(111) at 300 K [116]. The Cu 2p signal is damped and no change in the spectral shape upon the evaporation and subsequent oxidation of the nickel occurs, so a significant oxidation of the copper is ruled out. Minor amounts of Cu₂O, however, are still possible, as the binding energies for Cu₂O and metallic copper are very similar [120], so that an undetected minority species can not be ruled out. As oxygen was only found to interact very weakly with Cu(111), saturating at 0.45 ML after a linear coverage increase at an exposure of 1700 L oxygen at room temperature, the exposure of 320 L used for the oxidation of the nickel layers should only lead to a maximum of 0.08 ML Cu₂O. STM pictures revealed a very rough, cauliflower-like surface lacking both long and short range order. Annealing the surface to 500 K led to sharper pictures but did not improve the surface order. The annealing step was introduced to reduce the hydroxide contamination. Both the Ni 2p and Cu 2p spectra remain completely unchanged after the annealing step, showing no segregation of copper atoms on top of the NiO layers or of NiO into the bulk taking place up to this temperature. In the O 1s region, the annealing step leads to a conversion of some of the oxide shoulder species to the main oxide species, and a shift of the peaks to higher binding energies, which is again a similar behavior to the one observed for the NiO(111) layers on Ni(111). Due to these similarities, and similar STM pictures for the oxidation of Ni(111) at room temperature [76] to the ones we acquired for the NiO layers on Cu(111), it is assumed that the NiO(111) layers on Ni(111) also have this cauliflower like rough surface structure. In catalysis a rough surface is desired attribute, as it adds more potential reaction sites and thus we can conclude that the rough nature of the surface is favorable for catalysis.

The final NiO structure we prepared were nickel oxide clusters on Cu(111). For these, 0.5 ML thick nickel layers on Cu(111) were oxidized at room temperature and subsequently annealed to 500 K. The O 1s spectra are similar to the spectra from the thicker layers, with the two oxide peaks at slightly higher binding energies. The same binding energies were found during the onset of the oxidation of the 2 ML thick nickel layers. This points towards an influence of the copper substrate on the binding energy. A new feature in the O 1s spectra is a high energy tail, that is also found for oxygen on Cu(111). As oxygen on Cu(111) can only be a minority species here, due to the low exposure of 320 L, this tail is attributed to a general loss effect due to the copper substrate. The oxide shoulder peak is only very weak and

disappears completely after the annealing step. The Ni 2p spectra are very different from the ones found for all other oxide preparations. They can either be fitted with the same peak parameters, but then the NiO peaks are shifted by 1.1 eV towards lower binding energies and a contribution by metallic nickel atoms is found. These metallic nickel atoms would be attributed to undercoordinated atoms within the NiO layer in this model. Alternatively, in a different interpretation analogous to data of NiO on Pd(100) [127], the spectrum can be fitted without the metallic nickel in a way that attributes the main peak to a NiO wetting layer, that could be an undercoordinated NiO, most likely Ni₃O₄. The Cu 2p spectra again show no sign of oxidation. Cu₂O like structures [119, 133] seen in the STM pictures after the nickel oxidation at 300 K disappear after the annealing step, while the Cu 2p peak remains unchanged. As also the Ni 2p spectrum remains almost constant after annealing any copper or nickel diffusion is ruled out again. As copper was reported to diffuse on top of metallic nickel layers above 300 K [37] this also points to a complete oxidation of the nickel layers. Due to the structural likeness with the thicker NiO layers observed in STM an (111) orientation of the NiO seems most likely, and due to the complete disappearance of the oxide shoulder peak after annealing to 500 K the majority of the surface should be octopolar reconstructed. A remarkable difference between the NiO clusters and the thin NiO layers on Cu(111) is that almost no carbonate contamination is detected in the NiO clusters, although both show significant hydroxide contaminations.

5 Adsorption and reaction of C_2H_x species on clean and oxygen precovered Ni (111)

Simple hydrocarbons are among the most important raw materials in chemical industry [2]. For their functionalization, clean or partially oxygen covered transition metal surfaces are widely used as heterogeneous catalysts [134-136]. In order to be able to optimize the reactivity and selectivity of existing catalysts as well as to develop new catalysts with tailored properties, it is necessary to gain insight into the elementary steps of the desired reactions in great detail. That means one has to study each elementary step of the reaction starting right from the adsorption of the respective hydrocarbon(s). During reaction it is also important to identify all intermediates and their possible interactions as these might play a decisive role. A typical example for such a heterogeneously catalyzed reaction is the oxidation of small hydrocarbons to form epoxides. Kao et al. [137, 138] showed that it is of particular importance to study and characterize the coadsorption phase of the hydrocarbons and oxygen, as just one example of the interaction of different possible reactants, in order to understand the basics of the surface reactions. The study of the Ni(111) surface is also very important for the application of Nickel as a catalyst in technical chemistry, as these catalysts usually contain small particles on a support like Al_2O_3 . These small particles are nanosized single crystals that exhibit, among others, (111) facets [1].

The adsorption of ethene on Ni(111) has been investigated by ultraviolet photoelectron spectroscopy (UPS) [139], various types of vibrational spectroscopies such as RAIRS (reflection absorption infrared spectroscopy) [140] and HREELS (high resolution electron energy loss spectroscopy) [141-144], diffraction methods like PhD (photoelectron diffraction) [145] and LEED (low energy electron diffraction) [141, 146], NEXAFS [147] (near edge x-ray adsorption spectroscopy) and TPD (temperature programmed desorption) [146, 148]. The chemisorbed layer of C_2H_4 displays a (2x2) LEED pattern with a nominal coverage of 0.25 ML [141, 146]. In all of the above mentioned studies ethene is supposed to adsorb with its molecular axis parallel to the Ni(111) surface. However, the exact adsorption site is still under discussion, although the more recent studies seem to favor a model with ethene adsorbed at a bridge site with symmetric adsorption geometry. In this structure, both carbon atoms have equivalent local adsorption geometries above a Ni substrate atom [145, 147, 149, 150]. In contrast to this model, an ethene adsorption site with very low symmetry was deduced from vibrational spectroscopy [142], indicating nonequivalent local adsorption geometries for the two carbon atoms.

The dehydrogenation of adsorbed ethene to acetylene upon thermal treatment around 200 K was first reported by Demuth using UPS, TPD, LEED and HREELS [139, 143, 146]. Upon further thermal treatment acetylene dehydrogenates to nickel carbide, which was first reported by Hammer et al. based on HREELS experiments [144]. These findings were confirmed later on by various experimental techniques [141, 145, 148, 151] and theoretical calculations [149, 152]. In contrast, the coadsorption of oxygen and ethene has not been studied yet on Ni(111), but comparable experiments on Pd(111) [153] showed attractive interactions between oxygen and the hydrocarbons, influencing the adsorption geometry. Furthermore, on Pt(111), oxygen coadsorption results in major changes of the surface chemistry, leading to different reaction products [154].

Changes in the symmetry of an adsorbed molecule, in particular the local adsorption geometry of the carbon atoms in hydrocarbons, can lead to a clear shift in the C 1s binding energy in XP spectroscopy, as was shown in earlier studies [28, 155]. In other words, the number of different local adsorption geometries for carbon atoms within one molecule, should be reflected by a corresponding number of peaks in the C 1s XP spectra. For ethene this would mean that for a symmetric adsorption site with equivalent carbon atoms one C 1s peak is expected, as can be seen in the gas-phase spectrum of ethene [31], were both carbon atoms are truly equivalent, while for a non-symmetric site with non-equivalent carbon atoms two C 1s peaks will be found. Note in this context that high resolution XP spectra of hydrocarbons also show a vibrational fine structure that has to be considered in the analysis. This fine structure can also be used to identify the CH_x (x=0-4) species [28, 31].

Ethane adsorption on Ni(111) has been much less studied than ethene adsorption on this surface. The main reason for this is that ethane as a saturated hydrocarbon can not easily form a chemical bond to the surface, limiting the focus to low temperature physisorption studies. For the desorption temperature of physisorbed ethane values of 85 K [138] and 99 K [156] have been reported. This places the desorption temperature on the lower end of the temperature range easily accessible by cooling with liquid nitrogen, which makes studying the adsorption process experimentally demanding. Due to the saturated nature of ethane at least one of the C-H bonds has to be broken to achieve chemisorption. One possible method to provide the necessary energy for the breaking of the C-H bond is using a seeded supersonic molecular beam. With this approach Hamza and Madix [157] studied dissociative adsorption of ethane on Ni(100). T. Fuhrmann [54] used a combination of a supersonic molecular beam and synchrotron radiation based XPS-measurements to study the dissociative adsorption of ethane on Ni(111) over a wide range of kinetic energies. He showed that the saturation coverage of

ethyle (C_2H_5) on Ni(111) depends on the kinetic energy of the impinging molecules. He also noticed a strong influence of the vibrational excitation of the molecule on the adsorption behavior. The highest saturation coverage of ethyle (C_2H_5) was 0.22 ML C atoms for a kinetic energy of 0.84 eV [54]. There also exist gas-phase XPS measurements for ethane [30] which can be used for comparison of the spectra. Some of the data obtained by T. Fuhrmann [54] is reevaluated in this work with a refined fitting routine, to allow a clear assignment of the two peaks in the corresponding C 1s spectrum. The coadsorption of oxygen with ethane or ethyle on Ni(111) has not been investigated so far.

The adsorption and thermal evolution of acetylene (C_2H_2) on Ni(111) has been studied more extensively than the adsorption of ethane. Demuth was the first to study this system with UPS [139] and later with TPD and LEED [158], reporting a $p(2 \times 2)$ layer corresponding to a coverage of 0.5 ML C atoms. Hammer et al. [141] reported the existence of a $(\sqrt{3} \times \sqrt{3})R30^\circ$ phase with a coverage of 0.66 ML C atoms for higher acetylene exposures of about 30-100 L. In that study acetylene was assigned to be adsorbed in a bridge-bridge configuration for both ordered phases; however later photoelectron diffraction studies [159] and DFT calculations [152] showed that at least for the $p(2 \times 2)$ phase acetylene adsorbs with both C atoms in adjacent hollow sites. The work done by Thomas Fuhrmann [54] on the adsorption of acetylene on Ni(111) is presented in Chapter 5.3.1, so that it can be used for comparison with the other discussed adsorption systems; the data for the thermal evolution was completely reevaluated in the context of this work with new conclusions. For elevated temperatures from a HREELS study [142] a splitting of the C-C bond of acetylene without dehydrogenation was reported above 400 K, with subsequent dehydrogenation above 500 K. Other studies [160-162] report on a partial trimerization of acetylene (C_2H_2) to benzene (C_6H_6) around 300 K, although this was only found for high coverages of acetylene. For the coadsorption of oxygen and acetylene on Ni(111) Demuth [158] found that oxygen hinders the adsorption of acetylene, whereas the adsorption of a second acetylene derived species, which was proposed to be CH, was not hindered by the preadsorbed oxygen.

Please note that all coverages given in figures are given as number of C atoms, not number of molecules. All the coverages were obtained by comparing the C 1s intensity of the discussed layers to that of a saturated ethene (2×2) layer on Ni(111) (Figure 5.1), which corresponds to 0.5 ML C atoms per Ni-atom.

5.1 Ethene

5.1.1 Ethene on clean Ni(111)

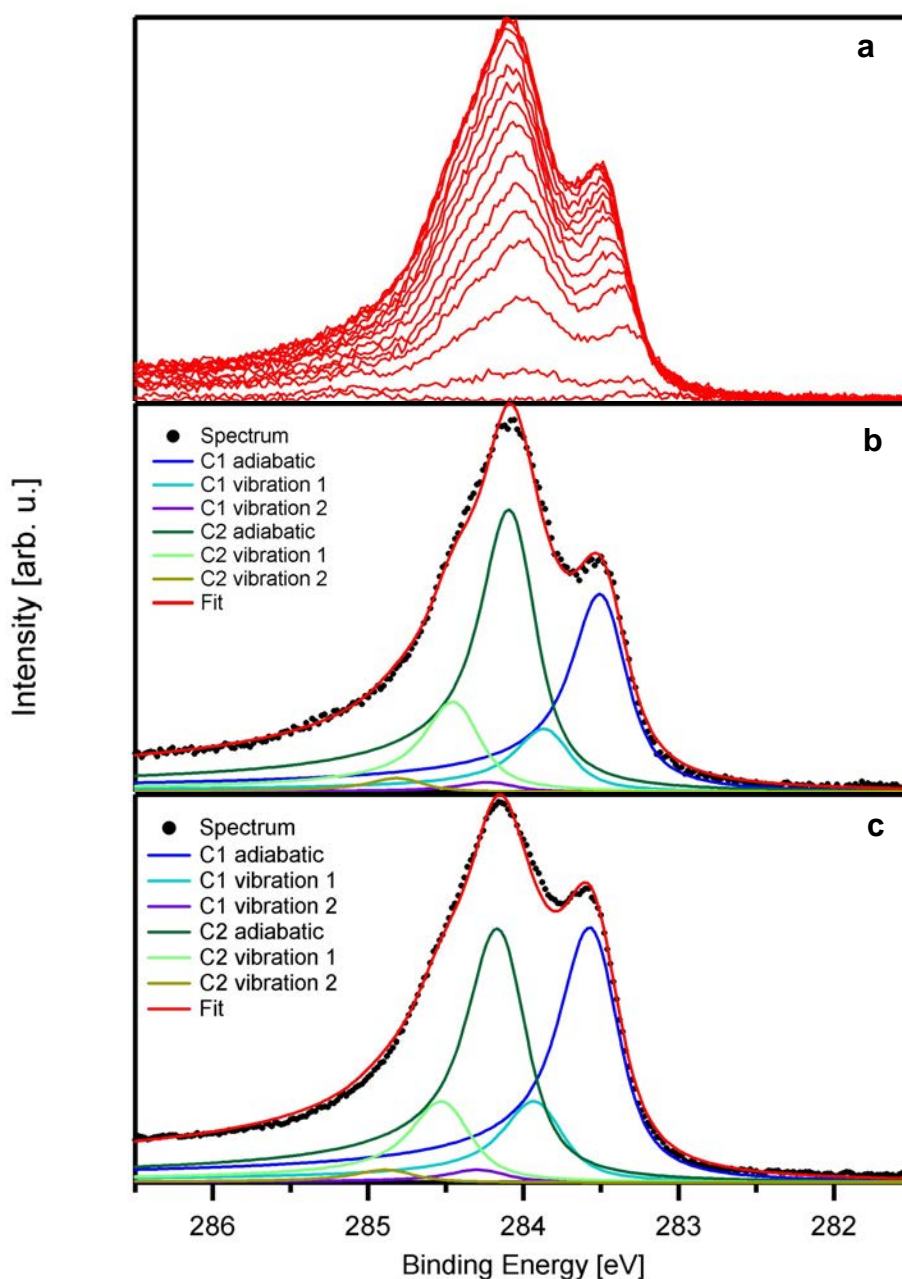


Figure 5.1: (a) Selected C 1s ($h\nu=380\text{eV}$) spectra of ethene adsorption on the clean Ni(111) surface, collected at 0° emission angle. (b) Fit of saturated ethene layer on Ni(111) collected at 0° emission angle. (c) Fit of saturated ethene layer on Ni(111) collected at 45° emission angle. Data for (a) and (b) taken from [54].

Ethene was adsorbed on clean Ni(111) at a surface temperature of 110 K. The corresponding C 1s spectra collected during the uptake can be seen in Figure 5.1. Thomas Fuhrmann [54] found for this system that two dominant peaks grow simultaneously at 283.35 and 283.98 eV, as obtained from the fitting procedure. For higher coverages the two peaks shift to higher binding

energies, with values of 283.48 and 284.07 eV, respectively, at saturation. The overall shape, i.e., the ratio of the peaks does not change during the uptake. These two peaks are assigned to the adiabatic Franck-Condon transitions from the vibrational ground state in the electronic initial state to the vibrational ground state in the ionic final state. There is general agreement in the literature [141, 146] that the coverage at saturation is 0.5 ML C atoms per Ni atom (0.25 ML ethene molecules). This saturated layer is used for the coverage calibration throughout Chapter 5, i.e., for all hydrocarbons adsorbed on Ni(111) and the NiO-layers. The fitting procedure used for the data is a refinement of the procedure used by Thomas Fuhrmann for this set of data [54], to test the validity of his results. The fit reveals four additional contributions to the spectra, two of which can be attributed to the transition from the vibrational ground state in the electronic initial state to the first excited C-H vibrational states in the final state ions; the other two can be assigned to transitions to the second vibrationally excited states. These peaks are shifted by 360 and 720 meV, respectively, to higher binding energies with respect to the adiabatic peaks at 283.48 and 284.07 eV. It should be noted, however, that fits with a vibrational splitting of 350-400 meV provided almost the same quality of the fit, with the splitting of 360 meV being the best fit, proving the assumptions made by Thomas Fuhrmann for this data set [54]. The S-factor, i.e., the ratio between the intensity of the vibrational contribution and the intensity of the adiabatic contribution [30, 31] is 0.32 ± 0.02 for the two peaks which are shifted by 360 meV in respect to the adiabatic peaks.

Steinrück et al. [28] showed that the C-H vibrational splitting in the ionic final state of simple hydrocarbons adsorbed on Pt(111) or Ni(111) is 5-10% larger than in the ground states. For ethene on Ni(111) previous HREELS [142] and RAIRS [140] studies found a value of 366 meV for the ground state, which is larger than the value of 360 meV that we found in the XP spectra. If we however take into consideration the range of 350-400 meV, in which we obtained reasonable fits, this result is still consistent with the general behavior observed by Steinrück et al [28]. In the same paper [28] it was shown that for simple hydrocarbons adsorbed on Ni(111) each C-H bond contributes 0.17 ± 0.02 to the S-factor. From the S-Factor of 0.32 ± 0.02 we therefore deduce that each carbon atom is bound to two hydrogen atoms as is expected for intact ethylene.

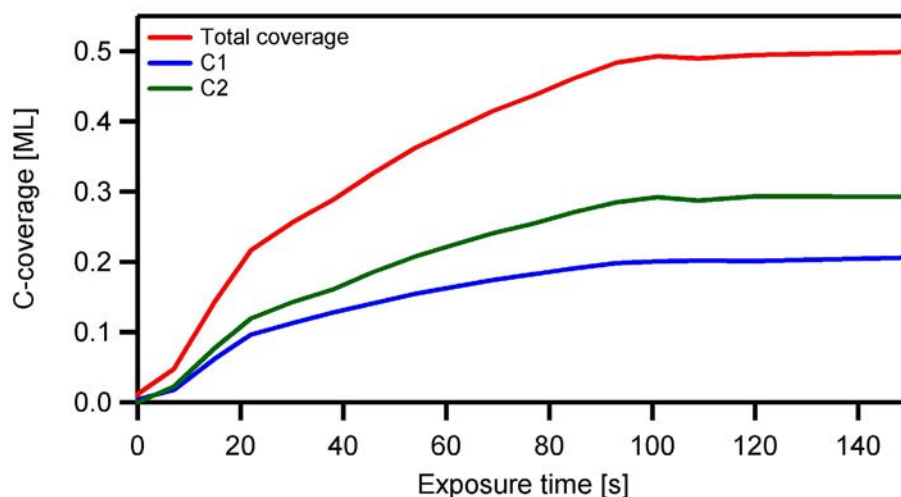


Figure 5.2: Quantitative analysis of the data from Figure 5.1 (a), taken from [54]

In Figure 5.2 the quantitative analysis of the data in Figure 5.1 is depicted. Evidently, the two main peaks (together with their vibrational contributions) grow simultaneously. From this and the identical S-factors and vibrational splittings we deduce that both peaks are due to molecular adsorption of a single ethene species. That leaves the question why the two adiabatic peaks show not the same intensity, as would be intuitively expected as they originate from the two carbon atoms of one ethene species. This can be attributed to photoelectron diffraction [163], which is a typical phenomenon observed at the low kinetic energies of around 100 eV used in our studies. If photoelectron diffraction plays a role, the intensity ratio between the two peaks should change if we measure at a different emission angle, which is indeed the case as can be seen from the comparison between Figure 5.1 (b) and (c). In Figure 5.1 (c), which shows data collected at 45° emission angle, the ratio between the two adiabatic peaks is indeed close to 1, as expected.

The existence of two peaks with different binding energies indicates that the two carbon atoms of the ethene species are in different chemical surroundings. Previous studies show that changes in the local adsorption geometry of a molecule can lead to clear shifts in the C 1s binding energies [28, 155], thus we conclude that both carbon atoms have to be adsorbed with different local geometries. We will now try to give an answer to the unsolved problem of the adsorption site of ethene on Ni(111), which is not solved in literature yet and which Thomas Fuhrmann also was not able to answer [54].

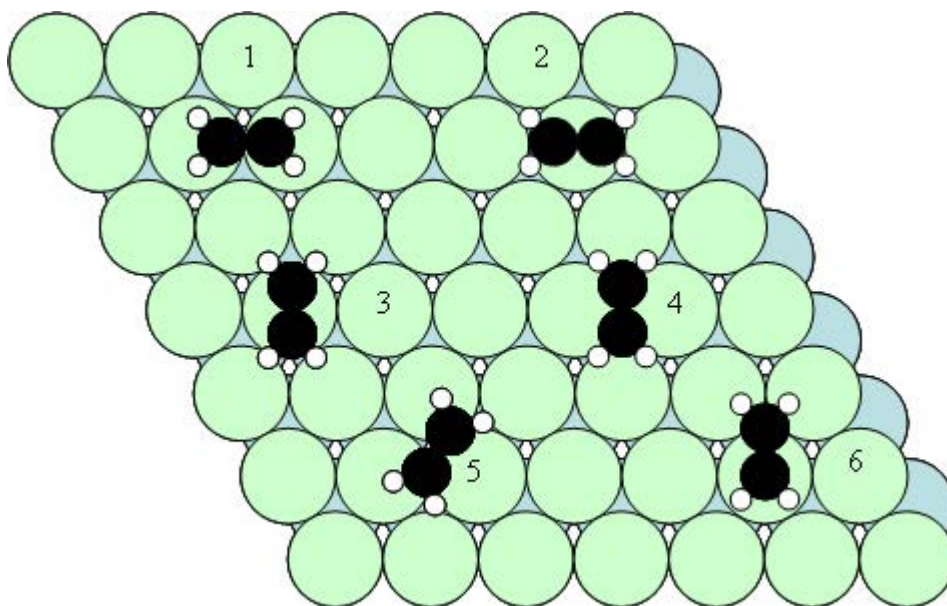


Figure 5.3: Schematic drawings of possible adsorption geometries on clean Ni(111) according to literature (see text)

In literature, there is no consensus about the adsorption geometry of ethene on Ni(111). From LEED studies it is known that the chemisorbed layer displays a (2x2) LEED pattern [141, 146]; hence the nominal coverage is 0.25 ML ethene molecules, which corresponds to 0.5 ML C atoms, at saturation. There is general agreement that the C-C axis is parallel or almost parallel to the surface, however there are many different suggestions for the symmetry of the adsorption site and the position of the C atoms. In a HREELS study by Baró et al. [164] it is proposed that the symmetry of the adsorption complex has to be either C_s (structures 5 and 6 in Figure 5.3) or C_2 (structures 1-4 in Figure 5.3) and possible adsorption sites were discussed in a LEED study [141]. The structure favored in most studies [145, 147, 149, 150] is structure 1 in Figure 5.3, with both atoms bound on adjacent Ni atoms in on-top positions. Other studies [141, 146] suggest a bridge/bridge geometry as depicted in structure 5 in Figure 5.3, or an on top/on top scenario where both carbon atoms are bound on top of the same Ni atom [149, 152] (Figure 5.3, structure 2).

However, all of these structures imply equal adsorption sites for the two carbon atoms of the ethene molecule. This situation should lead to only one adiabatic peak in the C 1s spectra, as is the case for acetylene and ethene adsorbed on Ni(100) [165], acetylene on Ni(111) [28] and ethene on Pt(111) [28]. Taking into account our findings of molecular adsorption, the long range order in a (2x2) superstructure and in particular the nonequivalent sites for the two carbon atoms, we can rule out all but one of the discussed possible adsorption geometries. We thus propose ethene to be adsorbed with one carbon atom on a hollow site and the second on an on-top like local

adsorption geometry as depicted in Figure 5.3, structure 6 and in Figure 5.4. When it comes to the assignment of the two peaks to the two adsorption positions it is noticeable that the binding energy of 283.48 eV is very close to the binding energy of 283.58 eV found for methyl on Ni(111) [28]. From density functional theory calculations [166] methyl is known to adsorb in a hollow position on Ni(111), and thus the peak at 283.48 eV is tentatively assigned to a C atom bound in a hollow site, the peak at 284.07 eV to a C atom bound in an on-top position. It should be noted, however, that these analogies have to be treated with some caution, since the comparison ignores differences in the bonding interaction to the substrate for the different species that might arise due to, e.g., the different hybridization of the carbon atom.

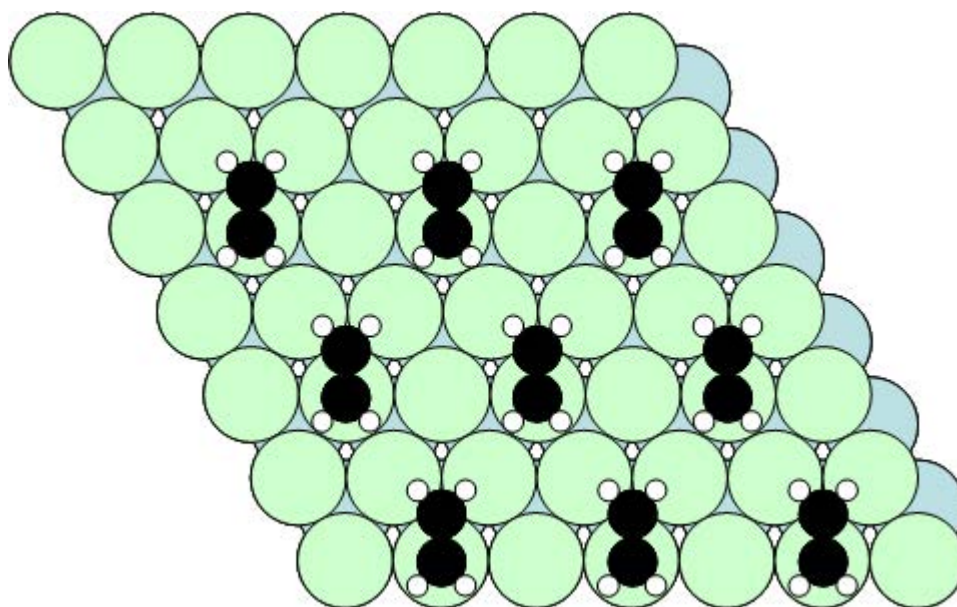


Figure 5.4: Schematic drawing of the proposed adsorption geometry of ethene on Ni(111) in a (2x2) superstructure.

The thermal evolution of the adsorbed ethene layers was studied by Thomas Fuhrmann [54] by applying a linear heating ramp of 0.5 K/s and continuously measuring spectra every 10 seconds. The resulting C 1s spectra are shown as a color-coded density plot in Figure 5.5 (a). The peaks at 283.48 and 284.07 eV start losing intensity around 170 K, and simultaneously a new peak at 283.35 eV evolves and gains intensity, with this process being finished at 220 K. The quantitative analysis, as displayed in Figure 5.5 (c), reveals that the total carbon coverage decreases in this temperature range from 0.50 ML C atoms to 0.26 ML. This can be attributed to partial desorption of ethene [146, 148]. The remaining peak is shown with detailed fitting in Figure 5.5 (b). The main peak at 283.35 eV is assigned to the adiabatic transition and the peak shifted to higher binding energies by 390 meV to the first vibrationally excited state of the final state ion with an S-factor of

0.19±0.02. This S-factor is typical for a hydrocarbon species with only one hydrogen atom per carbon atom [28]. The peak attributed to the second vibrationally excited state of the final state ion is shifted by 750 meV to higher binding energies in respect to the main peak. By comparing these results with the results of the adsorption of acetylene on Ni(111), as displayed in Chapter 5.3, the reaction intermediate is clearly identified as acetylene, which is also in accordance with the literature [139, 146].

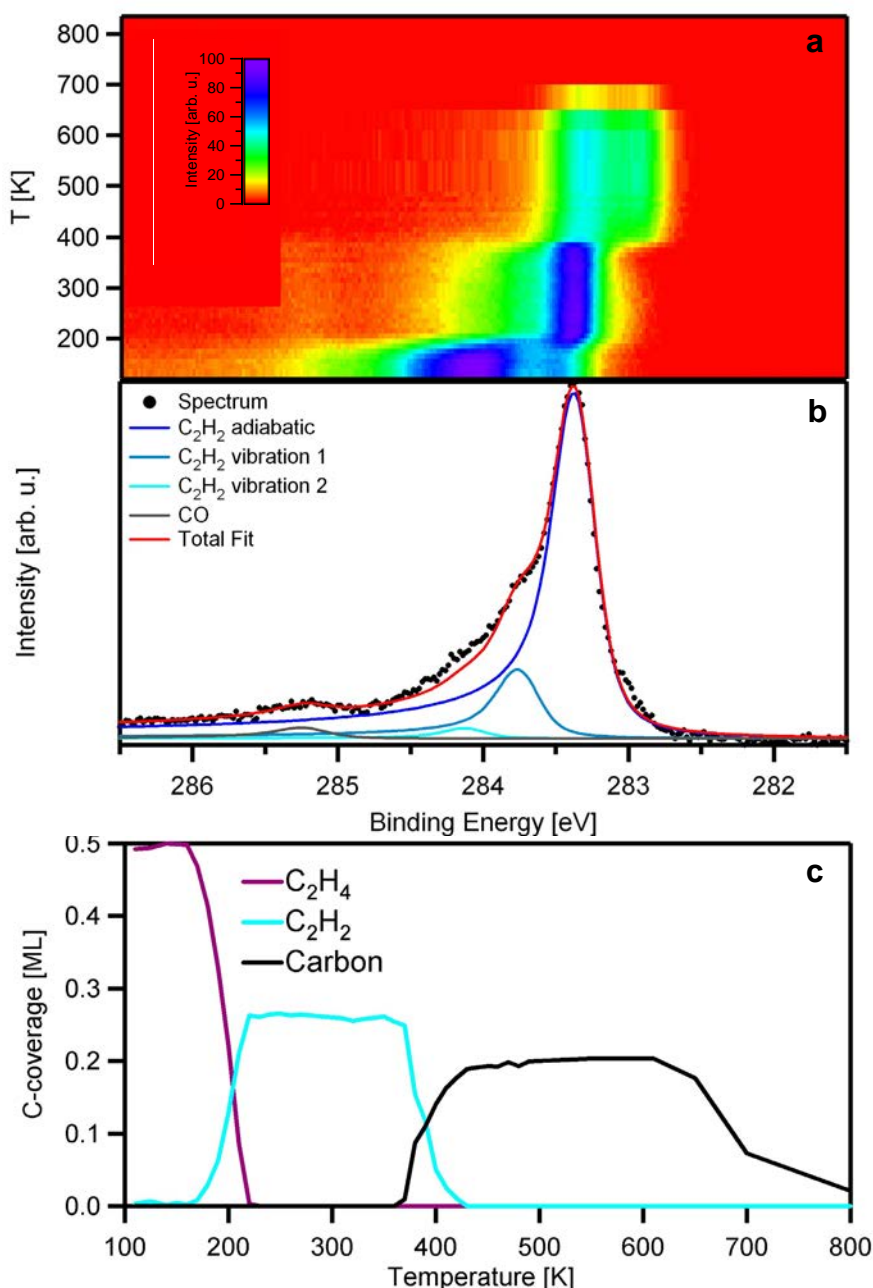


Figure 5.5: (a) Color coded density plot of the TPXPS experiment for a saturated ethene layer on Ni(111) (b) Acetylene spectrum and corresponding fit measured at ~300 K, from the data in (a); (c) Quantitative analysis of the data in (a). All data taken from [54] and obtained under an emission angle of 0°

Upon further heating a second and final reaction step occurs between 370 and 420 K. The intensity of the acetylene peak decreases and two new peaks at 282.92 and 283.29 eV appear. Both new peaks show no vibrational splitting. If the C_2H_2 molecule would decay by a cleaving of the C-C bond without dehydrogenation, as reported to happen in this temperature region [142], the resulting CH species should show a vibrational splitting. We thus can rule out CH and, due to the temperature regime the new species are stable within, assign them to carbidic carbon, resulting from further dehydrogenation of acetylene, in accordance with literature [144, 167-169]. These two contributions in the XP spectra for the carbidic carbon were observed for all dehydrogenation reactions on clean Ni(111) (see Chapters 5.2.1 and 5.3.1), and were also observed by other groups [168]. A possible explanation might be that one peak originates from stoichiometric nickel carbide and the other from a nonstoichiometric or slightly disordered carbide phase. No evidence for any trimerization of acetylene to benzene, which was suggested around 300 K [160-162] was found here.

5.1.2 Ethene coadsorbed with O on Ni(111)

To study the interaction of ethene with oxygen on Ni(111) an oxygen (2×2) layer was prepared on the surface, with a coverage of 0.25 ML atomic oxygen adsorbed in fcc hollow sites [3, 65, 66]. Ethene was dosed onto this oxygen precovered surface at a surface temperature of 105 K. The C 1s spectra that were collected during the uptake at an emission angle of 45° are shown in Figure 5.6 (a). In comparison with the spectra of ethene on clean Ni(111) the spectra are clearly different, as now only one main peak emerges at a binding energy of 283.27 eV and shifts to 283.34 eV for high coverages. In the detailed fit, as seen in Figure 5.6 (b), again a contribution due to vibrational excitation was found, with the peak assigned to transition from the vibrational ground state in the electronic initial state to the first excited C-H vibrational states in the same final state. The vibrational contribution is shifted by 350 meV to higher binding energies, with respect to the adiabatic main peak, and has a S-factor of 0.33 ± 0.02 . The peak for the second excited C-H vibrational state is shifted by 720 meV towards higher binding energies. All of these values are nearly identical to the ones for ethene on clean Ni(111), indicating molecular adsorption of the ethene. The major difference is that on oxygen precovered Ni(111) only one main C 1s peak is observed. As the binding energy of 283.34 eV is close to the binding energy of methyl on Ni(111), 283.58 eV [28, 54], it can tentatively be suggested that ethene adsorbs in a symmetric geometry with hollow adsorption sites for both carbon atoms, as depicted in Figure 5.7.

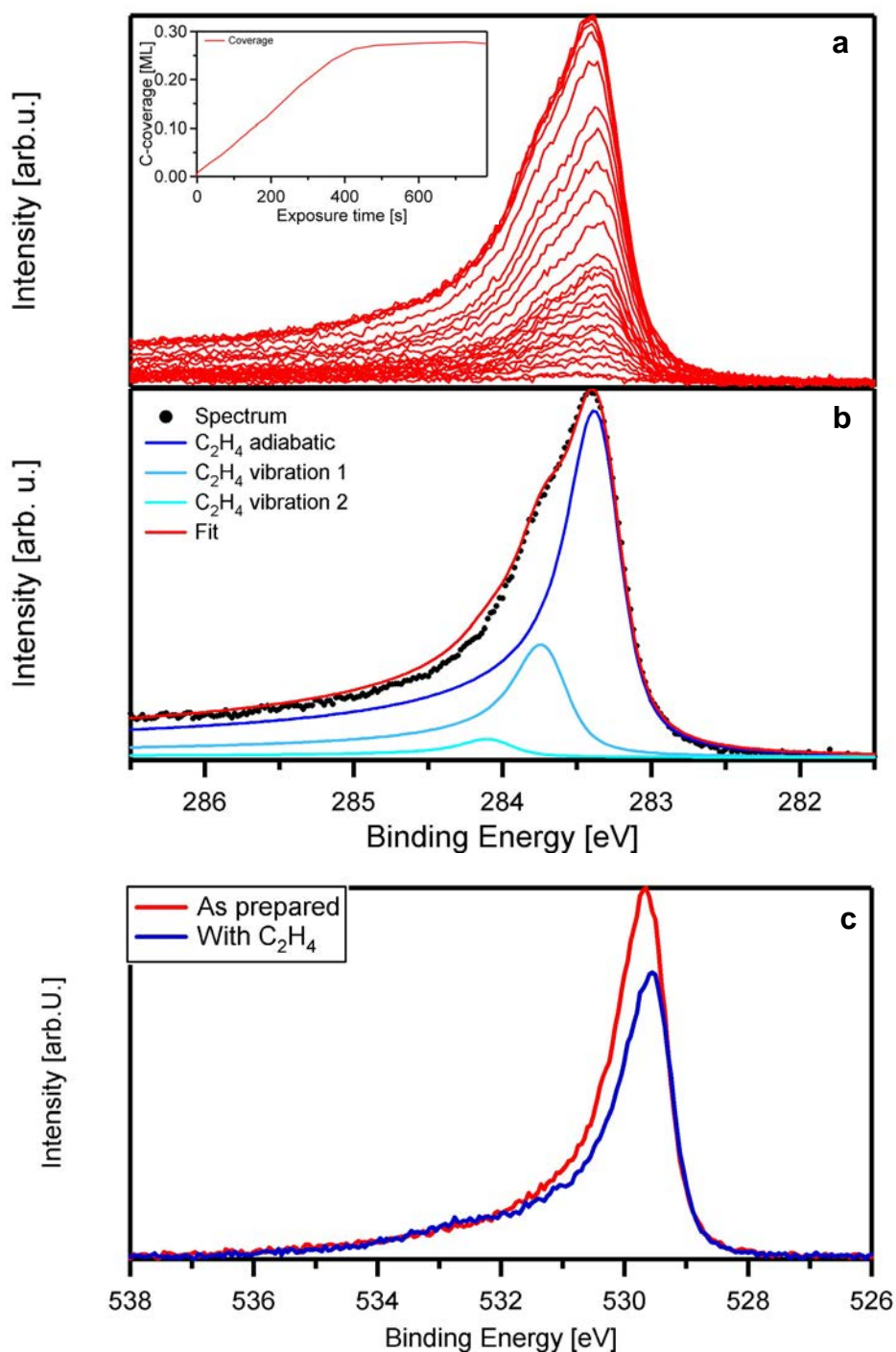


Figure 5.6: (a) Selected C 1s spectra of an ethene adsorption experiment on (2x2) O precovered Ni(111) surface, collected at an emission angle of 45° **Inset:** quantitative analysis of the data (b) fit of the spectrum of the saturated ethene layer (c) O 1s spectra before and after the uptake

The lateral arrangement of the ethene molecules was arbitrarily chosen such that the oxygen atoms on the surface have the largest distance from the ethene molecules. The suggestion of hollow adsorption sites for the carbon atoms is also strengthened by the comparison to the very similar binding energy of acetylene on Ni(111), which has a value of 283.35 eV [28].

Acetylene is known to adsorb with both carbon atoms in hollow positions as concluded from DFT calculations [152] and photoelectron diffraction studies [159].

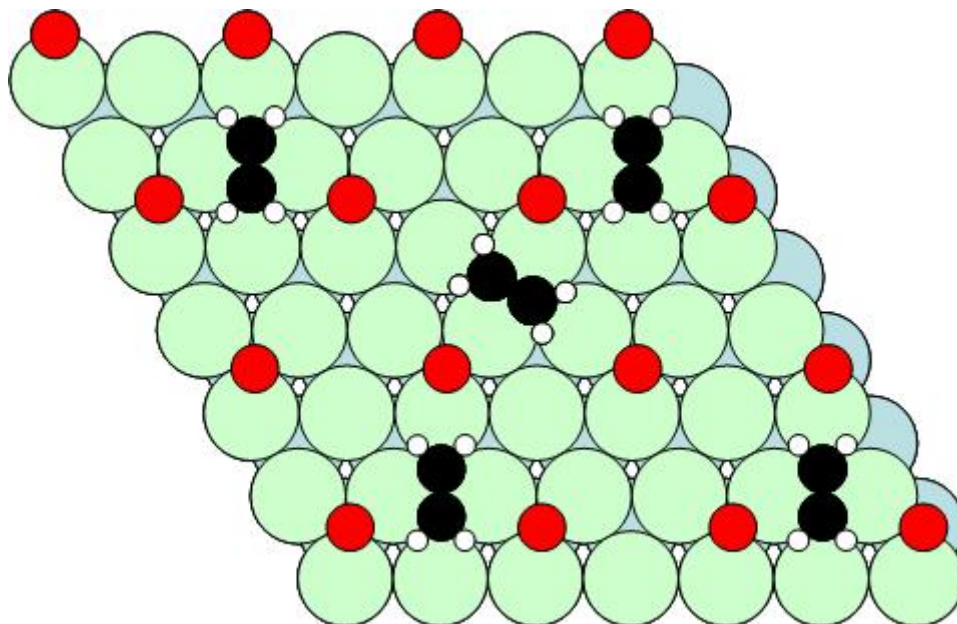


Figure 5.7: Proposed adsorption geometry for ethene on oxygen precovered Ni(111). The lateral arrangement of the ethene molecules was arbitrarily chosen such that the oxygen atoms on the surface have the largest distance from the ethene molecules.

A possible confusion of ethene on O/Ni(111) and acetylene due to the close binding energy can be ruled out, since the vibrational fine structure serves as a finger print for the species. The quantitative analysis in the inset of Figure 5.6 (a) shows that the ethene coverage on oxygen precovered Ni(111) reaches saturation at 0.28 ML C atoms. This is only roughly half the value of 0.50 ML C atoms found on the clean surface and clearly shows that oxygen blocks adsorption sites for ethene (see also Figure 5.4 and Figure 5.7). The oxygen coverage is apparently lowered by the ethene adsorption from 0.25 to 0.20 ML, as can be seen in Figure 5.6 (c). Since no damping by the ethene should take place, as the ethene adsorbs side by side to the oxygen instead of on top of the oxygen this coverage change is attributed to photoelectron diffraction. It is characterized as an apparent change in coverage instead of an oxygen loss since the coverage is restored after the ethene desorption, as is evident from Figure 5.8 (b).

The thermal evolution of ethene on the oxygen precovered Ni(111) surface was studied to gain insight on the influence of oxygen on the reactivity. For this the sample was heated to the temperatures denoted in Figure 5.8 (a) and subsequently an XP spectrum was recorded. The data reveal a strong

decrease in intensity up to 250 K as displayed in Figure 5.8 (b). Throughout this temperature range the shape of the spectra and the binding energy of the main peak remain unchanged, indicating the absence of any significant reaction. Only small amounts (less than 0.01 ML) carbonaceous species are formed, indicating some minority species that reacted. Possible explanations for this could be a slightly lower local oxygen coverage than the nominal value of 0.25 ML, reactions at defect sites or some minor beam damage. This thermal evolution, where ethene desorbs almost exclusively, is in strong contrast with the situation on the clean Ni(111) surface, where part of the adsorbed ethene dehydrogenates to acetylene upon heating. The difference is most likely due to steric reasons. It can be assumed that oxygen blocks the adsorption sites for hydrogen, which would be needed for the dehydrogenation. This is further strengthened by the fact that hydrogen is known both from experimental [170] and theoretical [171, 172] studies to adsorb in threefold-hollow sites on Ni(111), just like oxygen [65, 66].

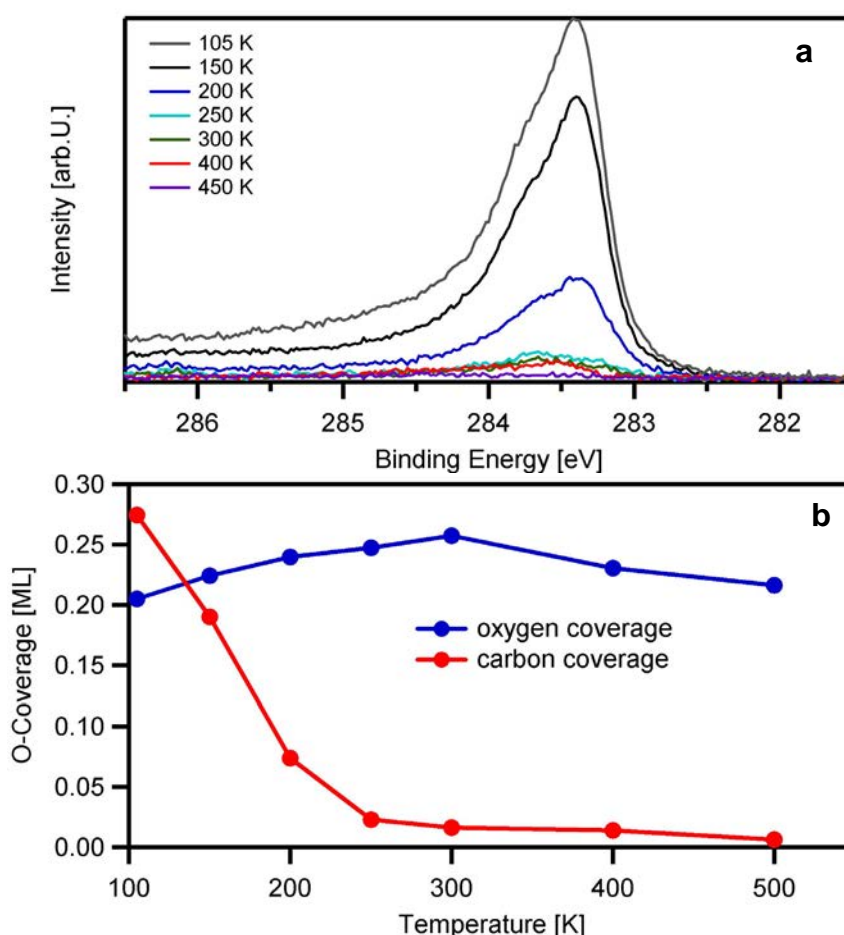


Figure 5.8: (a) Selected C 1s spectra of a TPXPS experiment for a saturated ethene layer on (2x2)O precovered Ni(111), collected at an emission angle of 45°. (b) Quantitative coverages during TPXPS

If the surface is further heated the remaining carbon starts to react with the oxygen to form CO, which is desorbing from the surface, leaving the surface devoid of any carbon containing species at 500 K. This can also be seen from a slight decrease of the total O coverage as displayed in Figure 5.8 (b). Another reaction contributing to the decrease of the total oxygen coverage is the formation of water from oxygen and the hydrogen formed in the minority dehydrogenation reactions. The water immediately leaves the surface as the desorption temperature for water on Ni(111) is 165 K as found in TPD experiments [173].

5.2 Ethane

5.2.1 Ethane on clean Ni(111)

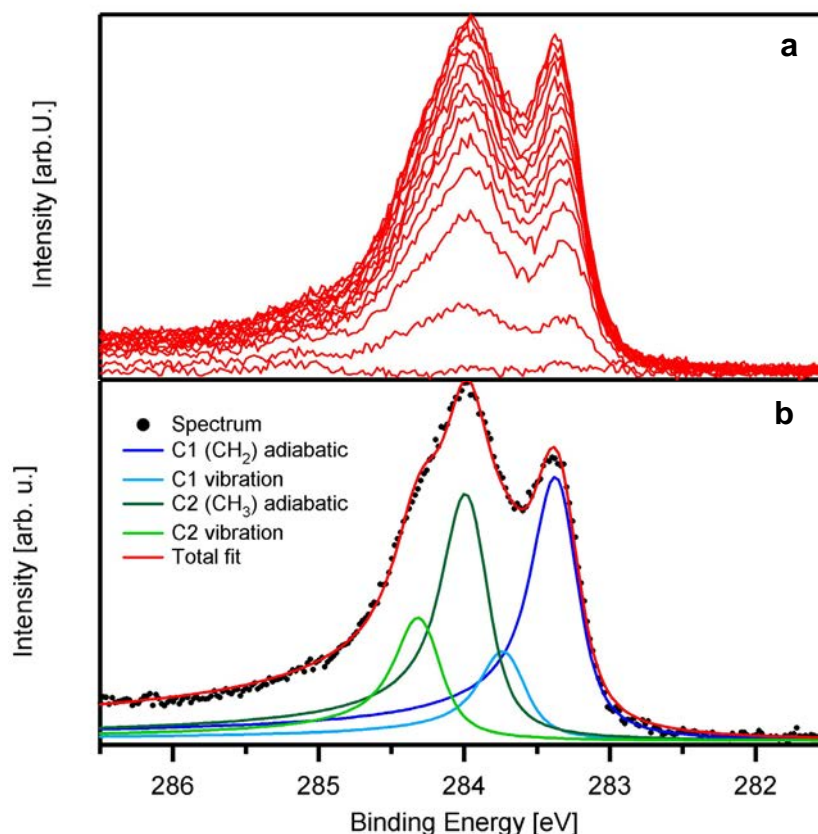


Figure 5.9: (a) Selected C1s spectra of the uptake of ethane (C_2H_6) on Ni(111) at a temperature of 110 K (b) Fit of the spectrum of the saturated ethyle (C_2H_5) layer on Ni(111). Data of (a) taken from [54]. All data obtained under an emission angle of 45°

For the interaction of C_2H_6 with Ni(111) Thomas Fuhrmann [54] conducted a large series of experiments. When C_2H_6 is dosed onto the Ni(111) surface from the background at a sample temperature of 103 K no adsorption on the surface is found. This is in good accordance with the literature, which provides

a TPD desorption temperature of 99 K for physisorbed ethane on Ni(111) [156]. To overcome the energy barrier for breaking of one C-H bond, which is a necessary prerequisite for chemisorption due to the saturated nature of ethane, ethane was dosed on Ni(111) with our supersonic molecular beam. A seeding ratio of 2 sccm C₂H₆ in 20 sccm He with a nozzle temperature of 873 K provides a kinetic energy per molecule of 0.84 eV [54], which can be used to break one of the C-H bonds upon impact on the surface. The resulting C 1s spectra for a surface temperature of 110 K can be seen in Figure 5.9 (a), as taken from [54]. Two dominant peaks emerge at binding energies of 283.28 and 283.94 eV, shifting to 283.33 eV and 283.95 eV, respectively, for higher coverages. In the context of this work a refined fitting procedure from the one used by Thomas Fuhrmann [54] was applied, to gain clearer insight into the vibrational splitting and allowing us to assign the two peaks better than possible within Fuhrmann's thesis [54]. The detailed fit, which is displayed in Figure 5.9 (b), reveals for both peaks a vibrational contribution due to C-H stretching vibrations at higher binding energies in respect to the main peak. The vibrational contribution of the peak at 283.33 eV has a distance of 360 meV to the main peak and an S-Factor of 0.34. The S-Factor is proportional to the number of C-H bond, with one C-H bond leading to an S-Factor of 0.16-0.19 for hydrocarbons on Ni(111) or Pt(111) [28]. Thus the S-Factor of 0.34 found for the peak at 283.33 eV is indicative of two H atoms bound to this carbon atom. For the second main peak at 283.95 eV a vibrational splitting of 320 meV is found with an S-Factor of 0.51 indicative of 3 C-H bonds. A possible explanation for the unusual low value of the splitting (see [28] for a table of typical values of ΔE) would be an intermixing of the C-H stretch vibration with the C-C stretch vibration which leads to a peak with a distance of 185 meV in gas phase measurements [30], which is below our resolution limit. A similar limitation was found for ethene on Ni(100) where a separation of the adiabatic and the first vibrational peak of 330 meV was detected [174]. Both main peaks grow simultaneously with an initial aspect ratio of 0.93 which changes monotonous to 0.7 during the course of the experiment. For the spectrum shown in Figure 5.9 (b) however the aspect ratio is 0.93 again as it was taken on a new spot not previously affected by the synchrotron light, so the constant decrease of the aspect ratio can be attributed to beam damage. Just like for ethene on Ni(111) (Chapter 5.1.1) it can be argued that the simultaneous growth is indicative of two carbon atoms of one molecule adsorbing in different chemical environments on the surface.

When combining these findings we can clearly conclude that C₂H₆ adsorbs on the surface as ethyle (C₂H₅), i.e. one C-H bond is broken to allow the molecule to adsorb on the surface, as already proposed by Fuhrmann [54]. The energy needed to break this bond comes from the kinetic energy supplied

by the supersonic molecular beam. This is in accordance with earlier findings of our group about the adsorption of CH_4 on $\text{Ni}(111)$ [28], for which also some kinetic energy is needed to break one of the C-H bonds for the molecule to be able to form a covalent bond to the surface. From the S-factor of the peak at 283.33 eV, which is indicative of two C-H bonds it is clear that the bond to the surface is made by the carbon atom that gives rise to this peak. The other carbon atom, which still is attached to three hydrogen atoms, gives rise to the XPS peak at 283.95 eV, of which the S-Factor is indicative of these three C-H bonds. A saturation coverage of 0.22 ML C atoms per surface Ni-atom, which corresponds to 0.11 ML C_2H_5 coverage, is reached after about 300 s.

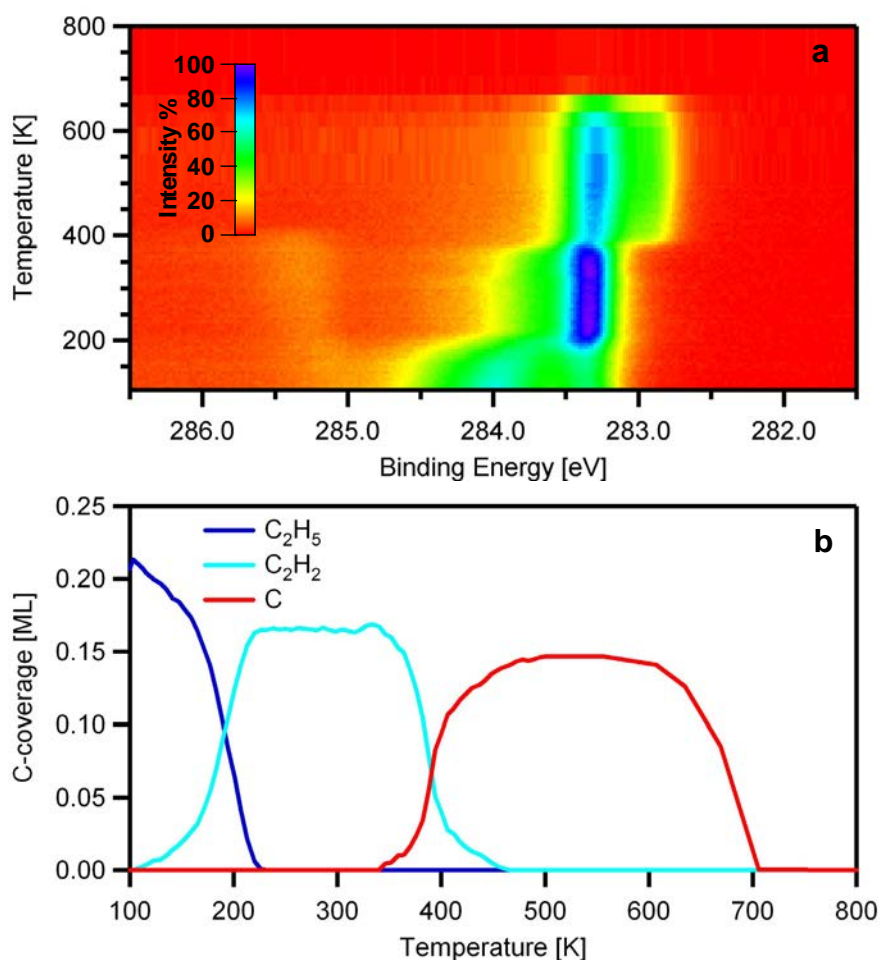


Figure 5.10: (a) Colour coded density plot of the TPXPS of 0.11 ML ethyle (C_2H_5) on clean $\text{Ni}(111)$ (b) Quantitative analysis of the data from (a). Data of (a) taken from [54]

To study the thermal evolution of the adsorbed C_2H_5 a linear heating ramp of 0.2 K/s was applied to the sample via the sample filament and a spectrum was taken every 6 K. The result is displayed in Figure 5.10 (a) as a color coded density plot. During heating a significant change in the spectra is occurring around 200 K. The spectral shape changes from the one characteristic for C_2H_5 to a new shape that is dominated by a single main

peak at 283.31 eV and has two vibrational contributions. The first vibrational contribution exhibits a S-factor of 0.18 and a binding energy shift of 380 meV to higher binding energies in respect to the main peak, and the second vibrational contribution has a S-Factor of 0.03 with a binding energy difference of 740 meV. By comparing this with the data obtained for acetylene on Ni(111) (Chapter 5.3.1) the new species on the surface can clearly be identified as acetylene, just like in the dehydrogenation path of ethene on Ni(111) (Chapter 5.1.1).

With the new fitting parameters for the ethyle used in this thesis the onset of the dehydrogenation is set at slightly higher temperatures than in the thesis of Thomas Fuhrmann [54], albeit the overall dehydrogenation path remains unchanged. At 400 K, a further change of the spectral shape is observed. Acetylene decomposes and two new peaks appear at 282.92 eV and 283.28 eV. Due to the lack of any vibrational fine structure in these peaks they are again assigned to two carbonaceous species, which can also be seen from the similar dehydrogenation path of ethene on Ni(111) (Chapter 5.1.1) and in accordance with literature [144, 167-169]. Above 700 K the carbon is diffusing into the bulk of the nickel crystal leaving a clean surface. In Figure 5.10 (b) the dehydrogenation path is shown quantitatively, with the "C" curve standing for the combined coverage of the two carbides. The conversion of C_2H_5 to C_2H_2 starts already at temperatures as low as 120 K and is finished around 220. The decrease in coverage from 0.22 to 0.17 ML C atoms can be attributed to either/or recombinative desorption of ethane or some dehydrogenation to and subsequent desorption of ethene. The second dehydrogenation step takes place between 360 and 440 K and goes along with a further decrease in coverage to 0.15 ML.

When the dehydrogenation of ethene (C_2H_4) (see Figure 5.5) is compared with the dehydrogenation of ethyle (C_2H_5), shown in Figure 5.10 the similarities of the two dehydrogenation paths are obvious. Both adsorbates first dehydrogenate to acetylene (C_2H_2) around 200 K. A noticeable difference is the earlier onset of the dehydrogenation of ethyle. One possible explanation for this behavior might be that it is a hint towards a minority species of ethene (C_2H_4) on the surface, formed from ethyle (C_2H_5) by removal of one hydrogen atom, which we are not able to resolve in our fitting procedure due to the small shift of the ethene binding energies compared to the binding energies of ethyle. As the overall shape of the spectrum undergoes no major changes below 160 K a dehydrogenation to ethene on a major scale can be ruled out however. Another noteworthy fact is the higher conversion rate of ethyle to acetylene when compared to the conversion of ethene to acetylene. The conversion rate is higher both in the percentage of conversion (~ 75 % of the adsorbed ethyle is converted to acetylene but only ~ 50 % of the adsorbed

ethene) as well as in the obtained acetylene coverage (0.17 ML and 0.13 ML acetylene for ethyle and ethene, respectively). As the acetylene coverages which were obtained in both cases are much lower than the saturation coverage found for acetylene on Ni(111) (Chapter 5.3.1) it seems likely that this is due to the rate for recombinative desorption of ethyle being lower than the direct desorption rate of ethene during the dehydrogenation step and/or that the conversion rate from ethyle to acetylene is higher than the conversion rate of ethene to acetylene. The second argument would also be in accordance with the lower onset of the acetylene formation in the dehydrogenation of ethyle, where the acetylene peak appears at temperatures as low as 112 K whereas in the dehydrogenation of ethene the first acetylene can be detected at 170 K. The second dehydrogenation step, i.e. the dehydrogenation of acetylene is identical in both dehydrogenation paths within the margin of error. Just as in the dehydrogenation path for ethene we find no evidence of acetylene trimerization to benzene.

The obvious similarities between the two dehydrogenation paths open up the exploration of a different interpretation of the data. Figure 5.11 (a) shows the previously discussed interpretation of the data, with the spectrum resulting from the exposure of the Ni(111) surface to ethane (C_2H_6) with 0.84 eV kinetic energy, acquired under an emission angle of 45° , fitted as ethyle (C_2H_5) as already displayed in Figure 5.9 (b). Figure 5.11 (b) shows the same spectrum, however this time it is fitted under the assumption that instead of one C-H bond two C-H are breaking upon adsorption, netting ethene (C_2H_4) as the adsorbed molecule. In this fit the peak for the first carbon atom resides at 283.35 eV, and the peak for the second carbon atom at 283.98 eV. The first vibrational contributions are shifted by 360 meV towards higher binding energies in respect to the adiabatic peaks, and the S-factor is 0.32 in both cases. Although the fit as C_2H_5 is a bit better than the fit as C_2H_4 , a comparison with genuine ethene spectra on Ni(111) shows the validity of this alternative interpretation.

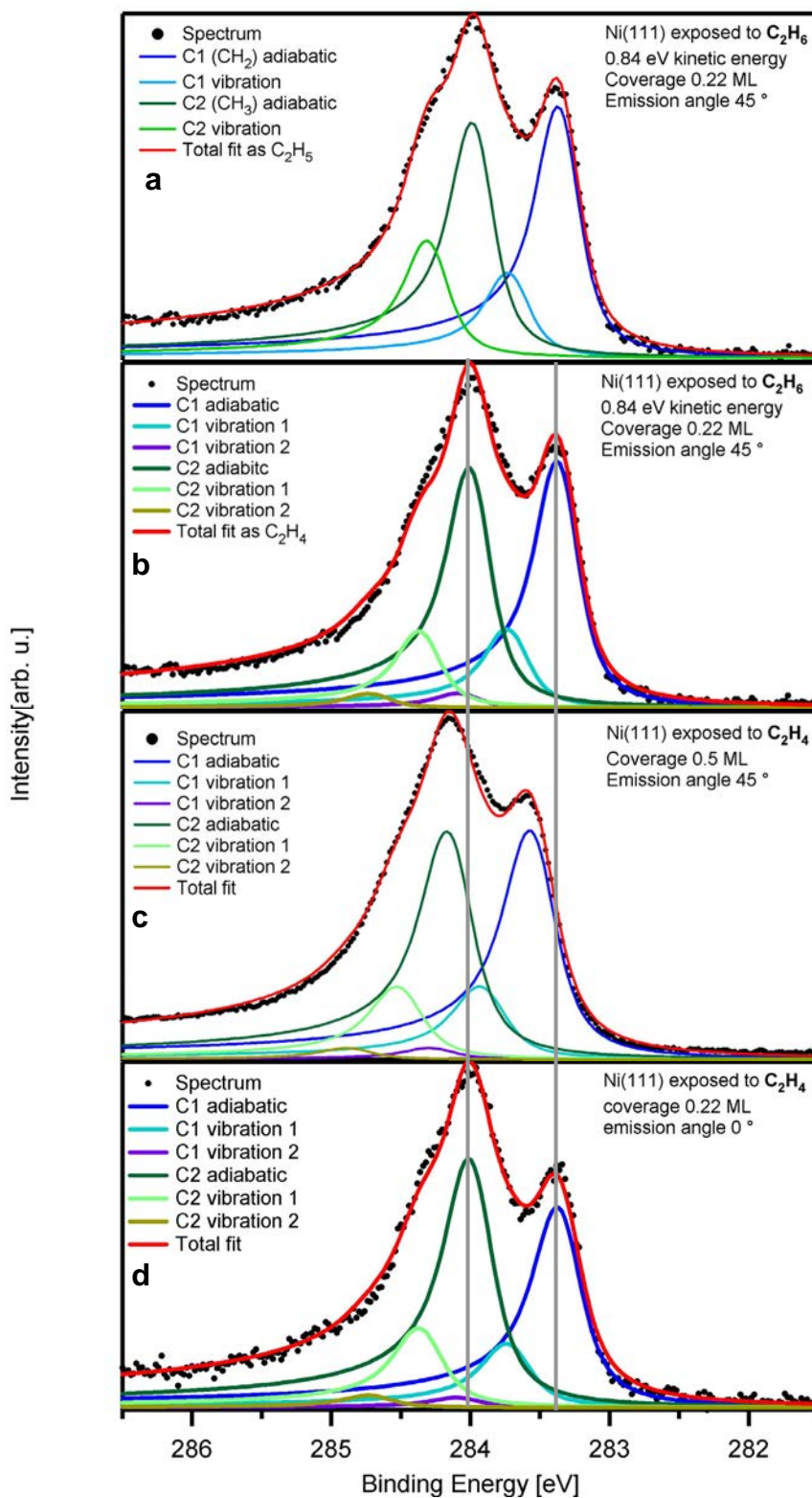


Figure 5.11: (a) and (b) Ethane dosed on Ni(111) with 0.84 eV kinetic energy, emission angle 45°, coverage 0.22 ML. (a) fitted as C_2H_5 . (b) fitted as C_2H_4 . (c) and (d) Ethene dosed on Ni(111). (c) coverage 0.5 ML and emission angle 45°. (d) coverage 0.22 ML and emission angle 0°.

Figure 5.11 (c) shows the fit of the C 1s spectrum of a saturated (0.5 ML C atoms) ethene layer on Ni(111). Just like the spectrum shown in Figure 5.11 (a) and (b), this ethene spectrum was recorded under an emission angle of 45 °. The fit shows very similar feature, especially the fact that the two adiabatic peaks have almost the same height in both in Figure 5.11 (b) and (c) demonstrates this similarities. A major difference is the position of the adiabatic peaks. The grey lines in Figure 5.11 show that the adiabatic peaks are shifted almost 200 meV towards higher binding energies in (c) in respect to their positions in (b). This can difference can be explained by the different coverages. In Chapter 5.1.1 it was discussed that the binding energy of adiabatic peaks in the spectra of ethene on Ni(111) depends on the ethene coverage, with the adiabatic peaks shifting to higher binding energies with increasing coverage. This can also be seen in Figure 5.1 (a). Figure 5.11 (d) shows a fit of 0.22 ML C atoms of ethene on Ni(111), the same coverage that was obtained for the dosing of ethane on the surface. Please note that this spectrum was acquired under a different emission angle of 0 °. The different height ratio between the two adiabatic peaks can be explained by photoelectron diffraction, as discussed in Chapter 5.1.1. The binding energies of the two adiabatic peaks here are exactly the same as for the fit in Figure 5.11 (b). The last remaining question in this alternate explanation would be why the dehydrogenation starts at lower temperatures after the exposure of the surface to ethane compared to ethene. This can also be attributed to the higher coverages reached after the exposure of the surface to ethene. As for the dehydrogenation of the ethene some free space is needed on the surface to accommodate the hydrogen, at first some ethene needs to desorb from the surface. As soon as this happens the dehydrogenation starts. After the exposure to ethane the surface is covered with less then 50 % of the amount found after the adsorption of pristine ethene, providing lots of empty sites for the dehydrogenation from the start of the experiment.

All of these arguments make the assignment of the adsorbate as C₂H₅ or as C₂H₄ equally likely, and for a clear assignment as one of the two species additional experiments with a different technique which is able to detect the number of hydrogen atoms would be needed, for example vibrational spectroscopies like HREELS. Such experiments have not been reported in literature up to now.

5.2.2 Ethane coadsorbed with O on Ni(111)

As the adsorption and especially the dehydrogenation behavior of both ethene (C₂H₄) and ethyle (C₂H₅), which was generated by dosing ethane (C₂H₆) on the clean Ni(111) surface with 0.84 eV kinetic energy per molecule, were

found to be rather similar, the question arises if these similarities also hold true in the coadsorption case with oxygen.

To investigate this, ethane (C_2H_6) was adsorbed with a kinetic energy of 0.84 eV per molecule (2 sccm C_2H_6 , 20 sccm He, nozzle temperature 873 K) on a Ni(111) surface covered with 0.19 ML O at a surface temperature of 101 K. The resulting C 1s spectra are shown in Figure 5.12 (a). The spectral shape remains constant during the uptake, however after the molecular beam is switched off a loss in intensity is observed (Figure 5.12 (b), Figure 5.13 (b)) due to desorption of physisorbed ethane. The corresponding peak, as derived from the subtraction of the first spectrum after the switchoff of the molecular beam from the last spectrum before the switchoff is displayed as well. This desorption causes a drop in coverage from 0.26 ML down to 0.22 ML C atoms. As can be seen from the figure the peak of the desorbing component is shifted to higher binding energies with respect to the peak for the remaining species, implying a different adsorption behavior. So the reason for this desorption is most likely that the sample temperature was in a range where a pressure dependent adsorption/desorption equilibrium is reached on the surface for the desorbing component. After the molecular beam is switched off the lower pressure leads to a subsequent desorption of the excess ethane. The assumed adsorption/desorption situation is in good agreement with a TPD study [156] of ethane on clean Ni(111), where ethane was physisorbed onto Ni(111) at 70 K and during heating a desorption maximum was found at 99 K. On the oxygen precovered surface the coverage increases linearly with time, however the coverage increase is slower as for the clean Ni(111) surface. On the clean surface a saturation coverage of 0.22 ML C atoms is reached after 300 s of ethane dosage. Using the same adsorption parameters on the oxygen covered surface a total of 1800 s were needed to reach the same coverage, as can be seen from the quantitative analysis in Figure 5.13 (b). From this a lower sticking coefficient for the oxygen precovered surface can be deduced. It should be noted, however, that no saturation was reached during the uptake on the oxygen precovered surface. As some of the adsorbed ethane desorbed after the lowering of the pressure, however, it can be argued that 0.22 ML is the saturation coverage for the experiment temperature of 101 K and the base pressure of the vacuum system.

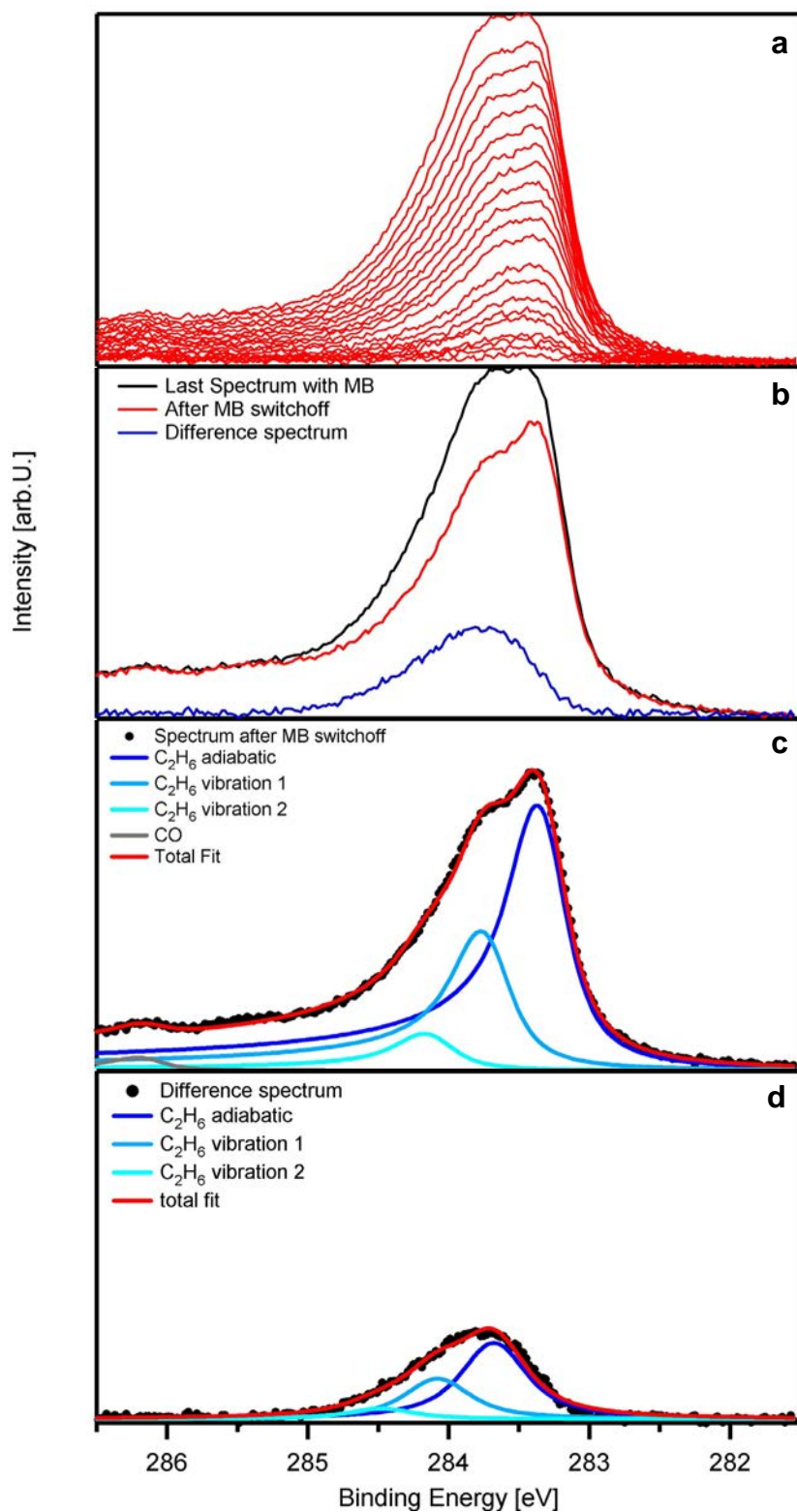


Figure 5.12: (a) Selected C 1s spectra of an ethane adsorption experiment with a kinetic energy of 0.84 eV per molecule on 0.19 ML O precovered Ni(111) surface at 101 K, collected at an emission angle of 45° (b) C 1s spectra before and after the switch off of the molecular beam (c) fit of the red spectrum from (b) (d) fit of the difference spectrum

Just like in the case of the ethene adsorption on the clean and the oxygen precovered Ni(111) surface (Chapter 5.1) the spectral shape of the adsorbate on the oxygen covered surface is clearly different from the one on the clean surface. Whereas the C 1s spectrum of the adsorbate on the clean Ni(111) surface features two distinct main peaks with their respective shoulders due to the vibrational contributions here for the adsorbate layer remaining on the surface after the desorption of the excess ethane, we only find one main peak with a rather strong shoulder. The detailed fitting result of the C 1s spectrum is shown in Figure 5.12 (c). A main peak at 283.33 eV is attributed to the adiabatic transition. Due to the presence of the excess ethane during the uptake, which alters the overall spectral shape, no information can be determined if the binding energy shifts during the uptake, like it was observed during the uptakes of both ethane and ethene on the clean surface and ethene on the oxygen precovered surface. In addition to the main peak two vibrational contributions are found, which are assigned to the transition to the first and second excited C-H vibrational states in the final state ions, respectively. The peak assigned to the first vibrational excitation is shifted by 400 meV to higher binding energies in respect to the main peak and has an S-Factor of 0.53. For the second vibrational excitation we find in respect to the adiabatic transition a shift of 800 meV and an S-Factor of 0.14. In Figure 5.12 (d) a fit of the difference spectrum for the ethane component that desorbed upon switchoff of the molecular beam is displayed. The spectrum can be fit with a similar set of three peaks as was used for the stronger bound component. The distances between the peaks of 400 meV each are the same as are the S-Factors of 0.53 and 0.14 for the first and second vibrational peak, respectively. A difference is found in the binding energy of the adiabatic peak, which lies at 283.67 eV. This clearly shows that this component is differently bound to the surface than the component remaining after the adsorption. This different adsorption behavior is also the most likely reason that the component has a lower desorption temperature. The binding energy difference between the peaks of 400 meV each corresponds well to the value of 404 meV found in gas phase measurements [30], but deviates from the vibrational energies of 360-370 meV found for ethane physisorbed on clean Ni(111) below 100 K with HREELS [156]. This difference is attributed to the fact that HREELS probes the electronic ground state and XPS the excited state. The difference of ~ 10% between the two values was found for a several hydrocarbons adsorbed on Ni(111) and Pt(111) [28]. Considering that for hydrocarbons adsorbed on Ni(111) each C-H bond contributes 0.17 ± 0.02 to the S-Factor [28] the S-Factor of 0.53 found here points to three C-H atoms per carbon atom, revealing the adsorbate to be molecular ethane (C_2H_6). This is quite surprising as the kinetic energy of the molecules upon adsorption was the

same as for the adsorption on the clean surface, where the ethane molecules are dissociatively adsorbed as C_2H_5 .

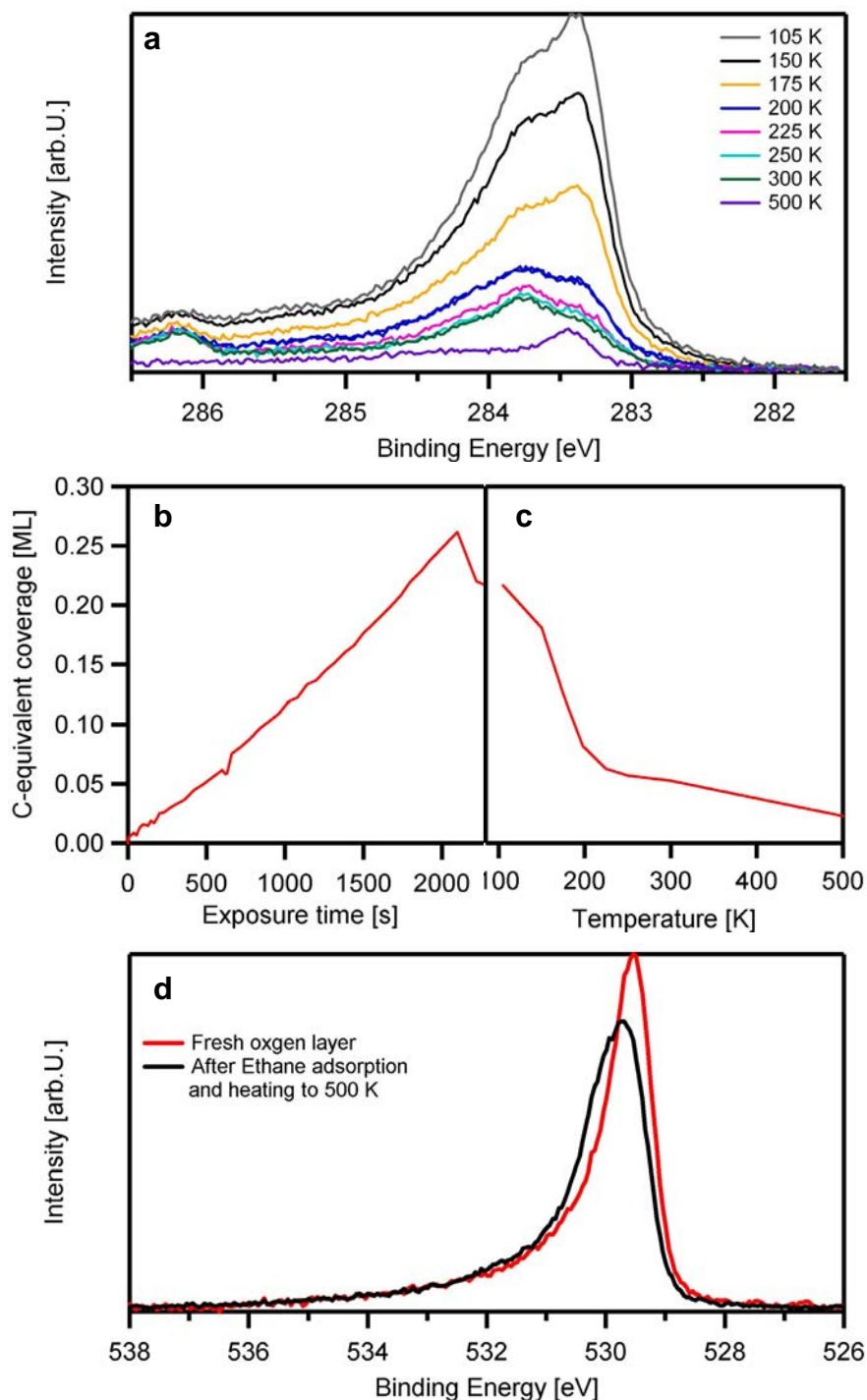


Figure 5.13: (a) C 1s spectra taken after heating a C_2H_6 layer on oxygen precovered Ni(111) to the denoted temperatures (b) Quantitative analysis of the ethane uptake (c) Quantitative analysis of the data from (a) (d) O 1s spectra before the ethane uptake and after the TPXPS

An explanation for this behavior could be that the oxygen blocks adsorption but stabilizes the physisorbed component on the surface. The fact that there is still ethane on the precovered surface at 103 K whereas we could not

adsorb any ethane on the clean surface at this temperature, where the desorption maximum is reported at 99 K [156] hints in this direction. Another argument in this direction is the presence of a variety of physisorbed hydrocarbons present on NiO (see Chapter 6.2.2) at temperatures where they have long desorbed on the clean Ni(111) surface. The absence of dissociative adsorption can be explained by steric reasons, i.e. that the oxygen blocks the adsorption sites for hydrogen that are necessary for the dissociative adsorption, just like in the case of ethene coadsorbed with O on Ni(111) (Chapter 5.1.2). This seems highly likely since hydrogen [170-172] and oxygen [65, 66] both are known to adsorb in threefold hollow sites on Ni(111). Haroun et al. [172] also found that CH₃ and H, which both adsorb in hollow sites on Ni(111), interact repulsively on Ni(111), leading to the conclusion that dissociative adsorption of methane (CH₄) on Ni(111) is only favored if the fragments do not interact. Since C₂H₅ also seems to prefer a hollow adsorption site (Chapter 5.2.1), it seems possible to compare the situation of the dissociative adsorption of methane and ethane. This means that a lower availability of hollow adsorption sites for the hydrogen due to the presence of oxygen on the surface will lead to more repulsive interactions between C₂H₅ and H making the dissociative adsorption of C₂H₆ unfavorable and leading to molecular physisorption of C₂H₆. To gain further insight whether or not the situation is comparable with the adsorption of ethene it is important to take a look into the thermal evolution of the adsorbed ethane layer.

The thermal evolution of this layer was studied by heating it via resistive heating stepwise to selected temperatures, acquiring spectra after each heating step. These spectra are shown in Figure 5.13 (a). Most of the adsorbed ethane is desorbing between 105 and 225 K, which is especially obvious from the quantitative analysis in Figure 5.13 (b), revealing that the total coverage drops from 0.22 ML to 0.05 ML C atoms in this temperature region. The coverage drops again when heating from 300 to 500 K. Together with the fact that the intensity of the oxygen peak is slightly lower at 500 K than before ethane adsorption (Figure 5.13 (d)) we can conclude that some of the oxygen reacts with carbonaceous species on the surface between 300 and 500 K to form CO or CO₂, which subsequently desorbs from the surface. A closer look at the spectrum at 225 K shows a peak near 283.3 eV which is assigned to acetylene (C₂H₂) from its binding energy value. As acetylene was found as dehydrogenation product of ethane on clean Ni(111) here the most likely source is also some dehydrogenation of ethane. Dehydrogenation is also a likely source for the other main contribution of the spectrum at 283.8 eV, of which the nature can not be determined. Another possible assignment of the peak at 283.33 eV would be that at least a part of the dosed ethane adsorbed dissociatively as ethyle (C₂H₅) or ethene (C₂H₄), just

like on the clean surface. However, the region of 225 to 300 K, in which the residual products are stable, makes this assignment unlikely since in this temperature region the ethylene has already dehydrogenated to acetylene on the clean surface. What is remarkable however is that here a much smaller adsorbate percentage reacts on the oxygen precovered surface than on the clean surface, with 0.05 ML of 0.22 ML and 0.17 ML of 0.22 ML remaining on the surface, respectively at 225 K. If we compare the situation here with the thermal evolution of ethene on the oxygen precovered surface it seems surprising that there we found no dehydrogenation on the surface (except for a very small minority of less than 0.01 ML), whereas here we have at least part of the species reacting. The best explanation for this is the lower oxygen coverage of only 0.19 ML in the coadsorption experiment for ethane and oxygen on Ni(111). From the ethene coadsorption experiment it could be deduced that the oxygen blocks the adsorption sites for the hydrogen, and thus completely blocking the dehydrogenation of the ethene. In the case of ethane some adsorption sites for hydrogen have to be available due to the missing 0.06 ML of oxygen, leading to dehydrogenation of some of the adsorbed ethane.

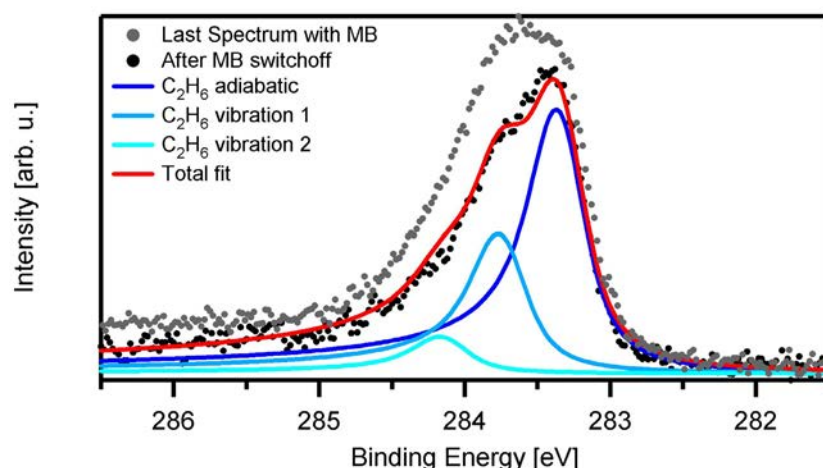


Figure 5.14: *C1s* spectrum of 0.07 ML C atoms of ethane adsorbed on Ni(111) precovered with 0.25 ML oxygen, after subtraction of surface contamination peak. Ethane dosed at 140 K with 0.84 eV kinetic energy

To further elucidate the role of the oxygen vacancies we also performed an adsorption experiment where ethane was dosed onto 0.25 ML oxygen on Ni(111), again with a kinetic energy of 0.84 eV at a surface temperature of 140 K for 1400 s. Subtracting peaks due to some contaminations (0.02 ML C-equivalent coverage) on the surface yields similar lineshape both prior and post desorption of the physisorbed component, as can be seen by comparing Figure 5.14 with Figure 5.12. The adiabatic component was again found at 283.33 eV, and also the differences in binding energy of 400 meV to the two

vibrational peaks and the S-factors of 0.53 and 0.14 for the first and second vibrational peak, respectively, are identical to the other experiment. The only difference is a slightly smaller line width that can be attributed to a slightly better resolution for this experiment. The coverage reached after 1400 s was 0.07 ML C atoms, which is significantly lower than in the first experiment, where 0.22 ML were reached after 1800 s. Considering that the coverage increase is linear over time (see Figure 5.13 (b)), and the difference in adsorption time between the two experiments is only ~ 25 %, the difference has most likely to be attributed to the higher sample temperature (140 K and 101 K for the second and first experiment, respectively), although an influence of the higher oxygen coverage can not be ruled out. During heating of this layer all of the adsorbed ethane desorbed again until 225 K, leaving only the contamination on the surface that was present before the uptake, with no difference in the contamination coverage before and after. As now dehydrogenation to acetylene or other dehydrogenation products can be found here this further backs the assumption that the oxygen blocks the adsorption sites for the hydrogen, and thus prevents the dehydrogenation of hydrocarbons on Ni(111). Interestingly additionally to blocking the dehydrogenation of hydrocarbons on Ni(111) the oxygen also seems to stabilize the physisorbed phases of hydrocarbons, as we find significant physisorption of ethane when it is coadsorbed with oxygen on Ni(111), whereas no physisorption was found on the clean Ni(111) surface.

5.3 Acetylene

5.3.1 Acetylene on clean Ni(111)

After studying the other two hydrocarbons with two carbon atoms, namely ethane and ethene, on Ni(111), the question remains if any of the trends observed there can also be found for acetylene.

Figure 5.15 (a) shows the C 1s spectra of an uptake experiment of acetylene (C_2H_2) on Ni(111) with a surface temperature of 105 K, the data set was taken from [54]. The inset shows that a coverage of 0.58 ML carbon atoms is reached after an exposure to 0.8 L acetylene. This coverage is slightly lower than the 0.66 ML carbon atoms Fuhrmann [54] assigned to this data set, due to a reevaluation of the coverage data. The detailed fit is displayed in Figure 5.15 (b). Unlike for the ethene and ethane adsorption the spectrum is dominated by a single peak, which starts at 283.33 eV and shifts to 283.40 eV for high coverages. Two vibrational contributions are shifted by 390 and 750 meV to higher binding energies in respect to the main peak. Their S-Factors are 0.19 and 0.03, respectively. The S-Factor of 0.19 of the first vibrational

contribution, which for hydrocarbon adsorption on Ni(111) is typical for one C-H bond per carbon atom [28], is a clear evidence for molecular adsorption of C_2H_2 . The absence of a second main peak, which was seen in the adsorption of ethene and ethane, indicates equivalent adsorption sites for both carbon atoms. From literature this adsorption site is known to be two adjacent hollow sites [152, 159]. The overall peakshape and the binding energy is in very good accordance with the acetylene species found in the dehydrogenation paths of ethene (C_2H_4) and ethyle (C_2H_5) in the previous chapters. It should be noted, however, that the coverage of 0.58 ML C atoms (0.29 ML C_2H_2 molecules) is much higher than the acetylene coverages obtained during the dehydrogenation of ethene or ethyle.

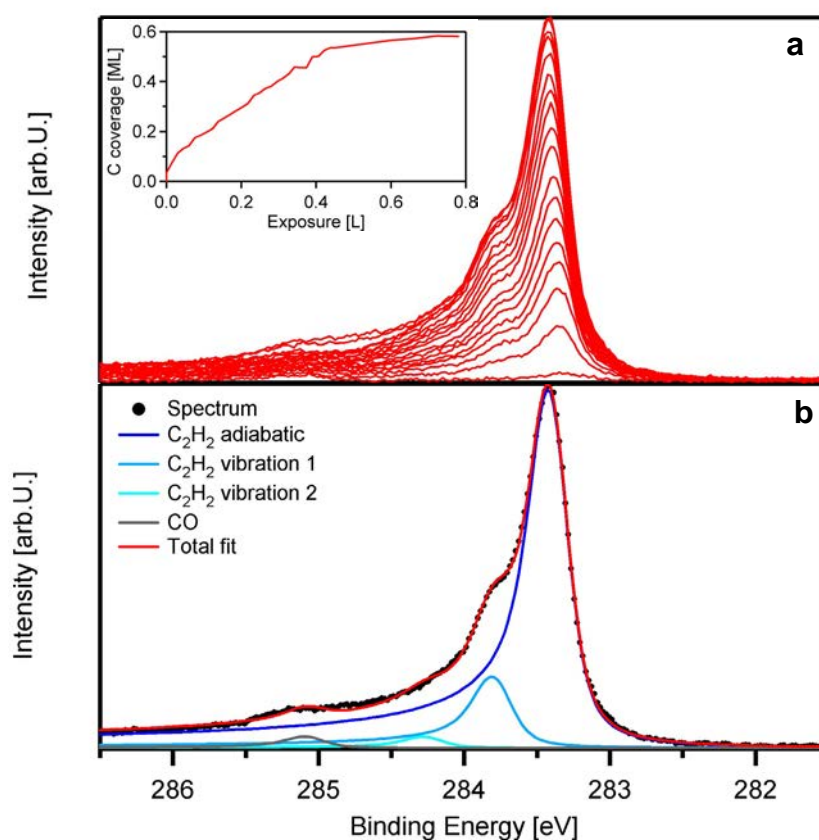


Figure 5.15: (a) Selected C 1s spectra of acetylene dosed on clean Ni(111) at 105 K. Inset: Quantitative plot of the uptake (b) detailed fit of spectrum with highest coverage. Data taken from [54]

The significance of this higher coverage becomes clear when looking at the thermal evolution of the adsorbed acetylene layer. In the previous chapters it was found that in the dehydrogenation path of adsorbed ethene and ethyle the formed acetylene dehydrogenated to carbonaceous species around 400 K. The same decay path was suggested by Thomas Fuhrmann [54] for this data set. However, a reevaluation of the data set paints a much more complex picture.

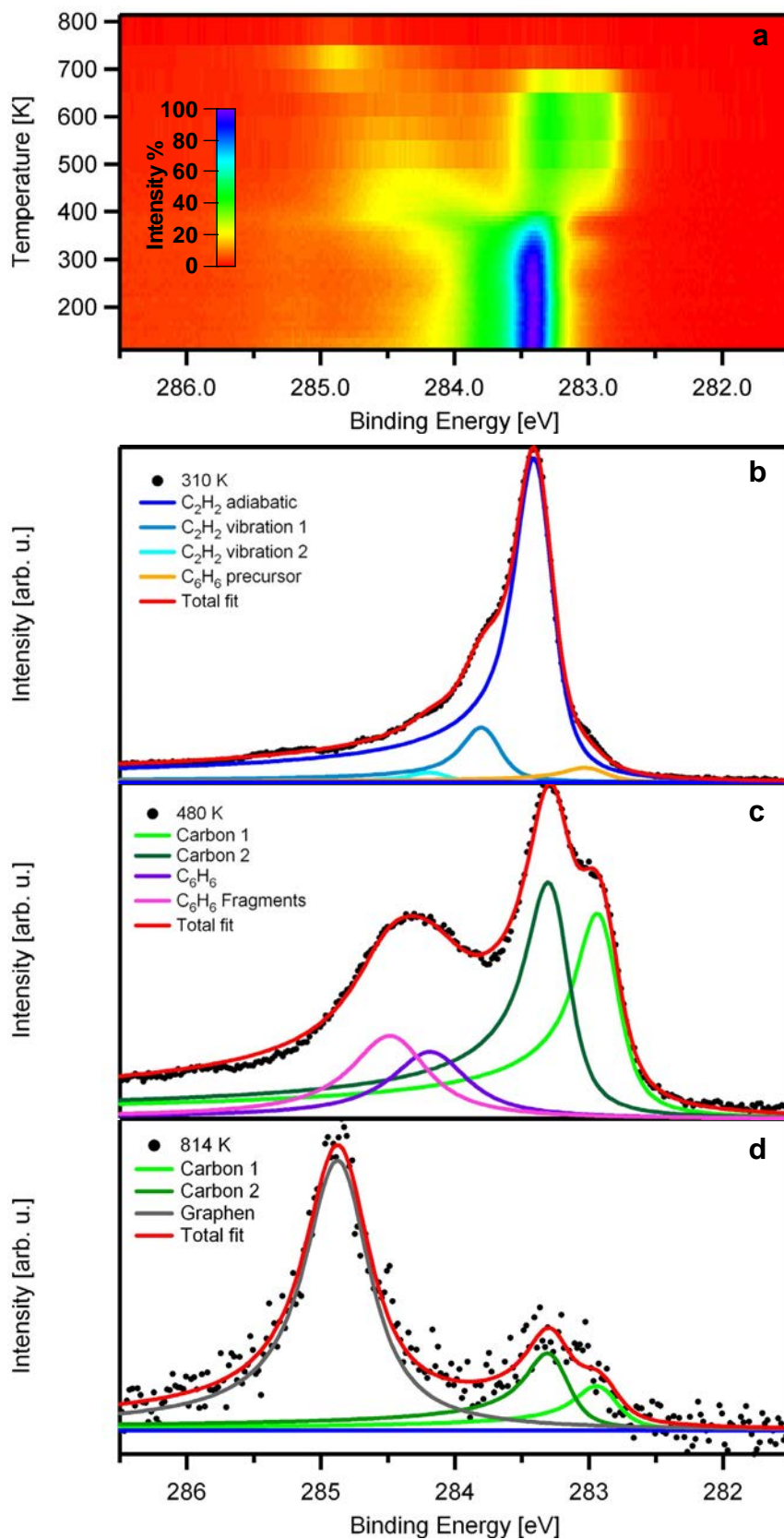


Figure 5.16: (a) Color coded density plot of the TPXPS experiment for a saturated acetylene layer on Ni(111) (b-d) Detailed fits of the spectra acquired at (b) 310 K (c) 480 K (d) 814 K

After the uptake of the acetylene on clean Ni(111) the layer was heated to 500 K with the sample filament with a rate of 0.5 K/s and a C 1s spectrum was taken every 10 K. Additional heating steps above 500 K were achieved using the resistive heating, the spectra were taken after the heating step in this temperature range. The density plot of this TPXPS is shown in Figure 5.16 (a) and the quantitative analysis in Figure 5.17. In Figure 5.16 (b-d) detailed fits are shown of temperatures where the reaction products discussed below can most clearly be seen. The displayed fit was the best achieved for this system, and the quality could not be improved further by including vibrational contributions for the C_6H_6 precursor, C_6H_6 and C_6H_6 fragments. The spectral shape and coverage remain unchanged up to 270 K; while above 270 K a new species appears at a binding energy of 282.98 eV (see Figure 5.16 (b)). The highest coverage found for this species is 0.04 ML C atoms at 340 K and at 370 K the species has disappeared from the surface. As the total C-atom coverage remains constant up to this temperature, and the C_2H_2 coverage is decreasing above 270 K it can be concluded that this new species has to be a decay or reaction product of acetylene, although a clear assignment is difficult. CH is a possible candidate, which would be in accordance with a study by Demuth et al. [158], who reported that CH was present on the surface as well as C_2H_2 after dosing 6 L of C_2H_2 on Ni(111) at room temperature. On the other hand CH was also found during TPXPS-Experiments of CH_3 on Ni(111) [54], where it appeared in the temperature range of ~150-270 K at a binding energy of 282.59 eV and reacted to acetylene at high temperatures. This would mean that at 270 K all CH should have been converted to C_2H_2 .

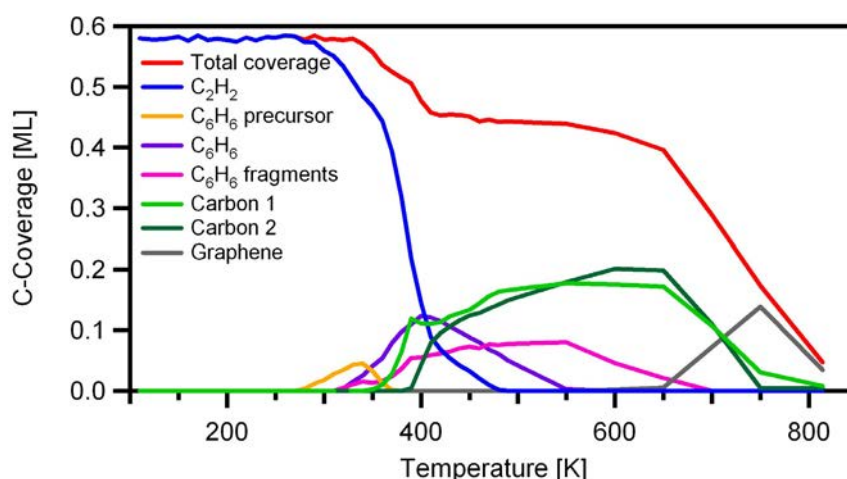


Figure 5.17: Quantitative analysis of data from Figure 5.16 (a)

Another possible assignment comes from the two species that start to appear at 284.17 and 284.47 eV above temperatures of 320 K (see Figure 5.16 (c)). The first species appearing at 284.17 eV reaches its maximum coverage of

0.12 ML C atoms at 400 K and starts to disappear again above 490 K. The second with a binding energy of 284.47 eV has its maximum intensity corresponding to 0.08 ML C atoms at 550 K and disappears above 650 K. The binding energy and thermal stability range of these two species suggest an assignment as hydrocarbon species. One possible candidate is benzene (C_6H_6), which has been reported before as an intermediate in the thermal evolution of acetylene on Ni(111) appearing around 300 K [160-162], which is close to the 330 K at which the species with the binding energy of 284.17 eV appears. The binding energy of the species at 284.17 eV is also in the region previously reported for low coverages of benzene on Ni(111) [175], and also the disappearance of the species above 490 K is consistent with TPD results of benzene on Ni(111) [176]. Therefore we assign the species as benzene. Benzene (C_6H_6) is formed from the acetylene through trimerization [160-162], and benzene adsorbs in a bridge site for coverages up to 0.6 ML C atoms [175, 177]. This means all carbon atoms are on top of Ni atoms in the first layer. So in order to trimerize to benzene the acetylene molecules have to leave their hollow-hollow positions. If the temperature range of 270-370K, in which the species with a binding energy of 282.98 eV exists is put into consideration as well as the disappearance of this species as soon as benzene starts to appear, it seems likely to assign this species to a benzene precursor state, i.e., either acetylene molecules that are displaced from their adsorption site in order to be able to trimerize or some benzene molecules that have not yet migrated to their preferred adsorption site. As benzene (C_6H_6) has been reported to dehydrogenate to C_6H_5 and C_6H_4 above 395 K [162] the species at 284.47 eV, which appears at higher temperatures than benzene, and does not increase in coverage after benzene is gone from the surface is attributed to hydrocarbons formed from the dehydrogenation of benzene. This assignment is further supported by the benzene TPD experiments conducted by Steinrück et al. [176], where hydrogen desorption from the surface was found up to 700 K, while benzene desorption was only detected up to 500 K. The quantitative analysis of our TPXPS experiment shows the same temperature threshold of 700 K for the disappearance of the C_6H_x fragments from the surface.

The next species, labeled as carbon 1 (light green in Figure 5.16 (c) and Figure 5.17), appears around 360 K at a BE of 282.90 eV. The coverage of this species increases up to 0.12 ML C atoms at 390 K and then remains almost constant until 430 K before increasing again to the maximum of 0.18 ML C atoms between 550 and 650 K and dropping to 0.03 ML at 750 K. Due to the lack of vibrational splitting, i.e. no C-H bonds on the carbon atoms this species can be clearly assigned as a carbon species. This is also in good agreement with the observed dehydrogenation of low acetylene coverages in

the decay path of ethene (C_2H_4) and ethyle (C_2H_5), as discussed in the previous chapters, and is also in agreement with literature on the thermal evolution of acetylene on Ni(111) [142]. The second carbon species (carbon 2, dark green line in Figure 5.16 (c) and Figure 5.17) found during the dehydrogenation of ethene and ethyle on Ni(111) is also found here. It appears at a binding energy of 283.26 eV and a temperature of 400 K. Its coverage increases up to 0.2 ML C atoms between 600 and 650 K before disappearing at 750 K. The final change in the spectral shape appears around 700 K, where another species appears at a BE of 284.86 eV (see Figure 5.16 (d)). The highest coverage found for this species is 0.14 ML C atoms at 750 K. This species evolution goes hand in hand with a drop in intensity of the two carbon species. Grüneis et al. [168] found that during propylene (C_3H_6) adsorption on Ni(111) at temperatures above 600 K the same two carbon species that we find here transform to graphene after longer exposure times. The XPS binding energy of the formed graphene layer was found to be 284.7 eV, which is very close to the binding energy of 284.86 eV we find for the high temperature species, and thus an assignment to graphene seems plausible. However in other experiments it was found that graphene layers on Ni(111) are thermally stable up to 1100 K [178], which is in contrast to the drop in intensity we observe for the species above 750 K (see Figure 5.17).

The total coverage remains constant at 0.58 ML C atoms from 110 to 340 K. In the temperature region of 340-420 K, where the transition of the acetylene to the hydrocarbons and the further transition to the two carbidic carbon species take place, it drops down to 0.45 ML C atoms. Such a decrease in the total coverage has also been observed for the acetylene dehydrogenation during the thermal evolution of ethene (see Figure 5.5 (c)) and ethyle (see Figure 5.10 (b)). In these cases no competing reaction, i.e. the benzene trimerization, exists besides the dehydrogenation of the acetylene. Molecular desorption of acetylene is ruled out from TPD experiments [158, 160], as there only H_2 was found to leave the surface. Thus this coverage decrease is attributed to photoelectron diffraction. Above 550 K the coverage decreases again slowly down to 0.4 ML at 650 K. As the slope of the decrease of the total coverage in this temperature range is the same as the decrease of the C_6H_x fragments, while the carbon coverage remains constant, this coverage decrease can be attributed to the desorption of the C_6H_6 fragments. However, photoelectron diffraction effects cannot be excluded either. Above 650 K carbon starts to diffuse into the bulk of the Ni(111) crystal [167] which decreases the coverage down from 0.45 ML C atoms at ~420-550 K to a remaining coverage of 0.05 ML C atoms at 800 K .

If we compare the thermal evolution of this acetylene layer with the thermal evolution of the acetylene formed during the dehydrogenation of either ethyle (C_2H_5) or ethene (C_2H_4) on Ni(111) we find both clear similarities and differences. In both cases acetylene reacts to another species around 400 K. For the pristine acetylene layer we find both a trimerization to benzene (C_6H_6) and a dehydrogenation to two carbidic carbon species, whereas for the acetylene formed during the dehydrogenation of ethyle and ethene we only found the second reaction channel. This behavior can clearly be attributed to the much higher acetylene coverage in the case of the pristine acetylene layer (0.58 ML) as compared to coverage of acetylene formed from ethene (0.26 ML) or ethyle (0.17 ML). Yang et al. [161, 162] attributed this behavior to the need for short diffusion lengths of acetylene on the surface prior to the trimerization, and found that coverages close to 0.5 ML of C_2H_2 are needed for the trimerization to take place. Although no exact threshold was given from the data presented here we can place this threshold now between the 0.26 ML acetylene formed during the dehydrogenation of ethene, at for this coverage no trimerization was observed, and the 0.5 ML for which Yang [161, 162] observed trimerization. Due to the high coverages of carbonaceous species formed from the pristine acetylene layer there is also evidence found for the formation of a new species at elevated temperatures, which could be graphene, whereas for the lower acetylene coverages the carbon is just diffusing into the bulk of the crystal.

5.3.2 Acetylene coadsorbed with O on Ni(111)

Since no or only minor traces of acetylene could be obtained in the thermal evolution of both ethene and ethane in coadsorption with oxygen on Ni(111), it is of special interest to study the coadsorption of acetylene and oxygen on Ni(111) directly. This experiment can give an answer to the question whether acetylene could not be detected in the thermal evolution of ethene and ethane coadsorbed with oxygen due to a blocking of the adsorption sites for hydrogen or because it is immediately desorbing from the surface.

The coadsorption of oxygen with acetylene was studied on a 0.23 ML containing preadsorbed oxygen layer, i.e., a slightly oxygen deficient 2×2 O layer. The resulting C 1s spectra can be seen in Figure 5.18 (a), and a detailed fit is displayed in Figure 5.18 (b). During the acetylene uptake a strong peak is growing at a binding energy of 283.34 eV, with no noticeable shifts during the uptake. Just like for acetylene adsorption on clean Ni(111) the main peak is attributed to adiabatic transition. The detailed fit reveals two vibrational contributions, which are shifted by 360 and 720 meV towards higher binding energies in respect to the main peak. Their S-Factors are 0.15

and 0.03, respectively, which points towards one C-H bond per carbon atom [28] and thus molecular adsorption of acetylene. As the binding energy and the vibrational splitting are almost identical to the values found for acetylene on clean Ni(111) (see Chapter 5.3.1) it can be concluded that acetylene adsorbs with both carbon atoms in hollow sites, just as it is the case for the clean surface [152, 159]. At exposures higher than 0.15 L a broad C 1s component appears around 284.97 eV with a coverage of ~ 0.05 ML C atoms. This component is attributed to physisorbed C_2H_2 due to the broad and unstructured spectral shape and the low thermal stability. The presence of a physisorbed component is remarkable, as for acetylene on the clean Ni(111) surface no such component exists in the same temperature range. The saturation coverage reached for the chemisorbed acetylene is 0.35 ML C atoms, which gives us a total saturation coverage of 0.4 ML C atoms together with the 0.05 ML C atoms physisorbed acetylene. This is also evident from the quantitative analysis of the uptake displayed in the inset of Figure 5.18 (a). As oxygen is also adsorbing in hollow sites on Ni(111) [65, 66] it blocks some adsorption sites for acetylene, resulting in the lower saturation coverage compared to the clean surface.

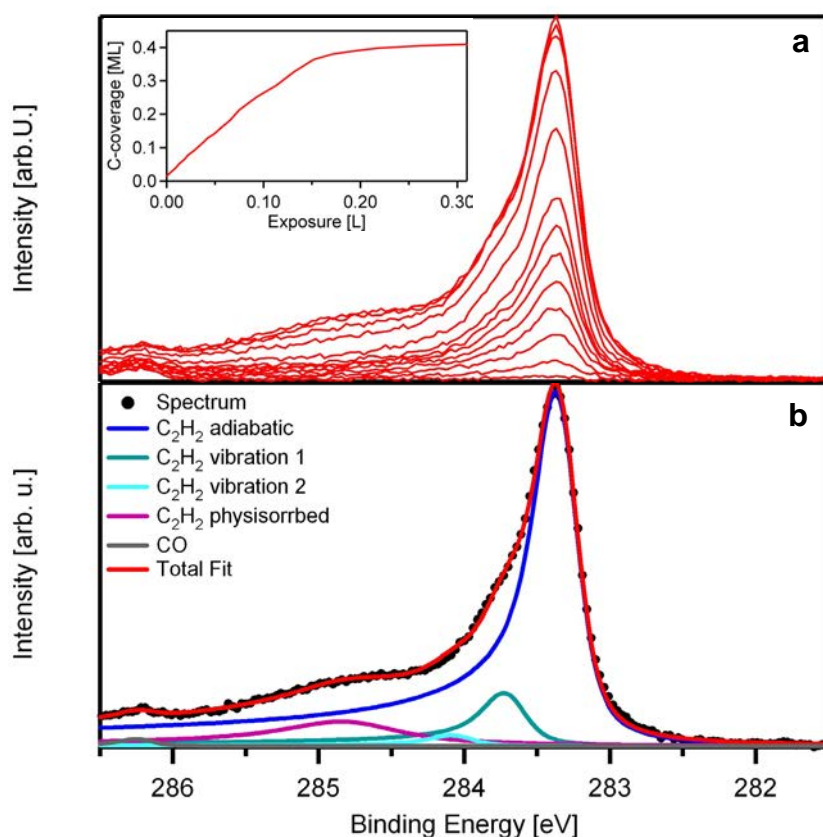


Figure 5.18: (a) Selected C 1s spectra of acetylene dosed on Ni(111) precovered with 0.23 ML O at 103 K. Inset: Total surface coverage as a function of exposure (b) detailed fit of spectrum with highest coverage

The thermal evolution for this adsorbate layer was studied applying a temperature ramp of 0.5 K/s per second with the resistive heating and taking a spectrum every 10 K. The resulting magnetic field affects the binding energy of the species in an unknown way, and thus no information can be given about this over the course of the TPXPS.

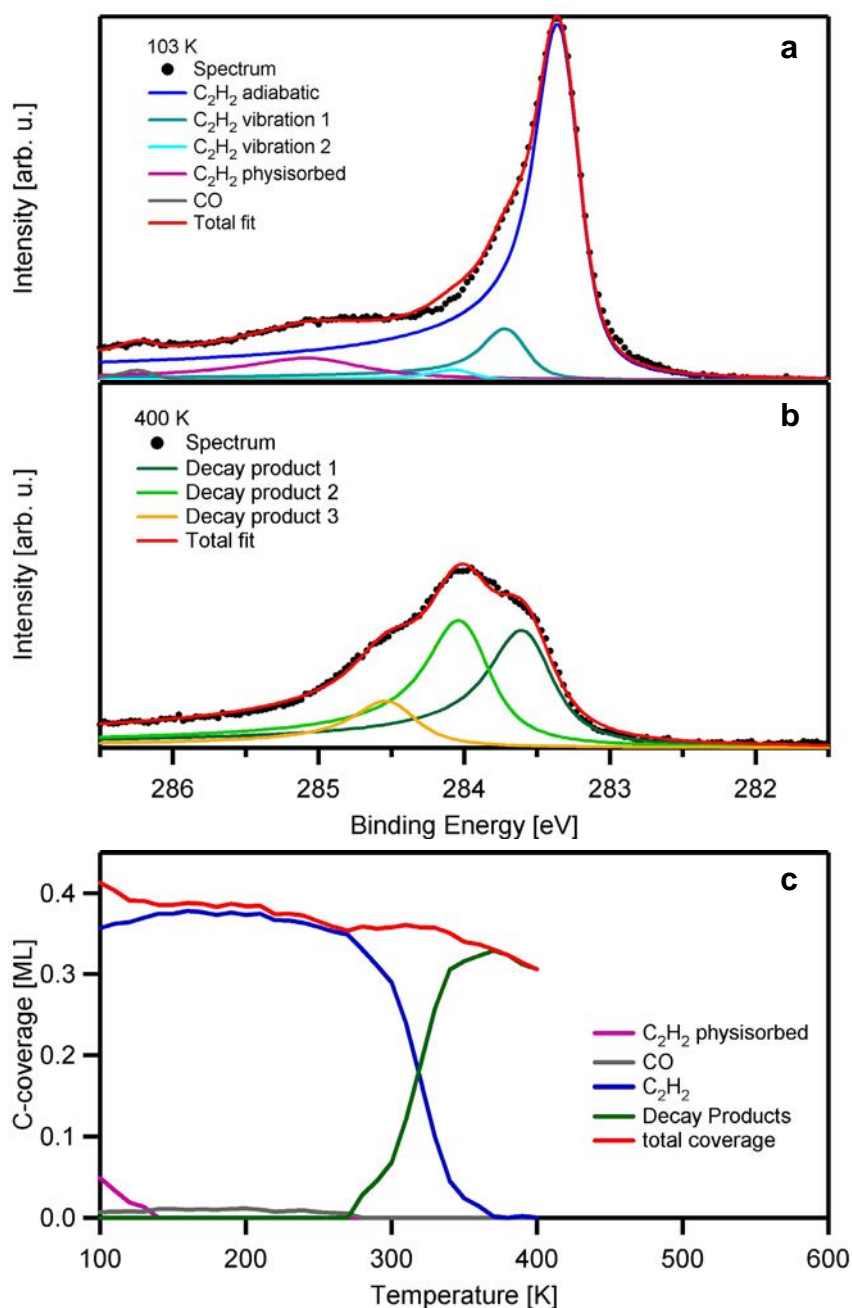


Figure 5.19: Thermal evolution of acetylene coadsorbed with oxygen on Ni(111) **(a)** detailed fit of the C 1s spectrum taken at 103 K **(b)** detailed fit of the C 1s spectrum taken at 400 K **(c)** quantitative analysis

The spectra at 100 K and 400 K however were taken without heating so the binding energies of the species present on the surface at the beginning and

the end of the experiment can be given. Careful comparison of the spectral shape of the spectra at 100 K (without heating) and 110 K (with heating) as well as of the spectra at 390 K (with heating) and 400 K (without) showed no change in spectral shape, so we are sure we can give valid information about the reaction behavior of the species. To compensate for the shifting BE we assumed a fixed BE distance between the mainpeak of the acetylene and the peaks of the decay products as well as fixed ratios and distances of the decay products among themselves, and allowed the BE of the acetylene main peak to shift. This should give us a good description of the decay process within a reasonable margin of error of the coverages of about 20%. The spectra at 100 and 400 K, which display the correct binding energies, are shown in Figure 5.19 (a) and (b), respectively. The quantitative analysis of the whole experiment is shown in Figure 5.19 (c).

The quantitative analysis shows desorption of the physisorbed acetylene up to a temperature of 140 K. At 280 K the chemisorbed acetylene starts to disappear and a set of three new peaks appear. At 400 K these peaks have binding energies of 283.56, 283.98 and 284.47 eV. The peak at 283.98 is 1.05 times larger than the peak at 283.56, and the peak at 284.47 is 0.37 the size of the peak at 283.56 eV. The ratio between the peaks at 284.47 eV and 283.98 eV is 0.35. From other data of hydrocarbons on Ni(111) (see [28] and the previous chapters) this could be interpreted as the adiabatic and first vibrational peak of a hydrocarbon species with two C-H bonds per carbon atom. However the distance between the two peaks is 490 meV and thus 100 meV larger than the highest vibrational splitting found on Ni(111) previously [28], making this interpretation highly unlikely. The transition between acetylene and the decay products takes place in the region between 270 and 370 K. Prior to this decay a small decrease of the acetylene coverage from 0.37 ML C atoms down to 0.35 ML C atoms is observed, which is attributed to a desorption of acetylene. Up to 330 K the total coverage remains constant suggesting an almost complete conversion of acetylene, and then falls slowly to 0.31 ML at 400 K. A clear assignment of the species is difficult. The species at 284.47 eV has the same binding energy as the C₆H₆ fragments on the clean Ni(111) surface, and also the temperature range in which the species appears is similar. If we assign this species to C₆H₆ fragments this implies that acetylene is also able to trimerize in the coadsorption case with oxygen. This raises the question however why we do not see the benzene peak at 284.17 eV, that appeared at the clean Ni(111) surface. Papp [27] observed for the coadsorption of benzene on Ni(111) with both CO and NO a shift of the benzene C 1s binding energies towards lower binding energies. As also a shift towards higher binding energies was observed for higher benzene coverages it was suggested that the binding

energy shift depends on the surface dipole induced by the coadsorbate (negative surface dipole for NO and CO and positive surface dipole for benzene-benzene coadsorption). Oxygen also induces a negative surface dipole so a shift towards lower binding energies is to be expected for the benzene binding energy, making an attribution of the peak at 293.98 eV as benzene possible. If we now further compare the TPXPS of acetylene on the clean Ni(111) surface with the TPXPS of acetylene on the oxygen precovered surface, it seems appropriate to assign the peak at 283.56 eV to a carbonaceous species.

5.4 Concluding Discussion

In studying the adsorption of ethane (and ethyle), ethene and acetylene on Ni(111) the importance of analyzing the vibrational fine structure of the adsorbates becomes evident, since it is of great importance for the identification of the adsorbates. Ethane (C_2H_6) exposed on the clean Ni(111) surface using a high energy molecular beam adsorbs dissociatively as ethyle (C_2H_5), whereas no adsorption was found when using a low energy beam. Both for ethene (C_2H_4) and acetylene (C_2H_2) molecular adsorption was found. While for acetylene (C_2H_2) adsorption the C 1s spectra are dominated by a single main peak, the spectra of ethene (C_2H_4) and ethyle (C_2H_5) both show two main peaks of similar height. The actual ratio of both peaks, however, was found to be dependent on the experimental geometry due to photoelectron diffraction. Since for both adsorbates the two peaks grow simultaneously over the whole timeframe of the uptake, it can be concluded that the two peaks originate from two carbon atoms within one molecule bound in different positions on the surface. Two different adsorption geometries for the molecules, as found e.g. for CO on Ni(111) [179] would lead to the two peaks growing consecutively instead of simultaneously. For ethene adsorption this observation helped to solve the old riddle of the adsorption geometry on Ni(111), as all but one of the adsorption geometries proposed by HREELS experiments show equivalent adsorption sites for the two carbon atoms. The remaining adsorption geometry has one carbon atom adsorbing in a hollow site and the second binding in an on-top position. Due to the similar binding energies the same adsorption geometry also seems likely for ethyle (C_2H_5) on the clean Ni(111) surface. Acetylene is widely accepted to adsorb in a hollow-hollow adsorption geometry on Ni(111), which is in good agreement with our data, showing only one main peak in the C 1s spectrum. All binding energies and adsorption geometries of the various C_2H_x are summarized in Table 5.1.

As on the clean Ni(111) surface all adsorbates adsorb with one carbon atom in a hollow position the binding energies of all three species are very close to each other. This further emphasizes the importance of analyzing the vibrational splitting to correctly identify the different adsorbates by their characteristic S-Factor. The mean S-Factor found for all adsorbates discussed in Chapter 5 is 0.17 ± 0.02 and is thus exactly the same value Steinrück et al. [28] found for various hydrocarbons adsorbed on Ni(111) and Pt(111).

Adsorbed Species	C ₁ /C ₂ Binding Energy [eV]	Vibrational Splitting for C1/C2	S-Factor for C1/C2	Coverage in ML C atoms	Adsorption Geometry
C ₂ H ₂ /Ni(111)	283.33-283.40/ Same as C1	390	0.19	0.58	Hollow/Hollow
C ₂ H ₂ /O/Ni(111)	283.34/ Same as C1	360	0.15	0.35	Hollow/Hollow
C ₂ H ₄ /Ni(111)	283.35-283.48/ 283.98-284.07	360/ 360	0.32/ 0.32	0.5	Hollow/On-top
C ₂ H ₄ /O/Ni(111)	283.27-283.34/ Same as C1	350	0.33	0.28	Hollow/Hollow
C ₂ H ₅ /Ni(111)	283.28-283.33/ 283.94-283.95	360/ 320	0.34/ 0.51	0.22 [54] (dependant on kinetic energy)	Hollow/CH ₃ group not interacting with surface
C ₂ H ₆ /O/Ni(111)	283.33/ Same as C1	400	0.53	0.22 (not saturated)	Hollow/Hollow

Table 5.1: Binding energies, vibrational data, coverages and adsorption sites for C₂H_x species on clean and oxygen precovered Ni(111)

In the study of the thermal evolution of the adsorbates on the clean Ni(111) surface an interesting coverage effect for acetylene could be confirmed. Both ethene (C₂H₄) and ethyle (C₂H₅) dehydrogenate to acetylene upon heating around 200 K. During these two dehydrogenation paths the formed acetylene further dehydrogenates to carbidic carbon species around 400 K. However, if acetylene is dosed directly onto Ni(111) upon heating a partial trimerization of

the acetylene to benzene (C_6H_6) is found. This can be attributed to the higher coverage reached when dosing pristine acetylene (0.58 C atoms) compared to the coverage of acetylene formed from the dehydrogenation of ethene and ethyle (0.26 and 0.17 ML, respectively). The higher coverage leads to shorter diffusion path lengths for acetylene prior to the trimerization. For even higher temperatures the benzene partly decays to the same carbidic carbon species found in the decay paths of the other two adsorbates, however, the achieved coverage of carbonaceous species is much higher than in the other cases, with 0.38 ML C atoms, compared to 0.20 ML C atoms formed in the dehydrogenation of ethene and 0.07 ML in the dehydrogenation of ethyle. Around 650 K the carbon diffuses in the bulk in all three cases, but for the highest coverage formed during the dehydrogenation of acetylene, the formation of a new species is found in this temperature region, for which no clear assignment is possible. In the other two cases the total amount of carbon is too low to allow this reaction path.

On oxygen precovered Ni(111) there are significant changes in the adsorption mechanisms for all the studied molecules. Ethane was found to adsorb molecularly on a Ni(111) surface precovered with 0.19 ML oxygen, even though it was dosed with the same kinetic energy that enabled dissociative adsorption on the clean surface. This molecular adsorption leads to a vastly different C 1s spectrum which is dominated by a single adiabatic main peak instead of the two main peaks found for ethyle on clean Ni(111). The reason for this molecular adsorption is that hydrogen formed during the dissociative adsorption favors hollow adsorption sites [170-172], which are blocked by oxygen [65, 66]. This blocking of the adsorption sites for hydrogen by the oxygen is also the most likely reason for the desorption of the majority of the adsorbed ethane without any dehydrogenation. Around 20% of the initial ethane coverage is converted to carbonaceous species and hydrocarbons, indicating some dehydrogenation is taking place despite the presence of the oxygen. Comparison with an ethane adsorption experiment on a Ni(111) surface precovered with 0.25 ML oxygen, where the ethane desorbed completely upon heating, showed that the carbonaceous species and hydrocarbons formed on the 0.19 ML O are only formed because the layer is oxygen deficient compared to a closed O (2x2) layer with 0.25 ML oxygen. It is unclear how the oxygen affects the saturation coverage for ethane on Ni(111). As can be seen from Table 5.1 the ethane coverage is 0.22 ML in both cases. However on the clean surface the saturation coverage depends strongly on the initial kinetic energy of the molecules as shown by Fuhrmann [54], and the adsorbate layer on the oxygen precovered surface is not saturated even though the adsorption time is already 6 times the adsorption time used on the clean surface.

Similar observations were made during a coadsorption experiment of ethene and 0.25 ML oxygen on Ni(111). Just like for the ethane the C 1s spectrum looks drastically different, with only one adiabatic main peak instead of two found for ethene adsorption on the clean surface. As the remaining peak has a binding energy of 283.34 eV which is typical for hydrocarbons adsorbed in a hollow position it is concluded that the presence of the oxygen changes the preferred adsorption site of ethene on Ni(111) from hollow-on top to a hollow-hollow geometry, which is also found for acetylene on Ni(111). A clear disambiguation between ethene and acetylene can be made by analyzing the vibrational finestructure, as they feature different S-Factors, as can be seen in Table 5.1. The oxygen presence on the surface leads also to a reduced saturation coverage, with a coverage of 0.28 ML C atoms. This is only 56% of the coverage obtained on the clean surface. Upon heating ethene desorbs completely up to 225 K with only very few traces of carbonaceous species formed. This can again be attributed to the blocking of the adsorption sites for hydrogen by the oxygen, inhibiting the dehydrogenation. The traces of carbonaceous species still formed are due to slight local variations in oxygen coverage.

The least changes to the behavior on the clean surface are found for the acetylene coadsorption with 0.23 ML oxygen. The spectral shape of the molecularly adsorbed acetylene is very similar to the situation on the clean surface. However the coverage is reduced to approximately 60% of the saturation coverage on the clean surface. This reduction is about the same size we find for the coadsorption of ethene and oxygen on Ni(111). Another interesting observation is that a physisorbed acetylene species with a coverage of 0.05 ML at 103 K exists on the oxygen precovered surface, although no such species is found on the clean surface. A similar finding was made for the coadsorption of ethane and oxygen on Ni(111), although there the physisorbed species is even less strongly bound, as at a temperature of 101 K it completely desorbs upon decreasing the pressure. This effect, that oxygen seems to stabilize physisorbed species on the nickel surface is even more strongly seen for the oxidized Ni(111) surface, as detailed in Chapter 6.2.2. In the context of this discussion it seems fair to mention that the exact nature of the bond of ethene and ethane coadsorbed with oxygen could not be determined. Although the binding energy, which is very similar for all the adsorbed species discussed in Chapter 5 hints at a chemisorbed species in all cases, the very low desorption temperatures, with desorption already starting below 150 K for ethane and ethene coadsorbed with oxygen, raises the question if an assignment as a physisorbed species would not be better. Such a fast desorption of the adsorbed species is not found for the coadsorption of acetylene and oxygen. Here a similar reaction path is found

as on the clean Ni(111) surface with a possible trimerization of the adsorbed acetylene to benzene, and other fractions of the acetylene dehydrogenating to carbonaceous species. This dehydrogenation is probably possible due to some oxygen vacancies on the surface since the layer studied is not a saturated O(2x2) overlayer. The oxygen however affects the binding energies of some of the reaction products, leading to a lower binding energy for benzene.

In summary for the adsorption of C_2H_x species on clean and oxygen precovered Ni(111) it was found that C_2H_5 , formed from the dissociative adsorption of C_2H_6 , and C_2H_4 adsorb in an asymmetric hollow/on-top adsorption geometry on clean Ni(111). C_2H_2 on the clean surface and all studied adsorbates on the oxygen precovered surface adsorb in a symmetrical hollow/hollow geometry. During heating C_2H_5 and C_2H_4 decay to C_2H_2 which further dehydrogenates to carbonaceous species which subsequently diffuse into the bulk. For high coverages acetylene trimerizes to benzene, and for high coverages of carbon graphene formation is suggested at high temperatures. Oxygen blocks or hinders the dehydrogenation of both ethene and ethane, leading to molecular adsorption of ethane and thermally instable adsorbates. It also reduces the saturation coverages for ethene and acetylene by 40% and increases the adsorption times needed for ethane to obtain higher coverages. Physisorbed species are stabilized by an oxygen precoverage and can be observed at higher temperatures compared to the clean Ni(111) surface.

6 Adsorption of hydrocarbons on Cu(111) and thin NiO layers

6.1 Acetylene adsorption and reaction on thin NiO surfaces

6.1.1 Acetylene adsorption on clean Cu(111)

In order to understand the adsorption behavior of acetylene (C_2H_2) on the Cu(111) surface covered with the NiO clusters (nominal coverage 0.5 ML), first the acetylene interaction with the clean Cu(111) surface has to be studied, since the cluster covered surface also has patches of this surface type.

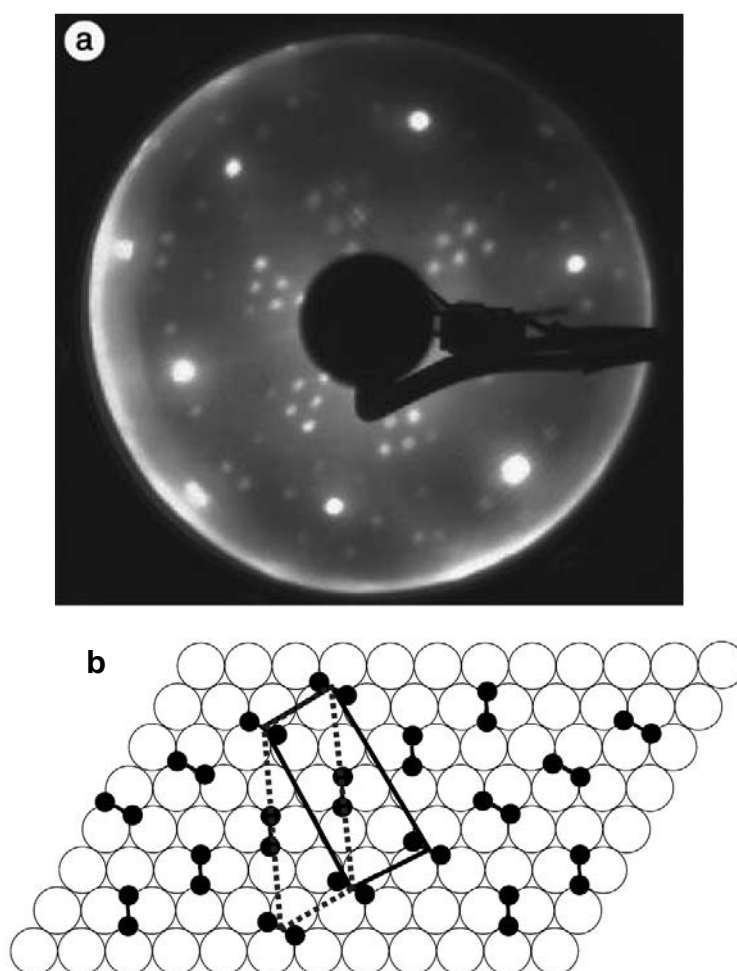


Figure 6.1: (a) LEED picture of a saturated C_2H_2 layer on Cu(111). (b) proposed adsorption geometry for this LEED structure. Both pictures taken from [180]

The adsorption and thermal evolution of acetylene on Cu(111) has been studied quite intensively so far. Demuth was the first to study the system with UPS [181], finding hints for a strong distortion of the molecule upon adsorption. Bandy et al. [182] found a rehybridisation of the molecule upon

adsorption with HREELS, and suggested a hollow-hollow adsorption geometry for the molecule with the C-C axis parallel to the surface, just as it is the case on Ni(111) (see Chapter 5.3.1). This requires the molecule to elongate the C-C distance to a value of 1.48 Å which is explaining the rehybridisation of the molecule [183]. This adsorption geometry was confirmed with various techniques, including PhD [183], STM [184] and DFT [185] studies. From a NEXAFS and He Scattering study [186] it was determined that the two hydrogen atoms are bent out of the molecular plane and face upward, away from the surface. A LEED study [180] revealed a rather complex diffraction pattern that can be notated as $\begin{pmatrix} 2 & 1 \\ 0 & 4 \end{pmatrix}$ and is displayed in Figure 6.1 (a). This structure corresponds to a coverage of 0.5 ML C atoms (0.25 ML C₂H₂ molecules), and the proposed adsorption geometry is displayed in Figure 6.1 (b). Upon heating a desorption temperature of 323 K was reported for acetylene [187]. A detailed TPD study [188] revealed that acetylene does not desorb molecularly but rather reacts to ethylene (C₂H₄), benzene (C₆H₆), butadiene (C₄H₆) and cyclooctatetraene (C₈H₈), which subsequently desorb from the surface. Isotope exchange experiments within the TPD study showed that the benzene formation is an associative mechanism, whereas in the formation of butadiene strong kinetic isotope effects were observed associated with C-H cleavage.

To characterize the interaction of acetylene with Cu(111) we dosed acetylene on the surface with the multicapillary array doser at a temperature of 112 K. The spectra were collected at an emission angle of 0° and to avoid beam damage the measuring spot was changed after each spectrum. The resulting C 1s spectra are shown in Figure 6.2(a). The spectra are dominated by an adiabatic peak with a binding energy of initially 283.36 eV, which shifts to 283.42 eV for higher coverage. The detailed fit, as displayed in Figure 6.2 (b), shows a vibrational contribution with a shift of 370 meV to higher binding energies in respect to the main peak. From the peak areas an S-factor of 0.21 is calculated. If the results from the Ni(111) surface (Chapter 5, [28]) and from Pt(111) [28] are taken into consideration this S-Factor is a proof of one C-H bond per carbon atom. This means that acetylene is adsorbing molecularly on the surface, in accordance with literature. Shifted by 740 meV towards higher binding energies a second vibrational peak is found. The absence of a second adiabatic peak, like we see for ethylene and ethyle on Ni(111) (see Chapters 5.1.1 and 5.2.1, respectively) points to chemically equivalent adsorption sites for the two C-atoms, again in good agreement with the reported hollow-hollow adsorption geometry [183, 185]. The inset of Figure 6.2 (a) shows the quantitative analysis of the uptake. The coverage of acetylene increases linearly with exposure until the saturation coverage is reached. The saturation

coverage is set to be 0.5 ML of C-atoms. This was determined as saturation coverage by LEED [180]. The thermal evolution of the layer was studied by heating the surface to the designated temperature and subsequent acquisition of a C 1s spectrum. The surface was shifted to a new spot after each spectrum to avoid beam damage.

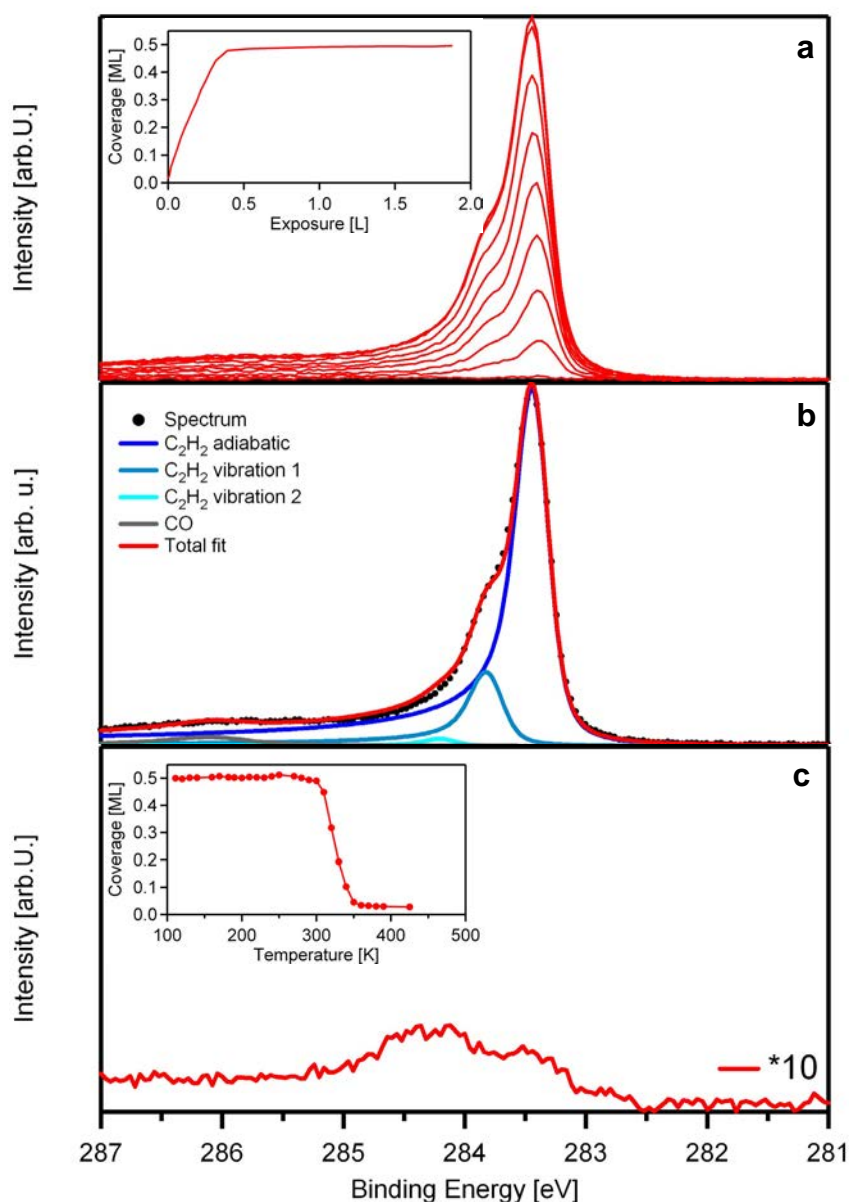


Figure 6.2: (a) selected C 1s spectra for C_2H_2 uptake on clean Cu(111) at 112 K, taken at an angle of 0° *Inset:* Quantitative analysis (b) detailed fit of saturation coverage spectrum (c) C 1s spectrum taken after heating to 425 K *Inset:* Quantitative analysis of the thermal evolution

The quantitative analysis of this TPXPS experiment is displayed in the inset of Figure 6.2 (c). The carbon coverage is starting to decrease slightly starting at 280 K until above 310 K a rapid decline of the coverage sets in, leaving a remaining coverage of 0.03 ML C-atoms on the surface at 360 K and above. Determination of the inflection point leads to a desorption/reaction

temperature of 325 K, which is very close to the value of 323 K reported in literature [187]. With this temperature an activation energy of 89 kJ/mol is estimated from the Redhead equation [189]. The spectral shape remains almost constant up to 350 K, where the spectrum of the residual adsorbates is noticeably different from the acetylene spectrum, see Figure 6.2 (c). The spectrum of the residual products shows two peaks at binding energies of 283.39 eV and 284.19 eV.

What is especially remarkable is that, apart from the minority residual species, no reaction products are observed. At first this seems in contradiction to the results of Kyriakou et al. [188] who reported that acetylene reacts to ethylene (C_2H_4), benzene (C_6H_6), butadiene (C_4H_6) and cyclooctatetraene (C_8H_8) in the temperature range where the reaction is observed. However most of these reaction products have very low desorption temperatures. For benzene a peak temperature of 225 K was found in TPD experiments [190], for butadiene the monolayer TPD peak lies at 195 K [191] and ethylene has the main desorption peak at 120 K [192], so these three reaction products are expected to immediately desorb from the surface as soon as they are formed, and are therefore not detected by XPS. Only the cyclooctatetraene has a high temperature desorption state with a desorption temperature of ~ 475 K [188]. Since cyclooctatetraene was found to be only a minority reaction product with a yield of $\sim 2.5\%$ this could be in line with the remaining coverage of 0.03 ML residual products on the surface, making an assignment of the two peaks at 283.39 eV and 284.19 eV to two carbon atoms of the C_8H_8 in different adsorption sites a possibility. Another explanation of these peaks would be the formation of carbon fragments due to some dehydrogenation, like we see for acetylene on Ni(111) (see Chapter 5.3.1). Since the binding energies reported for carbon on Cu(111) are in the range of 284.7-284.9 eV [193-195] this seems an unlikely assignment. The onset of reaction at around 280 K is also in agreement with the onset of benzene and butadiene formation as reported by Kyriakou et al. [188].

When the results obtained for the acetylene interaction with Cu(111) are compared with the acetylene adsorption and reaction on Ni(111), as presented in Chapter 5.3.1 the similarities are interesting. On the two surfaces the binding energies are almost identical, with the acetylene on Cu(111) spectrum switched by 20 meV towards higher binding energies in respect to the Ni(111) surface. The vibrational structure is also very similar with the distance between the adiabatic and first vibrational peak being smaller by 20 meV on the Cu(111) surface and the S-Factor being larger only by 0.02. These values are all within the margin of error. Such similarities are also found in the HREELS spectra of acetylene on these surfaces, as shown by Bandy et al. [182]. This very similar behavior can be attributed to the fact, that

the local adsorption structure on both surfaces is nearly identical within the margin of error as Bao and coworkers showed with photoelectron diffraction studies for acetylene on Cu(111) [183] and Ni(111) [159]. It is interesting to note however that both the saturation coverage, which is 0.08 ML larger on the Ni(111) surface, and the LEED pattern ($p(2 \times 2)$ for low exposures of acetylene on Ni(111) [158]; $\begin{pmatrix} 2 & 1 \\ 0 & 4 \end{pmatrix}$ structure for acetylene on Cu(111) [180])

differs between the two surfaces. If the thermal evolution of the adsorbed layer is compared the similarities continue. On both surfaces the acetylene starts to react around 270 K. For acetylene on Ni(111) a trimerization to benzene is confirmed by the data presented in chapter 5.3.1 and for Cu(111) it has been suggested in literature [188], but could not be confirmed due to the low desorption temperature of benzene on Cu(111). A notable difference is that no benzene precursor species was found on Cu(111). The activation energy for the reaction also seems to be slightly higher on Ni(111), as there acetylene is still found on the surface even above 400 K, whereas on Cu(111) all acetylene is used up or has desorbed at 360 K.

The similarities for the adsorption and reaction of acetylene on Ni(111) and Cu(111) are even more interesting when taking into consideration that most other adsorbates show strongly different behavior on the two surfaces, as can be seen e.g. for ethylene and ethane interaction with Ni(111) and Cu(111), see Chapters 5 and 6.2.1, respectively.

6.1.2 Acetylene adsorption on thin NiO layers

Even though NiO seems to be a suitable catalyst for carbon nanotube growth from acetylene [196], the actual interaction of acetylene with NiO has received very little attention so far. The only study was conducted by Demuth [158], who proposed that acetylene (C_2H_2) dissociated to CH on an oxidized Ni(111) surface at room temperature; however, some key arguments in this designation were later shown to be not valid [162].

The first NiO surface for which we discuss the interaction with C_2H_2 is Ni(111) oxidized at 550 K, as described in detail in Chapter 4.1.3. C_2H_2 was dosed using the multicapillary array doser at a surface temperature of 120 K. Figure 6.3 (a) shows selected C 1s spectra acquired during this uptake experiment. The spectra show two clearly separated peaks, the first of which emerges at 283.45 eV and shifts towards 283.26 eV for higher coverages while the latter starts at 285.21 eV and shifts towards 285.31 eV.

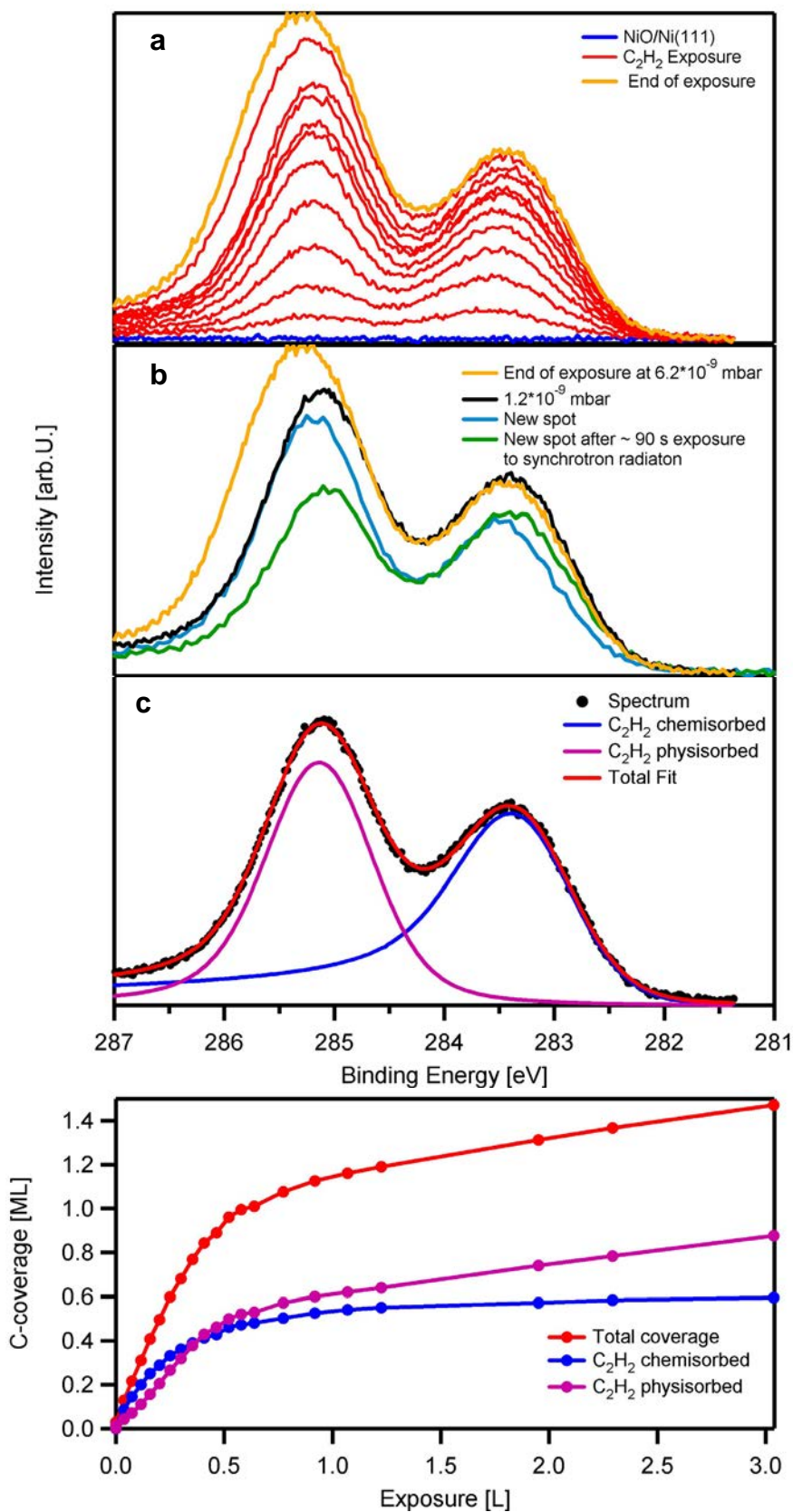


Figure 6.3: (a) Selected C 1s spectra acquired during exposure of Ni(111) oxidized at 550 K to C₂H₂ at 120 K, collected at an emission angle of 45° (b) Spectral changes after exposure to acetylene (c) Detailed fit of black spectrum from (b) (d) Quantitative analysis of the uptake experiment.

After the C_2H_2 pressure in the chamber was reduced at the end of the experiment the higher binding energy peak shifted back to 285.12 eV and lost intensity while the lower binding energy peak remained constant both in binding energy and intensity, see Figure 6.3 (b). Due to the intensity loss as the acetylene pressure is lowered this peak is assigned to physisorbed C_2H_2 . It is also close in binding energy to the physisorbed component found at 284.97 eV for the coadsorption of acetylene and oxygen on Ni(111). The other peak has a similar binding energy as chemisorbed acetylene on Ni(111), which appears at 283.40 eV and is thus assigned to a chemisorbed species. As the spectra were acquired under an emission angle of 45° , shifting sample position after each spectrum in order to avoid beam damage was not possible. Therefore after the uptake the position of the synchrotron light on the sample was changed to a different spot to examine if any beam damage had occurred. Figure 6.3 (b) shows that this led to an intensity loss for both peaks. Additionally both peaks shift slightly in binding energy to 283.42 and 285.17 eV, respectively. After an additional irradiation by the synchrotron light for ~ 90 s the peaks appear at 283.33 and 285.07 eV, respectively, with the first slightly gaining in intensity and the latter losing some intensity. Both the changes in intensity and binding energy can best be explained by beam damage.

As both peaks appear rather broad, and miss the obvious shoulders found in the spectra of chemisorbed acetylene on Ni(111) (Chapter 5.3.1) or Cu(111) (Chapter 6.1.1), it is very hard to tell if during the beam damage a new species is evolving. A closer investigation of the peaks also did not reveal any fine structure, and thus the two peaks were both fitted with a single, broad peak as shown in Figure 6.3 (c). The chemisorbed species shows a significant asymmetry, while the physisorbed species has an almost symmetrical peak shape.

A possible explanation for the broad peak shape of the chemisorbed species could be different adsorption sites, which might be expected due to the rough nature of the substrate discussed in Chapter 4. The adsorbate peaks of the different contributions cannot be individually resolved and in combination give rise to a very broad peak without resolvable substructure. In this context the peak shift for the chemisorbed peak during the beam damage experiment can be explained by a higher content of a dissociated species within the overall peak shape leading to a shift of the peak position. As there is also a slight increase in the intensity for the chemisorbed species, the dissociated species have to come mainly from the physisorbed layers, however the slight increase for the chemisorbed species could also be explained by lifted damping due to the partial desorption of the physisorbed component.

Figure 6.3 (d) shows the quantitative analysis of the uptake obtained from the fit. The coverages were referenced to the (2x2) ethylene layer on Ni(111) discussed in Chapter 5.2.1. The chemisorbed species saturates around 0.6 ML and the highest coverage found for the physisorbed component is 0.87 ML. At the new spot both components have a coverage of 0.48 ML each. The almost linear increase of the physisorbed component in the later stages of the uptake is in good accordance with a monotonous C₂H₂ pressure increase in the chamber during this phase of the experiment, and shows again that for this component an adsorption/desorption equilibrium dependent on the acetylene pressure in the chamber exists. The most remarkable aspect of the uptake is the almost simultaneous evolution of the chemisorbed and the physisorbed components. In most adsorption experiments for other adsorbate systems the physisorbed component only appears when a significant amount of the chemisorbed component is already present on the surface. There are two possible explanations for the almost simultaneous appearance of both components. The first would be that the physisorbed component does not adsorb as a multilayer on top of the chemisorbed acetylene, but instead in a different adsorption site directly on the oxide, but is not bound as strongly there as the chemisorbed component in its adsorption site. There are however several arguments against this possibility: firstly, it is highly unusual for an adsorbate to occupy a favorable and a less favorable adsorption site at the same time. Secondly, the total coverage of up to 1.47 ML seems much too high to fit into just one layer on the surface, even if we assume it as very rough, and lastly there is a small increase of the chemisorbed component as the physisorbed component desorbs as the acetylene pressure is lowered. This increase can be attributed to the lifting of a damping effect by the physisorbed component which implies that it sits on top of the chemisorbed one. Together these arguments favor the second possible explanation: The adsorption site for the physisorbed component is either due to energetic reasons or due to a much higher sticking coefficient so much favored over the chemisorbed adsorption site, that it is occupied as soon as it becomes available. The uniform rise of both peaks however implies that the adsorption site for the physisorbed component has to be either on top of the chemisorbed acetylene or close by and thus strongly influenced by the chemisorbed component. As soon as chemisorbed acetylene is adsorbed somewhere, the favorable multilayer sites become available and are filled. The “second physisorbed layer” on the other hand seems to be more unfavorable again, as the growth of the physisorbed component beyond the coverage of the chemisorbed component is limited by the background pressure of the acetylene.

A very similar situation is found if C_2H_2 is dosed on thin NiO layers on Cu(111). In order to avoid beam damage an uptake experiment was conducted, where a thin NiO layer grown from 2 ML Ni/Cu(111) was exposed to C_2H_2 at a constant surface temperature of 130 K. After each spectrum the sample was shifted to a position not yet exposed to the synchrotron radiation to minimize beam damage. This was possible here as the spectra were acquired under an emission angle of 0° .

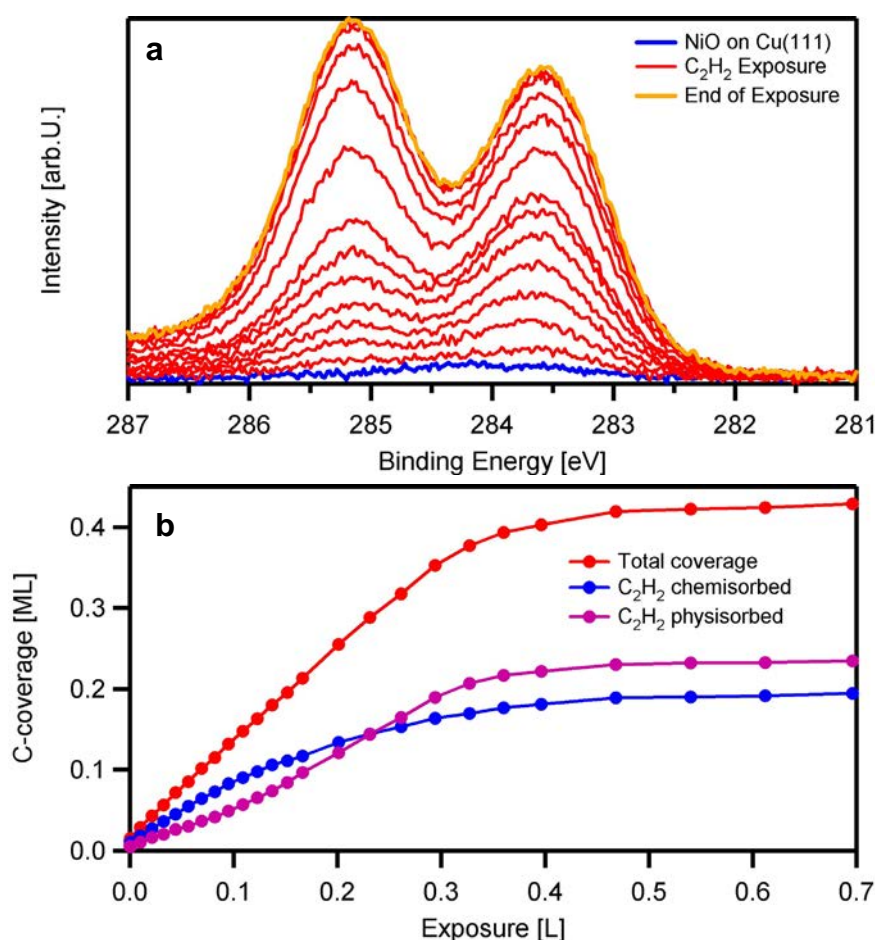


Figure 6.4: (a) Select C 1s spectra acquired during C_2H_2 exposure of a thin NiO layer on Cu(111) at 130 K. All spectra acquired at 0° emission angle with change of sample position after each spectrum. (b) quantitative analysis of data from (a).

Interestingly, the resulting spectral series, shown in Figure 6.4 (a), looks very similar to the one obtained on the NiO/Ni(111) layer shown in Figure 6.3 (a), even though the latter was found to be subjected to heavy beam damage. This confirms that the majority of the adsorbed molecules in both cases are not influenced by the photons. In the experiment depicted in Figure 6.4 (a) the chemisorbed species appears at 283.64 eV and shifts to 283.49 eV at saturation coverage. The binding energy region for the physisorbed component is smaller, ranging from 285.17 eV for low coverages to 285.13 eV at the end of the experiment. Figure 6.4 (b) shows the quantitative analysis of

the uptake, obtained with a very similar fit to the one shown in Figure 6.3 (c); the respective peak widths differ by less than 5 %. The saturation coverages found for the chemisorbed and physisorbed component are 0.19 and 0.23 ML C-atoms, respectively, however it should be mentioned that the coverage of the physisorbed species was found again to be dependent on the acetylene pressure in the chamber.

This saturation coverage is the only noticeable difference between the acetylene uptake on NiO/Cu(111) and the acetylene uptake on NiO/Ni(111) discussed earlier, where a saturation coverage of 0.48 ML was found. Another important similarity between the acetylene uptakes on the NiO layers on the different substrates is that we again find the surprising almost simultaneous growth of the physisorbed and the chemisorbed component.

If we combine all findings we have to conclude that the acetylene uptakes on both NiO layers are similar. Peak positions, peak shapes and uptake behavior are virtually the same on both surfaces. The only noticeable difference is the saturation coverage, with the saturation coverage for the chemisorbed component on NiO/Cu(111) only being 40% of the saturation coverage found on NiO/Ni(111). Due to the broad peak, which might imply different adsorption sites it is very hard to find an explanation for this behavior. A possible approach could be that the two surfaces, although both should be (111) oriented, as discussed in Chapter 4, could have different roughness. If the NiO/Ni(111) is rougher than on Cu(111), more adsorption sites would be available leading to higher coverages.

6.1.3 Thermal evolution of acetylene adsorbed on thin NiO layers

In order to study the thermal evolution of acetylene adsorbed on NiO/Ni(111) the layer was heated with the filament with a rate of 0.5 K/s. A spectrum was taken every 10 K under an emission angle of 45°, and the sample position was kept constant over the whole course of the series. The experiment was done on the new spot studied after the uptake was finished. The resulting spectra and analysis are shown in Figure 6.5. The density plot and the quantitative analysis show that the physisorbed species decreases in intensity from the start of the experiment and is completely gone from the surface at 190 K. As already at the end of the uptake some desorption was found this behavior was to be expected and it further strengthens the assignment as a physisorbed species. At 150 K, a new species starts to evolve at a binding energy of 284.62 eV. The fit of a spectrum taken at 500 K (Figure 6.5 (b)), at which temperature the species is fully evolved, shows that also this species has a very broad peak without any additional substructure.

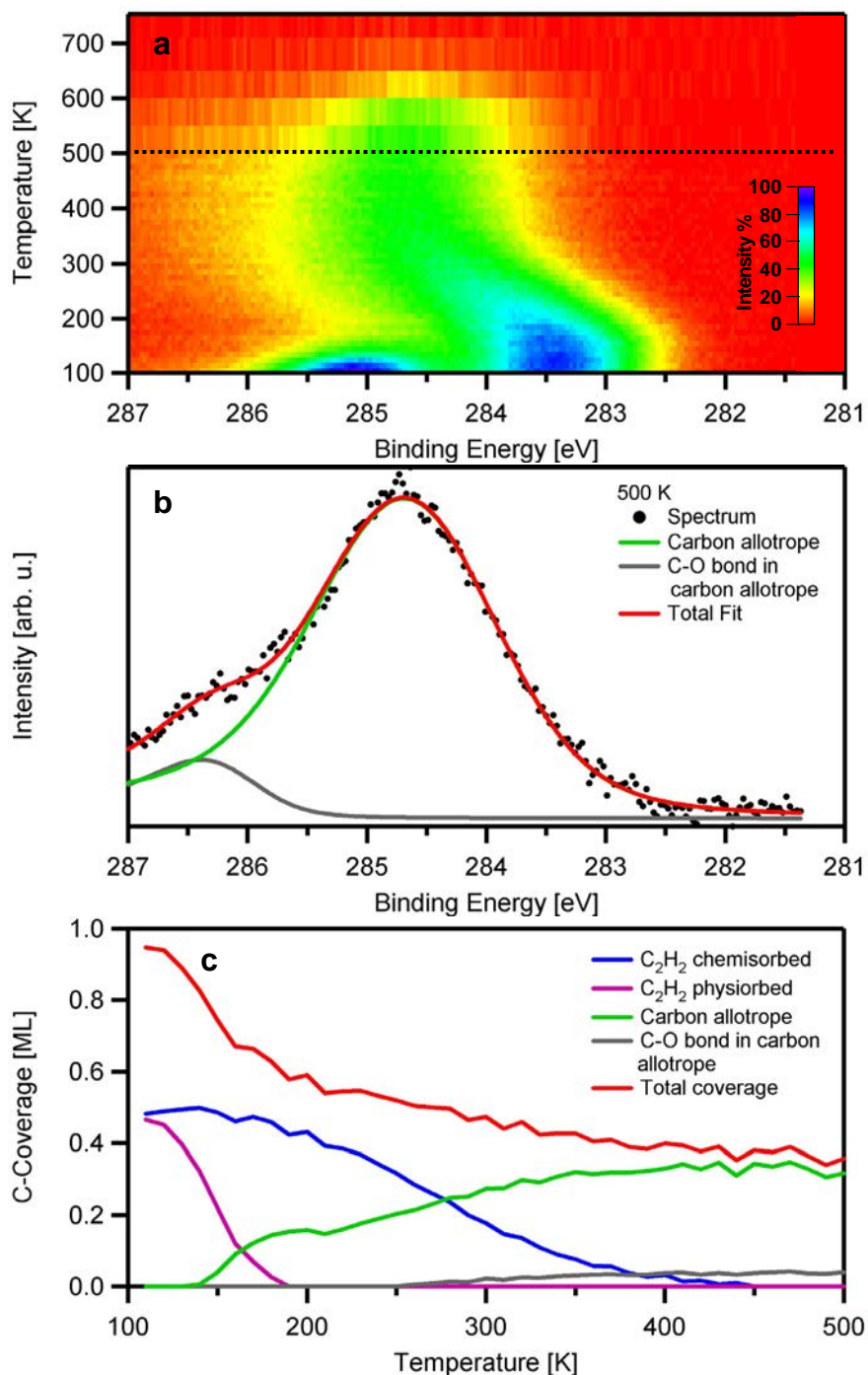


Figure 6.5: (a) Density plot of C 1s spectra acquired at an emission angle of 45° of C_2H_2 adsorbed on NiO/Ni(111). The heating rate was 0.5 K/s. (b) Detailed fit of the spectrum acquired at 500 K. (c) Quantitative analysis of the TPXPS experiment.

The highest coverage for this species is 0.35 ML in the temperature range between 400 and 500 K. Above 500 K, see Figure 6.5 (a), the intensity of this species starts to decline until it is mostly gone at 750 K. This intensity loss will not be discussed in detail as it mostly happens in a temperature range where the NiO layer itself is destabilizing. The chemisorbed C_2H_2 species starts to lose intensity around 150 K, where the new species at 284.62 eV appears,

and is completely gone from the surface at 450 K. The new species therefore has to be a reaction product of C_2H_2 , especially since the fast increase in intensity for the new species can only be explained if also some of the physisorbed C_2H_2 reacts to this species.

Since the peak shape shows no clear signs of vibrational splitting, we can get no information about the reaction product from it, so we have to resort to other means. On the one hand Demuth [158, 197] claimed dissociation of C_2H_2 to CH at room temperature on an oxidized Ni(111) surface, which would fit the temperature range we observe here, as the quantitative analysis shows a temperature range between 150 and 450 K for the conversion. Yang [161, 162] et al. later interpreted the corresponding HREELS spectra differently claiming C_6H_6 formation instead of CH formation. On the other hand the resulting species shows a high thermal stability up to the stability threshold of the surface. If it would be either CH or C_6H_6 it would seem strange that no dehydrogenation should occur within this temperature range. If the adsorbed species is already some dehydrogenated carbonaceous species this thermal stability would be perfectly reasonable and in line with the carbonaceous species found in the dehydrogenation paths of the species discussed in the previous chapters. The binding energy of 284.62 eV is in the typical binding energy range of 284.5-284.7 eV reported for a variety of carbon allotropes, like graphene oxide [198-201], carbon nanotubes [202, 203] and carbon nanofibers [204, 205]. NiO has been shown to be a suitable catalyst for the growth of such materials [204-207]. A peak in the same binding energy range was also found after the reaction of CH_4 and O_2 over a NiO catalyst [208] and as a result of the methanation of synthesis gas derived from biomass over a Ni/NiC/NiO catalyst on Al_2O_3 [209]. If we take all these arguments into account the species at 284.62 eV is clearly a dehydrogenated carbonaceous species. Further evidence that indeed a carbon network of some sort is formed on the surface comes from the next species appearing during the TPXPS.

At 250 K another new species appears at a binding energy of 286.23 eV. This species always remains a minority species with a maximum coverage of 0.04 ML around 500 K. Above 500 K it starts to disappear together with the carbonaceous species. The binding energy of this species is in the typical binding energy range for a carbon oxygen bond. The nature of this species however remains to be discussed. Both CO_2 and CO form CO_3 on the NiO surfaces which shows a peak around 289.0 eV, as discussed in detail in Chapter 7.3. Although 0.075 ML carbonate is present on the surface after the acetylene adsorption, at 250 K some of it has already decayed in agreement with the carbonate decay discussed in Chapter 7. An increase in coverage was never observed during the TPXPS. For CO another species has been

found at a binding energy around 287.5 eV, however this species is only found up to 350 K in CO adsorption experiments on NiO as discussed in Chapter 7.4.2, unlike this new species, which has the highest coverage at 500 K. A better match is found in literature about the carbon networks species. For graphene oxide [198-201], as well as for other carbon network materials [202, 204] a peak at the high binding energy side of the C-C peak is attributed to a C-O or C-OH single bond. The exact position of this peak varies for different materials, ranging from 285.3 eV for oxidized multiwall carbon nanotubes [202] to 286.1 eV for poly(p-hydroxystyrene) [199] and 286.6 [200] or 286.7 eV [198] for graphene oxide. The observed binding energy of 286.23 eV falls into this range. The peak separation between these two peaks is also in good accordance with the peak separation of 1.6-1.7 eV between the C-C peak and the C-O peak for phenol [210, 211] and phenol derivatives [212] on several surfaces. If we combine this information an assignment of the peak at 286.23 eV to a carbon atom within a carbon allotrope or an aromatic species bound to an O-atom. The final ratio between the peaks at 284.62 and 286.23 eV is 9:1. From this we can conclude that spectrum can not belong to a small aromatic species like phenol, because there a ratio of 5:1 would be expected which is much lower than the ratio we observe here. Due to this and the closeness of the binding energy for the C-C peak at 284.62 eV to the binding energies of carbon allotropes, as discussed in the previous paragraph, the best explanation for the reaction products is that some sort of carbon allotrope or a precursor thereof is formed on the surface and some of the oxygen from the support is either built into this network or the network is bound to the support via the oxygen atoms.

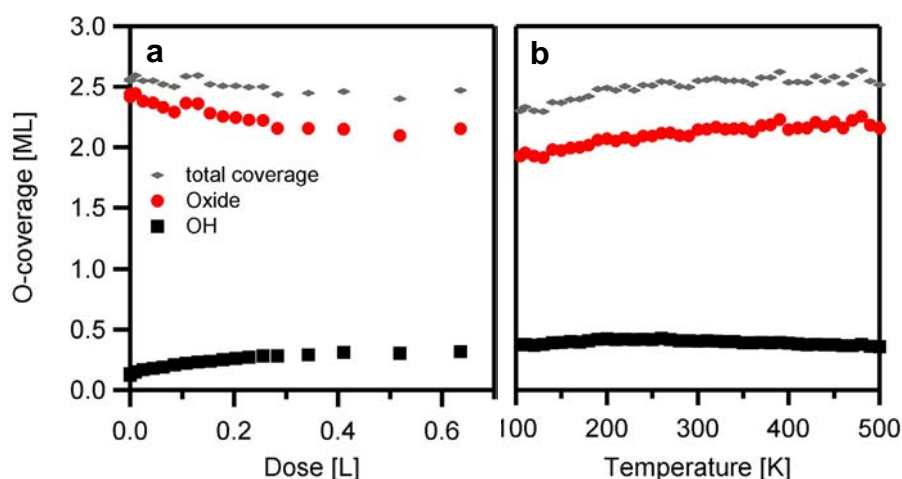


Figure 6.6: (a) Quantitative analysis of C_2H_2 exposure at 120 K on NiO/Ni(111) (b) Quantitative analysis of C_2H_2 on NiO/Ni(111) TPXPS. All data acquired at 45° emission angle. Oxide coverages corrected for damping by OH.

The acetylene interaction with NiO/Ni(111) was also studied in the O 1s region. The quantitative analysis of these experiments is shown in Figure 6.6. Please note that the oxide coverages have been corrected for the damping by OH with the method introduced in Chapter 7, but no corrections for the damping by the adsorbed acetylene have been made. The spectra (data not shown) show no discernible features besides the two oxide peaks and the hydroxide peak already discussed in Chapter 4. During the exposure of acetylene to the surface the oxide coverage, which is the combined coverage of the two oxide peaks found at 530.0 eV and 529.0 eV, decreases from 2.44 to 2.08 ML, while the peaks shift by 100 meV towards lower binding energies. As the damping by the hydroxide layers is already accounted for and the C 1s spectra showed no major carbonate contribution, this decrease in coverage is attributed to damping by the adsorbed acetylene. The hydroxide and carbonate coverage increases from 0.12 to 0.33 ML, with the corresponding peak located at 531.6 eV. As an increase of the hydroxide coverage within this order of magnitude was often observed during various uptake experiments within this thesis, this increase can not be attributed to dissociative adsorption of acetylene. It is more likely that this increase is due to some water, CO₂ or CO adsorption either from the residual gases in the chamber or from some contaminations within the acetylene. This is further strengthened by the observations from the C 1s region during the uptake and the subsequent TPXPS. The coverage of the chemisorbed C₂H₂ species is 0.48 ML and this coverage remains stable up to 150 K, which means no reaction is taking place below this temperature. So the only moment when a reaction, for example a dehydrogenation could take place would be directly upon adsorption of the molecules. As the peak now consist of only one species, this would mean that if some of the molecules would dehydrogenate upon adsorption, all of them would do so releasing at least 0.48 ML hydrogen. Given the generally observed high reactivity of the oxide surface towards hydroxide formation, a much larger increase of the hydroxide coverage than the observed 0.21 ML increase would be expected from this amount of hydrogen. So this leads to two conclusions: Firstly, the interpretation of the chemisorbed C₂H₂ species as molecularly chemisorbed acetylene has to be correct, i.e. no dehydrogenation happens below 150 K, and secondly that the increase of the hydroxide coverage is due to residual gases and not due to a dehydrogenation of the acetylene.

The TPXPS experiment was performed on a different spot on the sample, resulting in a lower oxide coverage of 1.93 ML. During the course of the experiment the oxide coverage increases again up to 2.16 ML at 500 K. The two oxide peaks shift from 529.8 to 530.2 eV and from 528.8 to 529.2 eV during this temperature range. This shift is in a similar order of magnitude as

the shifts observed for the TPXPS experiments of NiO discussed in Chapter 4. In these experiments in Chapter 4 a similar shift was also found in the Ni 2p region. Part of this shift is a reversal of the shift from 530.0 eV to 529.8 eV observed during the uptake. Interestingly the chemisorbed C₂H₂ species also undergoes a shift towards higher binding energies in this temperature range, shifting from 283.3 eV to 284.0 eV. As this shift is much larger than the shifts found in the O 1s region, and as the other C 1s species remain constant in binding energy it can, however, not be said whether or not this shift is a general effect affecting all binding energy regions. The hydroxide peak also shifts towards higher binding energies, from 531.5 to 532.0 eV. What is interesting is that the coverage of the hydroxide remains almost constant over the whole temperature range. The starting value of 0.37 ML increases slowly to a maximum of 0.42 ML at 220 K, and then slowly decreases again back to 0.36 ML at 500 K. The interpretation of this behavior is rather difficult, as a variety of effects can contribute to this. The initial increase falls into a temperature range where the total carbon coverage decreases due to desorption of the physisorbed C₂H₂. Thus a possible explanation for the increase would be the lowered damping by the C₂H₂. Some very rough estimates about the damping by C₂H₂ lead to a damping factor of ~ 0.8. Given that roughly 0.5 ML of physisorbed C₂H₂ desorb, and the coverage of OH increases by ~ 10%, this fits nicely. However, in the same temperature range also the dehydrogenation of the chemisorbed C₂H₂ is starting, so the resulting hydrogen could form additional hydroxide. The general decrease of the hydroxide coverage above 220 K can be attributed to the gradual decay of the hydroxide layers discussed in detail in Chapter 7.2. What is surprising in this regard is the relatively low loss of only 0.05 ML or 12 % of the hydroxide coverage between 220 and 500 K. On a NiO surface saturated with water, in the same temperature region the hydroxide coverage decreases by 65 % (see Chapter 7.2 for details), and on the hydroxide rich oxide layer prepared at 300 K, which is discussed in Chapter 4.1.2, the hydroxide content decreased by 30 % after heating to 500 K.

Three possible explanations are possible for this behavior: for one, due to the lower hydroxide coverage, a slower decrease might be energetically favorable as the coverage of 0.37 ML at 500 K is still lower than the value of 0.50 ML found in the decay of the fully water covered surface. If the potential saturation hydroxide coverage is dependent on temperature, as seems to be the case from the experiments discussed in Chapter 7.2, then a coverage well below this saturation coverage would not need to decrease upon an increase in temperature. In this model the slight decrease in coverage could be explained by local variations in the oxide structure, i.e., that locally the

hydroxide coverage is too high for a given temperature and thus has to decrease whereas elsewhere on the surface the coverage remains constant.

The second possible explanation for the relatively slow decrease comes from the observed acetylene dehydrogenation within this temperature region. The hydrogen from dehydrogenation forms additional hydroxide which adds to the total hydroxide coverage and thus slows the hydroxide decrease. The third effect which can contribute to the low slope of the hydroxide decay is again the lifted damping by the carbon species, as the total coverage in the C 1s region decreases by 0.2 ML within this temperature region. Due to the limited amount of information available from the O 1s spectra, and as all three explanations seem equally likely it is best to assume a combination of the three effects as the explanation for this behavior. The C-O species found in the C 1s spectra at 286.23 eV can not be resolved in the O 1s region, due to its relatively low coverage of maximum 0.04 ML. Literature reports a binding energy of around 532.8 eV for C-O bonds in graphene oxide [213], and in a study with several oxygen containing polymer films O 1s signals are found between 531 and 533 eV [199]. If we compare these binding energies with e.g. the spectra shown in Figure 4.3 (a), which show somewhat hydroxylated NiO layers like the ones used during this experiment, it is evident that a peak with a coverage of 0.04 ML at the given binding energies would disappear within the main oxide and /or the hydroxide peaks. There are also no new species found outside of this binding energy range.

On the thin NiO layer on Cu(111) the thermal evolution of adsorbed acetylene was studied in a similar manner, with the exception that after every spectrum the sample position was shifted to avoid beam damage. The quantitative analysis of this experiment is displayed in Figure 6.7 (c). The physisorbed component behaves almost identical to how it behaved on the NiO/Ni(111) with desorption from the start of the TPXPS, with the sole difference that here it is completely gone from the surface at 210 K while on NiO/Ni(111) this was already the case at 190 K. Another similarity is the appearance of a new species at 284.26 eV starting at 170 K. After a fast initial increase in coverage up to a coverage of 0.05 ML at 200 K the further increase is much slower, reaching a maximum coverage of 0.09 ML between 400 and 480 K before the coverage starts to decrease to 0.08 ML at 500 K. At 170 K also another species starts to appear at a binding energy of 285.91 eV. The coverage of this species increases in a similar manner as the species at 284.26 eV, although the maximum coverage here is smaller with a value of only 0.02 ML. This coverage remains relatively unchanged between 300 and 500 K. The appearance of these two species goes hand in hand with a decrease of the coverage of the chemisorbed C₂H₂ species, which starts at 170 K and gradually goes on up to 490 K where it has vanished. This behavior suggests

that the two new species at 284.26 and 285.91 eV are reaction products of the chemisorbed C_2H_2 .

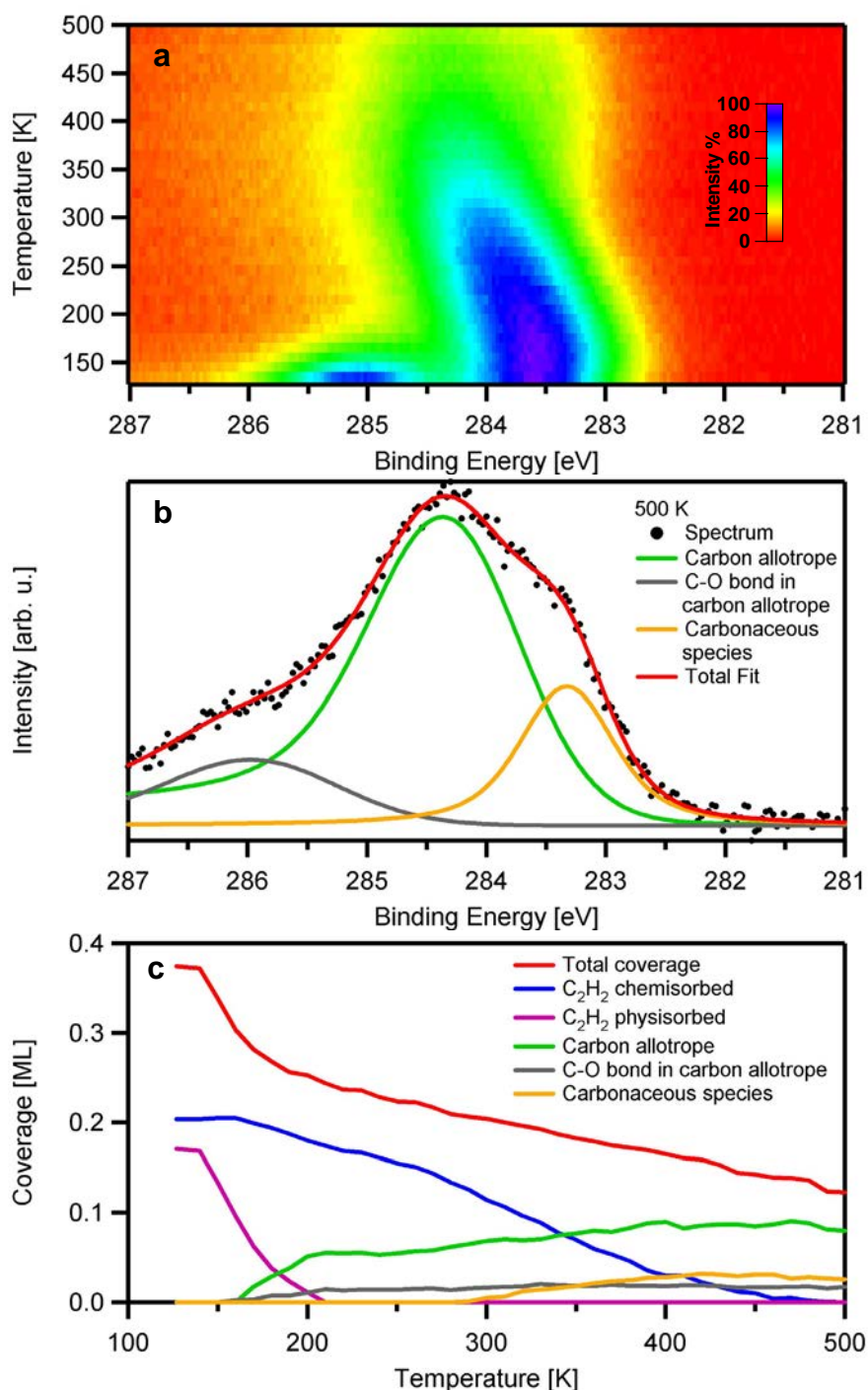


Figure 6.7: (a) Density plot of C 1s spectra acquired at an emission angle of 0° of C_2H_2 adsorbed on NiO/Cu(111). The heating rate was 0.5 K/s, and the sample position was changed after each spectrum (b) Detailed fit of the spectrum acquired at 500 K. (c) Quantitative analysis of the TPXPS experiment.

Although the binding energy of these two species is lower by ~ 0.35 eV than for the two reaction products found in the dehydrogenation of C_2H_2 on

NiO/Ni(111), due to the similar separation of 1.65 eV between the peaks (1.61 eV on NiO/Ni(111)), the similar temperature range in which the lower binding energy species appears, 170 K for NiO/Cu(111) compared to 150 K for NiO/Ni(111), and the much lower coverage of the species at 285.91 eV compared to the species at 284.26 eV, which is also found with the two respective species on NiO/Ni(111), we apply the same assignment for the two reaction products as on NiO/Ni(111). Thus the peak at 284.26 eV is assigned to either a carbon allotrope or a precursor species, and the peak at 285.91 eV is assigned to carbon atoms within this carbon allotrope/precursor species bound to an oxygen atom by a single bond, either an OH species or oxygen from the substrate. Interestingly this C-O species here already appears at the much lower temperature of 170 K compared to 250 K at the NiO/Ni(111) surface. A possible explanation for this behavior would be slight structural differences between the NiO on Ni(111) and the NiO on Cu(111). Although they are mostly similar, a noticeable difference is the higher hydroxide content for NiO/Cu(111), due to the different preparation temperatures as discussed in Chapter 4. As discussed in Chapter 7.2, hydroxide presence can lead to a restructuring of the surface. So we can tentatively assume that the structure present for the higher OH content promotes the formation of C-O bonds to the surface, enabling the appearance of the species at a lower temperature. Both reaction products appear here at lower binding energies than on NiO/Ni(111). A similar trend is found for physisorbed hydrocarbons on the different NiO preparations, as discussed in detail in Chapter 6.2.2. There the adsorbates have the highest binding energies on NiO/Ni(111), which is the thickest NiO layer. It seems plausible that the binding energy of the reaction products depends on the thickness of the NiO layers.

A big difference between the acetylene TPXPS on the two surfaces is that in the thermal decay of acetylene on NiO/Cu(111) starting at 300 K a new species starts to evolve at a binding energy of 283.32 eV. The maximum coverage found for this species is 0.03 ML above 400 K. For the carbon allotropes a matching species is neither reported in this binding energy range nor in this distance from the main carbon allotrope peak. The appearance of this species falls into a temperature range, where the decrease of the C₂H₂ coverage accelerates in Figure 6.7 although the coverage increase of the two carbon allotrope species does not get faster in a similar manner. Thus the species at 283.32 eV also has to be a reaction product of the chemisorbed C₂H₂. Due to this and the binding energy of 283.32 eV, which is close to the binding energy of 283.26 eV found for one of the carbonaceous species observed on the Ni(111) surface (see Chapter 5) this species is assigned to a carbonaceous species. Whether or not this is really a carbonaceous species on nickel is questionable, however, since the NiO layers stay fully oxidized

during the experiment, and also due to the fact that on the NiO/Ni(111) this species is not found. Even after taking into account a possible binding energy shift in the same direction as for the other two reaction species, all attempts of including this species into the fit have led to very inconsistent results, with the species appearing and disappearing randomly at different temperatures, instead of showing an evolution like on the copper substrate.

The total C 1s coverage is constantly decreasing over the whole temperature range. Below 160 K this decrease is attributed to desorption of the physisorbed C₂H₂. Interestingly between 160 K and 210 K the decrease of the total coverage is smaller than the decrease of the physisorbed C₂H₂, implying that also some of the physisorbed C₂H₂ has to react to the carbon allotrope species, explaining the quick initial rise in coverage for this species. The same observation was also made during the TPXPS of acetylene on NiO/Ni(111), where also the initial increase of the carbon allotrope species could not be explained by reaction of the chemisorbed C₂H₂ alone. Above 210 K the reason for the decrease is not as easily explained. The best explanation is that some of the carbon formed from the dehydrogenation of C₂H₂ reacts directly with some of the oxygen from the NiO support and leaves the surface as either CO or CO₂. Both molecules have physisorbed components on NiO/Cu(111) that desorb below 500 K. The question that remains is why no additional carbonate is formed, as on this surface, just like for acetylene on NiO/Ni(111), during no point of the TPXPS experiment an increase in the carbonate coverage is found. The most probable explanation is that the sites needed for the formation of the carbonate are blocked by the other adsorbates and thus any formed CO or CO₂ can not bind stable to the surface and thus has to desorb. Just like for NiO/Ni(111), for the NiO/Cu(111) substrate the O 1s spectral region (data not shown) only offers very limited information, with no species discernible besides the two oxide species and the hydroxide. The oxide coverage falls from 1.66 ML prior to the acetylene uptake down to 1.35 ML afterwards due to the damping by the acetylene and then goes up again to 1.49 ML after heating to 500 K as the carbon coverage decreases and the damping is lifted again. As the carbon coverage decreases from 0.37 ML to 0.13 ML between 100 and 500 K, which is a decrease by 65 %, whereas only 45 % of the “lost” oxide coverage is recovered in this region, the missing oxygen has either to be converted to hydroxide or to leave the surface as CO or CO₂ as discussed before. The hydroxide coverage increases from 0.22 ML prior to the uptake to 0.49 ML after the acetylene uptake and finally 0.56 ML at 500 K after the TPXPS experiment. As discussed for the NiO/Ni(111) substrate, this increase can be due to a number of reasons, with the increase during the acetylene uptake attributed completely to adsorption of water from the residual gas in the chamber

instead of dehydrogenation of the acetylene. The increase during the TPXPS can be attributed both to the dehydrogenation of the acetylene and additional adsorption of water from the residual gas. The Ni 2p and Cu 2p regions (data not shown) were also studied during the key steps of the experiment. Besides a damping by the adsorbates no other effects have been found there, especially no spectral changes which would indicate a reduction of the NiO or an involvement of the copper in the reaction.

6.1.4 Acetylene adsorption on NiO clusters on Cu(111)

The final system studied for acetylene adsorption was the acetylene exposure to the NiO cluster on Cu(111). The acetylene was dosed at a surface temperature of 130 K, and the resulting C 1s spectra are shown in Figure 6.8 (a). All spectra were recorded under an emission angle of 0° and the sample was shifted after each spectrum to a new spot to minimize beam damage. The spectra are dominated by two very different peaks, a narrow tall peak near 283.4 eV and a smaller but much broader peak near 285.0 eV. The detailed fit shown in Figure 6.8 (b) reveals that these two peaks can be fit with the assumption that they are due to a combination of acetylene adsorption on the bare Cu(111) patches between the clusters and on the NiO clusters.

Using the same parameters for the peaks as on the respective “pure” systems the spectra were fitted with a total of four peaks. A peak at 283.33 eV is attributed to the adiabatic transition for acetylene chemisorbed on the bare Cu(111) patches. The corresponding vibrational component is found at a binding energy of 283.69 eV. Both binding energies are shifted by 90 meV towards lower binding energies in respect to their positions on clean Cu(111), which is attributed to the coadsorption with NiO. The S-factor is 0.205 and thus very close to the S-factor of 0.21 found on the clean Cu(111). For acetylene adsorption on the NiO clusters we find a peak at 283.30 eV for the chemisorbed C_2H_2 component and one at 285.03 eV for the physisorbed C_2H_2 component. While the physisorbed component is close to the value of 285.01 eV found on the thin NiO layers on Cu(111), the binding energy of the chemisorbed component is shifted by almost 300 meV towards lower binding energies in respect to the 283.59 eV found for it on the thin NiO layers on Cu(111). This is much closer to the value of 283.33 eV found for acetylene on NiO/Ni(111). All of these binding energies remain constant throughout the experiment.

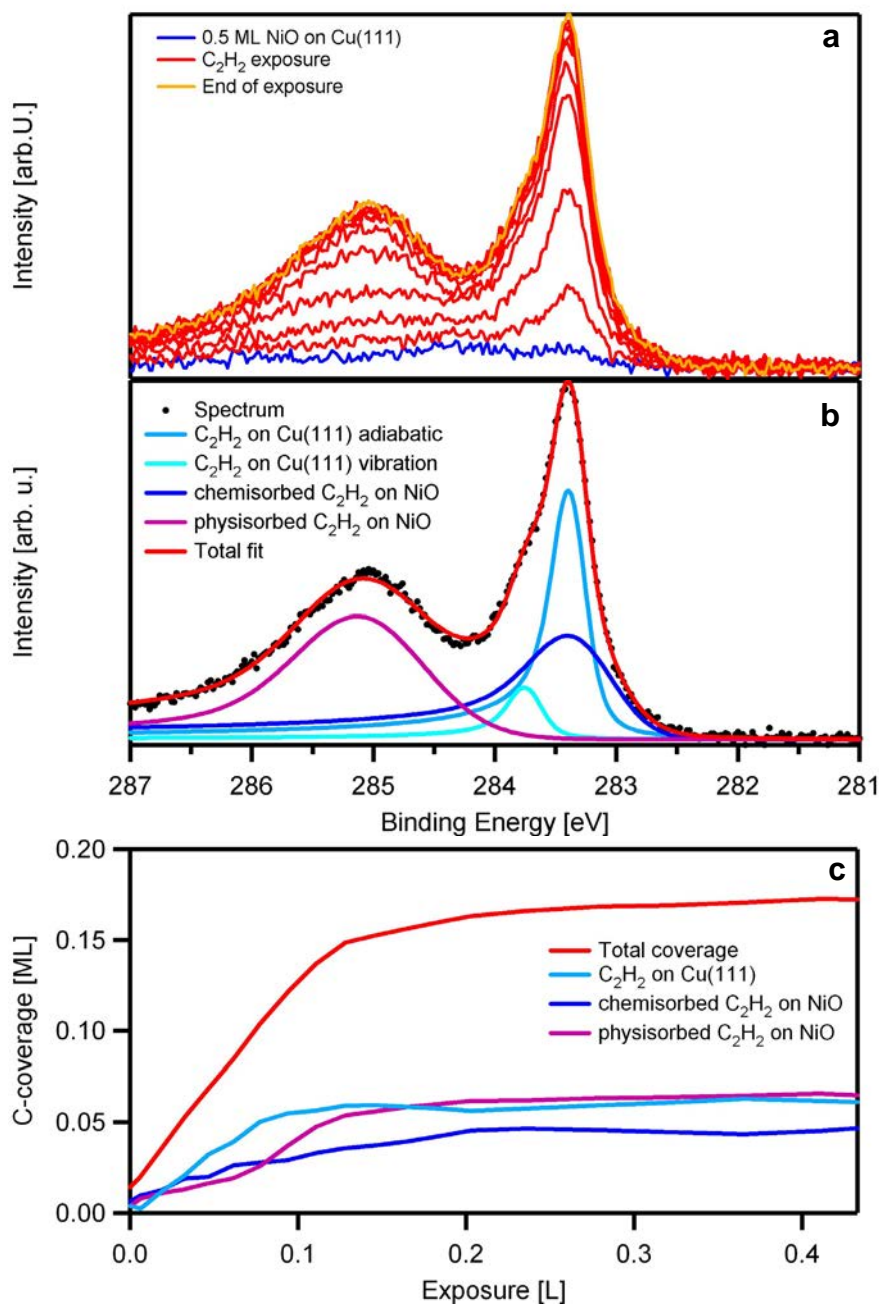


Figure 6.8: (a) Selected C 1s spectra recorded during acetylene exposure to NiO clusters on Cu(111) at 130 K (b) Detailed fit of the spectrum recorded at the end of exposure (c) Quantitative analysis of the data from (a)

The quantitative analysis of the uptake experiment shown in Figure 6.8 (c) reveals that the saturation coverages for all three species are very close to each other, with the saturation coverage for the C₂H₂ on Cu(111) being 0.06 ML, for the chemisorbed C₂H₂ on NiO 0.045 ML and 0.065 ML for the physisorbed C₂H₂ on the NiO, giving a total coverage of 0.17 ML. The C₂H₂ adsorbed on Cu(111) saturates at an exposure of 0.12 L, while the uptake on the NiO is a bit slower and saturates at an exposure of 0.21 L. The chemisorbed and physisorbed species on the NiO grow simultaneously, as

already observed for the adsorption on the thin NiO layers. Just like for the acetylene adsorption on thin NiO layers discussed in the previous Chapter, the coverage of the physisorbed C₂H₂ on NiO decreases when the acetylene pressure in the chamber is lowered after the exposure from $\sim 1 \cdot 10^{-9}$ torr to $1 \cdot 10^{-10}$ torr. 0.015 ML C₂H₂ desorb from the surface leaving 0.05 ML of physisorbed acetylene. A comparison to the earlier described adsorption experiments of acetylene on 2 ML NiO on Cu(111) and on the clean Cu(111) surface shows that the saturation coverages are much lower. On the clean Cu(111) surface an acetylene saturation coverage of 0.5 ML carbon atoms was found. As the NiO clusters were grown from 0.5 ML nickel atoms on the surface, we can estimate that roughly half of the surface should be covered by the NiO clusters, and the other half should be bare Cu(111). From this estimate we would expect a coverage of 0.25 ML carbon atoms of acetylene on the surface. Instead of this we only find 0.06 ML, which is 25 % of this expected coverage. For acetylene on NiO on Cu(111) we found saturation coverages of 0.19 and 0.23 ML C atoms for the chemisorbed and physisorbed component, respectively. So for the chemisorbed component we would expect 0.095 ML, but instead only find 0.045 ML which is 47 % of the expected value, and for the physisorbed component we find 0.05 ML, which is 43 % of the expected 0.115 ML. As all of these values are significantly lower than the expected values this effect can not be explained by a fault in the assumption that the surface is covered with equal shares of NiO and bare Cu(111), because then only one value would be expected to be too low and the other would be expected to be too high. A possible explanation for this behavior would be that acetylene can only adsorb on large enough patches of either NiO or bare Cu(111), and does not adsorb on the edges of the NiO clusters which make up a large percentage of the surface. If we further compare the slope of the total coverage curve on all three systems, we find that the uptake proceeds slightly but not significantly slower on the NiO clusters compared to the two “pure” surfaces. If now large areas of the surface do not adsorb C₂H₂ molecules, this means that they instead of adsorbing there directly they diffuse from these areas to the allowed surface areas for adsorption.

The thermal evolution was studied with a temperature ramp of 0.5 K/s and a spectrum was acquired every 10 K. The C 1s spectra acquired under an emission angle of 0° are shown as a color coded density plot in Figure 6.9 (a) with the quantitative analysis in Figure 6.9 (c) and a detailed fit of the 500 K spectrum in Figure 6.9 (b). Just like for the uptake, the sample was shifted to a new position after each spectrum to minimize beam damage. As expected the physisorbed component begins to desorb first, dropping down to a remaining coverage of <0.005 ML C atoms at 200 K. At 280 K the physisorbed C₂H₂ is completely gone from the surface, and the “tail” between

200 and 280 K can probably be attributed to a fitting artifact. At 150 K a new species starts to appear with a binding energy of 284.11 eV. After a very slow increase in coverage below 250 K, especially over 280 K its intensity increases much faster reaching a maximum coverage of 0.07 ML between 380 and 460 K before decreasing in coverage again down to 0.055 ML at 500 K. The appearance of this species falls into a range where the chemisorbed C_2H_2 species on the NiO starts to lose intensity. This intensity decrease proceeds gradually between 150 and 400 K, at which temperature the species disappears from the surface. The kinks in the coverage curve can be attributed to the relatively low coverage of the species discussed here, which makes the fits of the spectra complicated, and the kinks lie well within the usual margin of error for the coverage determination.

At 230 K, another new species appears at a binding energy of 283.38 eV. This species increases gradually in intensity up to a coverage of 0.02 ML at 320 K, and then remains more or less constant up to 450 K, before increasing again up to 0.025 ML at 500 K. The appearance and growth of this species falls into the same temperature range where the acetylene adsorbed on the Cu(111) patches disappears from the surface below 320 K, identifying the new species as a reaction product of acetylene. As the coverage of acetylene on Cu(111) was 0.06 ML at the start of the experiment, the coverage of 0.02 ML for the new species is not sufficient to explain the complete disappearance of the acetylene on the Cu(111) patches. The main intensity loss of the C_2H_2 on the Cu(111) patches between 280 and 320 K falls into the same temperature region where an increase in coverage is seen for the species at 284.11 eV.

We can thus conclude that this species is a reaction product both of the acetylene on the Cu(111) patches and on the NiO clusters. If we have a look at the total coverages, we see that most of the chemisorbed acetylene is converted to the two reaction products. Between 125 and 300 K the total coverage falls from 0.15 ML to 0.095 ML. Of the lost 0.055 ML 0.05 ML can be explained by desorption of the physisorbed C_2H_2 , leaving just minor amounts of other carbon containing species to leave the surface. Between 300 and 400 K, where all acetylene is gone from the surface, the total coverage decreases by another 0.01 ML leaving 0.085 ML of the reaction products on the surface.

What remains to be discussed is the assignment of the two reaction products. The binding energy of the species at 283.38 eV is very close to the binding energy of 283.32 eV found for the carbonaceous species found in the TPXPS of C_2H_2 on the thin NiO layers on Cu(111). Although this species already appears at 230 K on the surface covered with the NiO clusters, whereas it

only appears at 300 K on the thin NiO layers the similar binding energy and thermal stability makes this the best assignment.

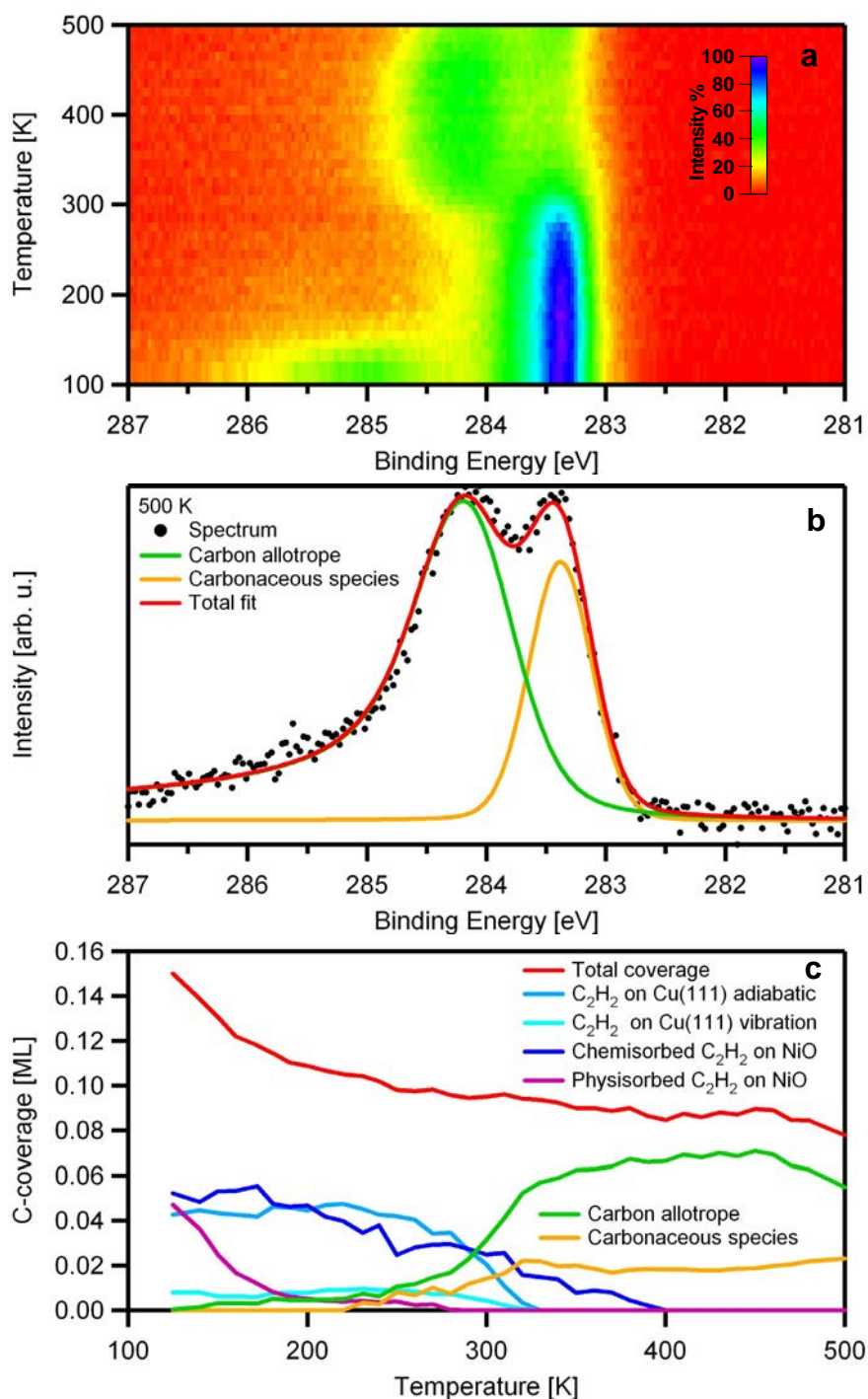


Figure 6.9: (a) Density plot of the thermal evolution of C_2H_2 on NiO clusters on Cu(111). Emission angle for all spectra was 0° , and the sample position was shifted after each spectrum. The heating ramp was 0.5 K/s . (b) Detailed fit of spectrum obtained at 500 K (c) Quantitative analysis of TPXPS experiment

The different formation temperatures can probably be explained by a higher reactivity of the NiO clusters in comparison to the thin NiO layers, due to the

higher number of edges present on clusters. The binding energy of the species at 284.11 eV is not too far away from the binding energy of the carbon allotropes/carbon allotrope precursors formed on the thin NiO layers on Cu(111) during the C₂H₂ decomposition. The 284.11 eV species also shows a similar thermal evolution, in that its coverage increase mainly mirrors the decrease in coverage of the chemisorbed C₂H₂ on the NiO clusters, except for the area between 280 and 320 K where a huge coverage increase is seen due to the reaction of the C₂H₂ on the Cu(111) patches. Due to these similarities the species at 284.11 eV is attributed to a carbon allotrope or carbon allotrope precursor just like on the other two studied NiO surfaces. The binding energy difference can be explained by the different structure of the NiO. Interestingly here we find no peak in the area around 286 eV, where on the other two surfaces a peak representative for C-O bonds within these carbon allotrope species was located. If we take a close look at the fit at 500 K displayed in Figure 6.9 (b), however, it seems possible that a minor amount of such a species might be present between 285.5 and 286.0 eV but can not be consistently included into the fit due to the low coverages on the surface.

These assignments are strengthened by another experiment, where acetylene was exposed to a Cu(111) surface covered with NiO clusters at a constant surface temperature of 400 K. The corresponding spectra acquired during the exposure at an emission angle of 0° are displayed in Figure 6.10 (a). Just like for the uptake at 130 K the sample was shifted to a new spot after each spectrum to minimize beam damage. As shown in Figure 6.10 (b) the resulting spectra can be fitted with the two components already found in the previous experiment. At the highest coverages the carbonaceous species has a binding energy of 283.40 eV and the carbon allotrope is found at 284.17 eV. The fitted spectrum is also very similar to the 500 K spectrum in the TPXPS experiments of acetylene on 2 ML NiO/Cu(111) displayed in Figure 6.7 (b). Apart from the different ratio between the two carbon species the major difference between the two spectra is that in Figure 6.10 (b) no C-O species is found, although a minor contribution from such a species cannot be fully excluded from the fit. The quantitative analysis is displayed in Figure 6.10 (c). After a fast initial increase of the carbonaceous species up to a coverage of 0.05 ML after an exposure of 10 L, the coverage increases more slowly until after an exposure of ~ 100 L the saturation coverage of 0.07 ML is reached. The carbon allotrope also shows the fast initial increase up to a coverage of 0.11 ML after an exposure of 10 L, and the coverage increase also slows down after this point but no saturation is reached. After an exposure to 770 L a coverage of 0.75 ML is reached for the carbon allotrope, giving a total coverage of 0.82 ML at this point. Upon heating to higher temperatures (data

not shown) the formed carbon deposits were found to be very stable. Both the total coverage and the distribution on the two species remain almost constant up to 900 K. As no further reaction was found, this supports the assignment of the two species as two forms of fully dehydrogenated carbon.

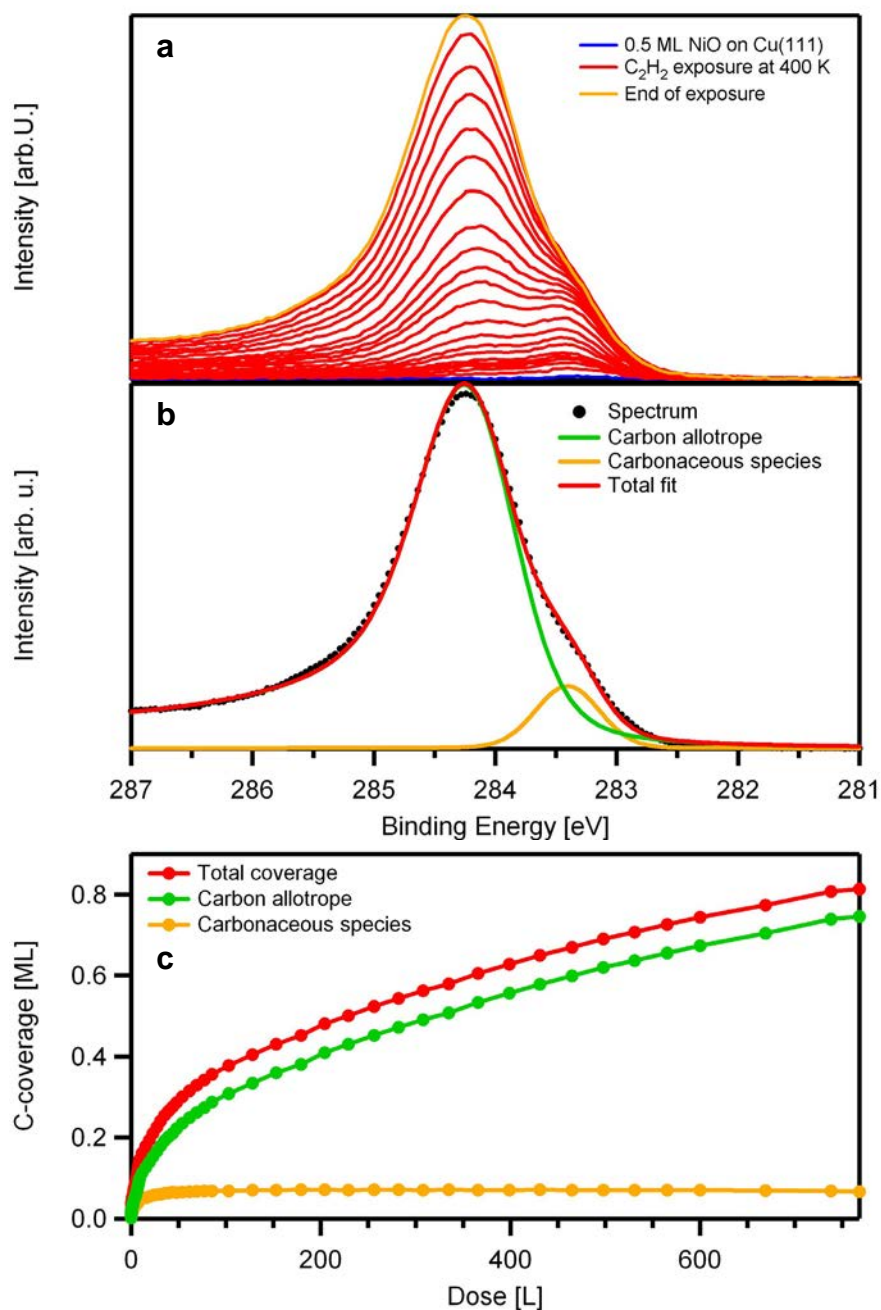


Figure 6.10: (a) C 1s spectra of C₂H₂ exposure on a Cu(111) surface covered with NiO clusters. All spectra acquired at 0° emission angle. The sample was shifted to a new spot for each spectrum. (b) Detailed fit of spectrum with highest coverage (c) Quantitative analysis of the experiment

In the O 1s region it is seen that after the exposure at 400 K the initial oxygen amount of 0.70 ML is reduced to 0.15 ML. The same is found in the Ni 2p region, where the spectra (data not shown) reveal that the oxidation of the

nickel clusters is lifted and the spectrum shows the metallic characteristics again, similar to the situation prior to the oxidation. For the acetylene uptake at 130 K, no intensity loss was found in the O 1s region after the C₂H₂ exposure, however after the TPXPS at 500 K a loss of 0.1 ML of oxygen is found. As the NiO clusters are stable up to 500 K, the loss is due to reaction with H₂ or CO/C, with the reaction products desorbing immediately. Since from the C 1s most of the coverage decrease could be attributed to the desorption of the physisorbed C₂H₂, this only leaves a small amount ~ 0.015 ML of carbon loss not yet accounted for. As less carbon than oxygen is lost, desorption as CO₂ seems more likely. Still to explain the total amount of oxygen missing from the surface some of the physisorbed C₂H₂ on the NiO also needs to dehydrogenate and react to CO or CO₂ to explain the total oxygen loss. A similar scenario, were some of the deposited carbon reacts with the oxygen from the support to form CO or CO₂ which subsequently desorbs can also be assumed for the acetylene uptake at 400 K. Just like for the acetylene reaction on the thin NiO layers discussed in the previous chapter, and due to the same reasons discussed there, the hydroxide coverage gives no hint towards the nature of the reaction products.

6.2 Physisorption of hydrocarbons on Cu(111) and thin NiO layers

6.2.1 Physisorption of hydrocarbons on Cu(111)

As the comparison of the acetylene spectrum on the NiO-cluster on Cu(111) (see Chapter 6.1.4) with the acetylene spectrum on clean Cu(111) (see Chapter 6.1.1) played an important role in the interpretation of the spectra, also for the other studied hydrocarbons ethane (C₂H₆), ethylene (C₂H₄), propylene (C₃H₆) and propane (C₃H₈) the interaction with the clean Cu(111) surface was studied. Of special interest is the question if the similarities found for acetylene adsorption on Cu(111), as discussed in Chapter 6.1.1 and on Ni(111) (Chapter 5.3.1) are also found for ethane and ethylene on these two surfaces.

The interaction of Cu surfaces with hydrocarbons is of general interest due to the use of hydrocarbons like C₃H₈ for the reduction of NO in Cu containing catalysts [214]. In a theoretical study [215] comparing the binding energies of carbon and various hydrocarbons on (111) surfaces of group VIII and IB metals, the Cu(111) surface was found to have the lowest binding energies for almost all adsorbates, ranking even lower than Au(111). Both for ethane and ethylene on Cu(111) the calculated adsorption energies suggest a desorption temperature of <150 K. The only study of ethane adsorption on Cu(111) has

been done by Fuhrmann et al. [186] who found a weakly bound physisorbed species with Helium scattering. Propane interaction with Cu(111) has only been studied at temperatures of 750 K so far, showing no interaction [216].

The adsorption of ethylene on Cu(111) has attracted quite some interest in the past. In an AES study by Canning et al. [187] ethylene was found to be π -bonded to the substrate, in contrast to the situation on Pt(111) where it is σ -bonded. From TPD a desorption peak was found at 120 K [192, 217] and the adsorption of ethylene was found to be completely reversible. The HREELS spectrum was almost identical to the gas-phase spectrum [192], and no long range order was found with LEED. The adsorbate was further characterized as being physisorbed by He-Scattering and NEXAFS in comparison with DFT calculations [186]. The NEXAFS spectra showed the adsorbate to be undisturbed, whereas the DFT results showed that a chemisorbed molecule would be heavily disturbed. DFT studies [186, 218] found several stable adsorption sites with very similar binding energies.

Only a small number of studies of C_3H_6 on Cu(111) have been reported. Lin and Bent [219] recorded the HREELS spectrum of propylene on Cu(111) at 120 K but only as a reference spectrum without detailed discussion. A brief discussion of the HREELS spectra is provided by Meyers and Gellman [220], who also recorded TPD spectra. They found both mono- and multilayer HREELS spectra very similar to gas-phase spectra of propylene, indicating no strong perturbation of the adsorbed molecule. The TPD spectra showed the onset of desorption slightly above 100 K with a peak around 120 K, from which a desorption energy of 24.7 ± 3.8 kJ/mol was estimated.

All coverages given in this Chapter are referenced to the saturated acetylene (C_2H_2) layer on Cu(111) discussed in Chapter 6.1.1, which has a nominal coverage of 0.5 ML C-atoms [180] (0.25 ML acetylene molecules).

6.2.1.1 Propylene physisorption on Cu(111)

Propylene (C_3H_6) was absorbed on Cu(111) at an initial sample temperature of 129 K, dropping to 122 K over the course of the experiment. To minimize beam damage the sample was shifted to a new spot after each sample. Some selected C 1s spectra, acquired at an emission angle of 0° , are displayed in Figure 6.11 (a). The spectra are dominated by a main peak that starts at 284.80 eV shifting to 284.84 eV for higher coverages, and a second large peak at 284.29 eV. Over the whole course of the uptake the spectral shape remains unchanged, i.e., all peaks grow simultaneously. For the two big contributions in the spectra this means that they belong to different carbon

atoms within the same molecule which adsorbs molecularly, just like it was found for ethylene and ethyle on Ni(111) in Chapter 5.1. The inset of Figure 6.11 shows the quantitative analysis of the experiment. After a fast initial increase up to a coverage of 0.16 ML C-atoms the coverage increases only slowly up to a final coverage of 0.21 ML C-atoms, at which point the background pressure was turned off.

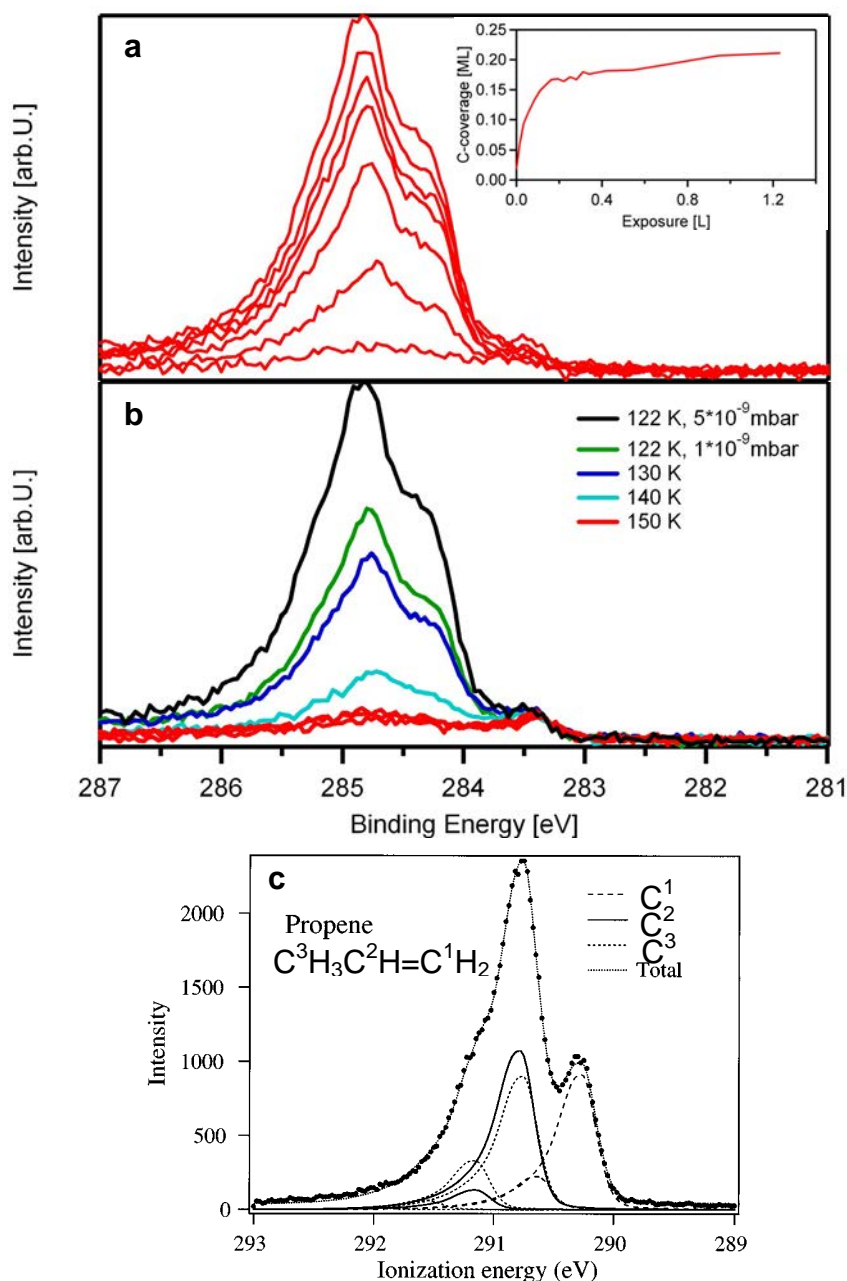


Figure 6.11: (a) Selected C 1s spectra of a propylene uptake on Cu(111) at < 129 K. **Inset:** quantitative analysis (b) C 1s spectra of thermal evolution of C₃H₆ on Cu(111) (c) Gas phase spectrum of propylene obtained by Saethre et al. [31]

The adsorption temperature used in this experiment of less than 129 K is well within the desorption peak of C₃H₆ on Cu(111), as reported from TPD data

[220]. If the C_3H_6 adsorption is reversible, as is shown below, we can assume an adsorption/desorption equilibrium for C_3H_6 on the surface dependent on the surface temperature and the C_3H_6 pressure in the chamber. Above 0.2 L exposure the sample temperature fell from 127 to 122 K and the C_3H_6 pressure in the chamber was rising from $3.6 \cdot 10^{-9}$ mbar to $4.8 \cdot 10^{-9}$ mbar. This is in good agreement with interpreting the slow coverage rise in this region as a slow shift of the adsorption/desorption equilibrium towards higher surface coverages with falling temperatures and rising adsorbate pressures in the chamber.

After the background pressure was lowered to $1 \cdot 10^{-9}$ mbar, desorption was observed, as shown in Figure 6.11 (b), with the coverage decreasing to 0.13 ML C-atoms. The adsorbate coverage dependence on the background pressure is in agreement with the assumed adsorption/desorption scenario. For the next step of the experiment the surface was heated to the temperatures shown in Figure 6.11 (b) with the resistive heating and subsequently a C 1s spectrum was acquired. All adsorbed propylene is gone from the surface at 150 K, in agreement with the TPD data [220], leaving behind only contaminations present on the surface already before the adsorption (less than 0.02 ML C-atoms). The spectral shape remains constant during the desorption which means that no thermal decay of the adsorbed propylene is observed, indicating a reversible adsorption.

As the HREELS spectra [220] for the physisorbed propylene molecules were very similar to gas-phase spectra of propylene, a comparison of the XPS data with the gas-phase XPS data obtained by Saethre et al. [31] could be helpful to understand the vibrational finestructure of the presented spectra. The corresponding spectrum, which is shown in Figure 6.11 (c), consists of two peaks that both show shoulders due to the vibrational finestructure. The two peaks are separated by 0.5 eV, which is very close to the peak separation of 0.55 eV we observe for high coverages, and the peak with the higher binding energy is larger by a factor of two. The peak at the lower binding energy is assigned to the carbon atom which is bound to two hydrogen atoms (labeled as C^1). The central carbon atom, which is bound only to one hydrogen (C^2), and the carbon atom from the methylene group (C^3) both make up the peak with the higher binding energy. Their binding energies are virtually the same. Based on the similarities in the spectral shape the fits shown in Figure 6.12 were carried out based on the assumption of three adiabatic peaks with vibrational contributions for the three carbon atoms in the molecule.

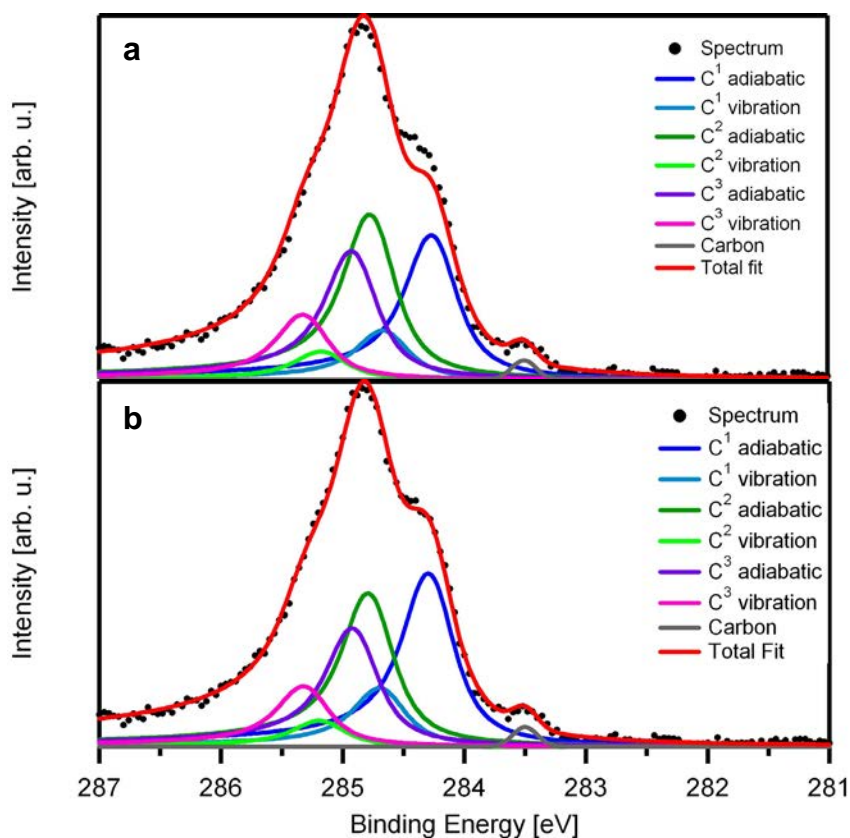


Figure 6.12: (a) Detailed fit of C_3H_6 on Cu(111) with equal intensity for all carbon atoms (b) Detailed fit of C_3H_6 with differing intensities for the carbon atoms

For the first fit which is shown in Figure 6.12 (a) it was assumed that all three carbon atoms contribute the same intensity to the spectrum, just like it was observed for the gas-phase [31]. Please note that this does not mean that the intensity of the adiabatic peak is the same for all three carbon atoms, but rather that the sum of the adiabatic and the vibrational peak is the same. The peak at 284.24 eV is attributed to the C^1 atom (see Figure 6.11 (c)). The corresponding vibrational peak is located at 284.64 eV, with an S-Factor of 0.34 or 0.17 per C-H bond. The peaks of the other two carbon atoms make up the larger peak, but due to the interaction with the surface they are found at slightly different binding energies unlike in the gas-phase where they shared a common binding energy [31]. The peak for the C^2 atom (see Figure 6.11 (c)) is located at 284.75 eV. The vibrational contribution for it has an S-Factor of 0.17 and a binding energy of 285.15 eV. The binding energy of the C^3 (see Figure 6.11 (c)) peak is 284.9 eV. The vibrational peak is found at 285.3 eV with an S-Factor of 0.51, which is also 0.17 per C-H bond.

As this fit lacks intensity in the area of the C^1 peak, another fit was made under the assumption that only the C^2 and C^3 peak have the same intensity, allowing the C^1 peak a higher intensity. The result is shown in Figure 6.12 (b). While the peak positions and the S-Factors remain unchanged, the C^1 peak

now has ~ 30 % more intensity than each of the other two peaks. The best explanation for this different intensity of one of the carbon atoms is photoelectron diffraction. A similar effect was found for ethene on Ni(111), which is discussed in Chapter 5.1.1, where the ratio of the intensities of the peaks for the two carbon atoms in the molecule varied with the emission angle. While the fit shown in Figure 6.12 (b) gives a very good description of the spectrum, it should be noted that it was also possible to achieve a fit of similar quality if the position of the C² and the C³ peak were reversed.

In summary propylene was found to physisorb on Cu(111) at temperatures of 122 K, showing an adsorption/desorption equilibrium dependent on the pressure of propylene in the chamber. The spectrum is very similar to the gas-phase spectrum, as was also found in HREELS studies on this system [220]. At 150 K all propylene is desorbed without any reaction products visible on the surface, strengthening the classification of the reaction as a reversible physisorption process.

6.2.1.2 Interaction of ethane, ethene and propane with Cu(111)

Figure 6.13 shows the C 1s spectra of the highest coverages obtained after dosing (a) propane, (b) ethane and (c) ethylene on clean Cu(111). Propane was dosed on the surface at a temperature of 110 K. As displayed in Figure 6.13 (a) the spectrum can be fitted with an adiabatic peak at 284.37 eV and a vibrational shoulder with a distance of 400 meV to the main peak. The S-factor of the vibrational peak is 0.54. If for propane (C₃H₈) an average of 2.67 C-H bonds per carbon atom are considered each C-H bond contributes ~0.20 to the S-factor. This is in line with the contributions per C-H bond to the S-factors found for C₂H₂ (0.21, see Chapter 6.1.1), but a bit higher than that for C₃H₆ (0.17, see Chapter 6.2.1.1) on Cu(111). Unlike the propylene discussed in the previous chapter, which shows a very similar spectrum both in the gas-phase and on Cu(111), the spectrum of propane adsorbed on Cu(111) at first appears vastly different from the gas-phase spectrum [221], which shows a multitude of peaks. However one has to consider that most of the additional peaks, which are assigned to the central carbon atom (which has fewer C-H bonds than the two outer ones) lie less than 100 meV away from the main peaks. As such small distances can not be resolved within our experimental conditions, these peaks then should disappear within the main peak, contributing to the asymmetry.

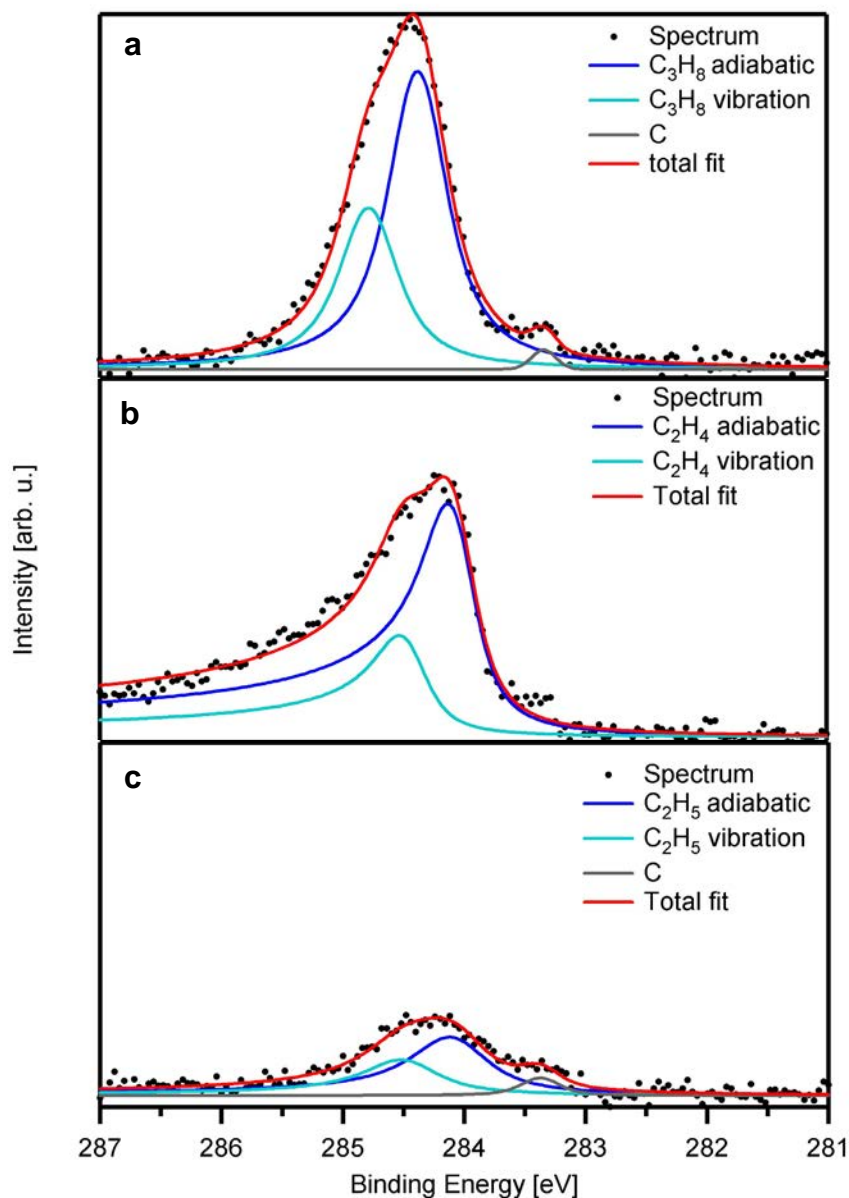


Figure 6.13: (a) Fit of C_3H_8 on Cu(111) at 110 K and a pressure of $5 \cdot 10^{-9}$ mbar (b) Fit of C_2H_4 on Cu(111) at 107 K and a pressure of $7.5 \cdot 10^{-9}$ mbar (c) Fit of C_2H_6 on Cu(111) at 110 K dosed with supersonic molecular beam. All spectra acquired at 0° emission angle, spectra in (b) and (c) scaled to the intensity of spectrum in (a)

Thus we can conclude that the physisorbed propane has a similar spectrum to its gas phase spectrum, just like propylene. Within this resolution limit all three carbon atoms have the same binding energy, which means that apparently the interaction of the molecules with the surface is weak enough that all three carbon atoms remain unaffected by it in respect to their chemical state. The spectrum displayed in Figure 6.12 (a) is equivalent to a coverage of 0.07 ML C-atoms, which was obtained at a surface temperature of 110 K at a C_3H_8 pressure in the chamber of $5.3 \cdot 10^{-9}$ mbar. Lowering the C_3H_8 pressure to $8.5 \cdot 10^{-10}$ mbar caused desorption of most of the adsorbate layer leaving a coverage of only 0.01 ML C-atoms on the surface. This shows clearly that the

experiment was done in an adsorption/desorption equilibrium, just like the propylene adsorption on Cu(111) discussed in the previous chapter.

Ethene was dosed on the Cu(111) surface at a temperature of 107 K. The resulting spectrum, as shown in Figure 6.13 (b) is dominated by a peak at 284.05 eV. Figure 6.13 (b) shows a tentative fit with an adiabatic main peak at this energy, and a vibrational contribution shifted by 400 meV towards higher binding energies in respect to the main peak. An S-factor of 0.43 is found for the vibrational contribution. Although this value is rather large, the contribution of 0.215 for each C-H bond (reasonably assuming two C-H bonds per atom, as the studied molecule is C₂H₄) is still in line with the contributions found for the other molecules on Cu(111). Just like for propane the displayed fit features just one peak pair. A fit with two equal adiabatic main peaks and vibrational splitting, like it was observed for ethene on Ni(111) (see Chapter 5.1.1) was tried, but was not possible. However, as the quality of the fit is not very good, we have to consider some things. The half width of the peak is rather large with 1.1 eV, whereas the propane peak only had a half width of 0.85 eV. In the gas-phase the half width of the spectra of both molecules is around 0.60 eV [31, 221]. A half width of 0.85 eV, like found for the propane peak on Cu(111) can also be estimated for the peaks of the propene spectrum on Cu(111) discussed in Chapter 6.2.1.1 and for the spectrum of ethene coadsorbed with oxygen on Ni(111) as discussed in Chapter 5.2.2. As the spectrum of ethene on Cu(111) thus shows a much larger broadening in respect to the gas phase than the other adsorbates, this could be an indication of the presence of several adsorbate sites with binding energies so close to each other that they cannot be resolved. DFT is predicting several different stable adsorption sites [186, 218]. The high asymmetry of the peak also points into the direction of several not resolved adsorption sites leading to spectral contributions in the high energy tail. Although the adsorption temperature of 107 K is below the desorption peak at 120 K it still lies in the desorption region [192, 217], leading to the same dynamic adsorption/desorption equilibrium situation also found for propane and propylene on Cu(111). The spectrum displayed in Figure 6.13 (b) was acquired at a C₂H₄ pressure in the chamber of 7.6*10⁻⁹ mbar and corresponds to a coverage of 0.09 ML C-atoms. The lowering of the C₂H₄ pressure to 5*10⁻¹⁰ mbar lead to desorption of half of this layer, leaving 0.045 ML on the surface. By annealing the sample to 120 K the remaining ethylene was completely removed from the surface.

As for ethane interaction with Ni(111) (see Chapter 5.2.1, [54]) additional kinetic energy from the supersonic molecular beam was required to enable dissociative adsorption as ethyle (C₂H₅), the same approach was used on Cu(111). Figure 6.13 (c) shows a spectrum during the exposure of the surface

to ethane with 0.84 eV kinetic energy, at a surface temperature of 110 K. With this method only very low adsorbate coverages of 0.02 ML C-atoms were obtained. The spectra were fitted with a set of an adiabatic main peak at 284.08 eV and a vibrational contribution with a distance of 400 meV and an S-factor of 0.5. This S-factor would be in line with an average of 2.5 C-H bonds per carbon atom, and thus a dissociative adsorption of C₂H₆. It should be noted however that due to the low total coverages fits of equal quality are obtained with an S-factor of 0.6, which would imply non-dissociative adsorption. On the other hand the thermal evolution of the adsorbate strengthens the assumption of C₂H₅ as the adsorbate. Unlike for the other molecules discussed in this chapter the coverage did not decrease as the pressure on the sample was lowered. Subsequent annealing the sample to higher temperatures led to a desorption of the adsorbate in the temperature range between 150 and 225 K. Zeigarnik et al. [215] calculated a lower molecular binding energy for C₂H₆ on Cu(111) compared to C₂H₄ on Cu(111). As C₂H₄ has its desorption maximum at 120 K, the desorption range for C₂H₆ should be even lower. For C₂H₅ on the other hand a higher binding energy was calculated. Xi and Bent [217] studied ethyle on Cu(111) formed from C₂H₅I, and found that it decomposes to ethylene which immediately desorbs from the surface between 225 and 250 K. Although this temperature is slightly higher than the desorption range witnessed in our data, it is in much better agreement with our data than an assumed ethane desorption at temperatures <120 K. The half width of the peak is around 1.1 eV, like for ethene and thus could hint at the presence of several adsorption sites close in binding energy.

6.2.2 Physisorption of hydrocarbons on NiO layers

Even though the three hydrocarbons (C₂H₆, C₂H₄ and C₂H₂) studied in Chapter 5 were adsorbed on the clean Ni(111) surface at very low temperatures, only chemisorbed species and in the case of C₂H₆ the dissociative adsorption as C₂H₅ were found, and no physisorption of the parent adsorbates was detected. For ethane this was explained by the reported desorption temperature of 85 K [138], while for ethene and acetylene no studies have been made at sufficiently low temperatures to achieve physisorption. Interestingly, as shown in Chapter 5.3.2, for acetylene coadsorbed with oxygen a physisorbed species was found that desorbed between 100 and 140 K from the surface, while in the same temperature range no physisorbed component was found on the clean Ni(111) surface. For the coadsorption of ethane and ethene with oxygen, as detailed in Chapters 5.2.2 and 5.1.2, respectively, there were physisorbed components found which were still partly present on the surface at 200 K and completely

desorbed at 250 K. This led to the conclusion, that oxygen stabilizes physisorbed components. This was again evident when studying acetylene on the thin NiO layers. There physisorbed components were found that desorbed in the temperature range between 100 and 200 K, which is 60 K higher than on the Ni(111) surface precovered with just 0.25 ML of oxygen. This led to the question if a similar effect is found for other hydrocarbons on NiO, with physisorbed components stable up to higher temperatures.

Figure 6.14 shows the C 1s spectra of the highest coverage obtained after exposing the different NiO preparations to ethane (C_2H_6), ethene (C_2H_4), propane (C_3H_8) and propene (C_3H_6). Ethane was dosed via the supersonic molecular beam with a kinetic energy of 0.84 eV, all other adsorbates were dosed with the microcappillary array doser. The NiO on Ni(111) was grown at 550 K for the ethene and propane experiments, and at 500 K for the ethane adsorption. The propene adsorption on NiO/Ni(111) was not studied. The spectra of the adsorbates on NiO/Ni(111) were acquired at an emission angle of 45° , all other spectra at an emission angle of 0° . The important temperatures, under which the adsorption experiments were performed, are shown in Figure 6.15, which shows the quantitative analysis both of the uptake and the subsequent TPXPS experiments.

The spectra in Figure 6.14 share some similarities for all adsorbates. All of the spectra are relatively broad and lack a visible structure like it was seen, e.g., for propene on Cu(111), see Chapter 6.2.1.1. They also all have a rather symmetric peak shape. In this they are similar to the acetylene peaks on the NiO layers. For C_2H_6 the peaks have approximately the same half width on all three substrates and for C_2H_4 this is the case at least on the two NiO preparations on Cu(111), while for C_3H_8 and C_3H_6 a noticeable difference is visible for different substrates, with the smallest half width found on the NiO clusters on Cu(111) and the largest half width on NiO/Ni(111). This difference is attributed to minor structural differences between the substrates, which lead to slightly different adsorption situations and was also seen to lead to different saturation coverages for acetylene (see Chapter 6.1).

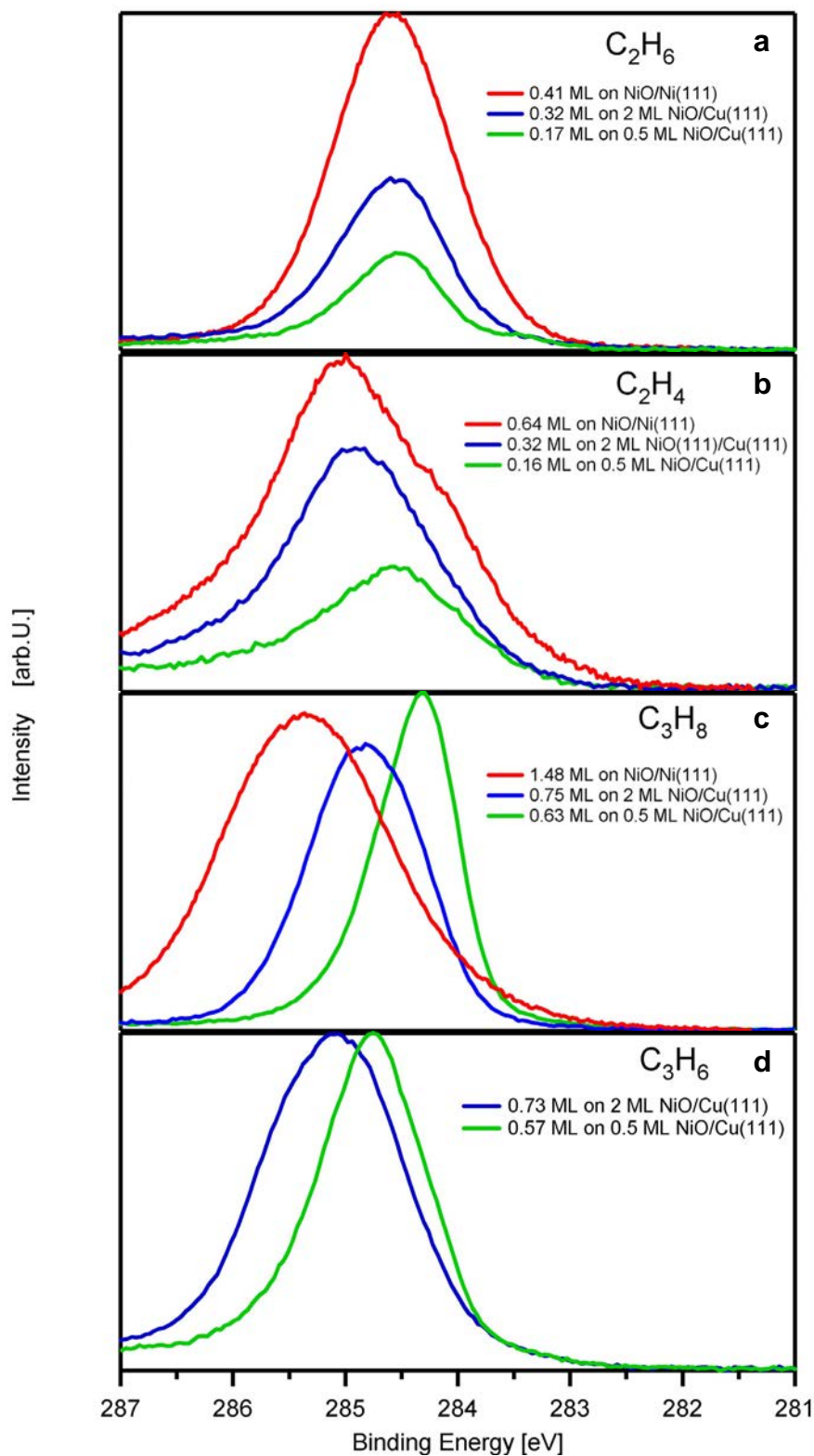


Figure 6.14: C 1s spectra of hydrocarbons adsorbed on the different NiO layers and clusters **(a)** C_2H_6 **(b)** C_2H_4 **(c)** C_3H_8 **(d)** C_3H_6 . All spectra of adsorbates on NiO/Ni(111) were acquired at an emission angle of 45° , all other spectra at 0° .

Adsorbate	NiO/Ni(111)	2 ML NiO/Cu(111)	0.5 ML NiO/Cu(111)
C ₂ H ₆	284.5-284.6 eV	284.5-284.6 eV	284.3-284.6 eV
C ₂ H ₄	284.0-285.0 eV	284.6-284.9 eV	284.4-284.6 eV
C ₂ H ₂ (physisorbed)	285.1-285.2 eV	285.0-285.2 eV	284.8-285.0 eV
C ₃ H ₈	284.7-285.4 eV	284.5-284.8 eV	284.3 eV
C ₃ H ₆	-----	284.5-285.1 eV	284.8 eV

Table 6.1: Observed binding energy ranges for physisorbed hydrocarbons on the different NiO preparations

Except for ethane, the binding energy of the adsorbates varies significantly on the different NiO preparations. Part of this difference is attributed to the different coverages displayed in Figure 6.14. For almost all adsorbates, except for propene and propane on the NiO clusters on Cu(111) the binding energy was found to shift towards higher binding energies as the coverage increased. A similar observation was made for all other physisorbed species on NiO, like the physisorbed acetylene components discussed in Chapter 6.1 and the physisorbed components of H₂O, CO₂ and CO discussed in Chapter 7. Table 6.1 lists the binding energy ranges for the different hydrocarbons on the different NiO surfaces. Please note that these ranges only hold true for the coverages prepared within this work, and that for higher coverages it is very likely that even higher binding energies could be found, although a saturation effect can be expected there as well when the adsorbate layer thickness reaches a point where it starts to behave like a hydrocarbon crystal. This shift towards higher binding energies can best be explained by adsorbate-adsorbate interactions. By looking at the binding energy ranges in Table 6.1 it becomes clear, however, that not all of the binding energy difference is explained by the different coverages. There is a clear shift towards higher binding energies with increasing thickness of the NiO layers (the NiO layers on Ni(111) are the thickest NiO layers).

What remains to be explained is why C₃H₈ and C₃H₆ on the NiO clusters don't undergo a binding energy shift. If we look at the binding energies, it is interesting to note that they are almost the same binding energies found for the respective molecules upon physisorption on clean Cu(111) in Chapter 6.2.1. In this context at least for propane it could be argued that also here the molecules adsorb mainly on the blank Cu(111) patches.

However, the coverage we found here is much higher than found in the adsorption experiment on the clean Cu(111), and the thermal stability is also higher with complete desorption up to 140 K instead of the 120 K found on the clean Cu(111). Also even though the binding energy found for propene on the NiO clusters on Cu(111) has the same value as the C_{2/3} peak for propene on clean Cu(111) in Chapter 6.2.1.1., the clear absence of the C₁ peak, which should be at 284.3 eV, makes an adsorption of the propene on the bare Cu(111) patches unlikely.

Further information about the adsorption process is obtained from the quantitative analysis in Figure 6.15. Both for ethane and ethene on all three surfaces a fast initial increase is followed by a much slower increase in coverage, without reaching saturation within the timeframe of the experiment. As the temperature was falling in all cases during the course of the uptake experiment, and as we are discussing physisorbed species here, the best explanation for this behavior is, that the studied temperatures lie within a temperature region where an adsorption/desorption equilibrium is established on the surface, which is dependent on the adsorbate pressure in the chamber and on the surface temperature. In this case the falling temperatures would allow higher adsorbate amounts on the surface to be stable, which is reflected by the slow increase in coverage. In between the end of the exposure and the beginning of the subsequent TPXPS experiment, the pressure in the chamber is reduced. As discussed before, this leads to a reduction of the coverage.

This confirms the assignment of the adsorbates as physisorbed species and the assumption of the pressure and temperature dependent saturation coverage. For the uptake experiments of propane and propene a similar evolution of the coverage is found, especially if the differently scaled exposure axis is taken into account. The only difference is, that for these two molecules an apparent saturation coverage is reached after the initial fast increase. The best explanation for this difference in behavior is that during these experiments a more stable temperature was reached near the end of the exposure, as well as a relatively stable background pressure. Upon decrease of the background pressure in between the uptake and the TPXPS the coverage decreases here as well.

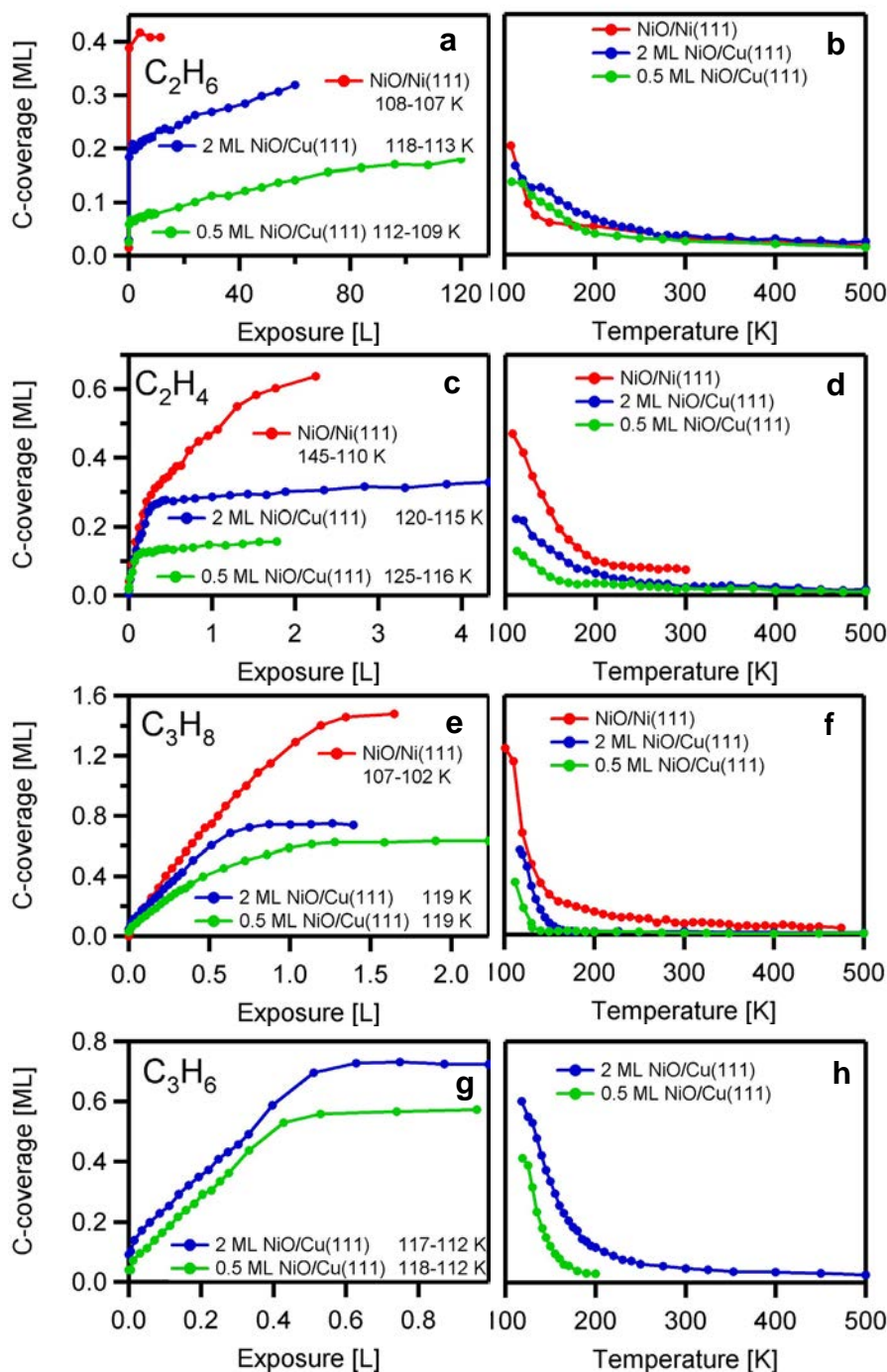


Figure 6.15 : Quantitative analysis of the C 1s spectra of the uptake and TPXPS experiments of the different adsorbates on the different NiO surfaces. (a) and (b) C₂H₆. (c) and (d) C₂H₄. (e) and (f) C₃H₈. (g) and (h) C₃H₆. All spectra of adsorbates on NiO/Ni(111) were acquired at an emission angle of 45°, all other spectra at 0°.

If we take a closer look at Figure 6.16 (a) and (b), depicting the coverage evolution on the thin NiO layers and the NiO clusters on Cu(111), respectively, for low exposures, the different behavior of the two C₃H_x species in regard to the two C₂H_x species becomes even more obvious. On both surfaces at the beginning of the uptake the coverages of C₂H₄, C₃H₆ and C₃H₈

evolve almost identical, while for C_2H_6 it is not as clear due to the much wider distance between the points. The offset between the different lines in Figure 6.15 (i) is attributed to different initial coverages due to residual gases prior to the uptake. After this initial uniform increase on both surfaces for ethane and ethene the slow increase starts while propane and propene continue to grow almost linearly and saturate at a similar coverage.

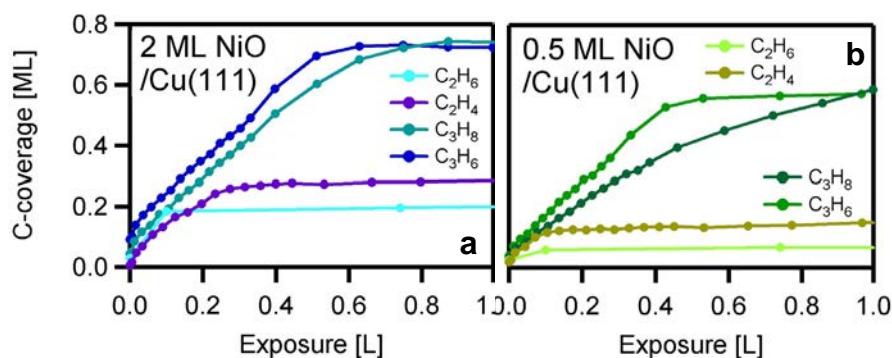


Figure 6.16: (a) all adsorbates on 2 ML NiO/Cu(111) (b) all adsorbates on 0.5 ML NiO/Cu(111). All spectra of adsorbates on NiO/Ni(111) were acquired at an emission angle of 45° , all other spectra at 0° .

For the coverages of all adsorbates there is a clear order of the three NiO preparations. The highest coverages are always found on NiO/Ni(111), while the lowest are found on the NiO clusters on Cu(111). This is in agreement with the observations made for the acetylene coverages on the three different surfaces. The coverage difference between NiO/Ni(111) and the two NiO preparations on Cu(111) can partly be explained by the different surface temperatures. As the coverage depends on the temperature, a lower temperature leads to a higher saturation coverage. For the two different NiO preparations on Cu(111), however, the surface temperatures are always either very close to each other, or are even higher for the thin NiO layers even though on these higher adsorbate coverages are found. This behavior is strong evidence that the physisorbed species mainly adsorb on the NiO clusters for the Cu(111) surface with the NiO clusters. As only part of the surface is covered with the NiO, whereas for the thin NiO layers on Cu(111) the whole surface is covered with it, this directly leads to a lower possible saturation coverage on the NiO clusters.

The last thing to be discussed is the thermal evolution of the adsorbates. Propane (C_3H_8) has desorbed from the NiO clusters on Cu(111) at 140 K and at 170 K from the thin NiO layers on Cu(111), while on NiO/Ni(111) some residues are still found on the surface at 300 K and above. On both NiO preparations on Cu(111) there also remain some residues on surface above the noted temperatures, but these species with a coverage of less than

0.02 ML are mostly attributed to contaminations already present on the surface prior to the propane adsorption. For NiO/Ni(111) it is not totally clear if this is also the case, as none such contaminations were present prior to the uptake. The spectral shape also remains constant during the propane desorption. On the other hand the residues in this case could be attributed to species generated by beam damage, as these spectra were recorded without switching to a new spot after each spectrum, unlike the spectra on the other two surfaces. Due to the rough nature of the NiO surfaces another explanation could be that indeed some propane molecules are adsorbed on very stable adsorption sites and only desorb as the surface undergoes some reconstruction processes, like also discussed for the TPXPS experiments of hydroxide and carbonate in Chapter 7. For propene (C_3H_6) we find a complete desorption from the NiO clusters on Cu(111) at 190 K. On the thin NiO layers, a similar coverage progression is found to the coverage progression of propane on NiO/Ni(111). However, the arguments discussed there do not hold true here due to two reasons: firstly, beam damage was ruled out as the surface was shifted to a new spot after each spectrum to minimize it. There were also a lot of contaminations present on the surface prior to the propene adsorption, and thus the coverage “tail” above 200 K here is attributed to these contaminations. Still it can be said from looking at the curves that propene desorbs at slightly higher temperatures from the surface on the thin NiO layers than on the NiO clusters on Cu(111). The same trend was already found for the propane desorption, with NiO/Ni(111) having the most stable adsorbates, and this trend holds also true for ethene (C_2H_4). As a residual tail due to contaminations and beam damage plays a role here for all three surfaces it is hard to tell when ethene is desorbed from the surface, but rough estimates of 160 K for the NiO clusters on Cu(111), 180 K for the thin NiO layers on Cu(111) and 200 K for NiO/Ni(111) show again the same trend that the adsorbates are most stable bound on NiO/Ni(111) and least stable on the NiO clusters. For ethane (C_2H_6) the situation is even less clear, as only for the NiO/Ni(111) surface a temperature of 150 K is given, where all of the ethane is desorbed from the surface and only the contaminations remain. On the two different NiO layers on Cu(111), the desorption proceeds much slower and is finished around 200 K on the clusters and around 300 K on the thin NiO layers on Cu(111). Why the NiO/Ni(111) is not the surface with the most stable adsorption sites in this case is not clear.

If we compare all of the adsorbates, some general rules can be found. For all adsorbates the coverage depends both on the surface temperature and on the pressure of the adsorbate in the chamber, which clearly identifies them as physisorbed components. The adsorbed species seem to be most strongly bound on the NiO/Ni(111) followed by the thin NiO layers on Cu(111), and

most weakly on the NiO clusters on Cu(111). This is seen both from reached coverages and from the temperatures, where all of the adsorbates are desorbed from the surface and only residues due to surface contaminations and beam damage remain on the surface, with the exception of the TPXPS of ethane on NiO/Ni(111), which does not follow this general trend. The most important observation, however, is that for all studied hydrocarbons we find physisorbed species in temperature ranges, where none are observed on the clean Ni(111) or Cu(111) surfaces, leading to the conclusion that oxygen stabilizes these physisorbed species.

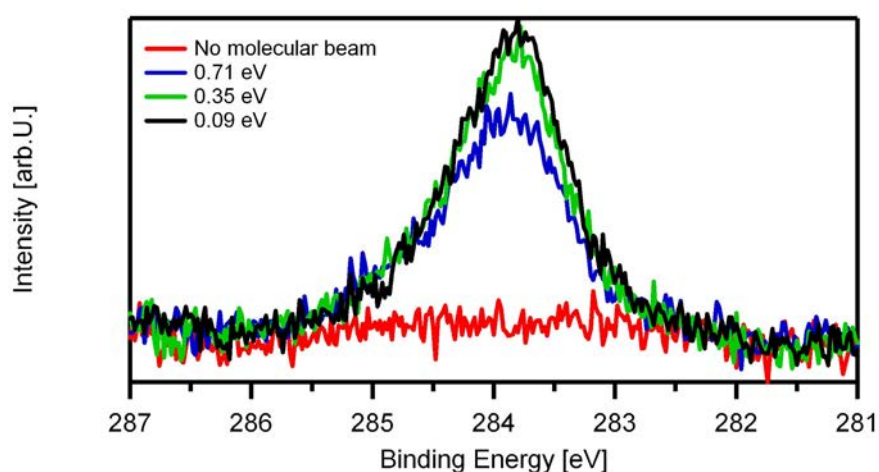


Figure 6.17: C 1s spectra of methane dosed on NiO/Ni(111) at 110 K with various kinetic energies provided by the molecular beam. All spectra acquired at an emission angle of 45°.

Apart from the discussed hydrocarbons, the interaction of methane (CH₄) with the various NiO surfaces was also studied. Even though a great range of different surface temperatures between 100 and 600 K and kinetic energies of the methane molecules up to 0.71 eV, provided by the supersonic molecular beam (for details on the energies available for methane adsorption experiments please see [54]), were tried, only a very weakly bound physisorbed species was found on NiO/Ni(111) at 110 K and no interaction with the other two surfaces at 120 K. The spectra of methane on NiO/Ni(111) are displayed in Figure 6.17. For all kinetic energies the physisorbed component was only present on the surface as long as the molecular beam was switched on, and desorbed immediately as soon as the beam was shut off. Interestingly for lower kinetic energies slightly higher coverages of 0.08 ML could be reached than for the highest kinetic energy of 0.71 eV, for which only a coverage of 0.07 ML was achieved. For methane on Ni(111) a desorption temperature of 50 K has been reported [138], which is much lower than the temperatures of 85 and 120 K reported for ethane and propane [138], respectively. So even if the physisorbed component is stabilized by the oxygen, it is not surprising that its desorption temperature on NiO is still so

low that it immediately desorbed from NiO/Ni(111) at 110 K when the molecular beam was switched off and did not adsorb on the other two surfaces at 120 K.

6.3 Concluding discussion

Unlike the Ni(111) surface, where chemisorbed species were found upon adsorption of ethane, ethene and acetylene (even though some additional kinetic energy had to be provided in the case of ethane), and these chemisorbed species reacted upon heating, the Cu(111) surface was found to be much less reactive. Although for acetylene interaction with the Cu(111) surface a chemisorbed species is found, just like on Ni(111), for ethene only a physisorbed species is discovered. For propane and propene we also found physisorbed species after exposure at low temperatures. The ethane interaction with the surface was found to be a bit more complicated. For ethane dosed from the background, no interaction with the surface was found. However, when the ethane was dosed from the supersonic molecular beam with a kinetic energy of 0.84 eV, a very low coverage of ethyle (C_2H_5) was formed on the surface, which was identified both by the applied fit and by its desorption temperature. All adsorbates except for propene show a single main adiabatic peak and were fitted with a combination of this adiabatic peak and a vibrational contribution at higher binding energies. The binding energies of all adsorbates as well as the data of the vibrational contributions are shown in Table 6.2.

Adsorbate	Binding energy [eV]	Vibrational splitting [meV]	Total S-Factor/ per C-H bond
C_2H_2	283.36-283.42	370	0.21 / 0.21
C_2H_4	284.05	400	0.43 / 0.215
C_2H_5 (from C_2H_6)	284.08	400	0.5 / 0.2
C_3H_6	284.29	400	0.34 / 0.17
	284.75	400	0.17
	284.9	400	0.51 / 0.17
C_3H_8	284.37	400	0.54 / 0.2

Table 6.2: Binding energies and vibrational data for hydrocarbons adsorbed on Cu(111)

The propene spectrum consisted of three peaks with vibrational splitting, one for each carbon atom in the molecule. Interestingly, the propene spectrum is very similar to the gas phase spectrum of propene. For the other adsorbates this similarity exists as well, however it is not as evident as many of the peaks seen in the gas phase spectrum cannot be resolved within our experimental conditions. The binding energies of all the adsorbates are very close to each other, with the exception of the acetylene binding energy which is lower by almost one eV. This is in accordance with the different nature of the acetylene bond, as it is the only adsorbate that is still present on the surface at room temperature while all other adsorbates leave the surface below 250 K, or at even lower temperatures. If we take a look at the S-factors, we find a mean S-factor of 0.20 ± 0.02 . This is significantly higher than the value of 0.17 ± 0.02 found in Chapter 5 for the adsorbates on Ni(111) and also found by Steinrück et al. [28] both on Ni(111) and Pt(111). This is a clear sign of the different behavior of the two surfaces. This different behavior is mostly evident here in the interaction of C_2H_4 and C_2H_5 with the two surfaces. On Ni(111) we found a chemisorbed species that reacted to acetylene which subsequently reacted to carbon. On Cu(111) both species are physisorbed and leave the surface at 120 K (ethene) and 225 K (ethyle). Although the ethyle is reported to dehydrogenate to ethene [217] prior to desorption, the situation is still rather different to the one on Ni(111) where in the end a complete dehydrogenation of the adsorbates was found. A similar behavior was found for C_3H_6 and C_3H_8 , with the former desorbing intact from the surface below 150 K and the latter already desorbing at 110 K upon lowering of the propane pressure in the chamber, which is lower than the desorption temperature of 120 K reported for propane on Ni(111) [138]. For the interaction of propene and Ni(111) no data exists for low temperatures. So the general trend observed is that the adsorbates interact much weaker with the Cu(111) surface than with the Ni(111) surface, leading to lower desorption temperatures and higher S-factors.

A very interesting exception to this trend is the interaction of acetylene with the two surfaces. The spectra of both adsorbates are very similar, with the binding energy, the vibrational splitting and the S-factor being so close to each other that they can be said to be identical within the margin of error. The same was found to be the case for the local adsorption geometry as shown by Bao and coworkers [159, 183]. Differences are found in the LEED structure ($p(2 \times 2)$ on Ni(111) and $\begin{pmatrix} 2 & 1 \\ 0 & 4 \end{pmatrix}$ on Cu(111)), and the saturation coverage which is 0.58 ML and 0.5 ML on Ni(111) and Cu(111), respectively. The thermal evolution is also very similar. On both surfaces around 270 K a reaction starts, where on Ni(111) mainly benzene and on Cu(111) benzene

and a variety of other hydrocarbons are formed, which immediately desorb from the surface on Cu(111) while on Ni(111) they stay on the surface and dehydrogenate.

The different behavior of acetylene and ethylene on Cu(111) is explained by a DFT study by Fuhrmann et al. [186]. They showed that for the acetylene molecule on Cu(111) the chemisorbed state, for which the molecule has to be distorted, provides a major energy gain in respect to an undistorted physisorbed state. For C₂H₄ on the other hand both states were shown to have similar energies, and additionally a large energy barrier lies between them, whereas for acetylene this energy barrier is significantly smaller. From this they concluded that the chemisorbed state is not favorable for ethene.

In contrast to the situation on Cu(111), where physisorbed species were found for all adsorbates, on clean Ni(111) no physisorbed species were found upon the adsorption of any of the studied C₂H_x molecules, even at temperatures as low as 100 K. This changed in the coadsorption case with oxygen, where for acetylene a physisorbed component was found to be present on the surface below 140 K, and the adsorbed ethene and ethane species could arguably be defined as physisorbed. This led to the assumption, that oxygen stabilizes the physisorbed components on the Ni surface. Upon studying the interaction of hydrocarbons with the NiO surfaces, this trend was found to be even more evident, with physisorbed components found for all of the studied molecules (C₂H₆, C₂H₄, C₂H₂, C₃H₈ and C₃H₆) except for methane. The C 1s spectra for these physisorbed species show one broad peak, without any visible structure which would be characteristic for a vibrational splitting. The positions of these peaks depend on the coverage, shifting to higher binding energies for higher adsorbate coverages. For all adsorbates, except for ethane, there is also an effect of the thickness of the NiO layers on the binding energy, with thicker NiO layers leading to higher binding energies. For all adsorbates the obtained coverages were found to depend both on the substrate temperature and on the pressure of the adsorbate in the chamber. Due to this, as the adsorbate pressure in the chamber was lowered in between the uptake and the TPXPS experiment a coverage decrease was found in all experiments. Upon heating, most adsorbates desorbed below 200 K, but for some, most notable propane on NiO/Ni(111), small quantities were found to be stable up to much higher temperatures. With the exception of ethane on NiO/Ni(111) a general trend was found, that the adsorbates were first gone from the NiO clusters on Cu(111) and remained longest on NiO/(Ni(111)). As the desorption temperatures are generally higher than the ones found on both clean Ni(111) and clean Cu(111), these experiments clearly show that the oxygen stabilizes the physisorbed components, and that thicker NiO layers lead to an even stronger stabilization.

While most of the hydrocarbons were found to only form a physisorbed adsorbate on the NiO, acetylene was found to also chemisorb on the different NiO layers. On NiO/Ni(111) the C 1s spectra of adsorbed acetylene shows two peaks at 283.26 and 285.21 eV, which are identified as physisorbed and chemisorbed acetylene, respectively. Both peaks are very broad and lack a clear vibrational structure, which is attributed to acetylene adsorbed on a variety of sites with small binding energy variations. Interestingly the two peaks develop almost simultaneously and not subsequently, as would be expected for the usual “multilayer” picture of a physisorbed component. This means that the population of the chemisorbed and the physisorbed adsorption site must be almost equally likely, with a slight favor for the chemisorbed site as this species develops slightly earlier. From the observation of a different spot on the sample it was deduced that both species are affected by the exposure to photons, as both the coverage and the binding energy was different on the new spot; however, adsorption is not due to beam damage. A very similar picture was found on the thin NiO layers on Cu(111). Here the C 1s spectra show the same two peaks, however at slightly different binding energies of 283.41 and 285.06 eV for the chemisorbed and physisorbed components, respectively. The uptake commences in same manner like on NiO/Ni(111), with the only difference being a much lower saturation coverage, the reason of which is not clear but is in line with the lower saturation coverages of the other (physisorbed) hydrocarbons on the NiO layers on Cu(111) in respect to their coverages on NiO/Ni(111). Upon heating the physisorbed component leaves the surface first in both cases, and is gone around 200 K.

At slightly lower temperatures the chemisorbed, and some of the physisorbed acetylene starts to react to a new species, for which the best assignment is some form of carbon allotrope or a precursor of such a species. The binding energies of all the acetylene species and reaction products on the different surfaces are listed in Table 6.3. Please note that the binding energies of the acetylene species on the NiO listed in the table may differ from the ones given for the uptake, as the binding energies were found to be somewhat dependent on the studied position on the sample, which is attributed to beam damage.

The assignment of the reaction species is based on its binding energy, thermal stability and the evolution of another reaction species, which appears at 170 K on the thin NiO layers on Cu(111) and around 250 K on NiO/Ni(111) in the area around 286 eV. This species is assigned to a C-O single bond within the carbon allotrope network. Up to 500 K all of the chemisorbed acetylene has reacted to these two species on NiO/Ni(111). On the thin NiO layers on Cu(111) a third reaction species is found to develop above 300 K, which is assigned as a carbonaceous species. The reason why this new

species only appears on the NiO layers on the Cu(111) could either be that it is directly adsorbed on the copper, although the binding energy would not fit. Or the structure of the NiO on Cu(111) enables the carbon atoms to bind to the nickel atoms, for which the binding energy would fit. The O 1s, Ni 2p and Cu 2p regions gave no deeper insight into the nature of the reaction products.

Species	Cu(111)	NiO/Ni(111)	2 ML NiO /Cu(111)	0.5 ML NiO /Cu(111)
C ₂ H ₂ on Cu(111) adiabatic	283.42 eV	-----	-----	283.33 eV
C ₂ H ₂ on Cu(111) vibration	283.78 eV	-----	-----	283.69 eV
Chemisorbed C ₂ H ₂ on NiO	-----	283.33-284.03 eV	283.59-284.17 eV	283.30 eV
Physisorbed C ₂ H ₂ on NiO	-----	285.01-285.12 eV	284.99-285.01 eV	285.03 eV
Carbon allotrope	-----	284.62 eV	284.26 eV	284.11 eV
C-O bond within carbon allotrope	-----	286.23 eV	285.91 eV	-----
Carbonaceous species	-----	-----	283.32 eV	283.38 eV

Table 6.3: Binding energies of C₂H₂ and reaction products on the various surfaces.

On the NiO clusters on Cu(111) the C 1s spectra were found to be a superposition of acetylene adsorbed on the bare Cu(111) patches between the NiO clusters and of acetylene both chemi- and physisorbed on the NiO clusters themselves. The saturation coverages for both components, however, are much lower than what would be expected for their respective surface coverages. As this is the case for all different adsorbates, this leads to the conclusion that the edges of the NiO clusters and their immediate vicinities are not populated by acetylene. During heating again the carbon allotrope/carbon allotrope precursor species found previously is formed, as

well as the carbonaceous species. The species assigned to a C-O single bond within the carbon allotrope is not found here. When acetylene is dosed on NiO clusters on Cu(111) at 400 K, the carbonaceous species saturates at 0.1 ML, while the carbon allotrope reaches much higher coverages, and could not be saturated even with exposures above 770 L. During the latter experiment the NiO was almost completely reduced, leaving just the metallic Ni on the surface.

An interesting comparison can be made between the clean Cu(111) surface and the Cu(111) surface covered with the NiO clusters. As discussed in Chapter 6.1.1, on the clean Cu(111) surface acetylene reacts at a temperature of 325 K to a variety of cyclic and non cyclic hydrocarbons that immediately desorb from the surface. On the Cu(111) surface precovered with the NiO clusters, the C₂H₂ adsorbed on the bare Cu(111) patches react at slightly lower temperatures, with a reaction temperature around 305 K. As no significant loss in the total C 1s coverage is observed in this temperature region, a reaction towards fast desorbing hydrocarbon species is ruled out. Instead we find the formation of carbon allotropes. Several possible explanations can be given for this difference. For acetylene adsorbed on Ni(111) we could show in Chapter 5 that a certain minimum amount of acetylene is needed on the surface to enable benzene formation. Since the amount of acetylene adsorbed on the Cu(111) patches was less than the expected value, assuming an equal coverage of the surface with Cu(111) patches and NiO clusters, the amount of acetylene could be too low to allow the formation of longer hydrocarbons. The second possible explanation is that Cu(111) patches could be too small to accommodate these longer hydrocarbons, although the STM pictures shown in Chapter 4.2.4 (Figure 4.18) seem to suggest rather large patches of bare Cu(111). On the other hand a minority of oxygen atoms (less than 0.05 ML as discussed in Chapter 4) could be present on the Cu(111) patches blocking adsorption sites needed for the formation of the longer hydrocarbons. The most important reason for the different reaction behavior, however, should be the presence of the NiO. As discussed in the previous chapter NiO is used as a catalyst in the synthesis of carbon allotropes [204-207] and thus apparently makes the carbon allotrope formation, and by this the complete dehydrogenation of the acetylene, more favorable than the formation of longer hydrocarbons.

7 Formation and thermal evolution of NiOH and NiCO₃

7.1 Introduction

Impurities on a surface, which can be caused, e.g., by residual gases, always play a very important role for the morphological and chemical properties of a material, e.g. by blocking of active sites. The most common impurity for most oxides is OH, due to interaction of the oxides with water from the atmosphere or from the residual gas in the UHV system, either during the growth process or later on [222]. McKay [110] found for NiO(100) surfaces, which were freshly prepared by cleaving a NiO crystal, only very weak interaction with water, which was shown to interact only with defect sites. These findings were confirmed by several groups, both for freshly cleaved surfaces [111] and thin NiO films with (100) orientation [79, 88, 89]. NiO(111) on the other hand was found to be very reactive to water, as reported by several groups using a wide range of different techniques including HREELS [85, 88-90], LEED [79, 85, 88, 89], AES [79, 88], STM [76, 79] and XPS [76, 79, 80, 88, 89, 91].

As discussed in detail in Chapter 4, the NiO(111) surface is a polar surface and thus thermodynamically unstable [84]. Several groups found that OH stabilizes the NiO (111) surface [79, 88, 89]. Langell et al [88] found it impossible to grow NiO(111) films on Ni(100) in the absence of OH; instead NiO(100) films are formed.

NiO(111) islands, which are present in NiO(100) films grown by oxidation of Ni(111) at 500 K with low oxygen doses [79, 81, 93], grow upon adsorption of water, but no nucleation of additional islands was observed [79]. This process was found to be reversible when heating the surface [93]. By taking photoelectron spectra under several emission angles, the OH groups were shown to reside at or near the surface of the films [79, 111]. A disagreement exists in literature over the coverage of OH, with estimates ranging from 0.4 ML [89] over 0.6-0.8 ML [88] up to 0.85-1ML [79], stabilizing the surface of a freshly grown oxide. After additional water adsorption a coverage of 1.5-2 ML OH has been estimated as saturation coverage for NiO(111)/Ni(111) [79], with the stacking sequence equal to β -NiOH. During adsorption of water at low temperatures (<200 K), additionally to the formation of OH also layers of physisorbed water are formed, giving rise to an XPS Peak at ~ 533 eV [111, 223].

Hydroxilated NiO has been studied with XPS by several groups so far [76, 79, 80, 88, 89, 91, 98, 99]. The binding energies reported by these groups in the

O 1s region for the oxide and the hydroxide peaks are given in Table 7.1. Although the peak positions differ by more than 1 eV between the publications the distance between these two peaks can be given as 1.7 eV \pm 0.1 eV, with only two exceptions in the works of Kitakatsu et al. [79] and Lorenz et al. [91], both of which feature only very small hydroxide shoulders making the determination of the peak position difficult.

System	Oxide Peak	Hydroxide Peak	Distance between Hydroxide and Oxide Peaks	Source
NiO(111)/Ni(111) grown at 100 K	529.0 eV	530.7 eV	1.7 eV	[76]
NiO(111)/Ni(111)	529.7 eV	531.3 eV	1.6 eV	[80]
NiO(111)/Ni(111)	Not given, ~ 529.8 eV	531.4 eV	1.6 eV	[89]
NiO(111)/Ni(111)	529.6 \pm 0.1 eV	531.4 \pm 0.1 eV	1.8 eV	[79]
NiO(111)/Ni(111)	530.2 eV	532.4 eV	2.2 eV	[91]
NiO(111)/Ni(100)	529.4 eV	531.2 eV	1.8 eV	[88]
NiO(100)/Ni(111)	530.1 \pm 0.1 eV	532.1 \pm 0.1 eV	2.0 eV	[79]
NiO(100) crystal	529.7 eV	531.4 eV	1.7 eV	[98]
Heated β -Ni(OH) ₂	529.7 eV	531.4 eV	1.7 eV	[99]

Table 7.1: List of oxide and hydroxide binding energies obtained from literature

The thermal evolution of these adsorbed layers was studied in less detail. On NiO(100) the physisorbed H₂O desorbs completely up to 275 K [111, 224], with a TPD Peak resulting from the H₂O multilayer at 150 K and the monolayer peak with its center at 200 K and a tail up to 300 K [224]. There is no known TPD data for water adsorption on NiO(111). For the OH coverage on NiO(100) Uhlenbrock et al. [111] claim no change in coverage for temperatures up to 573 K.

Rohr et al. [85] reported that heating to above 600 K removes the OH groups from a NiO(111) surface, leading to reconstruction of the surface, which is reversed by water adsorption at lower temperatures. Langell and Nassir [88] report a continuous decay of the hydroxide layers on NiO(111) from XPS

data, with coverage loss for both OH and oxidic oxygen starting at 400 K, and leading to conversion of the NiO(111) to NiO(100) at 600 K. Kitakatsu et al. [93] showed that NiO(111) islands within NiO(100) start to shrink at 550 K if they are weakly hydroxylated, but remain stable up to 600 K if they are strongly hydroxylated. A detailed in situ study of the thermal evolution over the whole temperature range from 100-600 K has not been conducted so far.

Another common atmospheric gas that can easily come into contact with NiO surfaces is carbon dioxide. CO₂ also plays an important role as either a reactant, or as reaction product in a variety of reactions catalyzed by transition metal oxides. Examples include the water-gas shift reaction [225], ketonization of carboxylic acids [226], CO₂ reformation of methane [227], carboxylation of epoxides [228] and oxidative coupling of methane [229], where CO₂ can also poison the catalyst. Lastly, the increasingly important question of CO₂ storage has to be mentioned [230].

The interaction of CO₂ with NiO surfaces was the topic of only a few publications so far. Behm and Brundle [231, 232] reported that CO₂ dosed onto an oxidized Ni(100) surface led to the formation of carbonate, with XPS binding energies of 289.0 eV and 531.2 eV in the C1s and O1s regions, respectively. The highest carbonate coverage obtained was 1.2 ML for simultaneous dosing of O₂ and CO₂ on Ni(100) at 130 K. It should be noted, however, that for the simultaneous dosing of O₂ and CO₂ the degree of oxidation of the surface was found to be lower than for the dosing of O₂ without CO₂. The carbonate was found to destabilize above 321 K decaying into O and CO₂, with the main CO₂ TPD Peak occurring at 418 K and the tail lasting up to 550 K. TPD experiments with isotopically labeled oxygen, where the carbonate layers were grown by coadsorption of C¹⁶O₂ and ¹⁸O₂, revealed desorption of atomic masses 44 (C¹⁶O₂) and 46 (C¹⁶O¹⁸O) in a ratio of 2:1. This led to the conclusion that all 3 oxygen atoms in the CO₃ are equivalent. From the close similarity of preliminary HREELS data of CO₃/Ni(100) with HREELS data of CO₃/Ag(110) [233], it is assumed that the CO₃ binds in the same manner to the substrate on both surfaces. For CO₃/Ag(100) the binding geometry is known from SEXAFS [234] and NEXAFS [235] to be flat lying and planar, with all three oxygen atoms bound to the surface.

For NiO(111)/Ni(111) Gordon et al [236] found 0.14 ML CO₃ after dosing of CO₂ at room temperature, with XPS binding energies of 290 eV and 530.7 eV. The TPD measurements showed peaks at 395 and 634 K, with the former disappearing, if the NiO layer was annealed to 570 K before CO₂ adsorption. Matsumoto [237] reported for NiO/Ni(111) a TPD peak of CO₂ at 160 K trailing up to 250 K after CO₂ was dosed at 123 K.

7.2 Water interaction with NiO layers

7.2.1 Determination of damping factors

In order to determine reaction pathways it is important to have knowledge about the actual coverages of the reacting species over the course of the reaction. When the adsorbate becomes adsorbed in multilayers at low temperatures, the apparent coverages of the lower lying layer, and also the coverage of the succeeding multilayers, determined from the spectra, are lower than the actual coverages due to damping. To determine the extent of this damping, which will be expressed by the damping factor a introduced in Chapter 2.3, we make use of some of the experiments discussed in the following chapters. Please note that only the aspects of the experiments necessary for the determination of the damping factors are discussed here, while all other aspects are discussed in the respective chapters.

Figure 7.1 (a) shows the quantitative analysis of the TPXPS experiment of water adsorbed on 2 ML NiO on Cu(111). As discussed in the following chapters, during adsorption of water hydroxide is formed as well as multilayers of physisorbed water. The important part of the experiment for the determination of the damping factor, a , is the section between 140 and 170 K. In this temperature range, which is marked with a green circle in Figure 7.1 (a), the multilayers of the physisorbed water desorb, leaving only a monolayer of physisorbed water on the surface which is subsequently desorbing. As the coverage of the physisorbed water falls from an apparent value of 3.86 ML down to 0.91 ML, the coverage of the oxide seems to increase from 0.47 up to 1.17 ML and the hydroxide coverage from 0.39 to 1.06 ML. Water was found to desorb molecularly from a NiO surface in this temperature region in a TPD experiment [224]. An increase in the hydroxide coverage seems unlikely since the hydroxide layer was saturated prior to the TPXPS experiment. Thus we conclude that the increase is only apparent, caused by the lifting of the damping by the adsorbed water multilayers. This leads to the conclusion that the oxide coverage prior and after desorption of the water multilayers should be the same. With this information we can now determine the damping factor a using Equation (13) from Chapter 2.3 to calculate actual coverages for several damping factors and looking for the best fit. For this it was assumed that water and hydroxide layers lead to equally strong damping. The first step in the calculation was a correction of the physisorbed water coverage itself, as lower layers of water in the multilayer are damped by the water layers on top of them. With this method a damping factor of 0.83 was determined for the water and hydroxide layers under an emission angle of 0° . This means that each full water layer reduces the signal strength of the lower layers by 17%.

Figure 7.1 (b) shows the coverages from Figure 7.1 (a) corrected with the determined damping factor.

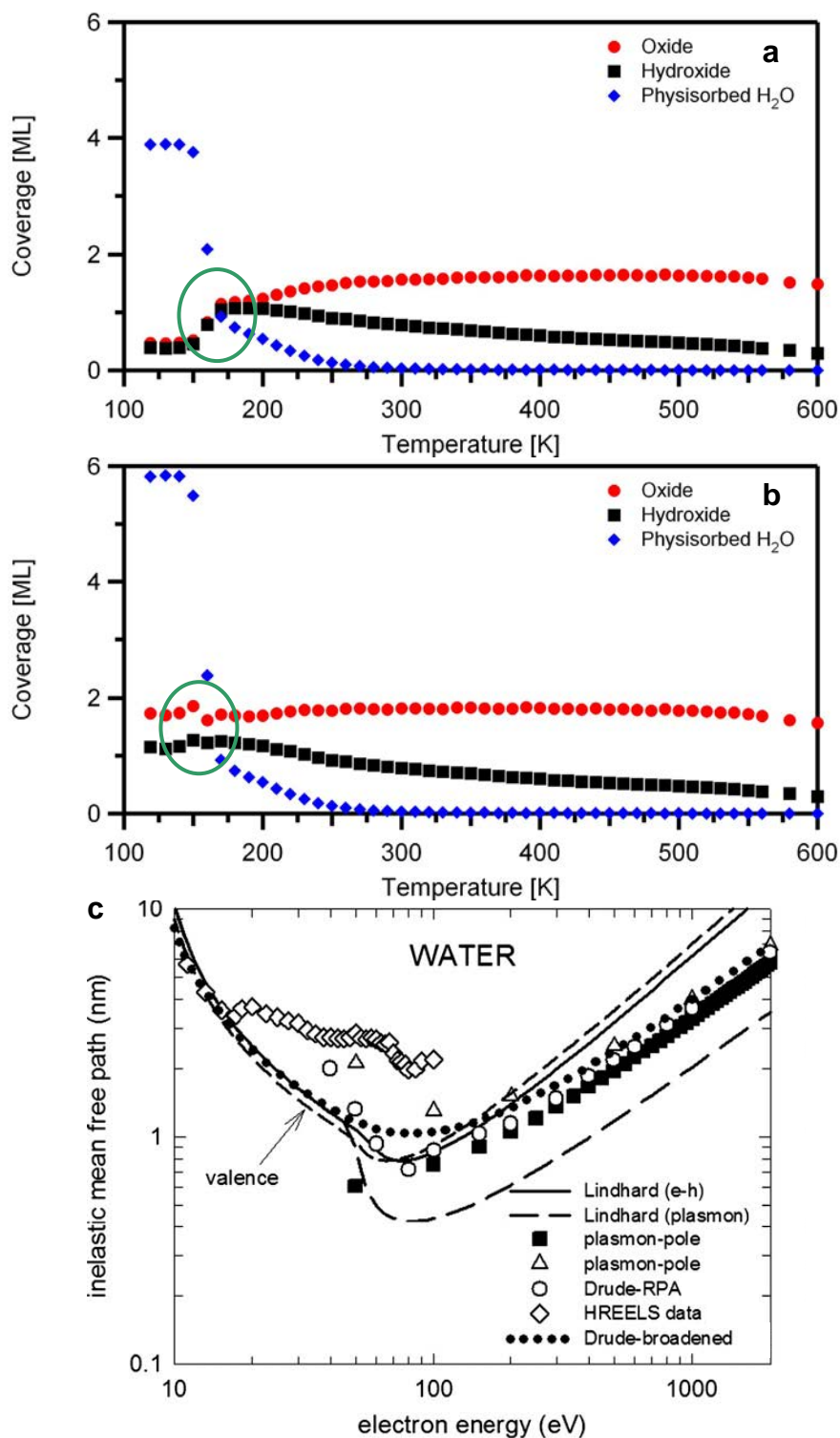


Figure 7.1: Quantitative analysis of TPXPS experiment of water on 2 ML NiO on Cu(111) (a) without correction for damping by the water and hydroxide adlayers (b) after correction for damping. Spectra acquired at an emission angle of 0°. (c) Inelastic mean free paths for water measured or calculated with various methods. Picture taken from [238].

The oxide and hydroxide coverages now are almost constant within the interesting temperature range, which is marked with a green circle. The deviations might originate from the very fast desorption of the water multilayers in this region, so that e.g. the time between the recording of the oxide and the water peaks leads to an incorrect ratio of the two peaks.

The same value for the damping factor is determined, if the damping of the copper or nickel signal is studied. The adsorption of H₂O on Cu(111) and Ni/Cu(111) is discussed in Chapter 7.2.2. For the adsorption of H₂O on NiO/Ni(111), which was studied under a different emission angle of 45°, the damping factor has to be adjusted. As a different emission angle increases the path the electrons have to travel through a water layer by a factor of $\cos 45^\circ = \frac{1}{\sqrt{2}}$, the damping by this layer increases by the same amount. As the damping factor is the remaining intensity after the photoelectrons travel through one layer, the intensity loss is $17\% * \frac{1}{\sqrt{2}} = 24\%$ at an emission angle of 45°, leading to a damping factor of 0.76 for experiments on NiO/Ni(111). These two damping factors were found to lead to reasonable results for almost all experiments, when used to calculate the real coverages from the apparent coverages determined from the fitting of the spectra. The quality of the correction was judged by the correction of sudden otherwise unexplained changes in the coverages, like the one discussed above.

Using Equation (3) from Chapter 2.3, we calculated the inelastic mean free path. We used the damping factor as the remaining intensity and 0.31 nm as the thickness of a water layer, as estimated by Ewing [239]. This gives us an IMFP of 1.67 nm at a kinetic energy of 120 eV. If we compare this value with results from literature compiled by Emfietzoglou et al. [238], displayed in Figure 7.1 (c), we see that this value is in between those determined by calculations from various groups [238, 240-243], and the IMFP determined from the HREELS data by Michaud et al. [244] at 100 eV. As all theoretical calculations were made for liquid water, which has a slightly higher density, the IMFP for ice (which we have in our experiments) should be a bit higher. In conclusion the IMFP of 1.67 nm and thus also our damping factor is reasonable.

7.2.2 Water interaction with copper and nickel surfaces

Just like in the case of the acetylene adsorption discussed in Chapter 6.1, the adsorption of water on the unoxidized metal surfaces was studied first as a reference for the other experiments.

Both water on Ni(111) and on Cu(111) have been quite extensively studied in the past. TPD experiments of water on Ni(111) [245-247] have revealed two desorption peaks. A peak at 168 to 171 K, dependent on the coverage, was shown to saturate at a coverage of 0.66 ML [247] and is attributed to water molecules directly chemisorbed to the nickel surface, while a second peak at 155 to 158 K could not be saturated. This second peak is attributed to desorption from ice multilayers. A close examination of this second peak also shows that it is composed of a component arising from a transition layer between the chemisorbed layer and the ice multilayers, and of the ice multilayer component. XPS spectra showed a peak around 533 eV [247].

On Cu(111) a binding energy of 533.5 eV has been reported for adsorbed water [248]. From this XPS study, a desorption between 140 and 160 K was reported. TPD experiments [249] showed desorption temperatures between 150 and 175 K, dependent on the initial coverage.

Water was dosed on the clean Cu(111) surface at 120 K. The corresponding O 1s spectra are displayed in Figure 7.2 (a). The spectra were acquired under an emission angle of 0° and after each spectrum the sample was shifted to a new spot to minimize beam damage. Right from the start of the exposure a peak at 533.3 eV is emerging, which shifts to 533.9 eV for higher coverages. The peak does not saturate and even continues to grow while the water pressure in the chamber is already being lowered. This behavior together with the binding energy, whose range includes the reported binding energy of 533.5 eV [248] for physisorbed water, allows to assign it to physisorbed water. A much smaller peak around 531.0 eV is assigned to hydroxide (OH), in agreement with Au et al. [248], who reported a peak of similar low intensity at 531.5 eV. As the total coverage of this peak does not exceed 0.04 ML, it can be assumed that the Cu(111) surface is rather inert towards hydroxylation, and the OH is only formed at steps or other defects. The final amount of water present on the surface was 4.5 ML. Please note that all coverages given in this chapter are referenced to CO (2x4) layers prepared on Ni(111) and 3 ML unoxidized nickel on Cu(111), for the experiments on the respective crystals. These layers are briefly discussed in Chapter 7.4.1. The coverages were also corrected for damping and self-damping effects of the water overlayers, as discussed in Chapter 4.2.1.

Similar uptake experiments were performed on Ni(111) and 2 ML unoxidized nickel on Cu(111), which were exposed to water at 125 K and 104 K, respectively. Representative spectra from these two systems are displayed in Figure 7.2 (b) together with a representative spectrum from the water uptake on the Cu(111) surface. Please note that the spectrum of water on Ni(111) has been acquired under an emission angle of 45°, unlike the other two,

which were acquired under 0°. On Ni(111) the water (ice) multilayers are found at 533.0 eV, in agreement with literature [247]. Upon increasing the coverage, there are only minor shifts in the binding energy of less than 100 meV. It is unclear why there are no large shifts in binding energy for higher coverages, even though such shifts are observed for almost all physisorbed species studied within this thesis. A possible explanation is that the observed coverage of 1.45 ML water is still too low for such shifts to occur.

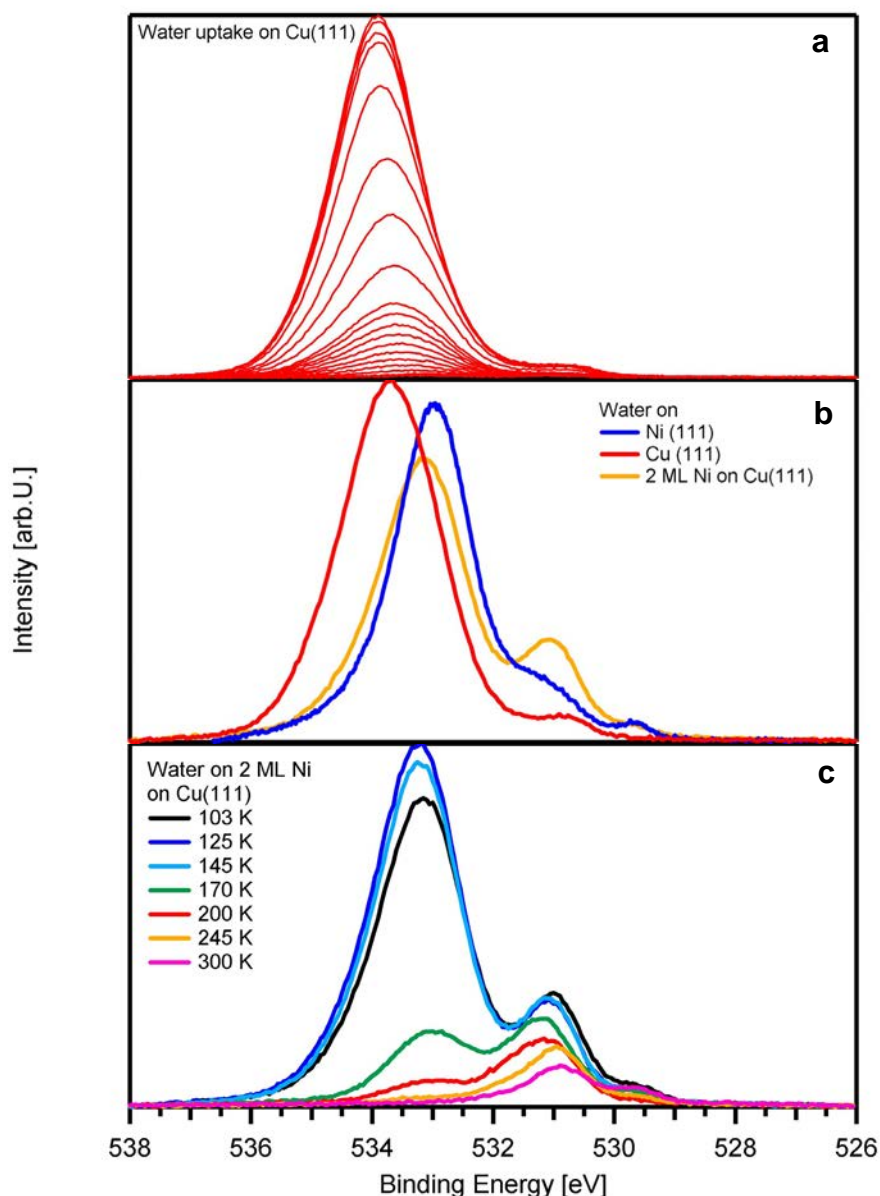


Figure 7.2: (a) O 1s spectra acquired during water adsorption on Cu (111) at 120 K (b) O 1s spectra of water on three different metallic surfaces. (c) Selected O 1s spectra acquired during TPXPS of water on 2 ML nickel on Cu(111)

On the nickel layers on Cu(111), the water peak emerges at 533.3 eV, and first shifts towards lower binding energies up to 533.0 eV before shifting back

again to 533.2 eV. The best explanation for this behavior is that the initial shift towards lower binding energies is attributed to the growth of the monolayer of water, while the later shift towards higher binding energies is attributed to the onset of the multilayer growth. A large difference between these two growth stages has been reported on several surfaces, for an overview see [222]. This interpretation is also in agreement with the observation that the backshift starts when a total surface coverage of 1 ML is reached. Even though some of this coverage is attributed to hydroxide (see below), it can still be argued that water on hydroxide is more similar to water on water than to water on Ni(111). Another possibility would be that the water molecules in the water layer forms hydrogen bonds with the OH.

In contrast to the water interaction with Cu(111), where only a very minor hydroxide component was detected, on the nickel surfaces hydroxide plays a larger role. On the Ni(111) surface it is found at 531.0 eV, and reaches a coverage of 0.07 ML. However, since the sample was not shifted to a new spot after each spectrum, and as there are no hints for H₂O dissociation in literature, the OH-peak is most likely due to beam damage. The peak at 529.6 eV with a maximum coverage of 0.02 ML is attributed to atomic oxygen. The formation of this atomic oxygen species is most likely also due to dissociation from beam damage, since no oxygen peak was reported in literature [247]. The situation is different for the nickel layers on Cu(111), as there the beam damage was minimized by shifting the sample after each spectrum. Here the hydroxide peak emerges at 531.3 eV and shifts towards 531.0 eV for higher coverages, a behavior that is also seen on the NiO layers. On this substrate, the highest hydroxide coverage reached is 0.18 ML. Oxygen, which is also present on this surface, reaches a coverage of 0.03 ML. As beam damage is excluded (the sample was shifted to a new spot after each spectrum), both oxygen and hydroxide have to emerge from dissociative adsorption of water. Since the water coverage of 1.35 ML here is similar to the 1.45 ML we observed on Ni(111), but the hydroxide coverage is higher, it can be concluded that the thin nickel layer on Cu(111) is more reactive in regards to this dissociative adsorption of water than the Ni(111) surface. The best explanation for this is a higher defect density in the thin nickel layers on Cu(111).

Upon heating the copper surface, water desorbed completely between 140 and 170 K, which is in agreement with literature [248, 249]. From the nickel layers on Cu(111), most of the water desorbed between 125 and 170 K. The initial increase in the water coverage between 103 and 125 K seen in the spectra displayed in Figure 7.2 (c), is due to ongoing water adsorption from the residual gas in the chamber. The water that remained on the surface at 170 K is desorbing much slower, but is gone from the surface at 245 K. Such

a behavior is not observed on the Ni(111) surface, where literature reports complete desorption below 200 K [245-247] (within this thesis the desorption of water from the Ni(111) surface has not been studied). So the question remains why water is more stable on the thin nickel layers on Cu(111). Pache et al [247] showed that on Ni(111) in the coadsorption case of water with oxygen a new desorption state labeled δ with a coverage up to 0.15 ML appears in the TPD spectra between 180 and 260 K. This state was assigned to chemisorbed water molecules stabilized on the surface by the oxygen atoms. As on the nickel layers on Cu(111), we only find minor traces of oxygen, it seems more likely that the water molecules here are stabilized by the OH layer. A similar high temperature tail for the water desorption is also visible for desorption of water from the NiO layers as discussed in the following chapters, where this tail is assigned to the monolayer desorption from the hydroxide covered NiO surface. Concurrently with the water desorption from the nickel layers on the Cu(111) surface, the hydroxide coverage is also decreasing. Due to the simultaneous occurrence of these two events, the decrease of the hydroxide coverage can be assigned to recombinative desorption of the hydroxide, i.e. hydroxide reacting with the hydrogen present on the surface from the dissociative adsorption to form water which is subsequently desorbing.

7.2.3 Water adsorption on NiO

As discussed in Chapter 7.1, hydroxide is the most common contamination on NiO(111), as it stabilizes the surface. Due to this, we investigated the adsorption process on differently prepared NiO layers. Figure 7.3 (a) shows the O 1s spectra acquired during the exposure of a NiO/Ni(111) layer to water vapor. As the NiO layer was grown at 550 K, and this temperature led to layers only weakly contaminated with OH as discussed in Chapter 4.1.3, it initially contained only 0.12 ML hydroxide. The spectra were acquired under an emission angle of 45°. Figure 7.3 (b) shows the detailed fit of the first spectrum of this adsorption series, Figure 7.3 (c) the detailed fit of the last spectrum, and Figure 7.3 (d) shows the quantitative analysis of this experiment. Please note that the coverages given in the quantitative analysis have been corrected for damping and selfdamping effects by the water and hydroxide layers, as discussed in Chapter 7.2.1.

Upon exposure of the surface to water, which was dosed using the multicapillary array doser, the hydroxide peak, which initially is found at 531.6 eV, starts to grow and shift towards lower binding energies; after an exposure of 0.65 L it is found at 531.0 eV.

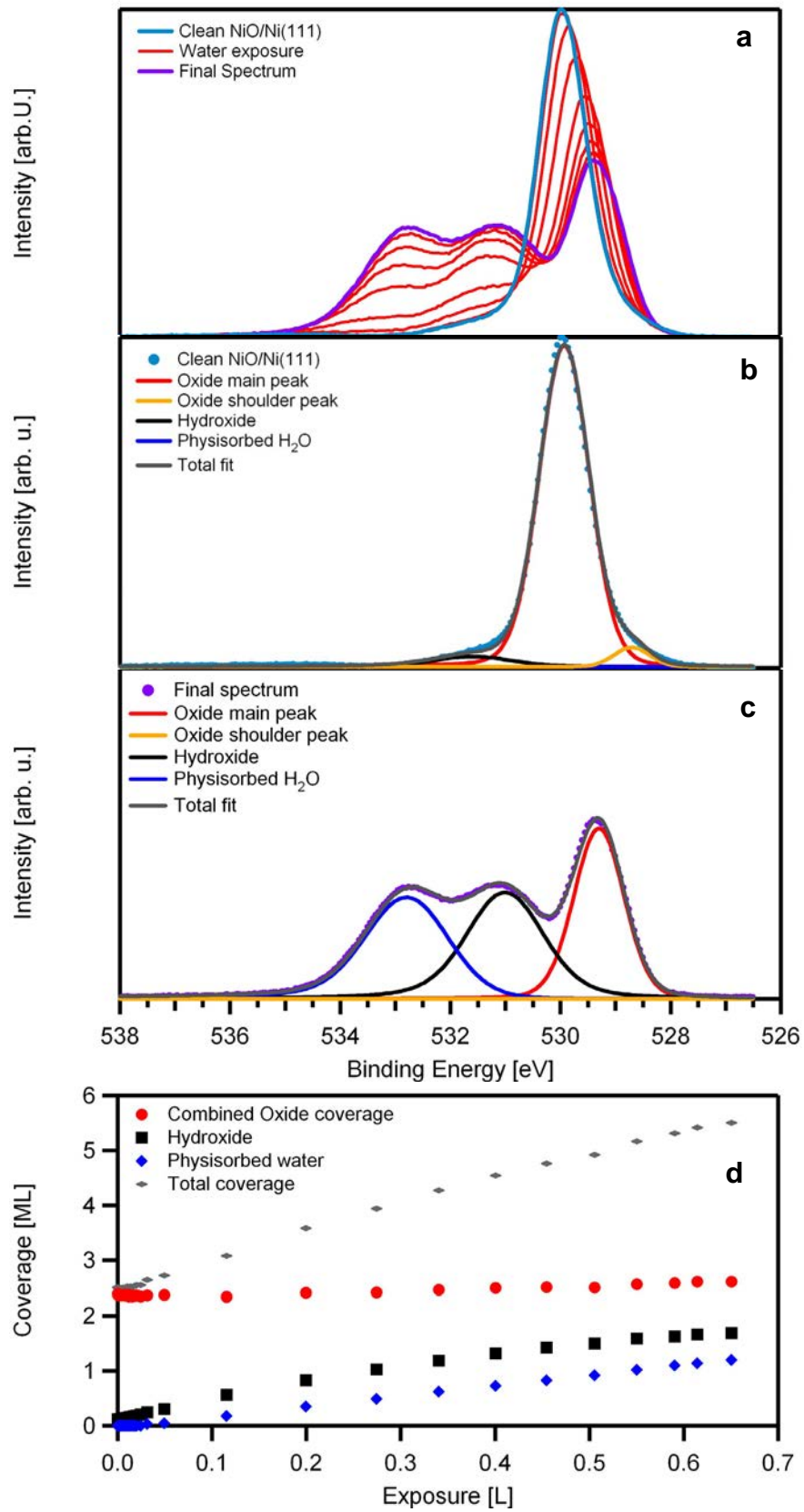


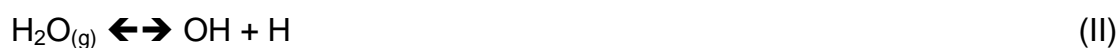
Figure 7.3 (on previous page): (a) Selected O 1s spectra acquired during the exposure of NiO/Ni(111) to water. All spectra acquired at an emission angle of 45°. (b) Detailed fit of the first spectrum (c) Detailed fit of the spectrum at 0.65 L. (d) Quantitative analysis of the uptake experiment; all coverages corrected for damping and selfdamping effects by water and hydroxide.

At an exposure of 0.03 L a new peak arises around 533.5 eV. This peak shifts towards lower binding energies with increasing coverage, and is located at 533.2 eV in the end of the experiment. This new peak is assigned to physisorbed water in agreement with literature [111, 223] and also in agreement with the results obtained on the unoxidized Ni(111) surface. The two oxide peaks here initially appear at binding energies of 529.9 eV and 528.7 eV for the main oxide and shoulder oxide species, respectively, as shown in Figure 7.3 (b). Upon water adsorption both species shift towards lower binding energies as well. The shoulder oxide peak continuously loses intensity and disappears completely before the end of the water uptake. The main oxide peak also loses intensity upon adsorption of the water, and shifts to 529.3 eV during the course of the experiment. The final situation without the oxide shoulder peak is shown in Figure 7.3 (c).

As discussed in Chapter 2.3, adsorption leads to damping of the surface core levels. In Chapter 7.2.1, the damping factor was determined to be 0.76. With the knowledge of this damping factor the real coverages are calculated from the coverages obtained from fitting the spectra. These corrected coverages are shown in Figure 7.3 (d). As the combined oxide coverage remains stable within the margin of error (although there is a conversion from the shoulder oxide species to the main oxide species), the observed decrease in intensity is attributed to the damping by hydroxide and water layers. With this knowledge we now discuss what the constant amount of oxide means in respect to the reaction of water with the surface. Normally, one would expect a behavior according to the following reaction scheme:



This scheme was found to hold true for many oxide surfaces, see [222] and [250] and references therein. Here a conversion of oxygen from the oxide to OH is proposed, which is also assumed for the reaction of our NiO layers. Since during the course of the reaction no change in the oxide coverage is observed, this leaves us with two possible interpretations: either the hydroxide formed from the oxide has a different binding energy than the hydroxide formed from water and thus is not distinguishable from the oxide, or that the oxide does not participate in the reaction and instead scheme (II) is valid.



However, to find out whether oxide oxygen atoms participate in the reaction we also have to consider the effect of the apparent oxide coverage discussed in Chapter 4.1.4. There it was shown that the intensity of the oxide peak is limited by selfdamping of NiO, as the IMFP is very short in the NiO layer, and thus it is not always clear if real quantitative information is obtainable from the oxide peak.

To avoid this problem, we studied the water adsorption on the thin NiO layers on Cu(111). In this case the whole NiO layer is sampled, thus allowing a quantitative analysis. Figure 7.4 (a) shows the O 1s spectra acquired during the exposure of 2 ML NiO/Cu(111) to water as a color coded density plot. Please note that these spectra were acquired under an emission angle of 0° . At the beginning of the uptake the spectra are dominated by the main oxide peak at 529.8 eV. Just like in the water uptake on NiO/Ni(111), during the exposure to the water this peak loses intensity and shifts towards lower binding energies, which leads to a binding energy of 529.6 eV at the end of the uptake experiment. The shoulder peak of the oxide has not been found here, as a fit of the data including it showed no improvement of the fit quality. The quantitative analysis in Figure 7.4 (c) shows that the hydroxide peak, which has an initial binding energy of 531.7 eV, as displayed in Figure 7.4 (a), starts growing immediately. This peak shifts to lower binding energies as well, and is located at 531.4 eV in the end. After an initial gain in intensity it loses intensity again for exposures above 0.32 L. The peak assigned to physisorbed water, which appears at 533.3 eV, starts growing at slightly higher exposures than the hydroxide peak. Unlike the other two peaks this peak shifts towards higher binding energies with increasing exposures, leading to a binding energy of 533.7 eV at the end of the experiment. Such a shift towards higher binding energies for higher coverages was also found for other physisorbed adsorbates on the different NiO layers, as discussed in Chapter 6, and was also seen for physisorbed water on the unoxidized metal surfaces discussed in Chapter 7.2.1. It is attributed to a slow conversion from the binding energy of the (monolayer) adsorbate to the binding energy the species would have in a crystal composed entirely of the adsorbate. For water, this binding energy would be 533.8 eV [251]. The shift towards lower binding energies for the oxide and hydroxide peaks is reversible if the hydroxide content is lowered again, as will be discussed in the following Chapter, and the shift in binding energy will be explained there.

Figure 7.4 (b) shows the detailed fit of the spectrum acquired after an exposure of 0.32 L. This spectrum was chosen, as here all three peaks have a similar height, whereas for higher exposures the spectra are dominated by the multilayer peak. The fit is similar to the one shown in Figure 7.3 (b), showing that both surfaces behave similarly when exposed to water.

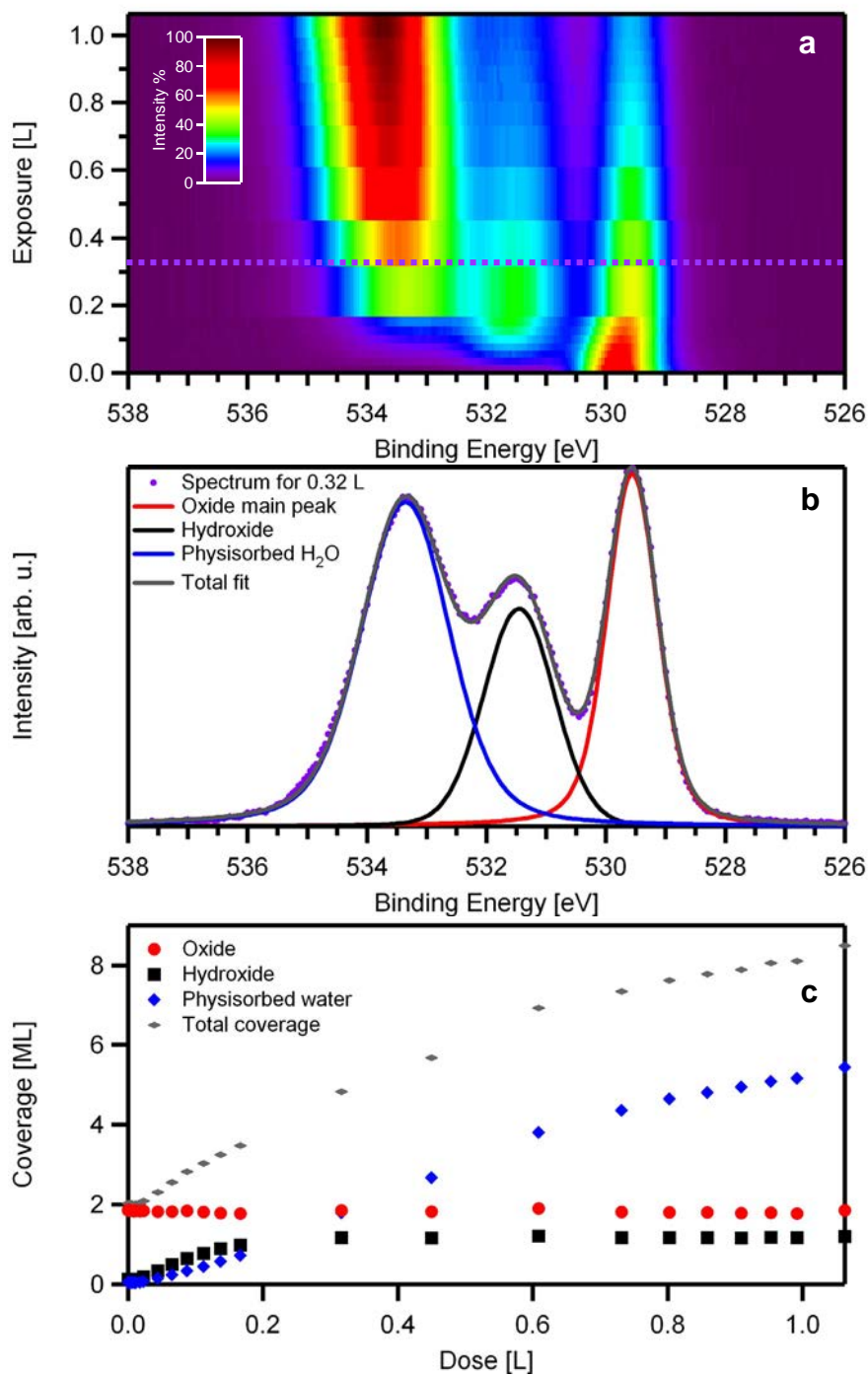


Figure 7.4: (a) Density plot of O 1s spectra acquired during exposure of 2 ML NiO/Cu(111) to water. All spectra acquired under an emission angle of 0° (b) Detailed fit of spectrum acquired after an exposure of 0.32 L (c) Quantitative analysis of uptake experiment. All coverages are corrected for damping and selfdamping effects by water and hydroxide.

Figure 7.4 (c) shows the quantitative analysis of the uptake experiments. As described in Chapter 7.2.1, all coverages are corrected for damping and selfdamping effects by the hydroxide and water adsorbate layers, using the damping factor of 0.83 for the emission angle of 0° (see Chapter 7.2.1). Please note that the enhancement factor for the multicapillary array doser is

not known and is disregarded when calculating the exposures. As can be expected for a physisorbed species, the water coverage is continuously rising without saturating and reaches a coverage of 5.44 ML at the end of the exposure. The hydroxide coverage on the other hand saturates at 1.17 ML after an exposure of 0.17 L, and stays constant afterwards. This means that the intensity decrease of the hydroxide, which is visible in Figure 7.4 (a), is attributed to the damping by the physisorbed water (ice) layers, and the hydroxide species is not involved in any further reaction. The most remarkable result here is, that just like for the water adsorption on NiO/Ni(111), the oxide coverage remains constant over the whole experiment. As now the whole oxide layer is sampled by our photoelectrons, excluding any apparent coverage effects, this means that the oxide atoms either don't participate in the hydroxide formation, or that their binding energy does not change upon hydroxylation.

The NiO clusters on Cu(111) react very similar to water as the other two discussed NiO surfaces. The density plot of the water uptake on the NiO clusters is shown in Figure 7.5 (a), and the detailed fit of the spectrum taken after an exposure of 0.12 L is shown in Figure 7.5 (b). The oxide peak remains almost stable at 529.8 eV over the course of the uptake, shifting only by 40 meV towards lower binding energies, while the hydroxide peak shifts from 531.3 eV to 531.1 eV. The water peak appears at 533.0 eV and shifts constantly towards higher binding energies, reaching 533.4 eV at the end of the experiment at an exposure of 0.81 L. The quantitative analysis, corrected for damping and selfdamping by the water and hydroxide, is shown in Figure 7.5 (c). The oxide coverage, which is 0.65 ML at first, rises up to an exposure of 0.2 L, where it reaches a value of 1 ML, before falling down to the initial value at 0.3 L and staying constant afterwards. This behavior is highly unusual, as in the two experiments discussed previously the oxide coverage remained constant throughout the experiment. If we assume that some of the oxide reacts with the water to form hydroxide, the oxide coverage should fall and not increase. As the sample position was changed after each spectrum in order to avoid beam damage, we scanned over a small area with a larger NiO coverage, before going back to the rest of the surface where the coverage was uniform. As the oxide was also saturated with oxygen prior to the uptake experiment, this leaves only one explanation for this behavior, namely a local variation of the nickel coverage and subsequently of the oxide coverage. One possibility for this local variation could be a local 3-dimensional growth of the NiO. Even though this behavior makes it difficult to discuss the oxide coverage in regards to the reaction responsible for the hydroxide formation, the fact that the oxide coverage is the same at the start and the end of the

experiment strongly hints at the same formation mechanism also found on the other two surfaces.

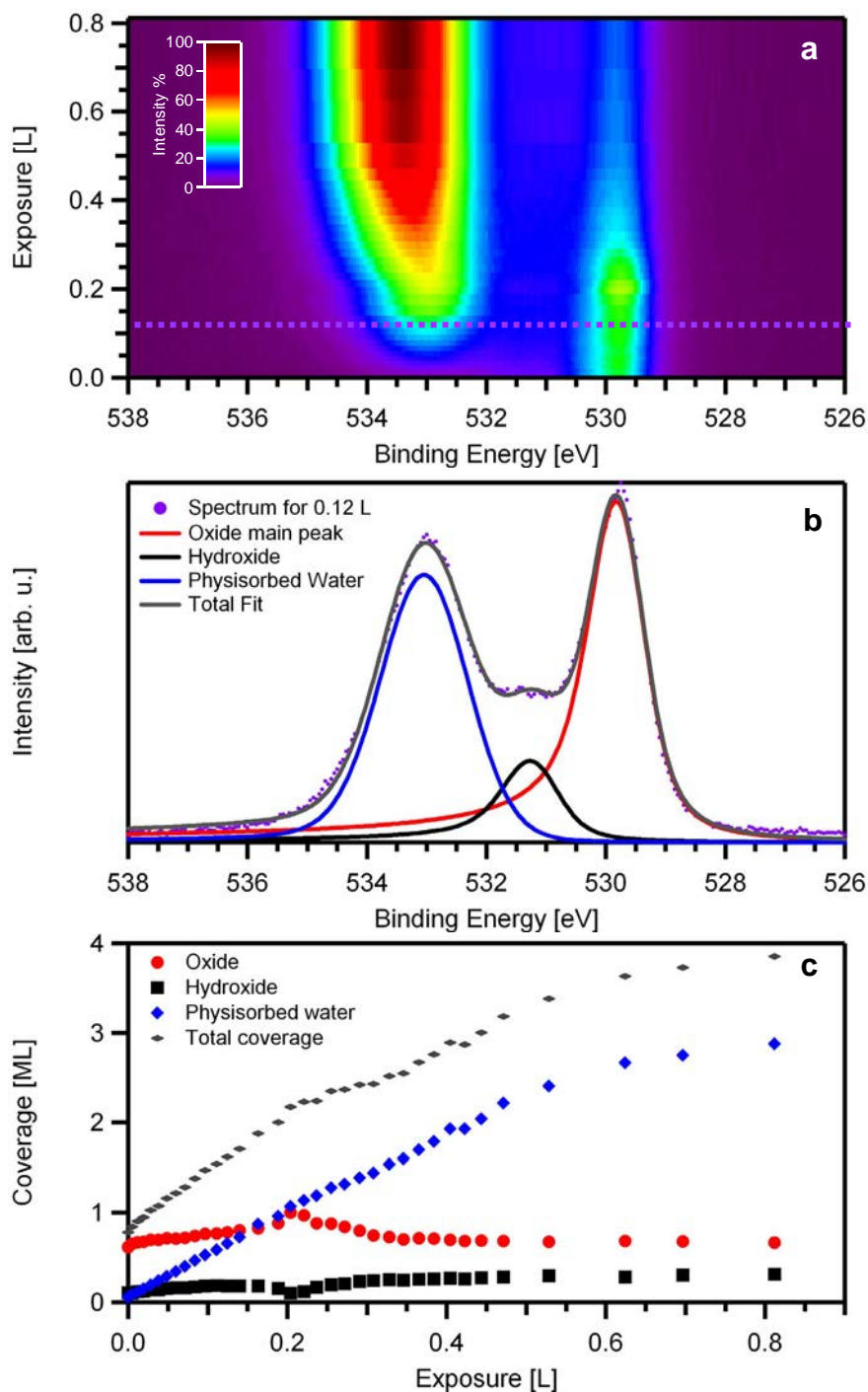


Figure 7.5: (a) Density plot of O 1s spectra acquired during exposure of 0.5 ML NiO/Cu(111) to water. All spectra acquired under an emission angle of 0° (b) Detailed fit of spectrum acquired after an exposure of 0.12 L (c) Quantitative analysis of uptake experiment. All coverages corrected are for damping and selfdamping effects by water and hydroxide.

The hydroxide coverage here rises slower compared to the water uptake on 2 ML NiO/Cu(111), and saturates at 0.30 ML. Just like on the 2 ML

NiO/Cu(111), this is approximately half of the coverage of the oxide. Interestingly at the spot on the sample surface, where the oxide coverage is the highest, which is reached at an exposure of 0.2 L, the hydroxide coverage is lower than in the vicinity. This is attributed to a higher resistance of this local oxide structure to hydroxylation, most likely due to the layer being more closed. The water multilayers behave like in the other two experiments, with a continuous increase that continued as long as there was water in the chamber.

7.2.4 Thermal evolution of hydroxide layers

The thermal evolution of the water and hydroxide adlayers on NiO/Ni(111) was studied by heating to the designated temperatures and subsequently recording a spectrum without heating. The resulting O 1s spectra are shown in Figure 7.6 (a) in the form of a color coded density plot.

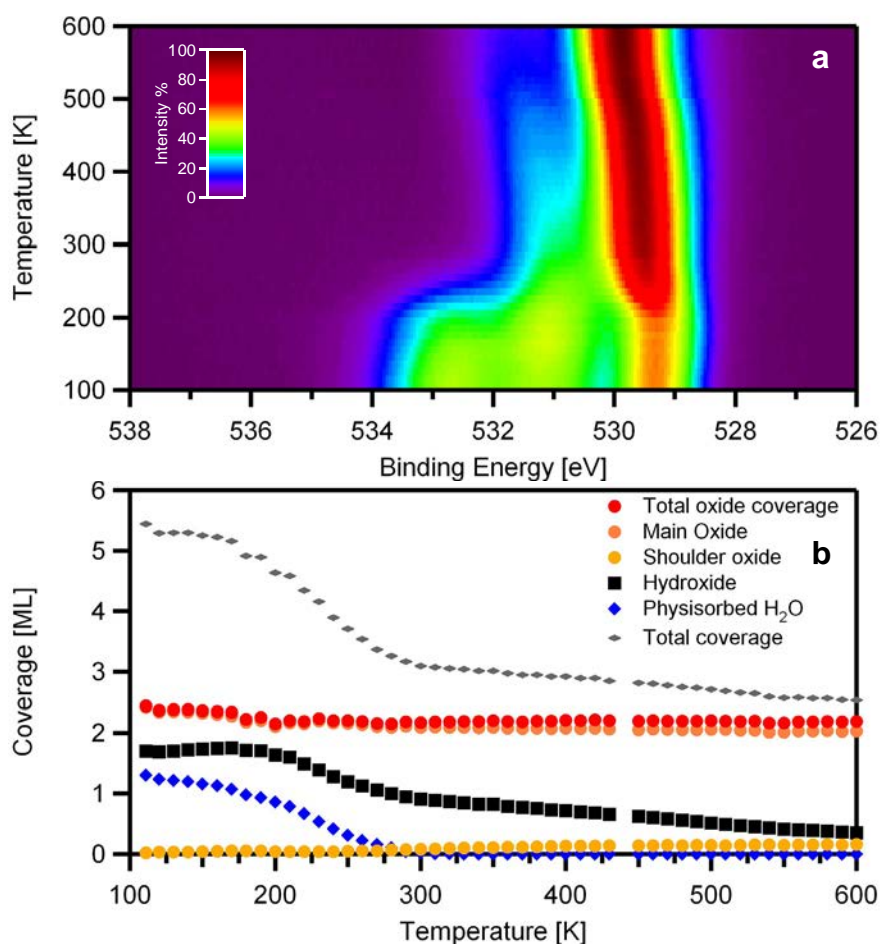


Figure 7.6: (a) Density plot of thermal evolution of water on NiO/Ni(111). All spectra recorded at an emission angle of 45°. (b) Quantitative analysis of data from (a), corrected for damping and self-damping effects by water and hydroxide.

The physisorbed water with its peak at 532.7 eV starts to desorb from low temperatures on. As the initial coverage is only slightly more than a monolayer, a clear distinction between desorption of the multilayers and that of the monolayer is not possible. At 300 K, all of the physisorbed water has left the surface, in agreement with TPD results by Reisner et al. [224]. This desorption temperature is higher than the corresponding value of 200 K [245-247] for Ni(111) as well as the value of 245 K for nickel layers on Cu(111). This again shows that the oxide stabilizes physisorbed species as discussed in Chapter 6.2.

The main oxide peak, which is initially located at 529.3 eV, increases in intensity above 200 K, and starts to shift towards higher binding energies. At 600 K it is found at 529.9 eV, which is the same position it was at prior to the water adsorption. Regarding the quantitative analysis in Figure 7.6 (b), which is corrected for damping effects, we see that the intensity increase of the main oxide peak is only apparent, as the damping is lifted when the physisorbed water is desorbing. Just like during the water adsorption experiment on this surface, the total oxide coverage remains almost constant over the whole course of the experiment. The only temperature range where the oxide coverage is not constant is below 200 K, where the total oxide coverage is falling slightly from 2.40 to 2.20 ML, i.e. less than 10%. A matching increase of the oxide coverage is seen at the end of the uptake experiment (see Figure 7.3 (c)). Such an increase in the oxide coverage should not happen, since this coverage is only an apparent coverage since the peak intensity is limited by the IMFP for the photoelectrons of lower oxide layers, as discussed in Chapter 4.1.4. An explanation for this behavior is the high coverage of physisorbed water in the same temperature/exposure ranges where the unrealistic high oxide coverages appear. This similarity shows that the changes in the oxide coverages are best explained by a slightly wrong damping factor. As a lot of factors contribute to slight miscalculation of this damping factor, like e.g. fitting procedure errors or errors in setting the emission angle, this deviation from constant oxide coverage is within the experimental error bar.

Between 200 and 300 K the shoulder oxide species at 528.3 eV starts to regain intensity. Just like the main oxide peak it shifts towards higher binding energies at higher temperatures, which leads to a binding energy of 528.8 eV at 600 K. At this temperature its coverage is 0.16 ML, which is 7% of the total oxide coverage, around the same value it was prior to the water adsorption. Due to this relatively low coverage it is challenging to determine the temperature when this species reemerges, but it is remarkable that the disappearance of this species during the water uptake is a fully reversible

process. This behavior coincides nicely with the assumption that the shoulder oxide species is a surface located oxide species.

The hydroxide is initially found at 531.0 eV, and its coverage of 1.75 ML remains constant up to 190 K. Around 0.14 ML of these 1.75 ML have to be attributed to carbonate, since the C 1s region revealed a carbonate coverage of 0.07 ML, which translates to double this amount in the O 1s region as discussed in Chapter 7.3. As carbonate behaves very similar to the hydroxide layers, and no displacement effects were found in coadsorption experiments as discussed in Chapter 7.5, this minor contamination (less than 8%) should have no major influence on the behavior of the hydroxide. Starting at 200 K, the coverage of the hydroxide quickly decreases, reaching 1 ML at 280 K and 0.92 ML at 300 K, from whereon the coverage decrease proceeds significantly slower. The coverage decrease between 300 and 600 K is almost linear, leading to a value of 0.36 ML at 600 K. This remaining coverage is in contrast to literature, which reports a complete removal of the hydroxide at 600 K [88]. If the surface is heated above 600 K (data not shown), the oxide layer starts to destabilize but even at temperatures as high as 730 K still some hydroxide is found on the surface. Over the course of this coverage decrease the binding energy of the hydroxide peak also shifts towards higher binding energies reaching a value of 531.4 eV at a temperature of 600 K.

The continuous decrease in hydroxide coverage was also observed when NiO/Ni(111) grown at 300 K was heated to elevated temperatures, as discussed in Chapter 4.1.2. Considering that the oxide coverage remains constant throughout this coverage decrease, when the damping by the hydroxide layer is accounted for, a decay of the hydroxide to oxide can be ruled out. Instead the hydroxide has to desorb recombinatively, as a diffusion of the hydroxide into the bulk would also increase the oxide coverage. The continuous decrease of the hydroxide coverage over the very long temperature range is highly unusual. If we consider the other adsorbates and reaction products discussed so far in this thesis, their desorption or reaction only spans a temperature range of no more than 200 K, with the exception of chemisorbed C₂H₂ on NiO which reacts over a temperature range of 300 K which is still smaller than the temperature range larger than 400 K we observe for the decay of the hydroxide layer.

As Ebensperger and Mayer showed [82], this behavior can be explained by changes in the structure of the surface. In Chapter 4.1., we discussed that NiO(111) is a polar surface and thus unstable. The charge of the polar surface is compensated by the adsorption of water and subsequent hydroxide formation. If the surface is hydroxide-free, it reconstructs to an octopolar structure displayed in Figure 4.1. (a). Ebensperger and Mayer [82] showed

that by an increase in temperature the hydroxylated surface is converted into the octopolar surface. However, they also showed that there is no simple transformation path between the two structures. In the first step of hydroxide removal from the surface, they claim the formation of a (2x1) missing row structure, where the hydroxide is removed from every second row of oxygen atoms. In the next step the octopolar reconstruction is formed by either removal of a NiO unit per unit cell from the surface or by adding one. Thus the transformation between the two surfaces involves activated transport processes for NiO on the surface, as well as the recombinative desorption of water. Since in between these structures a number of different transitory surface structures are energetically possible (for details see [82]), they claim that often not the thermodynamic most stable structure is present on the surface but rather one of the intermediates due to kinetic limitations, which leads to a stabilization of the partially hydroxylated intermediates. This model is in good agreement with our observed decay of the hydroxide over a large temperature range. These major reconstructions on the surface also explain the reversible shifts in the binding energies of the oxide and hydroxide, as the lowest values of the binding energies are attributed to the fully hydroxylated surface and the highest values to the fully octopolar reconstructed surface, with a continuity of transitory configurations in between. As the surface still contained a lot of hydroxide at 600 K, the binding energy of 531.4 eV is still lower than the initial position of 531.6 eV observed during the uptake. This also explains why after the oxidation of Ni(111) at 300 K (Chapter 4.1) the highly hydroxylated surface showed the oxide peak at a lower binding energy than after the oxidation at 500 K, which leads to an almost hydroxide free surface.

In a different adsorption experiment (data not shown), water was dosed onto NiO/Ni(111) at a surface temperature of 300 K. At this temperature no water physisorbed on the surface. The hydroxide layer grows similar to the adsorption at lower temperatures; however it saturates much earlier at a coverage of 0.65 ML after an exposure of 0.3 L. This value is lower than the value of 0.92 ML found for the low temperature uptake after heating to 300 K. The best explanation for this behavior is that for an uptake at a constant temperature of 300 K the surface has enough energy to reach a more hydroxyl free transitory state between the completely hydroxylated and the completely octopolar reconstructed surface. The oxide coverage remains constant throughout the water uptake, like during all other experiments. A slight conversion from the shoulder oxide species to the main oxide is found, but the shoulder oxide species does not completely disappear, which is in accordance with the hydroxide coverage of less than 1 ML. Upon heating,

the hydroxide coverage shows a linear decay leading to a value of 0.26 ML at 600 K.

Studying the thermal evolution of water on 2 ML NiO/Cu(111) provided very similar results. The spectra of this experiment, which were recorded at an emission angle of 0° after heating with the resistive heating to the designated temperatures, are displayed in Figure 7.7 (a) as a color coded density plot, and the quantitative analysis is shown in Figure 7.7 (b). The only remarkable difference to the situation on NiO/Ni(111) is that in this experiment we have much higher coverages of physisorbed water up to 6 ML, and due to this we can discern clearly between the desorption of the multilayers and the monolayer of physisorbed water. The coverage of physisorbed water remains constant until 140 K and then rapidly drops down to 0.92 ML at 170 K. Afterwards the coverage decreases slower until the species is completely gone around 300 K.

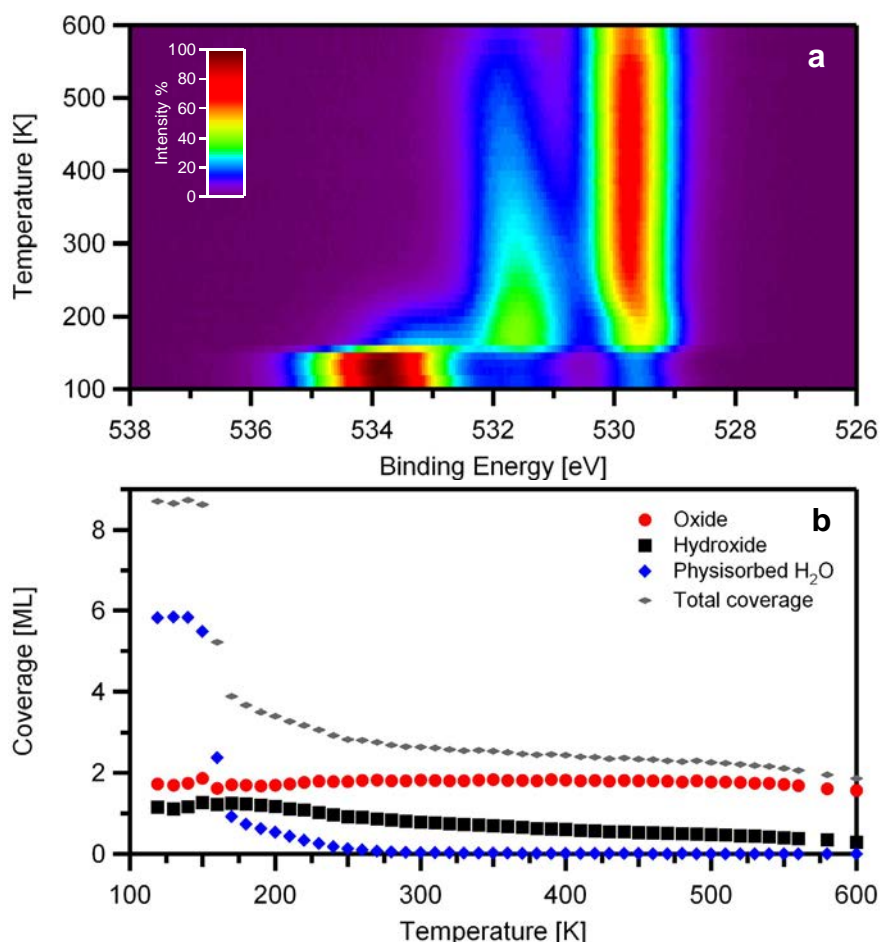


Figure 7.7: (a) Density plot of thermal evolution of water on 2 ML NiO/Cu(111). All spectra recorded at an emission angle of 0° . (b) Quantitative analysis of data from (a), corrected for damping and self-damping effects by water and hydroxide

Both the temperature range of 140-170 K for the multilayer desorption as well as 170-300 K for the monolayer desorption agree with the reported TPD peaks for water desorption from NiO(100) at 150 and 200 K [224], respectively, especially if we take into account that the monolayer TPD peak showed a tail up to 300 K just like we see it in our experiment. The peak of the physisorbed water is found at 533.8 eV at first, which is the binding energy of water in an ice crystal [251]. The slight shift in binding energy and higher coverage in comparison to the end of the uptake experiment can be explained by additional adsorption of water from the residual gas in the chamber in between the two experiments. After desorption of the multilayer, the peak for the water monolayer is found at 533.3 eV where it was also found initially during the uptake.

The total oxide coverage remains constant within $\pm 7\%$ over the course of the experiment. The main oxide peak is initially found at 529.6 eV shifting to 529.7 eV during the course of the experiment. The apparent intensity increase for this species around 150 K seen in Figure 7.7 (a) is due to the lifting of the damping by the desorbing water multilayers. Above 500 K the oxide coverage is decreasing due to the beginning destabilization of the NiO layers on the copper crystal, as discussed in Chapter 4.2.

The hydroxide evolution is almost the same as for the NiO/Ni(111). The slight initial rise from 1.15 ML prior to water multilayer desorption to 1.23 afterwards is attributed to a combination of errors in the damping correction and the fitting of the highly damped spectra for high water coverages. Starting at 170 K, the hydroxide coverage is decreasing quickly down to 0.79 ML at 300 K, from when on the coverage decreases slower but still steadily and reaches a coverage of 0.48 ML at 500 K. In this second temperature range the decrease is linear, a behavior that we already observed for hydroxide on NiO/Ni(111) in the same temperature region. However it proceeds slower here with a coverage loss of 0.155 ML / 100 K, compared to 0.19 ML / 100 K on NiO/Ni(111). The peak position changes from 531.5 eV at low temperatures to 531.8 eV at 500 K, showing the typical shift to higher binding energies when the hydroxide coverage decreases. Since the evolution of the hydroxide coverage is so similar to the situation on NiO/Ni(111) in all aspects, we attribute the slow decrease here also to the slow conversion of the hydroxylated surface to the octopolar reconstructed surface. The slow decrease in coverage is thus due to the kinetic limitations as NiO needs to be transported on the surface [82].

In Figure 7.8 (a) the O 1s spectra of the thermal evolution of water on 0.5 ML NiO/Cu(111) are displayed as a color coded density plot. These spectra were recorded at an emission angle of 0° after heating the surface with the resistive

heating to the designated temperatures. If we compare this density plot and the corresponding quantitative analysis displayed in Figure 7.8 (b) with the results from the other two surfaces, the similarities are evident. The coverage of the physisorbed water remains constant up to 140 K and then falls rapidly from 3.1 ML to 0.3 ML at 170 K. Just like on 2 ML NiO/Cu(111), the decrease then slows down but in contrast here all water is already gone at 250 K, 50 K earlier than on that surface.

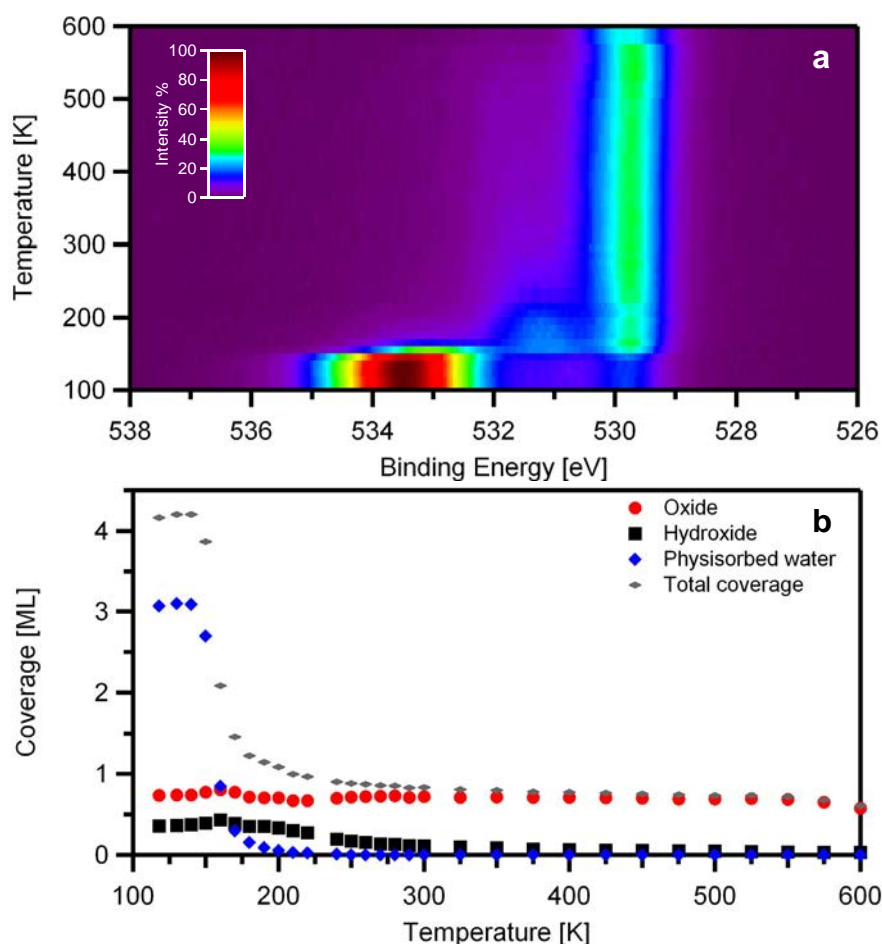


Figure 7.8: (a) Density plot of thermal evolution of water on 0.5 ML NiO/Cu(111). All spectra recorded at an emission angle of 0° . (b) Quantitative analysis of data from (a), corrected for damping and self-damping effects by water and hydroxide

As at 170 K only 0.3 ML water is left on the surface here no clear distinction between multi- and monolayer desorption exists. However, 0.3 ML could as well be the monolayer coverage for water on the NiO clusters, if we consider that in the acetylene adsorption experiment on the NiO clusters, which was discussed in Chapter 6.1.4, the acetylene coverages on the NiO clusters were found to be lower than what was expected if the surface coverage by the NiO was taken as basis of estimation. The temperature region for the multilayer desorption is the same as on the thicker NiO layers on Cu(111), but the threshold for complete desorption of the physisorbed water is lower here,

which is attributed to the influence of the copper substrate, since here we have still bare patches of Cu(111). On Cu(111) the water desorbed up to 170 K, and thus the copper patches can influence the stability of the physisorbed water on the NiO clusters. The binding energy of the physisorbed water peak is 533.5 eV for the multilayers, and 533.0 eV for the water monolayers.

The oxide peak is found at 529.7 eV during the whole experiment, and the oxide coverage remains almost constant around 0.73 ML throughout the experiment. The intensity increase for the oxide species in Figure 7.8 (a) is only an apparent one, due to the lifted damping by the physisorbed water. The decrease of the oxide coverage above 500 K is due to the destabilization of the oxide in this temperature region. The slight increase during the desorption of the physisorbed water is attributed to errors in the damping correction and in the fitting of the transitory spectra. This also leads to the slight increase of the hydroxide coverage during the desorption of the physisorbed water, which is reversed when the desorption is finished. Starting at 190 K the coverage of 0.35 ML quickly decreases down to 0.13 ML at 270 K, where the slower decrease already seen on the other two surfaces sets in, leading to a coverage of 0.04 ML at 500 K. Again the decay in this temperature region is almost linear, although much slower than on the other surfaces with 0.04 ML / 100 K due to the much lower hydroxide coverages. During this decay the peak position changes from 531.2 to 531.8 eV.

7.3 CO₂ interaction with NiO layers

7.3.1 CO₂ interaction with pure metal surfaces

For CO₂ interaction with Cu(111), literature reports no adsorption at room temperature [118] and very slow dissociative adsorption at 490 K, leading to 0.1 ML oxygen after a dose of $6 \cdot 10^8$ L of CO₂ [252]. A Cu(111) crystal with a high defect density was found to show a desorption peak for CO₂ in TPD experiments around 200 K [253]. The interaction of CO₂ with Ni(111) is likewise found to be very weak. Gordon and Lambert [236] reported that an exposure of 100 L at 300 K did not lead to adsorption. Wang et al. [254] calculated endothermic chemisorption energies for CO₂ on Ni(111), i.e. the chemisorption of CO₂ on Ni(111) is thermodynamically not favored.

We exposed a Cu(111) surface to CO₂ via the molecular beam with 20 sccm at a surface temperature of 115 K (data not shown). Even after an exposure of 100 L no changes were visible in the C 1s region, and in the O 1s only small changes in intensity were found for two very small peaks at 531.1 and

533.1 eV. These two peaks were present at the surface before the uptake and are attributed to small contaminations by OH and H₂O, respectively, in accordance with Chapter 7.2.2. The small variations in intensity for these two peaks are attributed to the presence of water in the residual gas in the chamber, leading to a continued growth of these peaks. No peaks associated with CO₂ were found in the O 1s region. Thus, the TPD peak for CO₂ at 200 K, which has been reported in literature [253], is attributed to adsorption of CO₂ on defects.

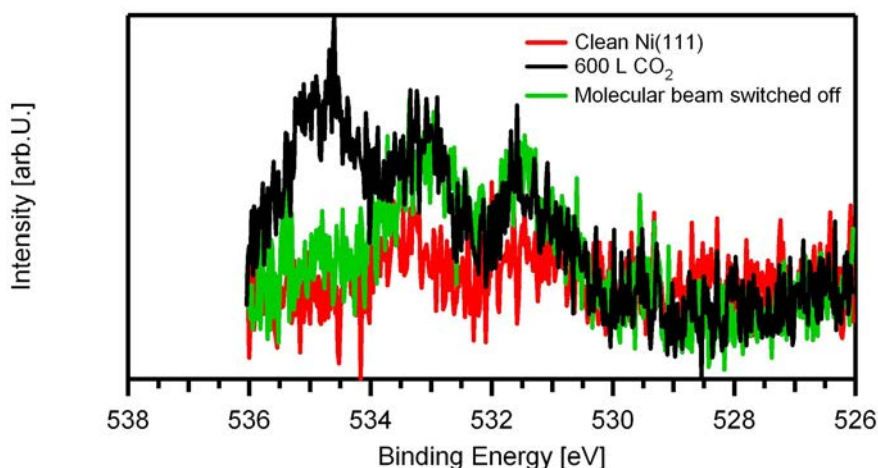


Figure 7.9: CO₂ on Ni(111) at a temperature of 102 K

CO₂ was dosed on a Ni(111) surface at a temperature of 102 K, using the molecular beam with a CO₂ flux of 10 sccm. The resulting O 1s spectra are displayed in Figure 7.9. The peak at 531.4 eV is attributed to hydroxide, and the peak at 533.1 eV to physisorbed water, in agreement with the results in Chapter 7.2.2. Just like on the Cu(111) surface both of these peaks were already present on the surface prior to the uptake experiments. The peak at 534.8 eV, however, appears only after the surface was exposed to CO₂. It disappears again when the molecular beam is turned off, and thus is attributed to physisorbed CO₂. A peak with matching behavior is found at a binding energy of 291.2 eV in the C 1s region (data not shown). The O 1s peak has a maximum coverage of 0.02 ML CO₂ molecules. A dissociative adsorption of CO₂ is ruled out under the described reaction conditions, as no peak at 529.6 eV is found. This binding energy is characteristic for atomic oxygen on Ni(111), see Chapter 4.1.1.

7.3.2 CO₂ Adsorption on NiO

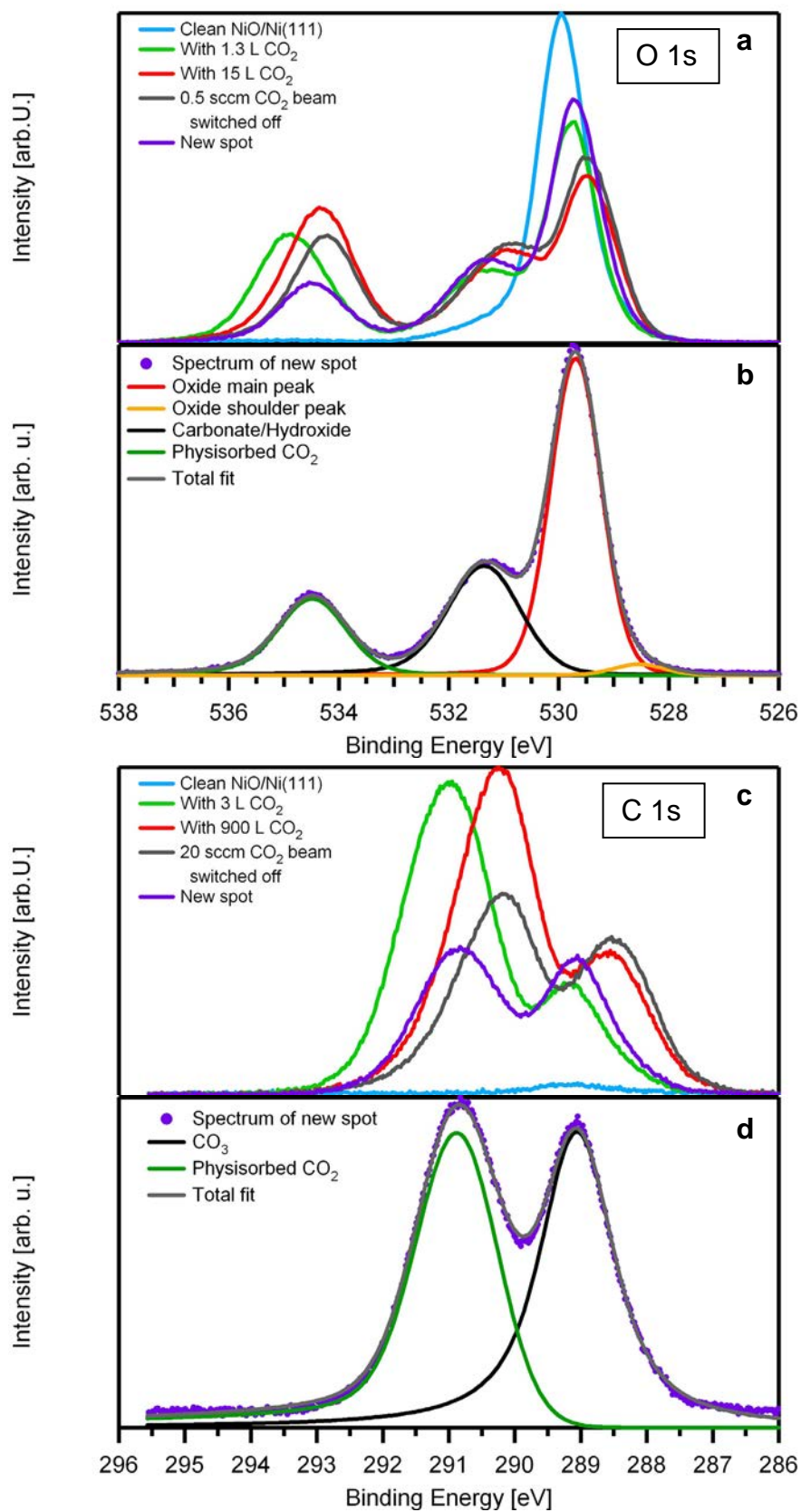


Figure 7.10 (on previous page): (a) Selected O 1s spectra of an exposure of NiO/Ni(111) to CO₂ at a surface temperature of 107 K. (b) Detailed fit of the O 1s spectrum acquired on the new spot after the CO₂ exposure. (c) Selected C 1s spectra of an exposure of NiO/Ni(111) to CO₂ at a surface temperature of 103 K. (d) Detailed fit of the C 1s spectrum acquired on the new spot after the CO₂ exposure. All spectra acquired under an emission angle of 45°.

In order to probe the capability of the NiO/Ni(111) layers to form NiCO₃, the layers were exposed to CO₂ at temperatures below 110 K. Figure 7.10 (a) shows selected O 1s spectra acquired during such an uptake experiment and Figure 7.10 (c) selected C 1s spectra of a separate uptake experiment. Please note that for these C 1s spectra a Shirley background was subtracted, unlike for the spectra of adsorbed hydrocarbons discussed in the previous chapters. All spectra were acquired under an emission angle of 45°. The NiO/Ni(111) layer used in the O 1s uptake was grown at 550 K, and the one used in the C 1s uptake was grown at 500 K, which leads to a slightly higher hydroxide contamination as discussed in Chapter 4. The CO₂ was dosed onto the surface using the supersonic molecular beam, but without Helium seeding or nozzle heating. The flux used was 0.5 sccm and 20 sccm for the experiments followed in the O 1s and C 1s region, respectively. Due to the direct exposure during the adsorption it was very rapid. Upon exposure to CO₂ four new peaks are observed, two each in the O 1s and the C 1s region. In the O 1s region these peaks are initially found at 531.3 and 534.8 eV, shifting gradually towards lower binding energies as the experiment proceeds, which is also the case for the two oxide peaks. In the C 1s region the new peaks emerge at 289.1 and 291.0 eV and also shift towards lower binding energies as the experiment continues. New spots were studied after the experiments were finished. The corresponding spectra (purple spectra in Figure 7.10 (a) and (c)) show that the observed binding energy shift is due to beam damage, as the shift completely reversed on the new spots returning all peaks to their initial positions. Even though the binding energy shifts gradually during the adsorption (gradual shift not shown), and the experiments are done on NiO which is generally characterized as an insulator, the direction of the shift speaks against an expected charging of the layer. An increasing positive surface charge should lead to a shift in the direction of higher binding energies, not towards lower binding energies like visible here, see difference between light green spectra (low exposure times) and red spectra (high exposure times) in Figures 7.10 (a) and (c).

The binding energies of the peaks at 289.1 eV and 531.3 eV are very close to the reported binding energies of 289.0 eV and 531.2 eV for carbonate [231, 232] on NiO(100). Due to this and due to their thermal stability, which is discussed in detail in Chapter 7.3.3, they are attributed to carbonate. The best explanation for the deviating binding energies of 290 and 530.7 eV reported

by Gordon et al. [236] for carbonate on NiO(111), are the very low signal intensity achieved in that study in the C 1s region and a similar beam damage as in our study in the O 1s region, respectively. If we compare the respective red and grey spectra in Figure 7.10 (a) and (c), we see that the peaks at 291.0 eV and 534.8 eV lose intensity when the CO₂ is switched off, while all other peaks gain in intensity. Due to this intensity loss and the low thermal stability of the peaks at 291.0 eV and 534.8 eV they are assigned to physisorbed CO₂. The intensity increase of the other peaks upon desorption of some of the physisorbed CO₂ is due to a lifting of the damping of these layers by the physisorbed CO₂.

Detailed fits of the spectra on the new spots are shown in Figures 7.10 (b) and (d) for the O 1s and the C 1s region, respectively. The O 1s carbonate binding energy of 531.2 eV is well within the binding energy window of 530.7-531.6 eV observed for hydroxide, which depends on its coverage. As discussed below, a comparison of the carbonate coverages obtained from the O 1s and C 1s region shows that a large amount of hydroxide is adsorbed on the surface, which is not too surprising giving the high reactivity of the surface towards water (see previous chapters). Due to the very similar binding energies, it was not possible to separate the carbonate and hydroxide contributions within the peak at 531.2 eV, and it is thus labeled carbonate/hydroxide.

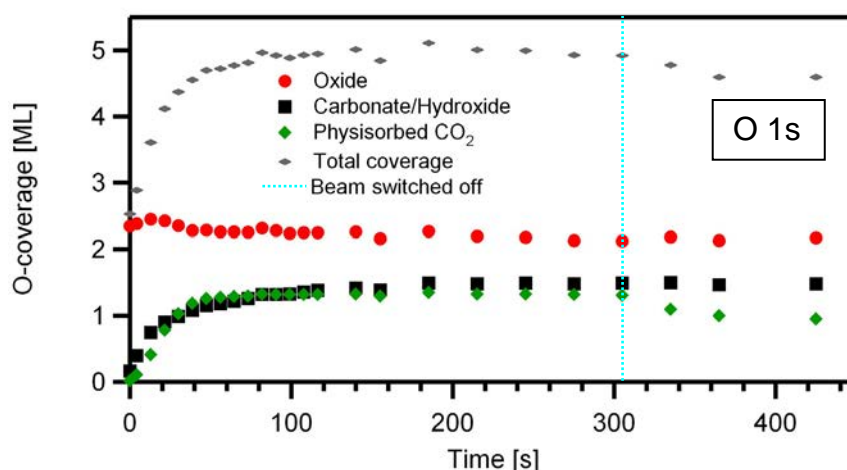


Figure 7.11: Quantitative analysis of data from Figure 7.10 (a), corrected for damping and selfdamping effects by the CO₂ and CO₃. Blue line marks end of CO₂ exposure.

Figure 7.11 shows the quantitative analysis of the uptake displayed in Figure 7.10 (a). The amount of physisorbed CO₂ starts to increase immediately and after 56 s (2.6 L), a coverage of 1.28 ML O-atoms is reached. Since one CO₂ molecule contains two oxygen atoms, this corresponds to 0.64 ML physisorbed CO₂ molecules. Thereafter, the coverage increases only slightly up to a maximum of 1.32 ML O-atoms, which is due to

a temperature decrease during the experiment. As soon as the molecular beam is switched off after 305 s (15 L, marked by the blue line in Figure 7.11), some of the physisorbed CO₂ starts to desorb, reducing the coverage down to 0.95 ML O atoms (0.47 ML CO₂ molecules) after 120 s. As discussed before, this intensity loss in the physisorbed CO₂ peak goes along with an increase of the other two peaks. Under the assumption that the intensities of the oxide and CO₃ peaks are constant, which is backed by their constant intensity prior to desorption of the physisorbed CO₂, we assign their apparent increase to damping. From this intensity increase we calculated the damping factors for this adsorption system. Just like for the water damping factors we assumed that both the physisorbed CO₂ and the chemisorbed CO₃ lead to equally strong damping and disregarded the differences between the damping factors of hydroxide and carbonate in the mixed carbonate/hydroxide adlayer. The mean value of the damping factor for CO₂/CO₃ determined from several experiments is 0.79 for an emission angle of 45° and a corresponding value of 0.85 for an emission angle of 0°. These factors are slightly lower than the factors of 0.76/0.83 determined for the damping by hydroxide and physisorbed water under emission angles of 45/0°, i.e. the damping by CO₂/CO₃ is weaker than the damping by H₂O/OH, due to its different electronic structure and geometry.

Similar to the water adsorption experiments discussed in the previous chapters, the oxide coverage remains almost constant during the experiment. The small variations in coverage are mainly attributed to errors due to the quick uptake and the determination of the damping factor. As the chemisorbing CO₂ needs to bind to one of the oxide oxygen atoms to form CO₃, the constant oxide coverage implies that the oxide oxygen atom does not change in binding energy upon formation of the CO₃. This is interesting as literature suggested all three carbonate atoms to be equal [233].

A fast initial increase of the carbonate coverage up to 0.91 ML O-atoms at 21 s (0.86 L) is followed by a further increase of the carbonate coverage with a slower rate. The saturation coverage of 1.48 ML O-atoms is reached after 185 s, which is equivalent to an exposure of 9 L. A comparison to the C 1s region shows a coverage of 0.38 ML CO₃ and 0.42 ML CO₂. The difference between the 0.42 ML CO₂ determined from the C 1s region, and the 0.47 ML CO₂ molecules determined from the O 1s region, is explained with the continued desorption after the experiment, which leads to even lower coverages at the start of the TPXPS experiment discussed in the next chapter. With the 0.38 ML CO₃ determined from the C 1s region we can calculate the OH content of the layer. From the constant oxide coverage we have learned that the oxide atom the CO₂ binds to in order to form CO₃ does not change in binding energy. This means that for each CO₃ only 2 atoms

contribute to the CO_3/OH peak at 531.2 eV and the third still contributes to the oxide peak. Thus in order to calculate the OH coverage we have to subtract two times 0.38 ML (determined from the C 1s region) from the total coverage of 1.48 ML determined from the O 1s region for the CO_3/OH peak, yielding 0.72 ML hydroxide. On the new spot a slightly lower carbonate coverage of 0.33 ML was observed. A similar decrease was found for the experiment shown in Figure 7.10 (c) where the adsorption was followed in the C 1s region. Here a carbonate coverage of 0.51 ML was found at the end of the adsorption and 0.42 ML when the sample was switched to a new spot. On the new spot a hydroxide content of 0.35 ML was found. Since coadsorption experiments discussed in Chapter 7.5 show that on a hydroxide precovered surface almost no carbonate is formed the lower hydroxide content is the explanation for the higher carbonate coverage observed there.

As the physisorbed CO_2 completely desorbs up to 200 K, (see next chapter), additional uptake experiments were performed at a sample temperature of 200 K. In these experiments (data not shown) coverages of 0.18 and 0.21 ML carbonate were achieved, with hydroxide coverages of 0.19 and 0.1 ML, respectively. No physisorbed CO_2 was detected.

Similar adsorption experiments were also done on the thin NiO layers on Cu(111), which were grown from 2 ML thick nickel layers. The spectra resulting from adsorption at 119 K, which was followed in the O 1s region, are shown in Figure 7.12 (a) and the spectra of an uptake at 116 K, which was followed in the C 1s region in Figure 7.12 (b). These spectra were acquired under an emission angle of 0° , and in order to minimize beam damage the sample was moved to a new spot after each spectrum. As already observed for the other studied adsorbates, this surface behaves very similar to the previously discussed NiO/Ni(111) layers, although the saturation coverages reached are lower. The carbonate peaks emerge at 289.1 and 531.6 eV in the C 1s and O 1s region, respectively, and shift slightly to lower binding energies during the uptake. At the end of the experiment they are found at 289.0 eV and 531.4 eV. A similar observation was made for the peaks assigned to physisorbed CO_2 , which shift from 291.2 to 290.9 and from 534.9 to 534.6 eV during the course of the uptake experiment. This shift is unusual, as the shift goes in the same direction as the shift induced by the beam damage in the previously discussed chapters, which was reversed when a new spot was studied. Here this beam damage was minimized by shifting the sample to a new spot after each spectrum, and thus even though some beam damage might still occur, the continuous shift over several spectra as observed here, is not due to beam damage.

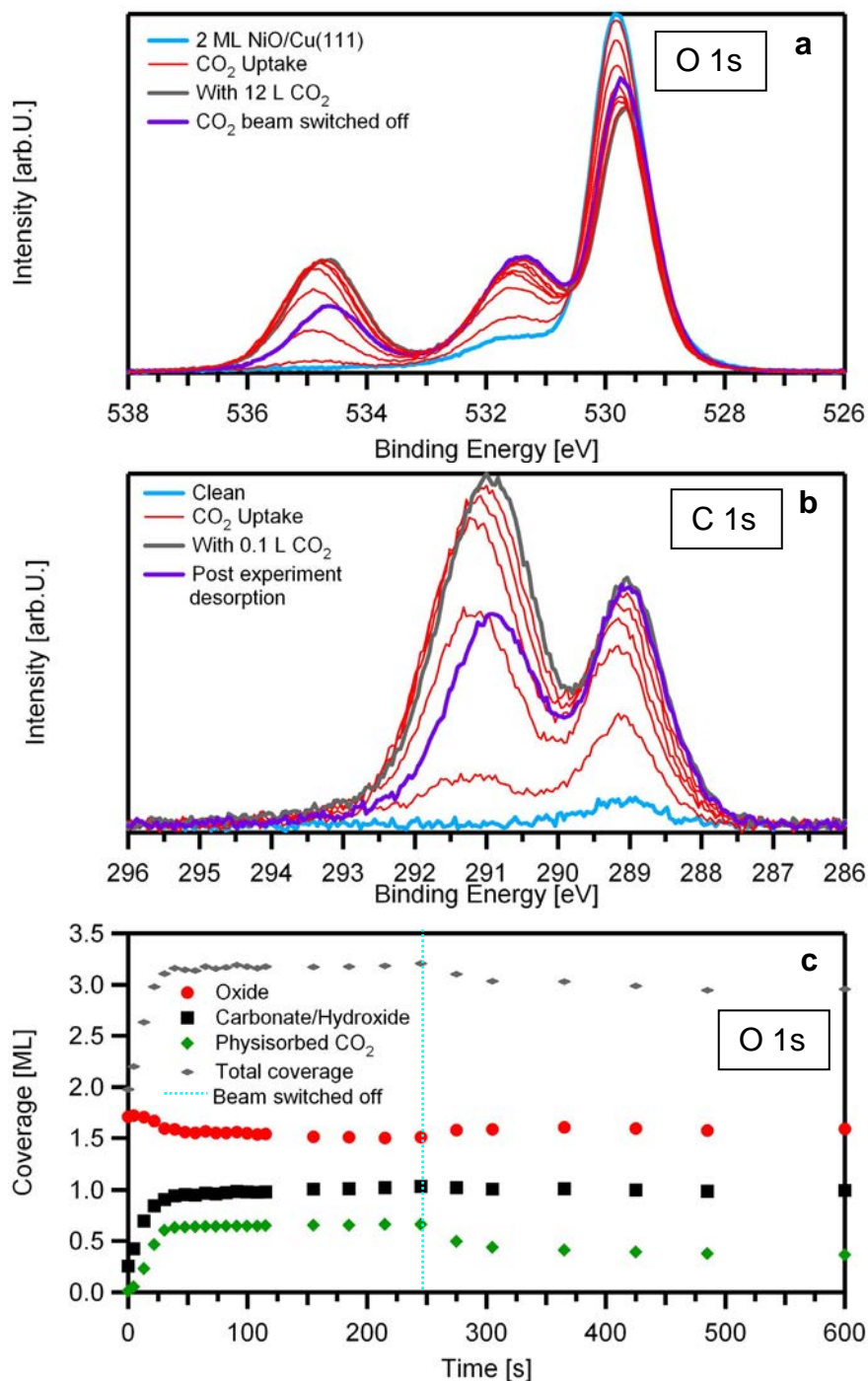


Figure 7.12: (a) Selected O 1s spectra acquired during the exposure of 2 ML NiO/Cu(111) to CO₂ at a surface temperature of 119 K. (b) Selected C 1s spectra acquired during the exposure of 2 ML NiO/Cu(111) to CO₂ at a surface temperature of 116 K. (c) Quantitative analysis of data from (a), corrected for damping and selfdamping effects by the CO₂ and CO₃. All spectra were acquired under an emission angle of 0°. The sample was shifted to a new spot after each spectrum.

Figure 7.12 (c) shows the quantitative analysis of the adsorption experiment displayed in Figure 7.12 (a). The evolution of the physisorbed CO₂ is very similar to the situation on NiO/Ni(111). After a fast increase around

39 s (1.7 L) a coverage of 0.63 ML O-atoms or 0.32 ML physisorbed CO₂ molecules is reached. After that, only a very slow increase up to 0.66 ML O-atoms is found, which is attributed to a slight decrease in temperature. When the molecular beam is switched off, after 245 s (12 L), the coverage of the physisorbed CO₂ starts to decrease down to 0.37 ML O-atoms after 360 s. Similar desorption of physisorbed CO₂ after the exposure was also observed on NiO/Ni(111). In the O 1s region discussed here, the peak at 531.6 eV already starts with a coverage of 0.25 ML. This is mostly attributed to hydroxide, as in the C 1s region prior to the uptake only a small CO₃ peak is found equivalent to 0.03 ML. In a similar fashion to the uptake of the physisorbed CO₂, a fast uptake of CO₃ up to a coverage of 0.94 ML O-atoms reached after 39 s (1.9 L) is followed by a slower increase up to 1.01 ML O-atoms reached after 185 s, (9 L). After this, the coverage stays almost constant, also during desorption of the physisorbed CO₂. The C 1s spectrum acquired after the adsorption (data not shown) revealed a final CO₃ coverage of 0.26 ML. From this, a hydroxide coverage of 0.49 ML is calculated. The coverage of physisorbed CO₂ determined from the C 1s region is 0.19 ML. This is close to the value of 0.18 ML CO₂ molecules determined from the O 1s region.

The oxide coverage shows a larger variation than on NiO/Ni(111). However, two aspects have to be considered: During the fast initial uptake of the CO₂ the oxide coverage remains almost constant, and the decrease down from 1.72 ML to 1.55 ML occurs after this point. And secondly, during the TPXPS experiments discussed in the next chapter, the oxide coverage remains constant. Thus, the drop in oxide intensity is not attributed to the reaction of CO₂ with the oxide, but instead to possible errors in the damping factor and to local variations of the oxide coverage on the surface.

The quantitative analysis of the C 1s spectra acquired during the uptake displayed in Figure 7.12 (b) provided similar results and is thus not shown separately. Here a carbonate coverage of 0.20 ML was reached with a hydroxide content of 0.45 ML. The physisorbed CO₂ had a maximum coverage of 0.39 ML, half of which desorbed when the molecular beam was switched off.

Unlike the adsorbates discussed previously, for which the NiO clusters on Cu(111) showed a lower but still significant adsorption capacity, the interaction of CO₂ with the NiO clusters is very weak. Figure 7.13 (a) and (b) show uptake experiments of CO₂ on NiO clusters on Cu(111) around 120 K followed in the O 1s and C 1s region, respectively.

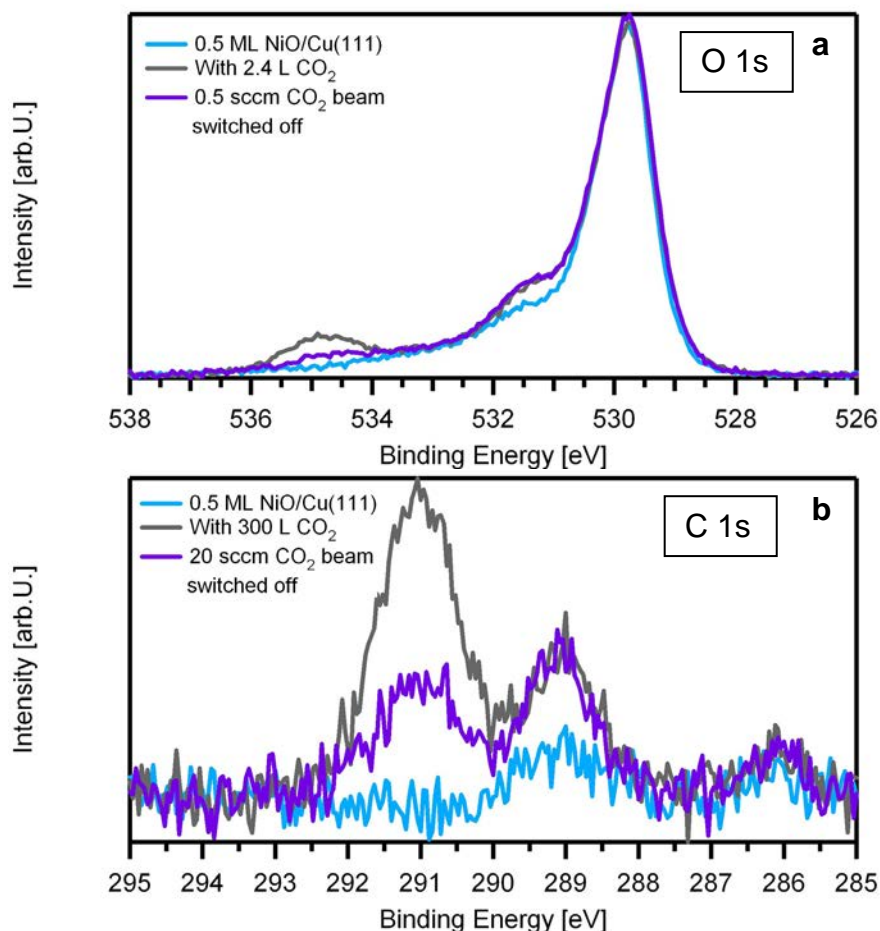


Figure 7.13: (a) Selected O 1s spectra acquired during the exposure of 0.5 ML NiO/Cu(111) to CO₂ at a surface temperature of 118 K. (b) Selected C 1s spectra acquired during the exposure of 0.5 ML NiO/Cu(111) to CO₂ at a surface temperature of 120 K. All spectra were acquired under an emission angle of 0°. The surface was shifted to a new spot after each spectrum.

All spectra were acquired under an emission angle of 0°, and the surface was shifted to a new spot after each spectrum in order to minimize beam damage. Please note that the binding energy range of the C 1s spectrum is shifted by 1 eV to lower binding energies, in comparison to all other C 1s spectra shown in this chapter so far, in order to accommodate an additional peak at ~286 eV. In the O 1s spectra displayed in Figure 7.13 (a) only a small increase of the hydroxide/carbonate peak around 531.4 eV is observed during exposure to CO₂. The coverage is found to increase from 0.05 ML to 0.10 ML. Assuming that all of this coverage increase is due to carbonate formation, and using the information that two of the oxygen atoms of the carbonate contribute to this peak this means a maximum carbonate amount of 0.025 ML. At 534.7 eV a peak attributed to physisorbed CO₂ appears, but almost completely desorbs when the CO₂ beam is turned off. The highest oxygen coverage of this species is 0.05 ML or 0.025 ML CO₂ molecules. After desorption the intensity is equal to 0.01 ML (0.005 ML CO₂).

In the C 1s region shown in Figure 7.13 (b) there is only a small increase of the carbonate peak at 289.0 eV visible during exposure to CO₂, leading to a saturation coverage of 0.02 ML carbonate. The physisorbed CO₂ is found at 291.0 eV and has a maximum coverage of 0.04 ML, dropping down to 0.02 ML when the CO₂ beam is switched off. Given the low overall coverages, these numbers are in good agreement with the coverages observed during the experiment followed in the O 1s region. The very small peak at 286.1 eV, which has a coverage of less than 0.01 ML is attributed to a contamination with CO adsorbing on Cu(111) patches.

7.3.3 Thermal evolution of carbonate layers

The thermal evolution of the carbonate layers was followed in the O 1s region by heating to the designated temperatures and taking spectra afterwards. Figure 7.14 (a) shows the O 1s spectra acquired during one of these experiments in the form of a color coded density plot. All spectra were acquired under an emission angle of 45°. The physisorbed CO₂ at 534.5 eV desorbs immediately, which is in line with the desorption of physisorbed CO₂ after the CO₂ beam was switched off at the end of the uptake experiment. As the physisorbed CO₂ desorbs, an apparent intensity increase is seen for the oxide and carbonate/hydroxide peaks. The quantitative analysis of the experiment displayed in Figure 7.14 (b) is corrected for the damping effects by carbonate and physisorbed CO₂. This analysis reveals that the increase is only apparent, due to the lifting of the damping by the physisorbed CO₂. The quantitative analysis also shows that desorption of the physisorbed CO₂ is mostly finished at 180 K, but some CO₂ remains on the surface up to 250 K. This is in agreement with the TPD data of Matsumoto et al. [237], who reported a CO₂ peak at 160 K with a tail up to 250 K for CO₂ on NiO/Ni(111).

The coverage of the carbonate/hydroxide peak at 531.3 eV remains constant at a value of 0.99 ML up to 130 K. From there on an almost linear decay of the layers starts, similar to the TPXPS experiments of adsorbed water above 300 K. This decay leads to a coverage of 0.40 ML at 400 K, which means the observed loss is 0.22 ML/100 K. Between 400 and 600 K the decay continues, but slows down, leading to a coverage of 0.25 ML at 600 K. Before further discussions, we have to consider that also hydroxide is in this layer, so in order to describe the temperature dependent decay of CO₃ the analysis of the C 1s region is important, as the hydroxide has no signal there.

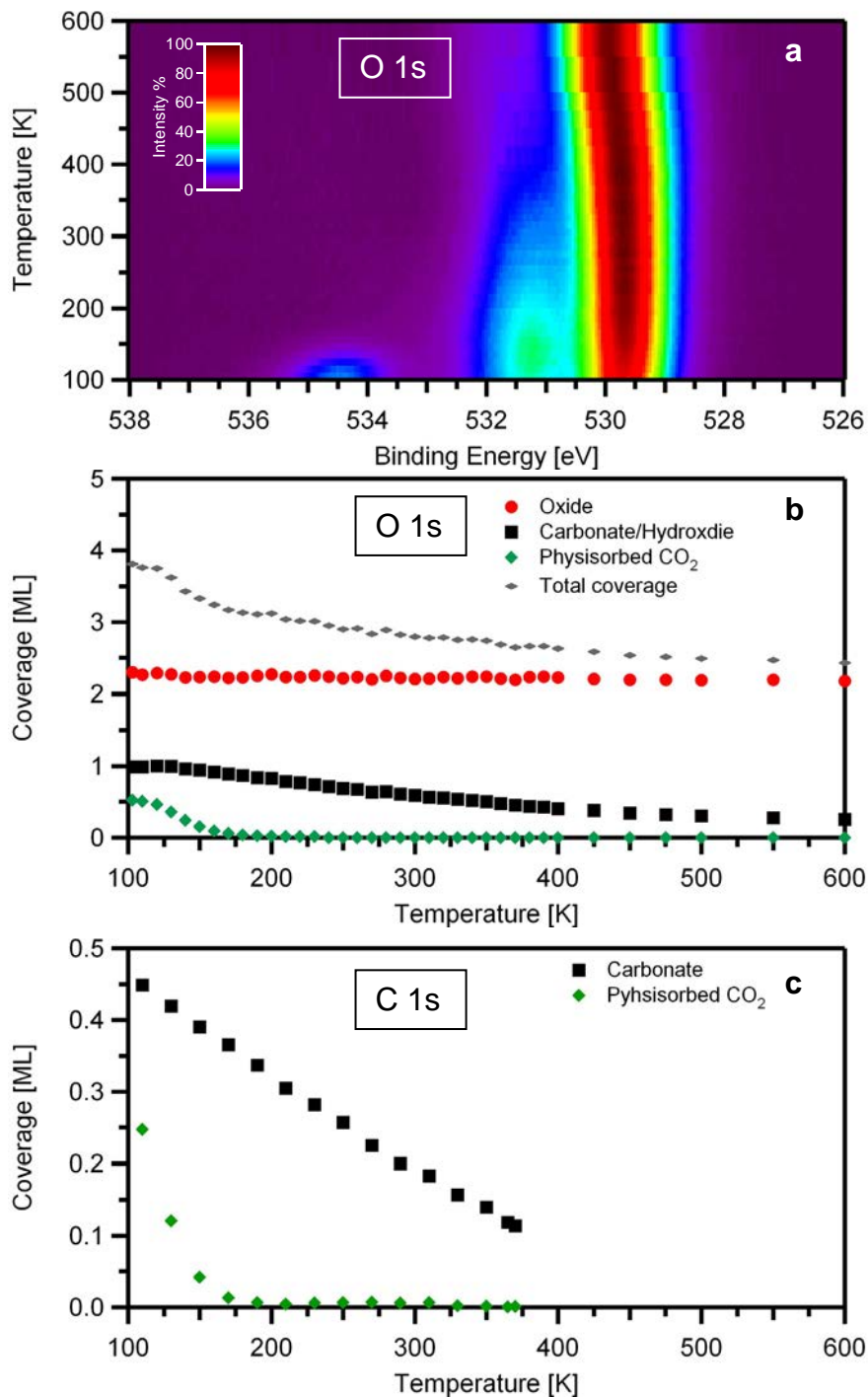


Figure 7.14: (a) Density plot of O 1s spectra acquired during TPXPS of carbonate on NiO/Ni(111). (b) Quantitative analysis of data from (a). (c) Quantitative analysis of TPXPS experiment of carbonate on NiO/Ni(111) followed in the C 1s region. All spectra were acquired under an emission angle of 45°. The quantitative coverages were corrected for damping and selfdamping effects by the CO₂ and CO₃, using a damping factor of 0.79.

Figure 7.14 (c) shows the quantitative analysis of a TPXPS experiment of carbonate on NiO/Ni(111), which was followed in the C 1s region. This TPXPS experiment was performed by heating the sample with the sample filament, using a ramp of 0.5 K/s, and taking a spectrum at designated

temperatures. The physisorbed CO₂ here behaves like in the previously discussed experiment, with most of it desorbing up to 190 K. The carbonate here seems to start to decay immediately, as compared to at ~ 130 K in the O 1s spectra. The intensity is going down linearly from 0.45 ML at 110 K to 0.22 ML at 270 K. The decay continues somewhat slower from there on with the coverage reaching 0.11 ML at 370 K, where the experiment was stopped. From looking at the TPXPS experiment of carbonate on 2 ML NiO/Cu(111) discussed below, however, it is likely that the decay would continue in a similar fashion above 370 K. This was also found when heating a carbonate layer which was prepared on NiO/Ni(111) at a temperature of 200 K (data not shown). There, the initial carbonate coverage of 0.21 ML decreased in a similar fashion as discussed before down to 0.02 ML at 500 K and was gone from the surface at 600 K. The start of the decay below 300 K is in contradiction to the work done by Behm and Brumble [231, 232], who observed no decay of carbonate on NiO(100) below 300 K. However, this is attributed to the different surface orientation used within this thesis, as the NiO layers discussed here have (111) orientation.

As hydroxide plays no role in the C 1s region, we can now be sure that carbonate shows a similar decay as hydroxide, with a continuous decay over a wide temperature range. In the case of hydroxide, we attributed this unusual decay behavior to a conversion from the hydroxylated NiO(111) surface to the octopolar reconstructed NiO(111) surface, involving NiO transport, in agreement with calculations by Ebensperger and Meyer [82]. If carbonate shows a similar decay behavior, this leads to the conclusion that it also has a similar effect on the NiO(111) surface as the hydroxide groups, most importantly stabilizing the flat NiO(111) surface by neutralizing the charge of the surface. As the evolution of the octopolar reconstructed NiO(111) surface is kinetically limited, carbonate shows a similar thermal stability as the hydroxide.

The thermal evolution of carbonate on 2 ML NiO/Cu(111) provided similar results as the one on NiO/Ni(111). Figure 7.15 (a) shows the O 1s spectra of the thermal evolution experiment as a color coded density plot, and Figure 7.15 (b) the respective quantitative analysis. Figure 7.15 (c) shows the quantitative analysis of a thermal evolution experiment of carbonate on 2 ML NiO/Cu(111) that was followed in the C 1s region. The thermal evolution experiments were performed by heating the sample to the designated temperatures with the resistive heating and subsequently recording the spectra under an emission angle of 0°. In the quantitative analysis the coverages were corrected for damping effects by the physisorbed CO₂ and the carbonate using a damping factor of 0.85.

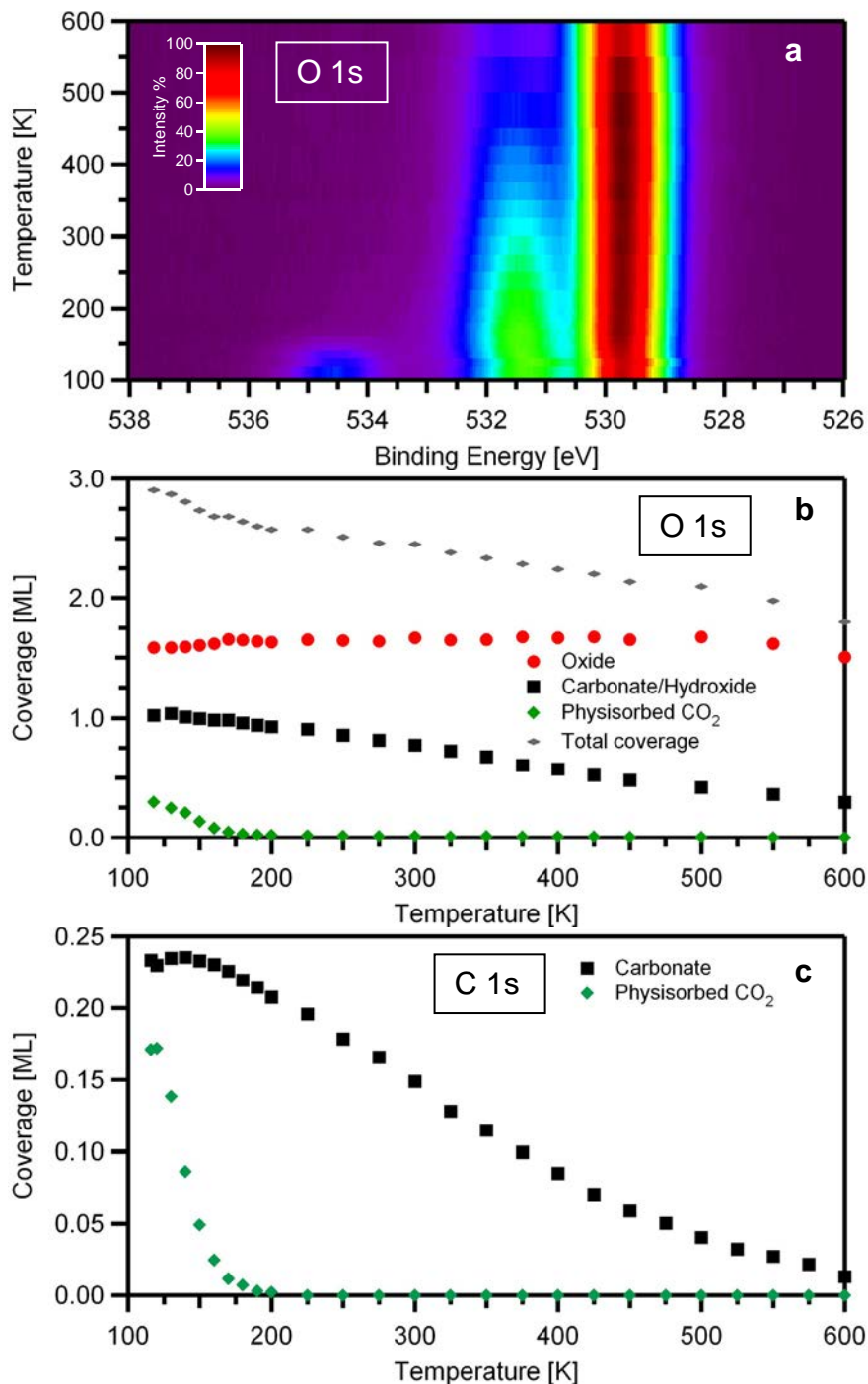


Figure 7.15: (a) Density plot of O 1s spectra acquired during the thermal evolution of carbonate on 2 ML NiO/Cu(111). (b) Quantitative analysis of data from (a). (c) Quantitative analysis of thermal evolution of carbonate on 2 ML NiO/Cu(111) followed in the C 1s region. All spectra were acquired under an emission angle of 0°. The coverages were corrected for damping effects by the CO₂ and CO₃, using a damping factor of 0.85.

In both experiments the physisorbed CO₂, which is found at binding energies of 534.5 and 290.9 eV in the O 1s and C 1s region, respectively, starts to desorb immediately and is completely gone from the surface at a temperature of 200 K, which is 50 K earlier than on NiO/Ni(111). The carbonate, which is

found at 289.0 eV in the C 1s region and as part of the mixed carbonate/hydroxide peak at 531.4 eV in the O 1s region, remains constant up to 150 K. Starting at 150 K, a linear intensity loss is observed in both experiments, which lasts up to around 450 K. In the experiment displayed in Figure 7.15 (b), the combined carbonate/hydroxide coverage drops from 1.00 ML to 0.48 ML in this temperature region, while in the experiment displayed in Figure 7.15 (c) a drop from 0.23 ML to 0.06 ML carbonate is observed. Above 450 K the decrease of the coverage continues in both experiments, although a bit slower than before. At 600 K most of the carbonate is gone from the surface, as in the C 1s region only 0.01 ML CO₃ are found; however, at this temperature the destabilization of the oxide layer has already begun, as discussed in Chapter 4 and evident from the decreasing oxide coverage in Figure 7.15 (b) above 500 K. Thus a carbonate contamination of the NiO layers cannot be removed by heating without destroying the oxide layer. The C 1s binding energy of 289.0 eV remains constant throughout the studied temperature range, while the O 1s peak shifts slightly from 531.4 eV to 531.5 eV. As such a shift to higher binding energies with decreasing coverages was observed for the hydroxide layers, the shift here is attributed to hydroxide content in the shared peak.

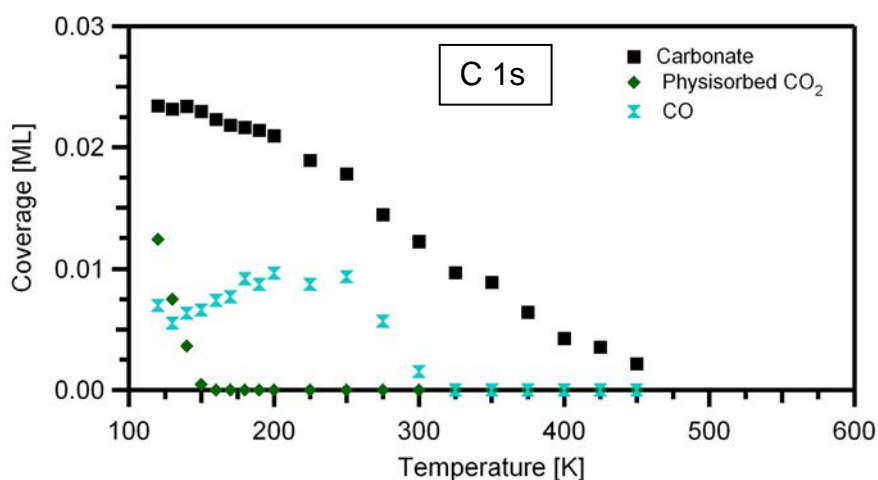


Figure 7.16: Quantitative analysis of TPXPS of carbonate on 0.5 ML NiO/Cu(111). All spectra acquired under an emission angle of 0°

The oxide coverage remains mostly constant over the whole range of the carbonate decay. This is further evidence that the oxide atom to which the CO₂ molecule binds in order to form the CO₃ does not change its binding energy. TPD experiments [236] showed that the CO₂ desorbs molecularly in the observed temperature ranges, so the third oxygen atom has to remain on the surface as part of the oxide. If this atom would have a different binding energy as part of the carbonate the oxide intensity would have to increase upon decay of the carbonate.

Even though the exposure of the NiO clusters on Cu(111) to CO₂ produced only very small amounts of carbonate and physisorbed CO₂, these small amounts show a similar thermal stability as the thicker carbonate layers found on the other two NiO surfaces. The quantitative analysis of a respective TPXPS experiment, where the sample was heated to the designated temperatures using the resistive heating and the spectra were subsequently acquired under an emission angle of 0°, is displayed in Figure 7.16. The physisorbed CO₂ desorbs even faster than on the 2 ML thick NiO/Cu(111), with complete desorption up to 150 K. At this temperature the decay of the carbonate layers starts slowly, and then gets a bit faster above 200 K. At 450 K only very small amounts of carbonate remain on the surface. The CO contamination desorbs completely between 250 and 300 K, with no noticeable effect on the carbonate coverage.

7.4 CO Interaction with NiO layers

7.4.1 CO Interaction with nickel and copper surfaces

The CO interaction with Ni(111) has been extensively studied in the past, see [125] and references therein. If CO is adsorbed on Ni(111) at temperatures around 180 K or below and subsequently annealed to 320 K, it forms a c(4x2) structure on the surface with a coverage of 0.5 ML [125]. This defined structure is used within this thesis to calibrate the coverages of the NiO/Ni(111) layers and of all adsorbates on NiO/Ni(111) discussed in Chapter 7. To prepare this structure 10 L CO were dosed on a clean Ni(111) surface at a temperature of 110 K. Afterwards the surface was heated to 320 K in order to desorb excess CO (for details on this excess CO see [125]).

The resulting O 1s and C 1s spectrum are shown in Figure 7.17 (a) and (b), respectively. Both spectra were acquired under an emission angle of 45° and are in agreement with literature [125]. Figure 7.17 (c) shows a LEED picture of the c(4x2) structure acquired at an electron energy of 96.6 eV. This LEED picture is also in agreement with literature [125]. Since this layer is solely used for coverage calibration of the adsorbates on NiO it will not be discussed further.

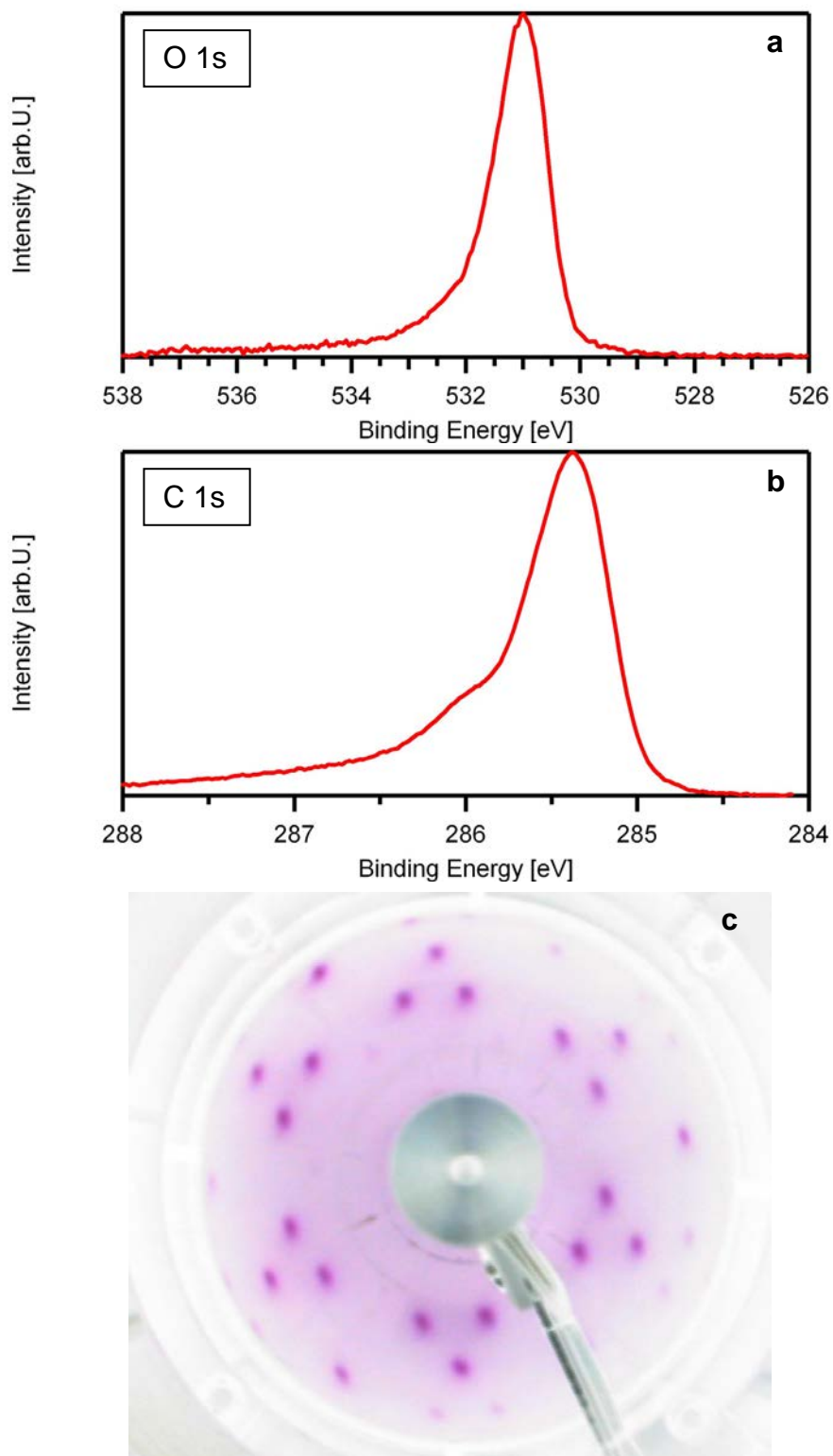


Figure 7.17: (a) O 1s spectrum (b) C 1s spectrum and (c) LEED picture at 96.6 eV of a CO c(4x2) structure on Ni(111). Both spectra acquired under an emission angle of 45°

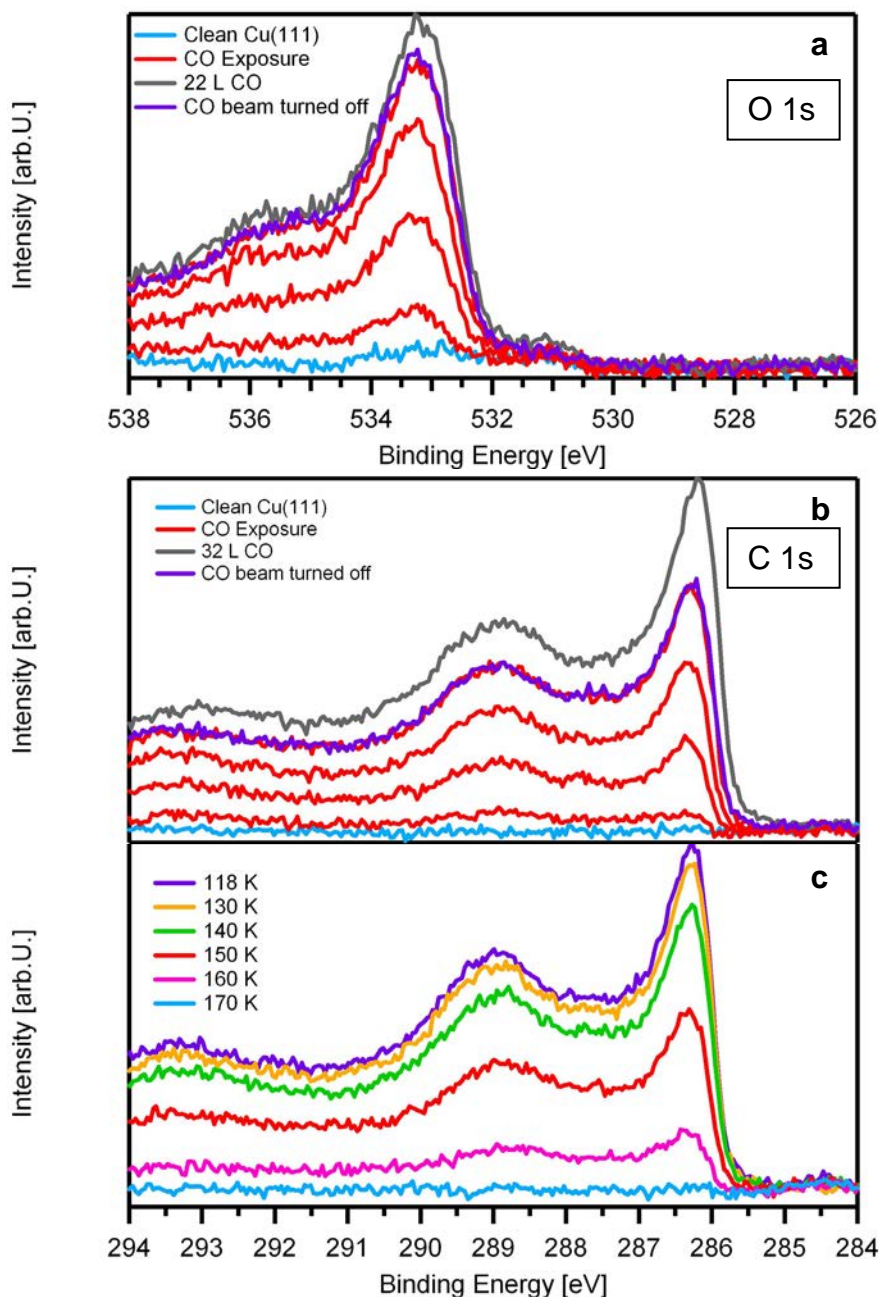


Figure 7.18: (a) Selected O 1s spectra of CO exposure to clean Cu(111) at 117 K. (b) Selected C 1s spectra of CO exposure to clean Cu(111) at 118 K. (c) Selected C 1s spectra of thermal evolution of CO on Cu(111). All spectra acquired under an emission angle of 0°

CO on Cu(111) is also a well known system. LEED studies at 89 K revealed three different ordered structures. First a $(\sqrt{3} \times \sqrt{3})R30^\circ$ with a coverage of 0.33 ML, then a structure with two domains of a hexagonal $(1.5 \times 1.5)R18^\circ$ mesh coexisting on the surface with a coverage of 0.44 ML and finally a (1.4×1.4) structure with a coverage of 0.52 ML [255]. TPD studies revealed three desorption peaks around 130, 150 and 170 K [256-258]. Raval [259] et al. showed with a combination of LEED, HREELS and FT-RAIRS that up to

coverages of 0.41 ML all CO molecules are bound in on-top positions, while for higher coverages also bridge bound CO molecules are found. This has also been confirmed by DFT [260, 261], although it has to be mentioned that this system is one where DFT often finds the wrong adsorption site, favoring the hollow position. In a XPS-study [262] very complex spectra were found, in which the main lines at 533.7 and 286.6 eV in the O 1s and C 1s regions, respectively, are each accompanied by two satellites at higher binding energies. These satellites were attributed to shake up features, and also appear in the spectra of CO on Cu(100) [263]. The system was also studied with AES [257, 264, 265], UPS [266], RHEED [257] and ellipsometry [265].

We studied the CO interaction with Cu(111) by exposing the surface to CO at temperatures below 120 K and taking spectra under an emission angle of 0°. Figure 7.18 (a) shows selected O 1s spectra of one uptake, while Figure 7.18 (b) displays selected C 1s spectra of a different uptake. In both spectral regions a set of peaks is found to grow simultaneously. In the O 1s region the main peak is found at 532.9 eV and the first satellite at 535.6 eV. The second satellite reported in literature [262] in a distance of 7.3 eV in respect to the main peak is not found, as it would be outside the measured binding energy window. In the C 1s region both satellite peaks are found, with the main peak at 286.1 eV and the two satellites at 288.9 eV and 293.2 eV. The peaks in both regions are shifted to lower binding energies in respect to the binding energies reported in literature for CO on polycrystalline copper, which lists the O 1s peaks at 533.7 and 536.0 eV and the C 1s peaks at 286.6, 289.4 and 294.0 eV [262]. However, the separation between the main peak and first satellite is identical with the one reported in literature in both regions. The binding energies of the main peaks are also close to the binding energies of 286.3 eV and 533.0 eV reported for the main peaks for CO on Cu(100) [263]. Thus our spectra are in good agreement with literature. Upon turning off the CO beam after the uptake experiment, some intensity is lost due to desorption of CO, as seen in both regions. This is not surprising, since the desorption from the α -desorption state at 130 K [256] starts already at 110 K for higher coverages. Due to the complex and very broad satellite structure the total peak areas are very hard to determine, and thus no attempt of giving quantitative coverages was made.

Figure 7.18 (c) shows selected C 1s spectra of the thermal evolution of adsorbed CO on Cu(111). Desorption starts immediately and at 170 K all CO has disappeared from the surface. This is in good agreement with the reported TPD data with desorption states at 130, 150 and 170 K [256-258].

7.4.2 CO Adsorption and thermal evolution on NiO/Ni(111) and 2 ML NiO/Cu(111)

CO Adsorption on NiO has mainly been studied for the NiO(100) surface so far. On this surface CO was found from photoelectron diffraction (PhD) studies [267, 268] to adsorb in on top adsorption sites on the Ni atoms, with the molecular axis tilted 12° away from the surface normal. This adsorption geometry was also reproduced with DFT [269]. From the PhD studies, the Ni-C bond was found to be significantly longer on NiO than on metallic nickel surfaces, and this was put into correlation with the lower desorption temperatures found for CO on this surface compared to the metallic surfaces. This desorption temperature is known from a TPD study [270], where for adsorption temperatures of 85 K a single desorption peak between 115 and 137 K, depending on coverage, was found for freshly cleaved NiO(100) surfaces. For thin NiO(100) films on Ni(100) the peak was found at slightly higher temperatures up to 150 K. On NiO(111) from a NEXAFS study [271] an adsorption on the NiO(100) microfacets of the octopolar reconstructed areas of the surface was proposed. Some low resolution XPS spectra of CO on NiO(100) showed a CO derived peak at ~ 5 eV higher binding energy than the oxide peak in the O 1s region and in the C 1s region two peaks with a distance of ~ 4.5 eV, whose binding energies were not explicitly given [267]. Another XPS study on powdered NiO samples at room temperature, with a similarly low resolution (>2 eV), showed a C 1s peak at 285 eV, which was attributed to a carbon contamination and a peak at 290.8 eV attributed to a surface carbonate [272]. In the O 1s region no respective peaks were found.

In order to study the interaction of CO with NiO, CO was dosed on NiO/Ni(111) and 2 ML NiO/Cu(111) with the molecular beam using a gas flux of 0.5 sccm and a sample temperature of less than 120 K. Selected O 1s and C 1s spectra from these experiments are displayed in Figure 7.19. The spectra of CO on NiO/Ni(111) were acquired under an emission angle of 45° , and the spectra of CO on 2 ML NiO/Cu(111) under an emission angle of 0° .

The O 1s region upon CO adsorption on NiO/Ni(111) is displayed in Figure 7.19 (a). While the oxide main peak at 529.9 eV loses some intensity, the hydroxide peak at 531.8 eV grows slightly. There also appears a new peak at 535.4 eV. When the molecular beam was switched off after a total exposure of 54 L CO, the new peak at 535.4 eV started losing intensity and both the oxide and the hydroxide peak regained intensity. This is the same behavior we already saw upon adsorption of CO₂, where the oxide and the hydroxide/carbonate peak were damped by the physisorbed CO₂, and this damping was lifted when part of the physisorbed CO₂ desorbed when the CO₂ beam was switched off.

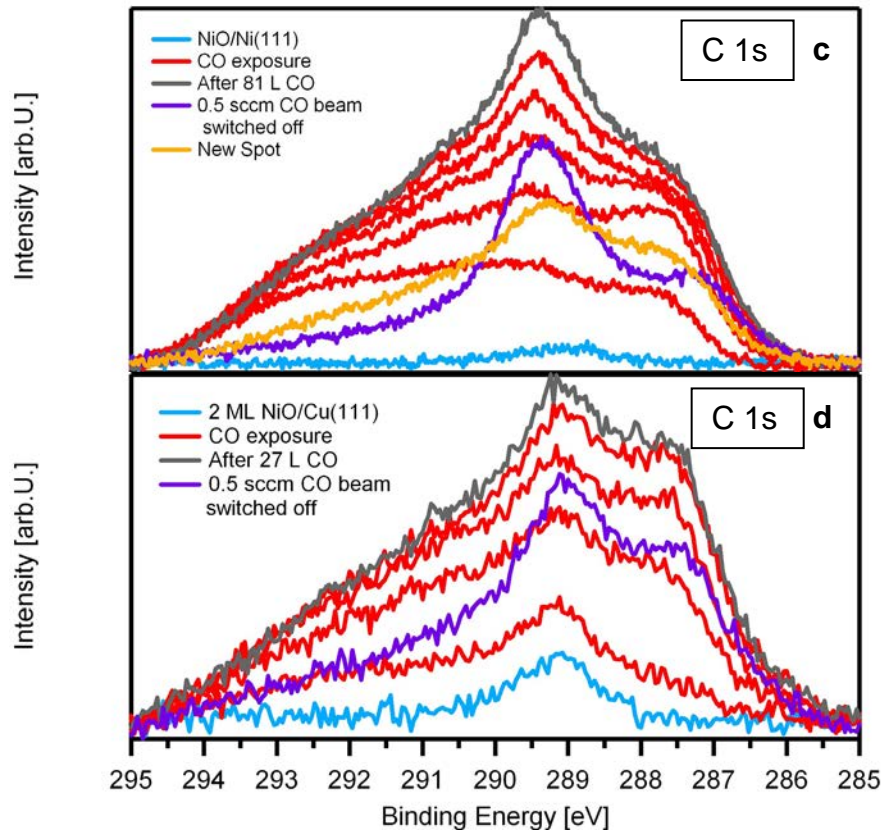
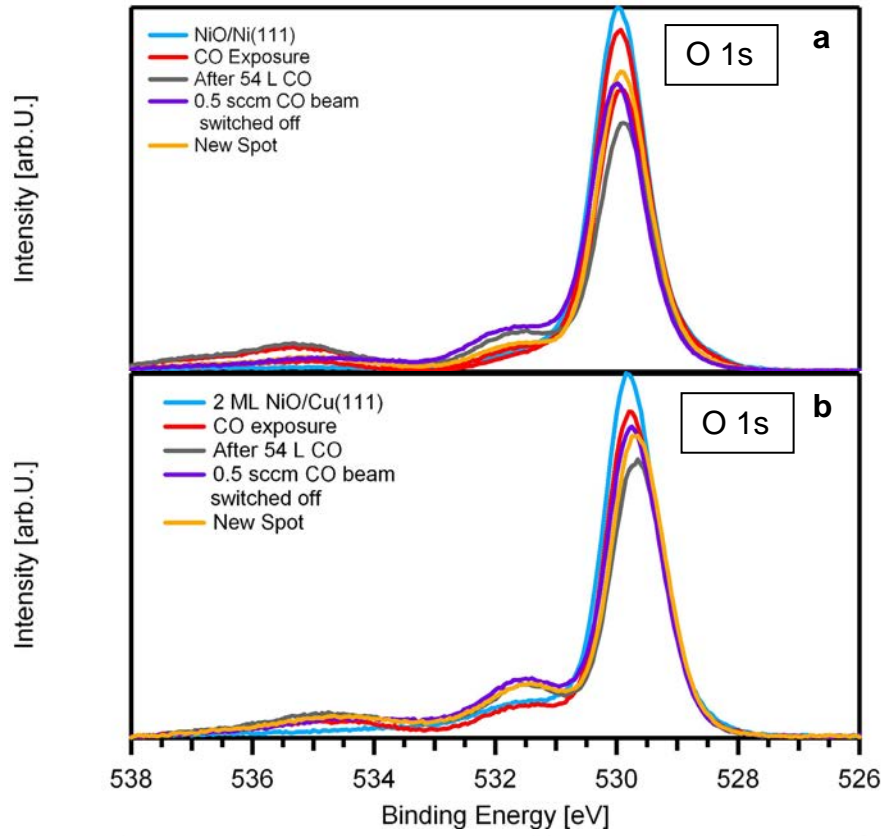


Figure 7.19 (on previous page): (a) Selected O 1s spectra of CO uptake on NiO/Ni(111) at 106 K. Spectra acquired under an emission angle of 45°. (b) Selected O 1s spectra of CO uptake on 2 ML NiO/Cu(111) at 117 K. Spectra acquired under an emission angle of 0°. (c) Selected C 1s spectra of CO uptake on NiO/Ni(111) at 102 K. Spectra acquired under an emission angle of 102 K. (d) Selected C 1s spectra of CO uptake on 2 ML NiO/Cu(111) at 117 K. Spectra acquired under an emission angle of 0°

The binding energy of 534.8 eV of the physisorbed CO₂ on NiO/Ni(111) is also similar to the value of 535.4 eV we find for the new peak. Due to these similarities, and the reported desorption temperature of 115 K of CO on Ni(100) [270] the peak at 535.4 eV is attributed to physisorbed CO. However, the presence of some physisorbed CO₂ due to residual gas can not be excluded, but due to reasons discussed below CO₂ cannot be responsible for all observations. After the experiment a spectrum was recorded on a new spot on the surface, in order to check if any beam damage had occurred. On the new spot (orange line in Figure 7.19 (a)) the intensity of the hydroxide peak was found to be lower, which indicates some beam damage and is in accordance with the observations from the C 1s spectra discussed below.

For 2 ML NiO/Cu(111) the O 1s spectra displayed in Figure 7.19 (b) provide very similar results. The oxide peak here is found at 529.8 eV and the hydroxide peak at 531.6 eV. The physisorbed CO appears at 535.0 eV here. Apart from the slightly different binding energies the three species behave just like on the other surface, although there is much less beam damage here.

The interesting question now is, if the growth of the hydroxide peak on these two surfaces is only due to formation of hydroxide from the residual gas or if some carbonate is formed here as well, just like it was formed during the CO₂ uptake. As the carbonate can not be separated from the hydroxide, as discussed in Chapter 7.3, we studied the C 1s region to answer this question.

Figure 7.19 (c) shows selected C 1s spectra acquired during a CO uptake on NiO/Ni(111). Upon CO exposure intensity develops over a wide spectral range. For high exposures (e.g. gray line in Figure 7.19 (c)) the highest intensity peak is found at 289.4 eV, with shoulders on both sides. As the CO beam was switched off after the experiment, an intensity loss over the whole spectral range was visible, with the high binding energy shoulder suffering the biggest losses. After the experiment a new spot was studied, in order to test for beam damage. The resulting spectrum is shown as the orange line in Figure 7.19 (c). Compared with the situation on the old spot the intensity of the central peak has decreased while the two shoulders regained some intensity. As the intensity loss of the shoulders after the experiment was an ongoing process, the intensity gain on the new spot can not be attributed to readsorption from the gas phase. Thus we conclude that these components

that make up the intensity in the shoulders are subject to desorption upon interaction with the photons. As not all intensity was regained, however, there has to be also some desorption due to the lowered CO pressure, just like for other physisorbed components discussed in this thesis. The central peak at 289.4 eV on the other hand has a lower intensity on the new spot, and thus the lost intensity can be attributed to a beam damage derived species. Most likely the reaction from the carbonate precursor to the carbonate (see below) is favored by the photons. Due to this heavy beam damage no quantitative analysis has been performed for this uptake, only for the thermal evolution as discussed below, where also the assignment of the species will be discussed.

On 2 ML NiO/Cu(111) the CO uptake provided similar spectra displayed in Figure 7.19 (d). In order to minimize the heavy beam damage witnessed on the other surface, here the sample was shifted to a new spot after each spectrum. Upon CO adsorption we find the same intensity evolution over a large spectral range. The central peak here is found at 289.1 eV, and features the same broad shoulder on the high binding energy side and a slimmer one on the low binding energy side. Upon turning the CO beam off, we also find some desorption here.

In order to assign the different peaks to species we have to take a look at the TPXPS of the adsorbate layer in the C 1s region. Figure 7.20 (a) shows the spectra of this TPXPS of CO on NiO/Ni(111) in the form of a color coded density plot. All spectra were acquired under an emission angle of 45° and the temperature ramp applied by the sample filament was 0.5 K/s. The quantitative analysis is shown in Figure 7.20 (d), and two representative fits of the spectra at temperatures of 100 K and 190 K are shown in Figure 7.20 (b) and (c), respectively.

The 100 K fit displayed in Figure 7.20 (b) reveals that the high binding energy shoulder can be reasonably well fit with a very broad peak centered at 290.3 eV. Although this may seem a bit arbitrary at first, it provides a good quality fit, with parameters for the other two species that also work at higher temperatures were the species at 290.3 eV has already desorbed, as visible in Figure 7.20 (c). Upon heating, this species immediately starts to decrease in intensity and is completely desorbed at 190 K. The initial coverage for this species was found to be 0.07 ML. As this species also suffered a massive intensity loss during the uptake when the CO beam was shut off, this behavior is in line with the other physisorbed species discussed in this thesis so far and thus this species is attributed to physisorbed CO.

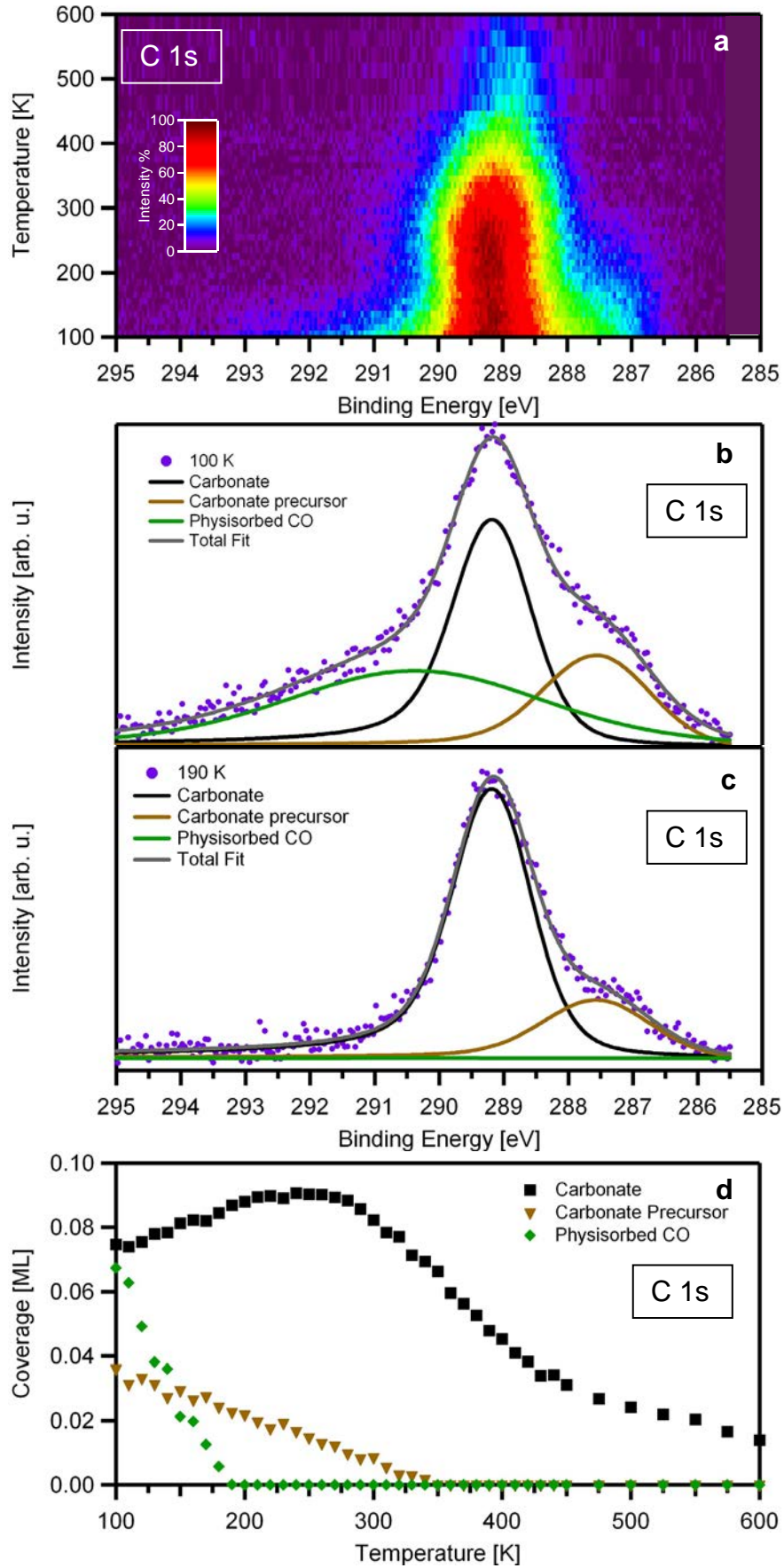


Figure 7.20 (on previous page): (a) TPXPS of CO on NiO/Ni(111) studied in the C 1s region displayed as a color coded density plot. The heating ramp used was 0.5 K/s. All spectra acquired under an emission angle of 45°. (b) Detailed fit of the C 1s spectrum acquired at 100 K. (c) Detailed fit of the C 1s spectrum acquired at 190 K, scaled to size of (b). (d) Quantitative analysis of data from (a), corrected for damping.

The low binding energy shoulder is located at 287.5 eV and has an initial coverage of 0.035 ML. Upon heating it shows linear coverage decay, and is completely gone from the surface at 350 K. To give an assignment for this species, we have to take a look at the final species. This species, which has the highest peak, is initially located at 289.1 eV and has a coverage of 0.075 ML. Unlike the other two species, the intensity of this species increases at first upon heating until a coverage of 0.09 ML is reached around 250 K. Starting at 300 K, this species also loses intensity linearly down to a coverage of 0.035 ML at 430 K. From this temperature on the intensity loss continues, however at a slower rate down to 0.015 ML at 600 K. Above 300 K there is also a binding energy shift found for this species towards lower binding energies. At 600 K, this species is found at 289.9 eV. Both the binding energy of this species and the two stage thermal decay above 300 K are so similar to the carbonate species formed upon CO₂ adsorption (see Chapter 7.3), that this species can be unambiguously assigned as carbonate. This leaves the question, why we see an intensity increase here up to 250 K, which is not present in the CO₂ experiments. Please note that the intensities shown in Figure 7.20 (d) have already been corrected for damping by the physisorbed CO and the species at 287.5 eV, using the same damping factor of 0.79 used for the CO₂ experiments discussed in Chapter 7.3. Thus this increase can not be explained by the lifting of the damping upon desorption of the physisorbed CO, especially since it continues even when all physisorbed CO has already desorbed. As the intensity increase goes hand in hand with the decrease of the species at 287.5 eV, it seems likely that the species at 287.5 eV reacts to carbonate upon heating. If we look closer at the intensity evolution of the two species up to 250 K we even find that the sum of the two coverages remains constant within the margin of error up to this temperature. Thus the species at 287.5 eV is assigned to a carbonate precursor species. Since the CO molecule has to bind to two surface oxygen atoms in order to form CO₂, a possible precursor species would be CO bound to a single oxygen atom from the oxide. A CO₂⁻ species would also be a possible candidate. However, the C 1s binding energy reported for such a species on Ni(110) is 286.6 eV [273] and thus far from our observed value of 287.5 eV.

The existence of the precursor species and its conversion to carbonate during heating can also explain why a carbonate formation from CO is possible at all. It is also one of a number of arguments, why we are sure that the carbonate is

formed mainly from the dosed CO instead of residual CO₂ in the chamber. The carbonate formation due to residual CO₂ in the chamber was seen on other occasions, but even during longer time periods, e.g. when trying to record LEED pictures of the NiO (which never revealed ordered patterns) or while waiting for the surface to cool down to 120 K after oxidation these did not exceed 0.02 ML. We can also exclude a contamination of the CO gas by CO₂, as this was checked after one of the adsorption experiments with the QMS.

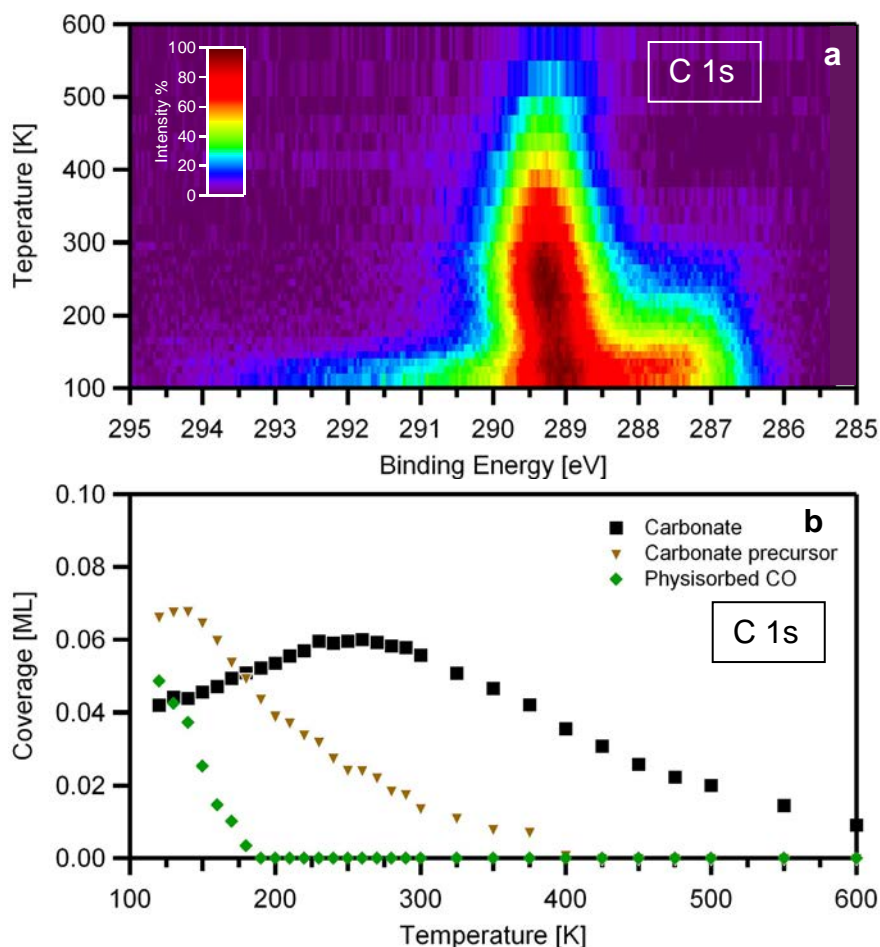


Figure 7.21: (a) C 1s spectra of thermal evolution of CO on 2 ML NiO/Cu(111) as a color coded density plot. All spectra acquired under an emission angle of 0°. (b) Quantitative analysis of data from (a), corrected for damping.

Figure 7.21 (a) shows the C 1s spectra of the thermal evolution of CO on 2 ML NiO/Cu(111) as a color coded density plot, and Figure 7.21 (b) the corresponding quantitative analysis. These spectra were acquired under an emission angle of 0° and the sample was shifted to a new spot after each spectrum in order to minimize beam damage. Apart from minor differences in coverages, binding energies and temperatures the thermal evolution is the same as on NiO/Ni(111). The physisorbed CO, which has an initial coverage of 0.05 ML here is completely desorbed at 190 K, the same temperature as on

NiO/Ni(111). The initial coverage of 0.065 ML of the carbonate precursor at 287.6 eV remains constant up to 140 K, where an intensity decrease starts that lasts up to 400 K, when the species is completely gone from the surface. Unlike on NiO/Ni(111), this decrease is not linear but instead slows down for higher temperatures. We also find a binding energy shift for this species down to 287.4 eV at 300 K, that was not seen on NiO/Ni(111).

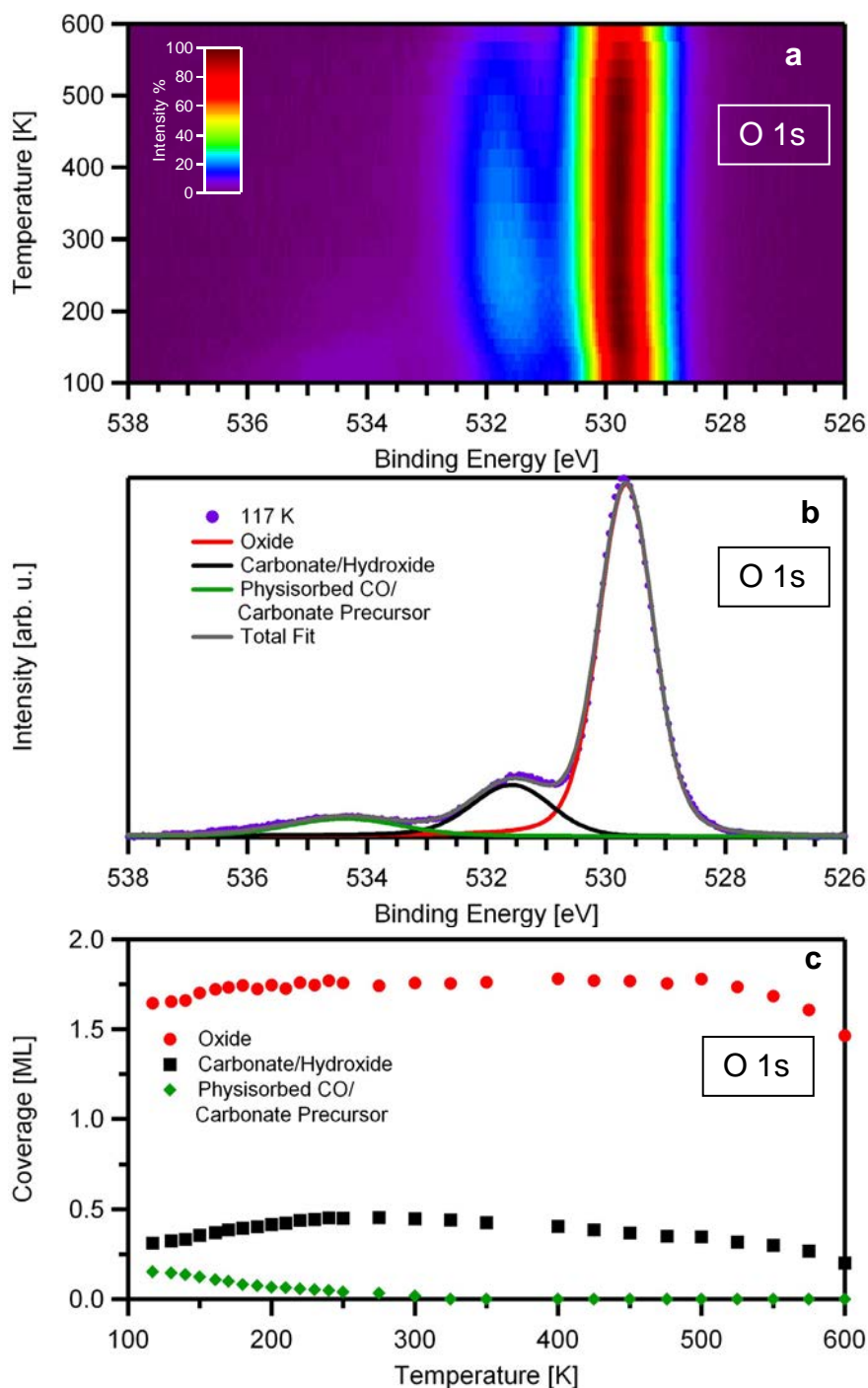


Figure 7.22: (a) O 1s spectra of thermal evolution of CO on 2 ML NiO/Cu(111) as a color coded density plot. All spectra acquired under an emission angle of 0° . (b) Detailed Fit of spectrum at 117 K (c) Quantitative analysis of data from (a), corrected for damping.

The carbonate is initially found at 289.1 eV and shifts to 289.2 eV for higher temperatures. Its coverage increases from 0.04 ML at 120 K up to 0.06 ML around 260 K. It has to be noted however that this increase is not as strong as the parallel intensity decrease of the carbonate precursor, which is another difference to NiO/Ni(111). Above 260 K, the intensity decrease of the carbonate starts, with a faster decay down to 0.025 ML at 450 K and thereafter a slower decay down to 0.01 ML at 600 K.

The low coverages for all the discussed species together with the inseparability of the carbonate and the hydroxide peak, as discussed in Chapter 7.3. and the damping of the oxide signal make both the analysis and interpretation of the O 1s region data rather difficult, as will be briefly discussed for the thermal evolution of CO on 2 ML NiO/Cu(111) below.

Figure 7.22 (a) shows the O 1s spectra of the thermal evolution of CO on 2 ML NiO/Cu(111) as a color coded density plot, with the quantitative analysis of the experiment displayed in Figure 7.22 (c). In Figure 7.22 (b) the fit of the lowest temperature spectrum at 117 K is displayed. Apart from the oxide peak at 529.7 eV and the carbonate/hydroxide peak at 531.6 eV a high binding energy peak at 534.4 eV is found. This peak was already seen during the adsorption of CO on the surface, and suffered a massive intensity loss as the CO beam was shut off, just like the physisorbed CO component in the C 1s region. Thus it would seem likely to assign this peak to physisorbed CO. On the other hand the quantitative analysis shows that this component is more stable than the physisorbed CO with a presence on the surface up to 300 K, and the initial coverage of this species (and also CO₂) of 0.15 ML is also higher than the coverage of physisorbed CO found at similar temperatures in the C 1s region. Since the thermal stability of the species is similar to that of the CO₃ precursor species found in the C 1s region, and since the CO₃ precursor species is also not found at another position in the spectrum we assume that this peak consists of contributions of both the physisorbed CO (and CO₂) and the CO₃ precursor species. The carbonate/hydroxide peak upon heating shows an intensity increase from 0.31 ML coverage at 117 K up to 0.45 ML at 250 K. Between 300 K and 500 K the intensity decreases again down to 0.35 ML. A separation of the carbonate component from the hydroxide component was impossible again. The initial increase in intensity was not seen in the thermal evolution of either pure hydroxide or the mixed carbonate/hydroxide layers derived from the adsorption of CO₂. However, it is in agreement with the increase of the carbonate amount found in the C 1s region. As the increase of 0.14 ML in this temperature region is much larger than the 0.02 ML increase found in the C 1s region one might speculate whether or not this means that in this case one or even both of the oxide atoms needed for the formation of the carbonate change their binding

energies. However, we have to keep in mind that this increase can also be due to hydroxide formation from the reaction of the surface with water from the residual gas, especially since the total coverage of the carbonate/hydroxide peak is still relatively low compared to the coverages discussed in Chapters 7.2 and 7.3, and thus the surface is likely not saturated. The oxide coverage initially increases as well, before remaining constant up to 500 K where the oxide starts to destabilize. The initial increase of the oxide coverage could be either due to an overestimation of the damping by the other adsorbates, as the coverages have been corrected for damping using the damping factor of 0.85 determined during the CO₂ adsorption experiments. Or they could be an indication of a locally lower oxide coverage, as the sample was shifted to a different spot after each spectrum in order to minimize beam damage.

7.4.3 CO interaction with NiO clusters on Cu(111)

Upon CO₂ adsorption, the NiO clusters, i.e. 0.5 ML nickel on Cu(111), were found to behave differently than the thicker NiO layers, as discussed in Chapter 7.3. On the NiO clusters almost no carbonate formation was found, whereas on the thicker layers significant carbonate formation was detected. Since for adsorption of CO on the thicker nickel layers significantly less carbonate was formed compared to the adsorption of CO₂, it is now interesting to study the interaction of CO with the NiO clusters.

Figure 7.23 (a) shows selected C 1s spectra acquired during the adsorption of CO on 0.5 ML NiO/Cu(111) at 119K, using the supersonic molecular beam with 0.5 sccm to dose the CO. The spectra were acquired under an emission angle of 0°. Upon CO exposure an intensity increase is observed over a wide spectral range. The highest peak is found at a binding energy of 286.1 eV, and another peak is formed around 288.9 eV. If we compare the overall spectral shape with the spectral shape of CO on clean Cu(111) displayed in Figure 7.18 (b), the similarities are obvious, with the binding energies of the main peak and the first satellite being identical. The second satellite found at 293.2 eV for CO on Cu(111) is not clearly visible in Figure 7.23 (a), however, since here a significant intensity increase in this binding energy region is found, it can be assumed that it is present as well. When the molecular beam is switched off at the end of the experiment, there is some intensity decrease over the whole spectral range, due to desorption. This was already seen for CO on Cu(111). Due to this similarities we attribute most of the intensity to CO adsorbed on the Cu(111) patches, although some other species might be present due to the high thermal stability discussed below. As discussed in Chapter 7.4.1., the satellite structure makes a determination of the coverage

very difficult. However, if we just compare the spectra of CO on Cu(111) and on the NiO clusters on Cu(111) by comparing the relative peak heights of the main peaks, we find that the CO coverage on the NiO clusters is roughly one third of the coverage found on clean Cu(111).

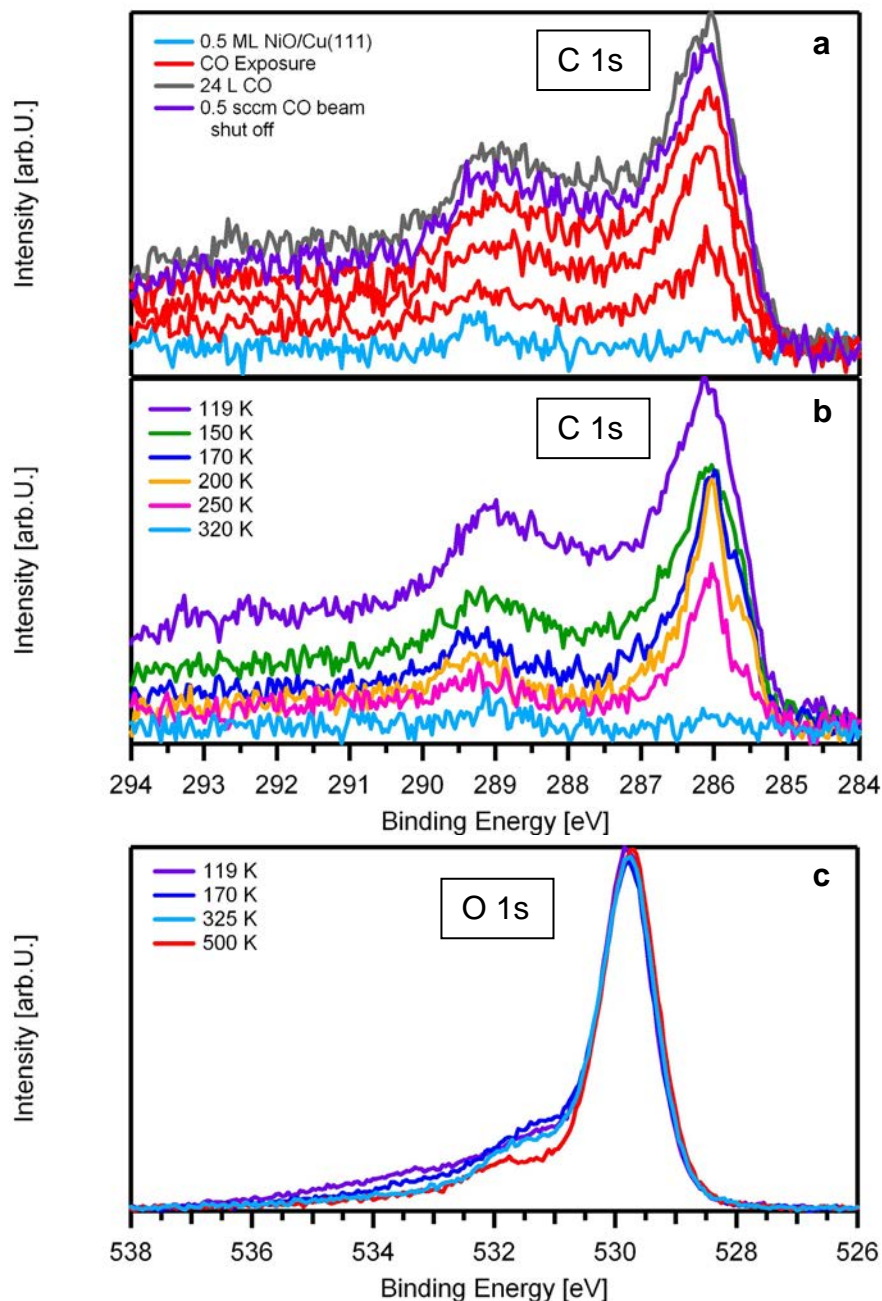


Figure 7.23: (a) Selected C 1s spectra acquired during a CO uptake on 0.5 ML NiO/Cu(111) at 119 K. (b) Selected C 1s spectra of the thermal evolution of CO on 0.5 ML NiO/Cu(111). (c) Selected O 1s spectra of the thermal evolution of CO on 0.5 ML NiO/Cu(111). All spectra acquired under an emission angle of 0° . Sample shifted to a new position after each spectrum.

Figure 7.23 (b) shows selected C 1s spectra of the thermal evolution of the adsorbed CO on the NiO clusters. In order to study the thermal evolution, the

surface was heated to the designated temperatures with resistive heating and subsequently the spectra were taken under an emission angle of 0° . Upon heating, the intensity decreases quickly over the whole spectral range up to 170 K. At this temperature, all CO had desorbed from the clean Cu(111) surface, but in this case we still find adsorbates on the surface. From 170 to 320 K, the loss of intensity proceeds much slower; at 320 K the adsorbed CO has desorbed and only a very small amount of CO_3 at 289.0 eV (less than 0.01 ML) remains on the surface, which was already present prior to the uptake. No additional CO_3 or other stable species were formed over the course of the experiment, but we can conclude that the NiO clusters stabilize some of the adsorbed CO so that some is present on the surface up to room temperature while on pure Cu(111) all adsorbed CO has desorbed up to 170 K.

In the O 1s region the CO adsorption and desorption leads only to small spectral changes. Figure 7.23 (c) shows selected O 1s spectra acquired during the thermal evolution of CO adsorbed on NiO clusters on Cu(111). The uptake is not displayed on its own, as the spectrum of the clean surface looked like the light blue (325 K) spectrum in Figure 7.23 (c) and the 119 K spectrum is the same as the final spectrum of the uptake. No desorption was found here upon turning the 0.5 sccm CO beam off after dosing 22 L CO. The adsorbed CO leads to new spectral features on the high binding energy side of the hydroxide peak. This is not surprising since on clean Cu(111) CO leads to peaks at 532.9 and 535.6 eV, as displayed in Figure 7.18 (a). Due to the location of these peaks on the tail of the oxide and hydroxide peaks in Figure 7.23 (c) and their relatively low intensity their exact position can not be determined. Upon heating to elevated temperatures, CO is desorbing again; at 320 K all adsorbed CO is gone from the surface, as evident from the stable intensity in the binding energy region above 532.5 eV, between 320 and 500 K. The intensity loss of the hydroxide peak at 531.8 eV is in accordance with the thermal evolution of hydroxide on the NiO cluster on Cu(111) as discussed in Chapter 7.2.4.

7.5 Coadsorption experiments on NiO layers

In this chapter we will briefly discuss two coadsorption experiments qualitatively. The relevant C 1s and O 1s spectra for the first of these two experiments are displayed in Figure 7.24 (a) and (b), respectively.

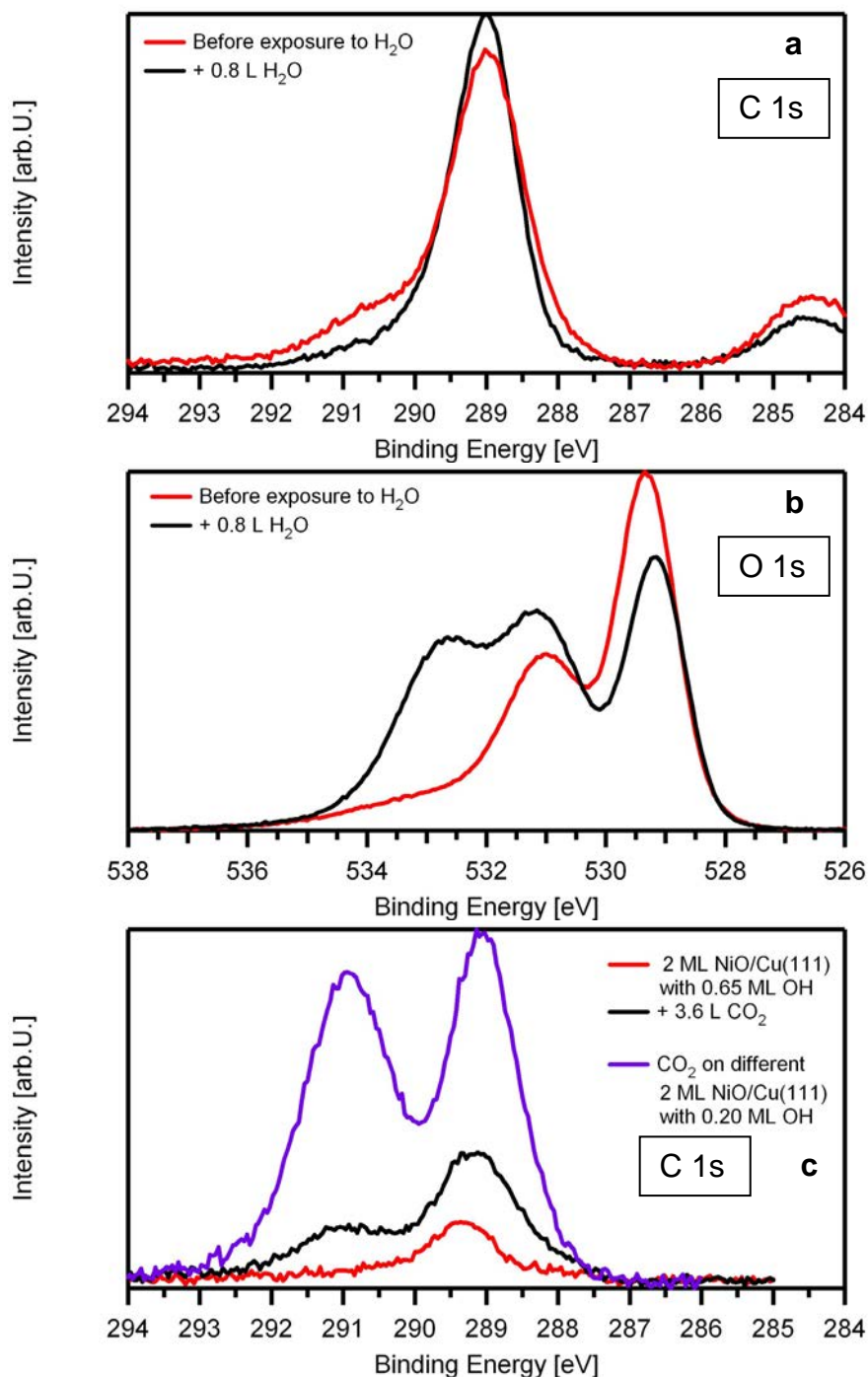


Figure 7.24: (a) C 1s spectra and (b) O 1s spectra of a saturated carbonate layer on 2 ML NiO/Cu(111) prior and after exposure to water. (c) C 1s spectra of two different carbonate exposure experiments on 2 ML NiO/Cu(111). All spectra acquired under emission angle of 0° .

In this experiment a saturated carbonate layer on 2 ML NiO/Cu(111) with a coverage of 0.21 ML (the deviation from the value of 0.23 ML in Figure 7.15 (c) is within the margin of error) was exposed to water at a temperature of 109 K. The layer was already partly hydroxylated prior to the water adsorption. The small peak visible in Figure 7.24 (a) at 284.5 eV is due to a small contamination by an adsorbed hydrocarbon. After an exposure of

0.8 L, which is suitable to saturate the hydroxide layer as discussed in Chapter 7.2.3, the O 1s spectrum is the same as found during the adsorption of water on a carbonate free surface. But even though the hydroxide layer is saturated now, the C 1s spectra show that the carbonate coverage remained almost constant. That means that at this temperature no displacement of adsorbed carbonate by hydroxide is possible.

There is also some evidence that preadsorbed hydroxide can block the carbonate formation from the experiments shown in Figure 7.24 (c). The red and black spectrum show a CO₂ uptake on 2 ML NiO/Cu(111) with a high hydroxide content of 0.65 ML. If we now compare the spectrum of the saturated layer (black curve in Figure 7.24 (c)) with the spectrum of a saturated carbonate/CO₂ layer on a different 2 ML NiO/Cu(111) preparation with a hydroxide content of 0.20 ML (purple line in Figure 7.24 (c), identical with purple line in Figure 7.12 (b)), it is evident that on the stronger hydroxylated surface the saturation coverage of both carbonate and physisorbed CO₂ are much lower. Thus we conclude that preadsorbed hydroxide can not be displaced by the CO₂. However, in order to quantify this site blocking, more experiments with different hydroxide precoverages would have to be made.

7.6 Concluding Discussion

In Chapter 7 we discussed the interaction of the three different NiO preparations with H₂O, CO₂ and CO, as well as the interaction of these molecules with the clean metal surfaces for reference. Table 7.2 lists the O 1s binding energy ranges of the species appearing on the surface upon adsorption of these molecules. The binding energy ranges of the oxide peaks have been excluded from this table and can be taken from Table 4.2. Table 7.3 lists the C 1s binding energies of the relevant adsorbates.

On the two metallic surfaces, water adsorption leads to the evolution of two peaks, one of which was attributed to hydroxide and the other to physisorbed water, in agreement with literature. On the Cu(111) surface only very small hydroxide coverages were found, due to dissociative adsorption on defect sites. The highest hydroxide coverages were found on a 2 ML thick nickel layer on Cu(111), where also some oxygen was formed from dissociative adsorption of water. Upon heating, water desorbed below 170 K on Cu(111), in agreement with literature. On the nickel layers on Cu(111), some of the physisorbed water remained on the surface up to 245 K.

Species\ Surface	Ni(111)	Cu(111)	NiO/Ni(111)	2 ML NiO/ Cu(111)	0.5 ML NiO/ Cu(111)
Hydroxide	531.0	531.0	531.0- 531.6	531.4- 531.8	531.1- 531.8
Physisorbed Water	533.0	533.3- 533.9	532.7- 533.5	533.3- 533.8	533.0- 533.5
Carbonate*	-----	-----	531.3	531.4- 531.6	531.4
Physisorbed CO ₂	534.8	-----	534.5- 534.8	534.5- 534.9	534.7
(Physisorbed) CO	531.0	532.9 #	535.4	534.4- 535.0	~532.9 #

Table 7.2: O 1s binding energy ranges [eV] of species discussed in this chapter. *Inseparable from hydroxide peak. # Binding energy for main peak.

Species\ Surface	Ni(111)	Cu(111)	NiO/Ni(111)	2 ML NiO/ Cu(111)	0.5 ML NiO/ Cu(111)
Carbonate	-----	-----	288.9- 289.1	289.0- 289.2	289.0- 289.1
Physisorbed CO ₂	291.2	-----	291.0	290.9- 291.2	291.1- 291.2
(Physisorbed) CO	285.4	286.1 #	290.3	291.0	286.1 #
Carbonate Precursor	-----	-----	287.5	287.4- 287.6	-----

Table 7.3: C 1s binding energy ranges [eV] of species discussed in this chapter. # Binding energy for main peak.

Upon exposing the NiO surfaces to water, the hydroxide peak, which is already present due to residual water in the chamber during the NiO growth (see Chapter 4), is gaining intensity and shifting towards lower binding energies. The lowest binding energies given in Table 7.2 for the hydroxide peak always belong to the highest hydroxide coverages. On all surfaces also a peak at higher binding energies appears that is attributed to physisorbed water. Unlike all other physisorbed species discussed in this thesis, this peak continues growing instead of losing intensity when the pressure of the adsorbing molecule is reduced. While this peak shifts towards lower binding energies on NiO/Ni(111) for higher coverages, on the other two surfaces a shift towards higher binding energies is observed. The shift towards higher binding energies is due to the multilayer character of the adsorbate, which gets closer to the properties of an ice crystal with increasing coverage. It is not fully understood, why on NiO/Ni(111) the peak for physisorbed water behaves differently. However, two things have to be considered. First, we have to take into consideration that the coverages of physisorbed water we studied on NiO/Ni(111) are much lower than on the other two surfaces, with the coverage never reaching a true multilayer regime. In the submonolayer regime studied here also on the other two surfaces a shift towards lower binding energies is found for low coverages, before a shift to higher binding energies starts. Secondly, on NiO/Ni(111) all peaks undergo a shift towards lower binding energies as the experiment continues. This effect can be partly attributed to beam damage, but also other aspects have to play a role like the structural changes due to the hydroxide formation. The hydroxide coverages found on the three different surfaces follow the trend observed for all other adsorbates so far, with the highest coverages found on NiO/Ni(111) and the lowest on the NiO clusters on Cu(111). The oxide peak shifts to lower binding energies on all three surfaces upon exposure to water, with the strongest shifts on NiO/Ni(111) and the smallest on the NiO clusters. There is also an intensity loss visible in the spectra for the oxide peak. However, upon further analysis this intensity loss could be shown to be due to damping by the adsorbed hydroxide and water layers. This in turn means that the oxide coverage stays constant throughout the adsorption experiments, but on NiO/Ni(111) a conversion of the shoulder oxide species discussed in Chapter 4 to the main oxide species was observed. On the 2 ML NiO/Cu(111) similar observations were made, but are not as clear as the intensity of the shoulder oxide species was very small.

Upon heating the adsorbed water and hydroxide layers, the physisorbed water desorbs up to room temperature, in agreement with literature. On the NiO layers on Cu(111), a clear distinction between the multilayer and the monolayer desorption of water is possible, as the multilayers desorb quickly

up to 170 K, whereas the monolayer is more stable and present on the surface up to 300 K. The hydroxide coverage initially remains constant on all three surfaces. Around 190 K (170 K for 2 ML NiO/Cu(111)) the hydroxide intensity falls and the peaks start to shift back towards higher binding energies, reversing the shifts observed during the adsorption. This intensity loss proceeds over a wide temperature range, and even at the temperatures of 600 K and 500 K, where the NiO layers on Ni(111) and Cu(111), respectively, start to destabilize, significant hydroxide amounts remain on the surface. On all three surfaces the decay is faster in the temperature range between 200 and 300 K than above 300 K, where a linear dependency of the coverage on the temperature is observed. During the entire temperature range of the hydroxide decay the oxide coverage stays constant on all three surfaces.

Two explanations are possible for this constant oxide coverage: the first explanation would be that an adsorbing water molecule forms only one hydroxide, and thus the oxide from the NiO surface does not take part in the reaction. In this case the excess hydrogen atom would either need to bind to the nickel atoms in the NiO surface or desorb. As a (111) surface of a rock salt like structure consists of only one of the two components, and the (111) surface of NiO is stabilized by OH [79, 88, 89], the surface should be oxygen terminated and no nickel atoms should be present. A desorption of the hydrogen atoms can be ruled out due to the constant oxide coverage during the thermal evolution of the layers. If no hydrogen is present on the surface, the decrease of the hydroxide coverage has to be facilitated by either direct desorption of the hydrogen from the OH or by recombinative desorption of one OH group with the hydrogen of another OH group. In both scenarios oxygen atoms remain on the surface, which would increase the oxide coverage. As such an effect is not seen, we can disregard the model where an adsorbing water molecule forms only one hydroxide. This leaves as with only one explanation: each adsorbing water molecule forms two hydroxide ions in interaction with the surface, but the hydroxide ion formed from the surface oxide atom retains its binding energy.

The slow, continuous decay of the hydroxide over a wide temperature range is explained by DFT calculations done by Ebensperger and Meyer [82]. The polar NiO(111) surface is unstable and can either be stabilized by hydroxylation or reconstruction to an octopolar structure. However, if the surface is heated and the hydroxide thus removed, there is no easy route towards the octopolar reconstructed surface, as the transition between the two structures involves activated material transport processes on the surface. A variety of transitory structures exists that can be present on the surface not because of thermodynamic, but kinetic limitations. This difficult and gradual

transition between the hydroxylated surface and the hydroxide free octopolar reconstructed surface leads to the slow continuous intensity decrease of the hydroxide layers observed within this thesis.

Upon exposing the Ni(111) and Cu(111) surface to CO, in both cases adsorption was found. On the Ni(111) surface and on a nickel layer on Cu(111), $c(2 \times 4)$ structures with coverages of 0.5 ML were prepared, according to literature [125], as coverage references for the other adsorbates. On Cu(111), relatively broad spectral features were observed in both the O 1s and C 1s region that are attributed to a main peak with shake up satellites [262]. The adsorbed CO desorbed completely up to 170 K in agreement with literature.

The exposure of Cu(111) to CO₂ at 115 K led to no adsorption. Exposing Ni(111) to CO₂ at 102 K resulted in very weak interaction with the surface, with the corresponding peaks (binding energies listed in Table 7.2 and 7.3) disappearing again when the molecular beam was turned off.

The exposure of NiO/Ni(111) and 2 ML NiO/Cu(111) to either CO₂ or CO led to the formation of a surface carbonate species that can best be characterized by its peak in the C 1s region at ~289.1 eV. In the O 1s region the binding energy of the carbonate overlaps with the binding energy range of the hydroxide peak. Since the NiO surfaces are never truly hydroxide free, and a separation of the two peaks in the fitting procedure was not possible, the C 1s region is better suited to study this species. Like for hydroxide, the saturation coverage of this carbonate species was higher on NiO/Ni(111) than on the 2 ML NiO/Cu(111). Here, one reason for this could be the higher hydroxylation of the NiO/Cu(111), as coadsorption experiments gave some evidence to an influence of the carbonate coverage on the hydroxylation of the NiO. Exposure of the surface to CO₂ leads to significantly higher carbonate coverages than exposure to CO. During the carbonate formation the oxide coverage stays constant, just like during the hydroxylation of the surfaces.

Apart from forming carbonate, CO₂ also physisorbs on NiO. This physisorbed CO₂ desorbed up to 200 K upon heating. A similar physisorbed component was also found upon CO adsorption. This component was found to have spectral intensity over a wide binding energy range. The physisorbed CO desorbed up to 170 K. During CO adsorption also a third component was found in the C 1s region, at a binding energy of ~287.5 eV. In the O 1s region the peak for this component can not be separated from the peak of the physisorbed CO due to its low intensity, and is thus not listed in Table 7.2. Upon heating, the intensity decrease of this species up to 250 K went hand in

hand with an intensity increase of the carbonate. Such an intensity increase of the carbonate was not observed when heating CO₂ derived carbonate, and thus the species at 287.5 eV was identified as a carbonate precursor.

Heating the carbonate layers shows a similar thermal evolution as the hydroxide layers, with a slow, continuous intensity decrease over a large temperature range. For the CO₂ derived carbonate layers the decay begins around 130 K, which is significantly earlier than the decay of the hydroxide layers. In the case of the CO derived carbonate layers the carbonate intensity increases at first, due to an ongoing reaction of the carbonate precursor species towards carbonate. Above 250 K, the intensity starts to decrease as well, but at first rather slowly indicating that still some carbonate is formed from the precursor species. As the thermal evolution of the CO derived carbonate above 300 K is the same as the one of the CO₂ derived carbonate, and the binding energy is the same, it is assumed that both are the same species. Thus it is very likely that also for the CO derived carbonate the decay starts around 130 K and is just not visible due to the ongoing carbonate formation from the precursor.

The constant oxygen coverage during the adsorption of CO₂ can be discussed in line with the constant oxygen coverage during the adsorption of H₂O. In order to form carbonate, the CO₂ has to bind to one oxygen atom from the oxide surface. If all three oxygen atoms within the carbonate would appear at the same binding energy in the spectrum, this would lead to a decrease of the oxide coverage, as the relevant oxide atom would appear at the carbonate binding energy after the CO₂ adsorption. Since this is not the case, we conclude that the oxide atom to which the CO₂ binds does retain its binding energy, similar to oxide atoms to which the additional hydrogen atom bonds during H₂O adsorption. This result is in disagreement to TPD experiments with isotopically labeled oxygen by Behm and Brumble [231, 232], who proposed all oxygen atoms in the carbonate to be equal. This difference is attributed to the different preparation of the carbonate layers in that study, as they were grown by coadsorbing oxygen and CO₂ on a Ni(100) surface, while in this study subsequent adsorption of oxygen and CO₂ on nickel surfaces with (111) orientation is used, which could result in a different surface structure. During CO adsorption, the evolution of the oxide coverage is not as clear. Since the carbonate coverages generated from CO are much lower, expected changes of the oxide coverages are small compared to the total oxide intensity, and are within the margin of error for the damping correction of the layers. If we also consider the overlap of the carbonate and the hydroxide peak in the O 1s region, we can not identify any significant changes of the oxide coverage due to CO adsorption.

As the carbonate layer shows a very similar thermal evolution as the hydroxide layer, especially the continuous decay over a large temperature range, while most other adsorbates desorb or react away in a much smaller temperature range, it is very likely that this is due to similar reasons. The slow decay of the hydroxide layers is explained by a complicated transition from the hydroxide stabilized flat NiO(111) surface to a hydroxide free NiO(111) surface that stabilizes itself by undergoing an octopolar reconstruction. Apparently carbonate can also stabilize the surface in an equal manner as the hydroxide group, and is also stabilized up to high temperatures due to the complicated transition to the octopolar reconstruction. To fully understand this process, however, further information from DFT calculations would be needed.

Another interesting question that can not be fully answered yet, is how CO can form carbonate on the surface. Unlike CO₂, it not only has to bind to one, but two surface oxide atoms in order to generate CO₃. That this process is much less likely can be seen from two observations: First from the achieved carbonate coverages upon CO adsorption, which are less than 25 % of the coverages achieved with CO₂ adsorption on both discussed surfaces. Secondly, the existence of a precursor species is a clear indication of more complicated reaction pathway. The most obvious candidate for a precursor species would be a CO molecule bound to a single oxide atom in the surface, forming a CO₂ species that further reacts towards carbonate. The absence of this precursor species in the CO₂ adsorption is explained by a lack of adsorption sites on the oxygen terminated surface for the oxygen atoms of the CO₂ molecule, so the molecule has to bind directly via the carbon atom to one of the surface oxygen atoms. This would mean that in this case the carbonate would be bound as a monodentate, while in the case of CO adsorption via the precursor species a bidentate binding geometry would be more likely. However, we have to consider that upon carbonate formation the surface should be able to reconstruct, as carbonate stabilizes the flat surface. During this reconstruction, the binding geometry of the carbonate could change again, allowing no clear assignment. Another possible candidate for the carbonate precursor species would be the reported adsorption of CO on nickel atoms in the NiO(100) microfacets of the octopolar reconstructed surface [271].

The NiO clusters on Cu(111) showed only very weak interaction with the CO₂. The small amount of carbonate formed showed the same slow thermal decay as on the other two surfaces; however, it was completely gone from the surface at 450 K whereas on the other two surfaces it could not be removed within the stability region of the oxide. CO adsorption on the NiO clusters led only to adsorption on the bare Cu(111) patches. The oxide, however,

stabilized some of the adsorbed CO, as during heating a temperature of 320 K was needed in order to completely remove the adsorbed CO, while on the pure Cu(111) surface all adsorbed CO was gone at 170 K.

8 Summary

In this thesis the adsorption and reaction of small molecules on various surfaces were investigated using in situ high resolution XPS. This technique allowed a detailed study of the involved processes and an identification of the reaction products. The main focus lies in the study of differently prepared NiO surfaces, but also of Ni(111) and Cu(111). NiO/Ni(111) and 2 ML NiO/Cu(111) were found to behave very similar in terms of growth and reactivity towards all studied adsorbates. NiO clusters on Cu(111), on the other hand often showed a different behavior than the other NiO layers, either by being less reactive or showing a mixed behavior of adsorption on the NiO and on clean Cu(111). In the following the most important results are summarized.

Growth of nickel oxide

Upon increasing the oxygen coverage on Ni(111) at 300 K from 0.25 ML for the well known $p(2 \times 2)$ structure to above 0.75 ML, a conversion of the asymmetric shape of the O 1s signal of chemisorbed oxygen to the symmetric shape of the oxide indicates the onset of oxidation. For higher exposures, the oxide thickness exceeded the escape depth of the photoelectrons, leading to saturation of the O 1s intensity and a complete transition of the Ni 2p peak, from the metallic to the oxidic shape. The oxide thickness was estimated as 11.3-20.0 Å. Its main O 1s peak is located at 529.6 eV, and as expected from literature a large OH peak is found, indicating a (111) orientation of the formed NiO. The OH peak position varied with coverage and temperature and the amount of hydroxide was lowered by heating. Besides the main oxide signal a new "shoulder oxide" species was found at 528.6 eV. This species is partially converted to the main oxide species upon heating. Oxidation at 500 and 550 K produced the same oxide layers, but with lower hydroxide content; these layers were used for the adsorption experiments on NiO/Ni(111). Above 600 K the oxide was found to destabilize.

In order to prepare thin NiO layers of defined thickness, nickel layers with thicknesses of 2 ML and 0.5 ML were evaporated on Cu(111), and subsequently oxidized at 300 K. The oxidation behavior of the 2 ML thick layers was very similar to the 300 K oxidation of Ni(111). This, together with a large hydroxide contamination, indicates a (111) orientation of the formed NiO. Higher oxidation temperatures were not possible due to copper segregation on top of the nickel layers, but after oxidation the NiO layers were annealed to 500 K in order to reduce the high hydroxide contamination.

Oxidation of the 0.5 ML thick nickel layers on Cu(111) was also performed at 300 K. After saturation of the O 1s peak, the Ni 2p region differed in shape and position from the Ni 2p spectra of the other two oxide layers. Two

interpretations are possible for this, either that some nickel atoms remain metallic or that this NiO forms a wetting layer on the surface with different properties than the other two NiO layers. The NiO was found to be almost OH free after oxidation, but is still reactive towards water, indicating a (111) orientation. STM pictures revealed the same cauliflower like structure as for the thicker layers. A major oxidation of the copper surface could be excluded.

Adsorption on and reaction of C₂H_x species on clean and oxygen precovered Ni(111)

Ethane dissociatively adsorbed as ethyle on clean Ni(111), when dosed with a high energy molecular beam. The C 1s spectra of both ethyle and ethene show two peaks with vibrational fine structure. For ethene the two peaks are explained by a geometry with carbon atoms bound in hollow and on-top positions; the same geometry is proposed for ethyle. For acetylene on Ni(111), the well known hollow-hollow geometry is found. Both ethyle and ethene dehydrogenate to acetylene around 200 K, which further dehydrogenates to carbonaceous species around 400 K. If acetylene is directly exposed to the surface, at much higher acetylene coverages a new reaction pathway is found, namely the trimerization to benzene. The formed benzene subsequently dehydrogenates, leaving high coverages of carbonaceous species on the surface, which give rise to another new, as yet unidentified species at high temperatures.

Adsorption of ethane and ethene on Ni(111) precovered with 0.25 ML oxygen in a p(2x2) structure was found to be quite different than on the clean surface. The spectra of both adsorbates only show one peak, indicating a change to a hollow-hollow geometry for both adsorbates. Even though ethane was dosed with the high energy molecular beam, it adsorbs molecularly. Ethene also adsorbs molecularly; for both adsorbates the saturation coverages are much lower than on the oxygen free surface. Upon heating, both adsorbates desorb up to 250 K, with only minor dehydrogenation; the latter is attributed to incomplete oxygen layers. Acetylene coadsorption with oxygen yielded lower saturation coverages than on the clean surface. The adsorption geometry remains unchanged, but in addition to chemisorbed acetylene a physisorbed component is observed that is not present at the same temperatures on the clean surface. At higher temperatures the same reaction pathway as for the clean surface is found, with trimerization to benzene and dehydrogenation. The S-Factor per C-H bond of all studied adsorbates on Ni(111) is 0.17 ± 0.02 .

Adsorption of hydrocarbons on Cu(111) and thin NiO layers

On Cu(111), ethane was dosed with the high energy molecular beam and dissociatively adsorbed as ethyle. Ethene, propane, propene and acetylene adsorbed molecularly. All C 1s spectra show a vibrational splitting, with an

S-Factor per C-H bond of 0.20 ± 0.02 . Except for acetylene, all spectra are similar to the gas-phase spectra, with the most obvious similarities for propene. These similarities and complete desorption of these adsorbates below 250 K are indicative for a very weak interaction with the surface. Acetylene is much stronger bound to the surface. It stays on the surface up to 325 K, when it is reacting to a range of products, which immediately desorb from the surface.

The adsorption of propane, propene, ethane, ethene, acetylene and methane on the three different NiO layers was studied at ~ 120 K. For all adsorbates physisorbed species were found. For methane a small signal was obtained only on NiO/Ni(111) with the molecular beam on. Most of the physisorbed molecules desorb below 200 K, but traces at defect sites are stable up to higher temperatures. For all adsorbates, except ethane, the physisorbed molecules adsorb strongest on NiO/Ni(111) and weakest on 0.5 ML NiO/Cu(111).

On all three NiO surfaces, only for acetylene a chemisorbed species was found in addition to the physisorbed component. At 120 K, both are populated almost simultaneously. On NiO/Ni(111), most of the physisorbed acetylene leaves the surfaces below 200 K, but small amounts are reacting to a carbon allotrope, which is also the reaction product of the chemisorbed acetylene up to 500 K. Besides a peak characteristic for C-C in carbon allotropes, a peak characteristic of C-O (single) bonds in carbon allotropes is found. For 2 ML NiO/Cu(111) an additional carbonaceous species is observed. On 0.5 ML NiO/Cu(111), acetylene adsorbed around 120 K both on the NiO clusters and on the bare Cu(111) patches in between; however, the cluster edges and their vicinity were not populated. Upon heating, the acetylene reacted to the carbon allotrope and the carbonaceous species that were also found on 2 ML NiO/Cu(111). The peak assigned to C-O bonds was absent here. Exposing 0.5 ML NiO/Cu(111) to acetylene at 400 K led to a continuing growth of the carbon allotrope and a complete reduction of the NiO.

Formation and thermal evolution of NiOH and NiCO₃

Water adsorption around 120 K on Ni(111), Cu(111) and Ni/Cu(111) led to small hydroxide formation on all three surfaces plus multilayers of physisorbed water, which desorbed on all surfaces below 250 K. For CO₂, at ~ 120 K no interaction was found with Cu(111) and only very weak interaction with Ni(111). CO adsorption on Cu(111) at 120 K led to very complex spectra both in the C 1s and the O 1s region, due to shake up features. CO completely desorbed from Cu(111) below 170 K. On Ni(111) and 3 ML nickel on Cu(111), we prepared CO in the c(2x4) structure, which has a nominal coverage of 0.5 ML and which is used as a reference for the coverages.

On the three different NiO surfaces, water adsorption around 120 K led to an increase of the hydroxide peak. In addition, physisorption of water was

observed. The physisorbed water and the formed hydroxide led to a damping of the photoelectrons originating from lower layers, which was accounted for in the quantitative analysis. The analysis showed that the oxide coverage is unchanged upon hydroxide formation. This is attributed to the fact that oxide atoms retain their binding energy upon attachment of hydrogen atoms, whereas the O signal of the hydroxide peak displays a different binding energy. The highest hydroxide coverages were found on NiO/Ni(111), the lowest on 0.5 ML NiO/Cu(111). Physisorbed water desorbed below room temperature. The hydroxide coverages stayed constant below 200 K and continuously decreased at higher temperatures; at 600 K still some hydroxide was left on the surface. This is explained by a complicated restructuring process of the surface between a flat hydroxyl-covered surface and a hydroxyl free surface, which is octopolar reconstructed to compensate for surface charges. The reconstruction involves material transport, leading to kinetic limitations together with the thermodynamic limitations and to the existence of several transitory states. The oxide coverage remains constant over the studied temperature range.

CO₂ adsorption on NiO/Ni(111) and 2 ML NiO/Cu(111) around 120 K led to the formation of carbonate layers and to the physisorption of CO₂. The saturation coverages of carbonate on NiO/Ni(111) were found to be higher than on 2 ML NiO/Cu(111). The oxide coverages remained constant throughout the uptake experiment; this indicates that the oxide atom participating in CO₃ formation retains its binding energy. Upon heating, the carbonate showed a similar thermal evolution as the hydroxide layers, with a slow continuous decay, starting at 130 K and going on over a wide temperature range. This leads to the conclusion that carbonate stabilizes the polar NiO(111) surface in a similar manner as the hydroxide, and that during the thermal decay a similar restructuring of the surface is taking place. On 0.5 ML NiO/Cu(111), only very small amounts of carbonate are formed when exposed to CO₂ around 120 K.

Upon CO adsorption on NiO/Ni(111) and 2 ML NiO/Cu(111) around 120 K carbonate was formed, but with much lower coverages than upon CO₂ adsorption. In the C 1s region there also appears a precursor species to carbonate, which completely reacts to carbonate when the surface is heated to room temperature. Up to 250 K, the carbonate coverage is increasing due to this ongoing reaction, while above 300 K the carbonate shows the usual behavior. CO also physisorbed on NiO, and desorbs again below 200 K. On 0.5 ML NiO/Cu(111), CO only physisorbed on the Cu(111) patches. A stabilizing effect of the NiO on the physisorbed CO was observed, as deduced from a higher desorption temperature compared to clean Cu(111).

9 Zusammenfassung

In dieser Arbeit wurde die Adsorption und Reaktion kleiner Moleküle auf verschiedenen Oberflächen mittels hochaufgelöster in-situ XPS untersucht. Diese Methode erlaubte die detaillierte Untersuchung der auftretenden Prozesse und eine Identifikation der Reaktionsprodukte. Das Hauptaugenmerk lag auf NiO Oberflächen, aber auch auf Ni(111) und Cu(111). NiO/Ni(111) und 2 ML NiO/Cu(111) verhielten sich sehr ähnlich, in ihrem Wachstumsverhalten und auch in ihrer Reaktivität gegenüber allen studierten Adsorbaten. NiO Cluster auf Cu(111) zeigten meist ein abweichendes Verhalten, d.h. sie waren entweder weniger reaktiv oder es wurde ein Mischverhalten mit Adsorption sowohl auf dem NiO als auch auf den unbedeckten Cu(111)-Bereichen beobachtet. Nachfolgend sind die wichtigsten Ergebnisse zusammengefasst.

Wachstum von Nickeloxid

Bei Erhöhung der Sauerstoffbedeckung auf Ni(111) bei 300 K, von 0.25 ML für die $p(2 \times 2)$ Struktur auf bis über 0.75 ML, zeigte ein Übergang vom asymmetrischen O 1s Signal des chemisorbierten Sauerstoffs zum symmetrischen Oxid signal den Beginn der Oxidation an. Bei höheren Sauerstoffdosen überschritt die Oxiddicke die Ausdringtiefe der Photoelektronen, was zu einer Sättigung des O 1s Signals führte. Gleichzeitig wandelte sich das Ni 2p Signal von der metallischen zur oxidischen Form. Die Dicke der NiO Schicht wurde auf 11.3-20.0 Å geschätzt. Der O 1s Hauptpeak fand sich bei 529.6 eV; auf Basis eines (aus der Literatur bekannten) großen OH Peaks wurde auf eine (111) Orientierung des NiO geschlossen. Die Position des OH Peaks variierte mit der Bedeckung und Temperatur, wobei Heizen die OH Bedeckung reduzierte. Neben dem Oxid fanden wir eine neue „Schulteroxid“-Spezies bei einer Bindungsenergie von 528.6 eV. Beim Heizen wurde diese Spezies zum Teil in die dominierende Oxidspezies umgewandelt. Die Oxidation bei 500 und 550 K ergab vergleichbare Oxidschichten, aber mit weniger Hydroxid; diese Schichten wurden für die Adsorptionsexperimente auf NiO/Ni(111) verwendet. Oberhalb von 600 K destabilisierte sich das Oxid.

Zur Herstellung dünner NiO Schichten mit definierten Dicken wurden Nickelschichten von 2 und 0.5 ML Dicke auf Cu(111) aufgedampft und anschließend bei 300 K oxidiert. Die Oxidation der 2 ML dicken Schichten verhielt sich sehr ähnlich zu der von Ni(111) bei 300 K. Zusammen mit einer starken Hydroxidkontamination ließ sich daraus auf eine (111) Orientierung des NiO schließen. Höhere Oxidationstemperaturen waren aufgrund von Kupfer-Segregation auf die Nickelschichten nicht möglich. Nach der Oxidation wurden die NiO Schichten auf 500 K geheizt um die Hydroxidverunreinigung zu verringern.

Die 0.5 ML dicken Nickelschichten auf Cu(111) wurden ebenfalls bei 300 K oxidiert. Nach Sättigung des O 1s Peaks unterschieden sich die Ni 2p Spektren in Form und Position von jenen der anderen beiden NiO Schichten. Dafür gibt es zwei Interpretationsmöglichkeiten. Entweder bleiben einige Nickelatome metallisch oder das NiO formt hier eine sogenannte „wetting layer“ mit

abweichenden Eigenschaften. Nach der Oxidation war das NiO fast hydroxidfrei. Die beobachtete Reaktivität gegenüber Wasser legte auch hier eine (111) Orientierung nahe. STM zeigte die gleiche „blumenkohlartige“ Struktur, die schon bei den dickeren NiO Schichten auf Cu(111) beobachtet wurde. Eine erhebliche Oxidation der Kupferoberfläche konnte ausgeschlossen werden.

Adsorption auf und Reaktionen von C₂H_x Spezies auf sauberem und Sauerstoff vorbedecktem Ni(111)

Bei Dosierung mit dem hochenergetischen Molekularstrahl adsorbierte Ethan dissoziativ als Ethyl auf Ni(111). Sowohl die Ethyl- als auch Ethenspektren zeigten zwei Peaks mit Vibrationsaufspaltung. Bei Ethen erklären sich diese durch eine Geometrie mit einem Kohlenstoffatom in einer „hollow“ Position und dem anderen in einer „on-top“ Position. Die gleiche Adsorptionsgeometrie wurde für Ethyl vorgeschlagen. Für Acetylen auf Ni(111) wurde die bekannte „hollow-hollow“ Adsorptionsgeometrie gefunden. Ethyl und Ethen dehydrierten beide um 200 K zu Acetylen, welches um 400 K zu einer Kohlenstoffspezies dehydrierte. Wenn Acetylen direkt auf die Oberfläche dosiert wurde, fand sich bei deutlich höheren Acetylenbedeckungen die Trimerisierung zu Benzol als neuer Reaktionspfad. Anschließend dehydrierte das Benzol, wodurch hohe Kohlenstoffbedeckungen auf der Oberfläche entstanden, welche die Ursache für eine neue, noch nicht identifizierte Spezies bei hohen Temperaturen sind.

Die Adsorption von Ethan und Ethen auf einer mit 0.25 ML Sauerstoff in einer p(2x2) Struktur vorbedeckten Ni(111) Oberfläche unterschied sich deutlich zum Verhalten auf der sauberen Oberfläche. Die Spektren beider Adsorbate zeigten nur einen Peak, was auf eine „hollow-hollow“ Adsorptionsgeometrie schließen ließ. Obwohl Ethan mit dem Hochenergie Molekularstrahl dosiert wurde, adsorbierte es intakt. Auch Ethen adsorbierte intakt, und für beide Adsorbate war die Sättigungsbedeckung deutlich niedriger als auf der sauerstofffreien Oberfläche. Beim Aufheizen der Oberfläche desorbierten beide Adsorbate unterhalb von 250 K und dehydrogenierten nur geringfügig, was mit Lücken in der Sauerstoffschicht erklärt wurde. Die Koadsorption von Acetylen mit Sauerstoff führte zu geringeren Sättigungsbedeckungen als auf der sauberen Oberfläche. Die Adsorptionsgeometrie änderte sich nicht, aber zusätzlich zum chemisorbierten Acetylen fand sich eine physisorbierte Spezies, die auf der sauberen Oberfläche bei gleicher Temperatur nicht vorlag. Bei höheren Temperaturen fand sich der gleiche Reaktionsweg wie auf der sauberen Oberfläche, d.h. Trimerisierung zu Benzol und Dehydrierung. Der S-Faktor pro C-H Bindung für die untersuchten Adsorbate auf Ni(111) ist 0.17 ± 0.02 .

Adsorption von Kohlenwasserstoffen auf Cu(111) und dünnen NiO Schichten

Ethan wurde mit dem hochenergetischen Molekularstrahl auf Cu(111) dosiert und adsorbierte dissoziativ als Ethyl. Ethen, Propan, Propen und Acetylen adsorbierten intakt. Alle C 1s Spektren zeigten eine Vibrationsaufspaltung mit

einem S-Faktor pro C-H Bindung von 0.20 ± 0.02 . Die Spektren aller Adsorbate außer Acetylen hatten eine große Ähnlichkeit mit Gasphasenspektren, am deutlichsten für Propen. Diese Ähnlichkeiten und die vollständige Desorption dieser Adsorbate unterhalb von 250 K wiesen auf eine sehr schwache Wechselwirkung mit der Oberfläche hin. Acetylen war deutlich stärker an die Oberfläche gebunden. Es blieb bis 325 K auf der Oberfläche. Bei dieser Temperatur reagierte es zu einer Reihe von Produkten, die sofort desorbierten.

Die Adsorption von Propan, Propen, Ethan, Ethen, Acetylen und Methan wurde bei Temperaturen um 120 K auf den drei unterschiedlichen NiO Schichten untersucht. Bei allen Adsorbaten wurden physisorbierte Spezies gefunden. Im Fall von Methan wurde nur ein kleines Signal bei laufendem Molekularstrahl auf NiO/Ni(111) beobachtet. Die meisten physisorbierten Moleküle desorbierten unterhalb von 200 K, aber auf Defektstellen waren einige bis zu höheren Temperaturen stabil. Alle Adsorbate (außer Ethan) waren auf NiO/Ni(111) am stärksten gebunden und am schwächsten auf 0.5 ML NiO/Cu(111).

Auf allen NiO Schichten wurde nur für Acetylen neben der physisorbierten auch eine chemisorbierte Spezies gefunden. Bei Adsorption um 120 K wurden beide beinahe gleichzeitig besetzt. Auf NiO/Ni(111) desorbierte das meiste physisorbierte Acetylen unterhalb von 200 K. Eine kleine Menge der physisorbierten Spezies reagierte zu einem Kohlenstoffallotrop, welches auch unterhalb von 500 K das Reaktionsprodukts der chemisorbierten Spezies war. Die charakteristischen Peaks für C-C Bindungen und C-O Einzelbindungen in Kohlenstoffallotropen wurde beobachtet. Auf 2 ML NiO/Cu(111) fand sich eine zusätzliche Kohlenstoffspezies, auf 0.5 ML NiO/Cu(111) adsorbierte Acetylen um 120 K auf den NiO Clustern und auch auf den blanken Cu(111) Flächen dazwischen. Die Ränder der Cluster und ihre Umgebung waren nicht besetzt. Beim Heizen reagierte das Acetylen zu dem Kohlenstoffallotrop und der Kohlenstoffspezies, die bereits auf 2 ML NiO/Cu(111) aufgetreten war. Der C-O Einzelbindungspeak fand sich hier nicht. Dosierung von Acetylen auf 0.5 ML NiO/Cu(111) bei 400 K führte zu fortgesetztem Wachstum des Kohlenstoffallotrops und vollständiger Reduktion des NiO.

Bildung und thermische Entwicklung von NiOH und NiCO₃

Wasseradsorption um 120 K auf Ni(111), Cu(111) und Nickel auf Cu(111) führte zur Bildung geringer Hydroxidmengen auf allen drei Oberflächen sowie zur Bildung von Multilagen physisorbierten Wassers, welche in allen Fällen unterhalb von 250 K desorbierten. Für CO₂ wurde bei ~120 K keine Adsorption auf Cu(111) gefunden und nur eine sehr schwache Wechselwirkung mit Ni(111). CO, welches unterhalb von 120 K auf Cu(111) adsorbiert wurde, führte aufgrund von shake-up Strukturen sowohl im C 1s als auch im O 1s zu sehr komplexen Spektren. CO desorbierte von Cu(111) unterhalb von 170 K vollständig. Auf Ni(111) und 3 ML Nickel auf Cu(111) wurden c(2x4) Adsorbatstrukturen mit einer nominalen Bedeckung von 0.5 ML von CO präpariert. Diese wurden als Referenz für Bedeckungen verwendet.

Auf den drei verschiedenen NiO Oberflächen führte Wasseradsorption um 120 K zu einer Zunahme des Hydroxidsignals und zur Physisorption von Wasser. Das physisorbierte Wasser und die Hydroxidschichten führten zu einer Dämpfung der Photoelektronen der darunterliegenden Schichten, was in der quantitativen Analyse berücksichtigt wurde. Diese zeigte, dass sich die Oxidbedeckung während der Hydroxidbildung nicht ändert. Dies erklärt sich dadurch, dass Oxidsauerstoffatome ihre Bindungsenergie bei Aufnahme eines Wasserstoffes nicht ändern. Der Hydroxidpeak hat eine andere Bindungsenergie. Die höchsten Hydroxidbedeckungen wurden auf NiO/Ni(111) gefunden, die niedrigsten auf 0.5 ML NiO/Cu(111). Das physisorbierte Wasser desorbierte unterhalb von Raumtemperatur. Unterhalb von 200 K blieben die Hydroxidbedeckungen konstant und verringerten sich bei höheren Temperaturen kontinuierlich; bei 600 K war noch Hydroxid auf der Oberfläche vorhanden. Dies erklärt sich aus einer komplizierten Restrukturierung der Oberfläche, zwischen der flachen Hydroxid-bedeckten Oberfläche und der Hydroxid-freien Oberfläche, die oktopolar rekonstruiert ist um Oberflächenladungen zu kompensieren. Diese Restrukturierung benötigt Materialtransport, was zusätzlich zur thermodynamischen auch zu kinetischer Limitierung führt und dadurch zur Existenz mehrerer Übergangszustände. Die Oxidbedeckung blieb innerhalb des untersuchten Temperaturbereichs konstant.

CO₂ Adsorption unterhalb von 125 K führte zur Bildung von Carbonatschichten und zur Physisorption von CO₂. Die Sättigungsbedeckung von Carbonat auf NiO/Ni(111) war höher als auf 2 ML NiO/Cu(111). Die Sauerstoffbedeckung blieb während der Adsorption konstant. Dies bedeutet, dass das Oxidsauerstoffatom im CO₃ seine Bindungsenergie beibehält. Beim Heizen zeigte die Carbonatschicht ein ähnliches thermisches Verhalten wie das Hydroxid, d.h. einen langsamen thermischen Zerfall, der bei 130 K begann und über einen großen Temperaturbereich andauerte. Dies zeigt, dass das Carbonat, ähnlich wie Hydroxid, die polare NiO(111) Oberfläche stabilisiert und während des thermischen Zerfalls eine vergleichbare Restrukturierung der Oberfläche stattfindet. Auf 0.5 ML NiO/Cu(111) bildeten sich nur geringe Carbonatmengen, als es um 120 K CO₂ ausgesetzt wurde.

Auf NiO/Ni(111) und 2 ML NiO/Cu(111) führte CO Adsorption um 120 K zu Carbonatbildung, allerdings mit niedrigerer Sättigungsbedeckung als bei CO₂ Adsorption. In der C 1s Region tauchte eine Vorgängerspezies auf, welche bei Heizen auf Raumtemperatur vollständig zu Carbonat reagierte. Unterhalb von 250 K wuchs die Carbonatmenge aufgrund dieser fortgesetzten Reaktion, oberhalb von 300 K zeigte die Carbonatschicht das bekannte Verhalten. CO physisorbierte auch auf NiO, und desorbierte wieder unterhalb von 200 K. Auf 0.5 ML NiO/Cu(111) physisorbierte CO nur auf den Cu(111) Flächen. Ein stabilisierender Effekt von NiO auf das physisorbierte CO wurde aus der im Vergleich zu sauberem Cu(111) höheren Desorptionstemperatur abgeleitet.

Literature

- [1] Larsen, J.; Chorkendorff, I.; *Surf. Sci. Rep.* **1999**, 35, p. 163-222
- [2] Weissermel, K.; Arpe, H.-J., *Industrial Organic Chemistry: Important Raw Materials and Intermediates*. 4 ed.; Wiley VCH: Weinheim, **2003**.
- [3] Mac Rae, A.; *Surf. Sci.* **1964**, 1, p. 319-348
- [4] Kato, H.; Kudo, A.; *J. Phys. Chem. B* **2001**, 105, p. 4285
- [5] Miseki, Y.; Kato, H.; Kudo, A.; *Energ. Environ. Sci.* **2009**, 2, p. 306
- [6] Sohn, J.; Kim, H.; Park, M.; Park, E.; Kim, J.; Park, S.; *Appl. Catal. A-Gen.* **1995**, 128, p. 127-141
- [7] Sohn, J.; Kim, H.; Park, M.; Park, E.; Kim, J.; Park, S.; *Catal. Today* **2002**, 73, p. 197-209
- [8] Sohn, J.; Lee, S.; *Appl. Catal. A-Gen.* **1997**, 164, p. 127
- [9] Wendt, G.; Finster, J.; Schöllner, R.; *Z. Anorg. Allg. Chem.* **1982**, 488, p. 197-206
- [10] Hu, X.; Hu, C.; *J. Chem. Technol. Biot.* **2010**, 85, p. 1522
- [11] Xu, Q.; Lan, P.; Zhang, B.; Ren, Z.; Yan, Y., *Energ. Fuel* **2010**, DOI: 10.1021/ef1010995
- [12] Zhang, A.; Zhang, R.; Zhang, N.; Hong, S.; Zhang, M.; *Kinet. Catal.+* **2010**, 51, p. 710-713
- [13] Dubowik, J.; Stobiecki, F.; Szymanski, B.; Goscianska, I.; Röhl, K.; Lee, Y.; *Phys. Status Solidi B* **2004**, 241, p. 1613-1616
- [14] Soeya, S.; Nakamura, S.; Imagawa, T.; Narishige, S.; *J. Appl. Phys.* **1995**, 77, p. 5838
- [15] Matsuda, A.; Kasahara, M.; Watanabe, T.; Hara, W.; Otaka, S.; Koyama, K.; Yoshimoto, M., *Mater. Res. Soc. Symp. P.* **2007**, 962, P09-04
- [16] Lindahl, E.; Ottoson, M.; Carlsson, J.-O.; *Surf. Coat. Tech.* **2010**, 205, p. 710-716
- [17] Li, F.; Chen, H.; Wang, C.; Hu, K.; *J. Electroanal. Chem.* **2002**, 531, p. 53-60
- [18] Sabbatini, L.; Morelli, B.; Zambonin, P.; *J. Chem. Soc. Faraday T. 1* **1979**, 75, p. 2628
- [19] Medway, S.; Lucas, C.; Kowal, A.; Nichols, R.; Johnson, D.; *J. Electroanal. Chem.* **2006**, 587, p. 172-181
- [20] Sarantaridis, D.; Atkinson, A.; *Fuel Cells* **2007**, 7, p. 246-258
- [21] Purushothaman, K.; Muralidharan, G.; *J. Sol.-Gel Sci. Techn.* **2008**, 46, p. 190-194
- [22] Bandara, J.; Weerasinghe, H.; *Sol. Energ. Mat. Sol. C* **2005**, 85, p. 385-390
- [23] Hotovy, I.; Huran, J.; Spiess, L.; Hascik, S.; Rehacek, V.; *Sensor. Actuat. B-Chem.* **1999**, 57, p. 147-152
- [24] Kumari, L.; Li, W.; Vannoy, C.; Leblanc, R.; Wang, D.; *Cryst. Res. Technol.* **2009**, 44, p. 495-499
- [25] Einstein, A.; *Ann. Phys.-Leipzig* **1905**, 17, p. 132-148
- [26] Hüfner, S., *Photoelectron Spectroscopy: Principles and Applications*. 2nd ed.; Springer: Berlin, **2003**.

- [27] Papp, C. *In-situ investigations of adsorbed hydrocarbons - model systems of heterogeneous catalysis*. PhD Thesis, FAU Erlangen-Nürnberg, Erlangen, **2007**.
- [28] Steinrück, H.-P.; Fuhrmann, T.; Papp, C.; Tränkenschuh, B.; Denecke, R.; *J. Chem. Phys.* **2006**, 125, p. 204706
- [29] Cederbaum, L.; Domcke, W.; *J. Chem. Phys.* **1976**, 64, p. 603
- [30] Osborne, S.; Sundin, S.; Ausmees, A.; Svensson, S.; Saethre, L.; Svaeren, O.; Sorensen, S.; Végh, J.; Karvonen, J.; Aksela, S.; Kikas, A.; *J. Chem. Phys.* **1997**, 106, p. 1661
- [31] Saethre, L.; Svaeren, O.; S. Svensson; Osborne, S.; Thomas, T.; Jauhiainen, J.; S. Aksela; *Phys. Rev. A* **1997**, 55, p. 2748
- [32] Hergenbahn, U.; *J. Phys. B.-At. Mol. Opt.* **2004**, 37, p. R89-R135
- [33] Somarjai, G., *Chemistry in two dimensions: surfaces*. Cornell University Press: Ithaca, **1981**.
- [34] Seah, M.; Dench, W.; *Surf. Interface Anal.* **1979**, 1, p. 2-11
- [35] Woodruff, D.; Bradshaw, A.; *Rep. Prog. Phys.* **1994**, 57, p. 1029-1080
- [36] Tanuma, S.; Powell, C.; Penn, D.; *J. Electron Spectrosc.* **1990**, 52, p. 285-291
- [37] Domnick, R.; Held, G.; Koschel, H.; Ammon, C.; Steinrück, H.-P.; *Surf. Sci.* **2001**, 482-485, p. 1292-1297
- [38] Frank, F.; van der Merwe, J.; *P. Roy. Soc. Lond. A. Mat.* **1949**, 198, p. 205-216
- [39] Elder, F.; Gurewitsch, A.; Langmuir, R.; Pollock, H.; *Phys. Rev.* **1947**, 71, p. 829-830
- [40] Hofmann, A., *The physics of synchrotron radiation*. Cambridge University Press: New York, **2004**.
- [41] Wiedemann, H., *Synchrotron radiation*. Springer Verlag: Berlin Heidelberg, **2003**.
- [42] Wille, K., *Physik der Teilchenbeschleuniger und Synchrotronstrahlungsquellen*. Teubner: Stuttgart, **1996**.
- [43] de Broglie, L. *Recherches sur la théorie des quanta*. Paris, **1924**.
- [44] Wood, E.; *J. Appl. Phys.* **1964**, 35, p. 1306
- [45] Park, R.; Madden, H.; *Surf. Sci.* **1968**, 11, p. 188-202
- [46] Held, G.; *Bunsen-Magazin* **2010**, 12, p. 124-131
- [47] Pendry, J., *Low Energy Electron Diffraction*. Academic Press: London, **1974**.
- [48] Van Hove, M.; Tong, S., *Surface Crystallography by LEED*. Springer: Berlin, **1979**.
- [49] Van Hove, M.; Weinberg, W.; Chan, C.-M., *Low-Energy Electron Diffraction*. Springer: Berlin, **1986**.
- [50] Clarke, L., *Surface Crystallography - An Introduction to Low Energy Electron Diffraction*. Wiley: Chichester, **1985**.
- [51] Scoles, G., *Atomic and molecular beam methods*. Oxford University Press: New York, **1988**.
- [52] Becker, E.; Bier, K.; *Z. Naturforsch.* **1954**, 9a, p. 975
- [53] Kinne, M. *Kinetische Untersuchungen von Oberflächenreaktionen mittels hochaufgelöster Röntgen-Photoelektronenspektroskopie - Oxidation von Co auf Pt(111) und zugehörige Elementarschritte*. PhD Thesis, Friedrich-Alexander Universität Erlangen-Nürnberg, Erlangen, **2004**.

- [54] Fuhrmann, T. *Elektronenspektroskopische Untersuchungen zur aktivierten Adsorption und thermischen Entwicklung von einfachen Kohlenwasserstoffen auf Platin und Nickel Einkristalloberflächen*. PhD Thesis, FAU Erlangen-Nürnberg, Erlangen, **2005**.
- [55] Denecke, R.; Kinne, M.; Whelan, C.; Steinrück, H.-P.; *Phys. Rev. Lett.* **2002**, 9, p. 797-801
- [56] Sawhney, K.; Senf, F.; Gudat, W.; *Nucl. Instrum. Meth. A* **2001**, 467-468, p. 466-469
- [57] Taylor, A.; *J. Inst. Metals* **1950**, 77, p. 585
- [58] Straumanis, M.; Yu, L.; *Acta Crystallogr.* **1969**, 25A, p. 676
- [59] Denecke, R.; *Appl. Phys. A* **2005**, 80, p. 977-986
- [60] Bronstein, I.; Semedjajew, K., *Taschenbuch der Mathematik*. Teubner: Stuttgart, Leipzig, **1996**.
- [61] Shirley, D.; *Phys. Rev. B* **1972**, 5, p. 4709
- [62] Doniach, S.; Sunjic, M.; *J. Phys.* **1970**, 3, p. 285
- [63] Clendenen, R.; Drickamer, H.; *J. Chem. Phys.* **1966**, 44, p. 4223
- [64] Bergemann, C.; *J. Prakt. Chem.* **1858**, 75, p. 239-244
- [65] Pedio, M.; Becker, L.; Hillert, B.; D'Addato, S.; Haase, J.; *Phys. Rev. B* **1990**, 41, p. 7462
- [66] Grimsby, D.; Wu, Y.; Mitchell, K.; *Surf. Sci.* **1990**, 232, p. 51-55
- [67] Li, T.; Bhatia, B.; Sholl, D.; *J. Chem. Phys.* **2004**, 121, p. 10241
- [68] Holloway, P.; Hudson, J.; *Surf. Sci.* **1974**, 43, p. 141-149
- [69] Okazawa, T.; Nishizawa, T.; Nishimura, T.; Y., K.; *Phys. Rev. B* **2007**, 75, p. 033413
- [70] Mitchell, D.; Graham, M.; *Surf. Sci.* **1982**, 114, p. 546-562
- [71] Narusawa, T.; Gibson, W.; Törnqvist, E.; *Phys. Rev. Lett.* **1981**, 47, p. 417
- [72] Fehner, F.; Mott, N.; *Oxid. Met.* **1970**, 2, p. 59-99
- [73] Holloway, P.; Hudson, J.; *Surf. Sci.* **1974**, 43, p. 123-140
- [74] Norton, P.; Tapping, R.; *Faraday Discuss.* **1975**, 60, p. 71
- [75] Tyuliev, G.; Kostov, K.; *Phys. Rev. B* **1999**, 60, p. 2900
- [76] Knudsen, J.; Merte, L.; Peng, G.; Vang, R.; Resta, A.; Laegsgaard, E.; Andersen, J.; Mavriakakis, M.; Besenbacher, F.; *ACS Nano* **2010**, 4, p. 4380
- [77] Zion, B.; Hanbicki, A.; Sibener, S.; *Surf. Sci.* **1998**, 417, p. L1154-L1159
- [78] Badyal, J.; Zhang, X.; Lambert, R.; *Surf. Sci.* **1990**, 225, p. L15-L19
- [79] Kitakatsu, N.; Maurice, V.; Hinnen, C.; Marcus, P.; *Surf. Sci.* **1998**, 407, p. 36-58
- [80] Norton, P.; Tapping, R.; Goodale, J.; *Surf. Sci.* **1977**, 65, p. 13-36
- [81] Hildebrandt, S.; Hagendort, C.; Doege, T.; Jeckstiess, C.; Kulla, R.; Neddermeyer, H.; Uttich, T.; *J. Vac. Sci. Technol. A* **2000**, 18, p. 1010
- [82] Ebensperger, C.; Meyer, B., *Phys. Status Solidi B* **2011**, 248
- [83] Christensen, T.; Raoul, C.; Blakely, J.; *Appl. Surf. Sci.* **1986**, 26, p. 408-417
- [84] Wolf, D.; *Phys. Rev. Lett.* **1992**, 68, p. 3315
- [85] Rohr, F.; Wirth, K.; Libuda, J.; Cappus, D.; Bäumer, M.; Freund, H.-J.; *Surf. Sci.* **1994**, 315, p. L977-L982
- [86] Ventrice Jr., C.; Bertrams, T.; Hannemann, H.; Brodde, A.; Neddermeyer, H.; *Phys. Rev. B* **1994**, 49, p. 5773

- [87] Barbier, A.; Renaud, G.; Mocuta, C.; Stierle, A.; *Surf. Sci.* **1999**, 433-435, p. 761-764
- [88] Langell, M.; Nassir, M.; *J. Phys. Chem.* **1995**, 99, p. 4162-4169
- [89] Cappus, D.; Xu, C.; Ehrlich, D.; Dillmann, B.; Ventrice Jr., C.; Al Shamery, K.; Kuhlbeck, H.; Freund, H.-J.; *Chem. Phys.* **1993**, 177, p. 533-546
- [90] Andersson, S.; Davenport, J.; *Solid State Commun.* **1978**, 28, p. 677-681
- [91] Lorenz, M.; Schulze, M.; *Surf. Sci.* **2000**, 454-456, p. 234-239
- [92] Lescop, B.; Galtayries, A.; Fanjoux, G.; *J. Phys. Chem. b* **2004**, 108, p. 13711-13718
- [93] Kitakatsu, N.; Maurice, V.; Marcus, P.; *Surf. Sci.* **1998**, 411, p. 215-230
- [94] Kortan, A.; Park, R.; *Phys. Rev. B* **1981**, 23, p. 6340-6347
- [95] Domnick, R.; Held, G.; Witte, P.; Steinrück, H.-P.; *J. Chem. Phys.* **2001**, 115, p. 1902
- [96] Hufner, S., *Photoelectron Spectroscopy: Principles and Applications*. 2nd ed.; Springer: Berlin, **1996**.
- [97] Briggs, D.; Seah, M., *Practical Surface Analysis*. 2nd ed.; Wiley: Chichester, **1996**; Vol. 1.
- [98] Roberts, M.; Smart, R.; *J. Chem. Soc. Faraday T.* **1984**, 80, p. 2957-2968
- [99] Moroney, L.; Smart, R.; Roberts, M.; *J. Chem. Soc. Faraday T.* **1983**, 79, p. 1769
- [100] Ebersperger, C.; Meyer, B., *Personal Communication* **2011**,
- [101] Evans, S.; Pielaszek, J.; Thomas, J.; *Surf. Sci.* **1976**, 56, p. 644-662
- [102] Baer, Y.; Hedén, P.; Hedman, J.; KLasson, M.; Nordling, c.; Siegbahn, K.; *Phys. Scr.* **1970**, 1, p. 55-65
- [103] Grosvenor, A.; Biesinger, M.; Smart, R.; McIntyre, N.; *Surf. Sci.* **2006**, 600, p. 1771-1779
- [104] Karis, O.; Svensson, S.; Rusz, J.; Oppeneer, P.; Gorgoi, M.; Schäfers, F.; Braun, W.; Eberhardt, W.; Mårtensson, N.; *Phys. Rev. B* **2008**, 78, p. 233105
- [105] van Veenendaal, M.; Sawatzky, G.; *Phys. Rev. Lett.* **1993**, 70, p. 2459-2462
- [106] Soriano, L.; Preda, I.; Gutiérrez, A.; Palacín, S.; Abbate, M.; Vollmer, A.; *Phys. Rev. B* **2007**, 75, p. 233417
- [107] Alders, D.; Voogt, F.; Hibma, T.; Sawatzky, G.; *Phys. Rev. B* **1996**, 54, p. 7716-7719
- [108] Towler, M.; Harrison, N.; McCarthy, M.; *Phys. Rev. B* **1995**, 52, p. 5375
- [109] Kuhlbeck, H.; Odörfer, G.; Jaeger, R.; Illing, G.; Menges, M.; Mull, T.; Freund, H.-J.; Pöhlchen, M.; Staemmler, V.; Witzel, S.; Scharfschwerdt, C.; Wennemann, K.; Liedtke, T.; Neumann, M.; *Phys. Rev. B* **1991**, 43, p. 1969-1986
- [110] McKay, J.; Henrich, V.; *Phys. Rev. B* **1985**, 32, p. 6764
- [111] Uhlenbrock, S.; Scharfschwerdt, C.; Neumann, M.; Illing, G.; Freund, H.-J.; *J. Phys.-Condens. Mat.* **1992**, 4, p. 7973-7978
- [112] Sawatzky, G.; Allen, J.; *Phys. Rev. Lett.* **1984**, 53, p. 2339-2342
- [113] Peng, T.; Xiao, X.; Han, X.; Zhou, X.; Wu, W.; Ren, F.; Jiang, C.; *Appl. Surf. Sci.* **2011**, 257, p. 5908-5912
- [114] Domnick, R.; Held, G.; Steinrück, H.-P.; *Surf. Sci.* **2002**, 516, p. 95-102

- [115] Sánchez-Agudo, M.; Yubero, F.; Fuentes, G.; Gutiérrez, A.; Sacchi, M.; Soirano, L.; Sanz, J.; *Surf. Interface Anal.* **2000**, 30, p. 396-400
- [116] Stanescu, S.; Boeglin, C.; Barbier, A.; Deville, J.-P.; *Phys. Rev. B* **2003**, 67, p. 035419
- [117] Barbier, A.; Stanescu, S.; Boeglin, C.; Deville, J.-P.; *Phys. Rev. B* **2003**, 68, p. 245418
- [118] Habraken, F.; Kiefer, E.; Bootsma, G.; *Surf. Sci.* **1979**, 83, p. 45-59
- [119] Wiame, F.; Maurice, V.; Marcus, P.; *Surf. Sci.* **2007**, 601, p. 1193-1204
- [120] Fleisch, T.; Mains, G.; *Appl. Surf. Sci.* **1982**, 10, p. 51-62
- [121] Kessler, J.; Thieme, F.; *Surf. Sci.* **1977**, 67, p. 405-415
- [122] Kirstein, W.; Krüger, B.; Thieme, F.; *Surf. Sci.* **1986**, 176, p. 505-529
- [123] Netzer, F.; Madey, T.; *J. Chem. Phys.* **1982**, 76, p. 710
- [124] Koschel, H.; Held, G.; Steinrück, H.-P.; *Surf. Sci.* **2000**, 453, p. 201-213
- [125] Held, G.; Schuler, J.; Sklarek, W.; Steinrück, H.-P.; *Surf. Sci.* **1998**, 398, p. 154-171
- [126] Rizzi, G.; Petukhov, M.; Sambì, M.; Granozzi, G.; *Surf. Sci.* **2003**, 522, p. 1-7
- [127] Höfert, O.; Zhao, W.; Gotterbarm, K.; Papp, C.; Steinrück, H.-P., *In preparation*, **2011**
- [128] Agnoli, S.; Orzali, T.; Sambì, M.; Granozzi, G.; Schoiswohl, J.; Surnev, S.; Netzer, F.; *J. Electron Spectrosc.* **2005**, 144-147, p. 465-469
- [129] Agnoli, S.; Sambì, M.; Granozzi, G.; Atrei, A.; Caffio, M.; Rovida, G.; *Surf. Sci.* **2005**, 576, p. 1-8
- [130] Sambì, M.; Sensolo, R.; Rizzi, G.; Petukhov, M.; Granozzi, G.; *Surf. Sci.* **2003**, 537, p. 36
- [131] Orzali, T.; Agnoli, S.; Sambì, M.; Granozzi, G.; *Surf. Sci.* **2004**, 569, p. 105
- [132] Preda, I.; Gutiérrez, A.; Abbate, M.; Yubero, F.; Méndez, J.; Alvarez, L.; Soriano, L.; *Phys. Rev. B* **2008**, 77, p. 075411
- [133] Matsumoto, T.; Bennett, R.; Stone, P.; Yamada, T.; Domen, K.; Bowker, M.; *Surf. Sci.* **2001**, 471, p. 225-245
- [134] Zaera, F.; *Prog. Surf. Sci.* **2001**, 69, p. 1-98
- [135] Zaera, F.; *Catal. Lett.* **2003**, 91, p. 1
- [136] Somorjai, G.; McCrea, K.; Zhu, J.; *Top. Catal.* **2002**, 18, p. 157
- [137] Kao, C.-L.; Carlsson, A.; Madix, R.; *Top. Catal.* **2001**, 14, p. 63
- [138] Kao, C.-L.; Madix, R.; *Surf. Sci.* **2004**, 557, p. 215-230
- [139] Demuth, J.; Eastman, D.; *Phys. Rev. Lett.* **1974**, 32, p. 1123-1127
- [140] Cooper, E.; Raval, R.; *Surf. Sci.* **1995**, 331-333, p. 94-99
- [141] Hammer, L.; Hertlein, T.; Müller, K.; *Surf. Sci.* **1986**, 178, p. 693-703
- [142] Lehwald, S.; Ibach, H.; *Surf. Sci.* **1979**, 89, p. 425-445
- [143] Demuth, J.; Ibach, H.; Lehwald, S.; *Phys. Rev. Lett.* **1978**, 40, p. 1044
- [144] Hammer, L.; Dötsch, B.; Harder, C.; Müller, K.; *Vacuum* **1990**, 41, p. 121-125
- [145] Bao, S.; Hofmann, P.; Schindler, K.; Fritzsche, V.; Bradshaw, A.; Woodruff, D.; Casado, C.; Asensio, M.; *Surf. Sci.* **1995**, 323, p. 19-29
- [146] Demuth, J.; *Surf. Sci.* **1978**, 76, p. L603-L608
- [147] Sham, T.; Carr, R.; *J. Chem. Phys.* **1986**, 84, p. 4091
- [148] Zhu, X.-Y.; Castro, M.; Akhter, S.; White, J.; Houston, J.; *J. Vac. Sci. Technol. A* **1989**, 7, p. 1991

- [149] Lam, M.; Boyd, R.; Kreuzer, H.; *Chem. Phys. Lett.* **1996**, 253, p. 129-134
- [150] Fahmi, A.; van Santen, R.; *Surf. Sci.* **1997**, 371, p. 53-62
- [151] Hammer, L.; Müller, K.; *Prog. Surf. Sci.* **1991**, 35, p. 103-111
- [152] Vang, R.; Honkala, K.; Dahl, S.; Vestergaard, E.; Schnadt, J.; Laegsgaard, E.; Clausen, B.; Norskov, J.; Besenbacher, F.; *Surf. Sci.* **2006**, 600, p. 66-77
- [153] Nascente, P.; Van Hove, M.; Somorjai, G.; *Surf. Sci.* **1991**, 253, p. 167-176
- [154] Steininger, H.; Ibach, H.; Lehwald, S.; *Surf. Sci.* **1982**, 117, p. 685-698
- [155] Baraldi, A.; Comelli, G.; Lizzit, S.; Kiskinova, M.; Paolucci, G.; *Surf. Sci. Rep.* **2003**, 49, p. 169-224
- [156] Bürgi, T.; Trautman, T.; Gostein, M.; Lahr, D.; Haug, K.; Ceyer, S.; *Surf. Sci.* **2002**, 501, p. 49-73
- [157] Hamza, A.; Madix, R.; *Surf. Sci.* **1987**, 179, p. 25-46
- [158] Demuth, J.; *Surf. Sci.* **1977**, 69, p. 365-384
- [159] Bao, S.; Hofmann, P.; Schindler, K.; Fritzsche, V.; Bradshaw, A.; *Surf. Sci.* **1994**, 307-309, p. 722-727
- [160] Bertolini, J.-C.; Massardier, J.; Dalmai-Imelik, G.; *J. Chem. Soc. Farad. T. 1* **1978**, 74, p. 1720
- [161] Yang, Q.; A.Johnson; Maynard, K.; Ceyer, S.; *J. Am. Chem. Soc.* **1989**, 111, p. 8748
- [162] Yang, Q.; Maynard, K.; Johnson, A.; Ceyer, S.; *J. Chem. Phys.* **1995**, 102, p. 7734
- [163] Woodruff, D.; Bradshaw, A.; *Rep. Prog. Phys.* **1994**, 57, p. 1029-1080
- [164] Baró, A. M.; Lehwald, S.; Ibach, H.; **1982**, p. 215
- [165] Whelan, C.; Neubauer, R.; Denecke, R.; Steinrück, H.-P.; *Surf. Rev. Lett.* **2002**, 9, p. 789-795
- [166] Michaelides, A.; Hu, P.; *J. Chem. Phys.* **2001**, 114, p. 2523
- [167] Wiltner, A.; Linsmeier, C.; *Surf. Sci.* **2008**, 602, p. 3623
- [168] Grüneis, A.; Kummer, K.; Vyalikh, D.; *New J. Phys.* **2009**, 11, p. 073050
- [169] Tanaka, K.; Hirano, H.; *Catal. Lett.* **1992**, 12, p. 1-6
- [170] Christmann, K.; Behm, R.; Ertl, G.; Hove, M. V.; Weinberg, W.; *J. Chem. Phys.* **1979**, 70, p. 4168-4184
- [171] Greeley, J.; Mavrikakis, M.; *Surf. Sci.* **2003**, 540, p. 215-229
- [172] Haroun, M.; Moussounda, P.; Légaré, P.; Parlebas, J.-C.; *Eur. Phys. J. B* **2010**, 78, p. 353-358
- [173] Gallagher, M.; Haq, S.; Omer, A.; Hodgson, A.; *Surf. Sci.* **2007**, 601, p. 268-273
- [174] Neubauer, R.; Whelan, C.; Denecke, R.; Steinrück, H.-P.; *J. Chem. Phys.* **2003**, 119, p. 1710
- [175] Papp, C.; Fuhrmann, T.; Tränkenschuh, B.; Denecke, R.; Steinrück, H.-P.; *Phys. Rev. B* **2006**, p.
- [176] Steinrück, H.-P.; Huber, W.; Pache, T.; Menzel, D.; *Surf. Sci.* **1989**, 218, p. 293
- [177] Schaff, O.; Fernandez, V.; Hoffmann, P.; Schindler, K.; Theobald, A.; Fritzsche, V.; Bradshaw, A.; Davis, R.; Woodruff, D.; *Surf. Sci.* **1996**, 348, p. 89-99
- [178] Zhao, W.; Papp, C., *Personal Communication*, **2010**

- [179] Held, G.; Schuler, J.; Skalerk, W.; Steinrück, H.-P.; *Surf. Sci.* **1998**, 398, p. 154-171
- [180] Ennis, C.; Carr, P.; McCash, E.; *Surf. Sci.* **2003**, 539, p. L574-L576
- [181] Demuth, J.; *IBM J. Res. Dev.* **1978**, 22, p. 265
- [182] Bandy, B.; Chesters, M.; Pemble, M.; McDougall, G.; Sheppard, N.; *Surf. Sci.* **1984**, 139, p. 87-97
- [183] Bao, S.; Schindler, K.-M.; Hofmann, P.; Fritzsche, V.; Bradshaw, A.; Woodruff, D.; *Surf. Sci.* **1993**, 291, p. 295-308
- [184] Konishi, Y.; Sainoo, Y.; Kanazawa, K.; Yoshida, S.; Taninaka, A.; Takeuchi, O.; Shigekawa, H.; *Phys. Rev. B* **2005**, 71, p. 193410
- [185] Hermann, K.; Witko, M.; *Surf. Sci.* **1995**, 337, p. 205-214
- [186] Fuhrmann, D.; Wacker, D.; Weiss, K.; Hermann, K.; Witko, M.; Wöll, C.; *J. Chem. Phys.* **1998**, 108, p. 2651-2658
- [187] Canning, N.; Baker, M.; Chesters, M.; *Surf. Sci.* **1981**, 111, p. 441-451
- [188] Kyriakou, G.; Kim, J.; Tikhov, M.; Macleod, N.; Lambert, R.; *J. Phys. Chem. B* **2005**, 109, p. 10952-10956
- [189] Redhead, P.; *Vacuum* **1962**, 12, p. 203
- [190] Xi, M.; Yang, M.; Jo, S.; Bent, B.; Stevens, P.; *J. Chem. Phys.* **1994**, 101, p. 9122
- [191] Huang, W.; Wei, W.; Zhao, W.; White, J.; *J. Phys. Chem. B* **2006**, 110, p. 5547-5552
- [192] Linke, R.; Becker, C.; Pelster, T.; Tanemura, M.; Wandelt, K.; *Surf. Sci.* **1997**, 377-379, p. 655-658
- [193] Constant, L.; Speisser, C.; Le Normand, F.; *Surf. Sci.* **1997**, 387, p. 28-43
- [194] Shih, J.-J.; Kuo, K.-H.; Yang, C.-M.; Lin, J.-L.; Fan, L.-J.; Yang, Y.-W.; **2008**, 602, p. 3266-3271
- [195] Syed, J.; Sardar, S.; Yagi, S.; Tanaka, K.; *J. Vac. Sci. Technol. A* **2004**, 22, p. 3
- [196] Chen, B.; Fujimura, Y.; Katsumata, T.; Takikawa, H.; Hibi, Y.; Sakakibara, T.; Itoh, S.; *T. Mrs. Jap.* **2004**, 29, p. 559-562
- [197] Demuth, J.; Ibach, H.; *Surf. Sci.* **1978**, 78, p. L238-L244
- [198] Gao, Y.; Yip, H.-L.; Chen, K.-S.; O'Malley, K.; Acton, O.; Sun, Y.; Ting, G.; Chen, H.; Jen, A.; *Adv. Mater.* **2011**, 23, p. 1903
- [199] Langley, L.; Villanueva, D.; Fairbrother, D.; *Chem. Mater.* **2006**, 18, p. 169-178
- [200] Liu, S.; Tian, J.; Wang, L.; Sun, X.; *Carbon* **2011**, 49, p. 3158-3164
- [201] Liu, K.; Chen, L.; Chen, Y.; Wu, J.; Zhang, W.; Chen, F.; Fu, Q.; *J. Mater. Chem.* **2011**, 21, p. 8612
- [202] Wang, L.; Ge, L.; Rufford, T.; Chen, J.; Zhou, W.; Zhu, Z.; Rudolph, V.; *Carbon* **2011**, 49, p. 2022-2032
- [203] Chopra, N.; McWhinney, H.; Shi, W.; *Mater. Charact.* **2011**, 62, p. 635-641
- [204] Bououdina, M.; Grant, D.; Walker, G.; *Carbon* **2005**, 43, p. 1286-1292
- [205] Hoshi, F.; Tsugawa, K.; Goto, A.; Ishikura, T.; Yamashita, S.; Yumura, M.; Hirao, T.; Oura, K.; Koga, Y.; *Diam. Relat. Mater.* **2001**, 10, p. 254-259
- [206] Jiang, Z.; Song, R.; Bi, W.; Lu, J.; Tang, T.; *Carbon* **2007**, 45, p. 449-458
- [207] Hanus, M.; Linkson, P.; Harris, A.; *Carbon* **2010**, 48, p. 3931-3938

- [208] Liu, S.; Xiong, G.; Yang, W.; Sheng, S.; *React. Kinet. Catal. Lett.* **1999**, 68, p. 243-247
- [209] Czekaj, I.; Loviat, F.; Raimondi, F.; Wambach, J.; Biollaz, S.; Wokaun, A.; *Appl. Catal. A-Gen.* **2007**, 329, p. 68-78
- [210] Serafin, J.; Friend, C.; **1989**, 209, p. L163-L175
- [211] Xu, X.; Friend, C.; *J. Phys. Chem.* **1989**, 93, p. 8072
- [212] Mourcel, P.; Pham, M.-C.; Lacaze, P.-C.; Dubois, J.-E.; *J. Electroanal. Chem.* **1983**, 145, p. 467-472
- [213] Yang, D.; Velamakanni, A.; Bozoklu, G.; Park, S.; Stoller, M.; Piner, R.; Stankovich, S.; Jung, I.; Field, D.; Ventrice Jr., C.; Ruoff, R.; *Carbon* **2009**, 47, p. 145-152
- [214] Morales, J.; Caballero, A.; Holgado, J.; Espinós, J.; González-Elipe, A.; *J. Phys. Chem. B* **2002**, 106, p. 10185-10190
- [215] Zeigarnik, A.; Valdés-Pérez, R.; Myatkovskaya, O.; *J. Phys. Chem. B* **2000**, 104, p. 10578-10587
- [216] van Kooten, W.; Kragten, D.; Gijzeman, O.; Geus, J.; *Surf. Sci.* **1993**, 290, p. 302-308
- [217] Xi, M.; Bent, B.; *J. Vac. Sci. Technol. B* **1992**, 10, p. 2440
- [218] Torres, D.; Lopez, N.; Illas, F.; *J. Catal.* **2006**, 243, p. 404-409
- [219] Lin, J.-L.; Bent, B.; *Chem. Phys. Lett.* **1992**, 194, p. 208-212
- [220] Meyers, J.; Gellman, A.; *Surf. Sci.* **1995**, 339, p. 57-67
- [221] Karlsen, T.; Borge, K.; Saethre, L.; Wiesner, K.; Bäessler, M.; Svensson, S.; *J. Am. Chem. Soc.* **2001**, 124, p. 7866
- [222] Thiel, P.; Madey, T.; *Surf. Sci. Rep.* **1987**, 7, p. 211-385
- [223] Carley, A.; Rassias, S.; Roberts, M.; *Surf. Sci.* **1983**, 135, p. 35-51
- [224] Reissner, R.; Radke, U.; Schulze, M.; Umbach, E.; *Surf. Sci.* **1998**, 402-404, p. 71-75
- [225] Shido, T.; Asakura, K.; Iwasawa, Y.; *J. Catal.* **1990**, 122, p. 55
- [226] Sugiyama, S.; Sato, K.; Yamasaki, S.; Kawashiro, K.; Hayashi, H.; *Catal. Lett.* **1992**, 14, p. 127-133
- [227] Rostrup-Nielsen, J.; Hansen, J.-H.; *J. Catal.* **1993**, 144, p. 38
- [228] Yano, T.; Matsui, H.; Koike, T.; Ishiguro, H.; Fujihara, H.; Yoshihara, M.; Maeshima, T.; *Chem. Commun.* **1997**, 1997, p. 1129
- [229] Lunsford, J.; *Angew. Chem. Int. Edit.* **1995**, 34, p. 970
- [230] Holloway, S.; *Annu. Rev. Energy Environ.* **2001**, 26, p. 145-166
- [231] Behm, R.; Brundle, C.; *J. Vac. Sci. Technol. A* **1982**, 1, p. 1223
- [232] Behm, R.; Brundle, C.; *Surf. Sci.* **1991**, 255, p. 327-343
- [233] Stuve, E.; Madix, T.; Sexton, B.; *Chem. Phys. Lett.* **1983**, 89, p. 48-53
- [234] Bader, M.; Hillert, B.; Puschmann, A.; Haase, J.; Bradshaw, A.; *Europhys. Lett.* **1988**, 5, p. 443
- [235] Madix, R.; Solomon, J.; Stöhr, J.; *Surf. Sci.* **1988**, 197, p. L253-L259
- [236] Gordon, D.; Lambert, R.; *Surf. Sci.* **1993**, 287/288, p. 114-118
- [237] Matsumoto, T.; Kubota, J.; Kondo, J.; Hirose, C.; Domen, K.; *Langmuir* **1999**, 15, p. 2158-2161
- [238] Emfietzoglou, D.; Kyriakou, I.; Abril, I.; Garcia-Molina, R.; Petsalakis, I.; Nikjoo, H.; Pathak, A.; *Nucl. Instrum. Meth. B* **2009**, 267, p. 46-52
- [239] Ewing, G.; *Chem. Rev.* **2006**, 106, p. 1511-1526
- [240] Tanuma, S.; Powell, C.; Penn, D.; *Surf. Interface Anal.* **1993**, 21, p. 165
- [241] Akkerman, A.; Akkerman, E.; *J. Appl. Phys.* **1999**, 86, p. 5809
- [242] LaVerne, J.; Pimblott, S.; *Radiat. Res.* **1995**, 141, p. 208

- [243] Emfietzoglou, D.; Nikjoo, H.; *Radiat. Res.* **2007**, 167, p. 110
- [244] Michaud, M.; Wen, A.; Sanche, L.; *Radiat. Res.* **2003**, 159, p. 3-22
- [245] Stulen, R.; Thiel, P.; *Surf. Sci.* **1985**, 157, p. 99-118
- [246] Madey, T.; Netzer, P.; *Surf. Sci.* **1982**, 117, p. 549-560
- [247] Pache, T.; Steinrück, H.-P.; Huber, W.; Menzel, D.; *Suf. Sci.* **1989**, 224, p. 195
- [248] Au, C.; Bri-Za, J.; Roberts, M.; *Chem. Phys. Lett.* **1979**, 66, p. 340
- [249] Hinch, B.; Dubois, L.; *J. Chem. Phys.* **1992**, 96, p. 3262
- [250] Henderson, M.; *Surf. Sci. Rep.* **2002**, 46, p. 1
- [251] Krepelová, A.; Newberg, J.; Huthwelker, T.; Bluhm, H.; Ammann, M.; *Phys. Chem. Chem. Phys.* **2010**, 12, p. 8870-8880
- [252] Campbell, C.; Daube, K.; White, J.; **1987**, 182, p. 458-476
- [253] Fu, S.; Somorjai, G.; **1992**, 8, p. 518-524
- [254] Wang, S.-G.; Cao, D.-B.; Li, Y.-W.; Wang, J.; Jiao, H.; *J. Phys. Chem. B* **2005**, 109, p. 18956-18963
- [255] Hollins, P.; Pritchard, J.; *Surf. Sci.* **1980**, 99, p. L389-L394
- [256] Kirstein, W.; Krüger, B.; Thieme, F.; *Surf. Sci.* **1986**, 176, p. 505-529
- [257] Fusy, J.; Menaucourt, J.; Alnot, M.; Huguet, C.; Ehrhardt, J.; *Appl. Surf. Sci.* **1996**, 93, p. 211-220
- [258] Berlowitz, P.; Peden, C.; Goodman, D.; *Mater. Res. Soc. Symp. Proc.* **1987**, 83, p. 161
- [259] Raval, R.; Parker, S.; Pemble, M.; Hollins, P.; Pritchard, J.; Chesters, M.; *Surf. Sci.* **1988**, 203, p. 353-377
- [260] Gajdos, M.; Hafner, J.; *Surf. Sci.* **2005**, 590, p. 117-126
- [261] Neef, M.; Doll, K.; *Surf. Sci.* **2006**, 600, p. 1085-1092
- [262] Norton, P.; Tapping, R.; Goodale, J.; *Surf. Sci.* **1978**, 72, p. 33-44
- [263] Antonsson, H.; Nilsson, A.; Martensson, N.; *J. Electron Spectrosc.* **1990**, 54/55, p. 601-613
- [264] Baker, M.; Canning, N.; Chesters, M.; *Surf. Sci.* **1981**, 111, p. 452-460
- [265] Mesters, C.; Koster, A.; Gijzeman, O.; Geus, J.; *Appl. Surf. Sci.* **1984**, 20, p. 1-12
- [266] Freund, H.-J.; Eberhardt, W.; Heskett, D.; Plummer, E.; *Phys. Rev. Lett.* **1983**, 50, p. 768
- [267] Kittel, M.; Hoefl, J.; Bao, S.; Polcik, M.; Toomes, R.; Kang, J.-H.; Woodruff, D.; Pascal, M.; Lamont, C.; *Surf. Sci.* **2002**, 499, p. 1-14
- [268] Hoefl, J.; Kittel, M.; Polcik, M.; Bao, S.; Toomes, R.; Kang, J.-H.; Woodruff, D.; Pascal, M.; Lamont, C.; *Phys. Rev. Lett.* **2001**, 87, p. 086101
- [269] Rohrbach, A.; Hafner, J.; Kresse, G.; *Phys. Rev. B* **2004**, 69, p. 075413
- [270] Wichtendahl, R.; Rodriguez-Rodrigo, M.; Härtel, U.; Kuhlenbeck, H.; Freund, H.-J.; *Surf. Sci.* **1999**, 423, p. 90-98
- [271] Schönnenbeck, M.; Cappus, D.; Klinkmann, J.; Freund, H.-J.; Petterson, L.; Bagus, P.; *Surf. Sci.* **1996**, 347, p. 337-345
- [272] Roberts, M.; Smart, R.; *Surf. Sci.* **1980**, 100, p. 590-604
- [273] Wambach, J.; Illing, G.; Freund, H.-J.; **1991**, 184, p. 239-244

Danksagungen

An dieser Stelle gebührt all jenen Personen Dank, die zum Gelingen dieser Arbeit beigetragen haben:

- Prof. Dr. H.-P. Steinrück für die Gelegenheit, diese Arbeit in seiner Arbeitsgruppe durchzuführen. Dabei gilt besondere Dank für seine große Geduld und die sehr angenehme Atmosphäre in der Arbeitsgruppe, die durch ihn ermöglicht wird
- Dr. C. Papp für die Betreuung bei der Datenauswertung. Vielen Dank für die Geduld bei den langen Diskussionen und das Stellen entscheidender Fragen
- Dr. A. Bayer und Prof. Dr. R. Denecke für die Betreuung bei der Experimentauswahl und Datensammlung. Danke für die gute Atmosphäre während der Messzeiten bei BESSY II
- Dr. R. Streber, O. Höfert, W. Zhao und K. Gotterbarm für die exzellente Zusammenarbeit und die gute Arbeitsatmosphäre in den letzten Jahren, sowohl in Berlin als auch in Erlangen
- Dr. B. Tränkenschuh, S. Wickert, E. Darlatt, Y. Lykach und F. Bebensee für die Unterstützung bei Strahlzeiten in Berlin
- Dr. H. Marbach, Dr. F. Buchner und E. Zillner für die Durchführung von STM Messungen
- Prof. Dr. Bernd Meyer und C. Ebensperger für die Durchführung von DFT-Berechnungen
- H.-P. Bäumlner für die stets schnelle und kompetente Hilfe bei elektrischen und elektronischen Problemen
- B. Kreß für die kompetente Hilfe bei UHV-Problemen
- Allen Mitarbeitern der Werkstatt und besonders F. Wölfel für die stets schnelle und unkomplizierte Hilfe
- Allen Mitarbeitern von BESSY II in Berlin für die Unterstützung beim Ablauf der Messzeiten
- Allen Mitarbeitern am Lehrstuhl PC II in Erlangen für die freundschaftliche und angenehme Arbeitsatmosphäre
- Meiner Familie und meiner Lebensgefährtin, die mich stets unterstützt haben

Lebenslauf

Persönliche Angaben

Name	Lorenz
Vornamen	Michael Peter Andreas
Geburtsdatum	24.08 1979
Geburtsort	Schwabach
Nationalität	Deutsch
Familienstand	Ledig

Promotion

05/2006-12/2011	Lehrstuhl für Physikalische Chemie II Universität Erlangen-Nürnberg
-----------------	--

Abschlüsse

03/2006	Physik Diplom
07/2002	Physik Vordiplom
06/1999	Abitur

Studium

09/2003-06/2006	Hauptstudium Physik an der Universität Erlangen-Nürnberg
09/2002-07/2003	Physikstudium an der University of York in Großbritannien
09/2000-07/2002	Grundstudium Physik an der Universität Erlangen-Nürnberg

Zivildienst

08/1999-06/2000	Therapiezentrum Wolkersdorf
-----------------	-----------------------------

Schule

09/1990-06/1999	Adam-Kraft-Gymnasium Schwabach
09/1987-07/1990	Grundschule Katzwang (Nürnberg)

Erlangen, den 19.12.2011